Growth of Semiconductor Thin Films using Single-Source Precursors

A thesis submitted to the University of Manchester for the Degree of Doctor of Philosophy in the Faculty of Science and Engineering

January 2004

Mohammad Afzaal

Department of Chemistry

The University of Manchester

Oxford Road

Manchester

M13 9 PL

ProQuest LLC.
789 East Eisenhower Parkway
P.O. Box 1346
Ann Arbor, MI 48106 – 1346

Table of Contents

List of Figures

List of Tables

Abstract

The growth of metal sulfide and selenide semiconductor thin films often involves the decomposition of organometallic or metal-organic compounds. The research described in this thesis concerns the synthesis and characterisation of single-source precursors which contain the elements essential to the preparation of a particular material. These complexes may be used for the deposition of thin film materials by chemical vapour deposition (CVD) growth processes.

Ternary metal chalcogenides such as $CuME_2$ (M = In, Ga; E = S, Se) are potentially useful materials for solar cells. Such materials have been deposited using precursors based on dithio- or diselenocarbamates. The deposited materials show a preferred orientation along (112) plane regardless of growth temperatures. Similarly, silver indium sulfide materials also have been grown from novel bimetallic thiocarboxylate compounds employed as single-source precursors.

Another class of metal-organic single-source compounds based on bis(dialkylphosphanylamines) *e.g.*, $[NH(SeP^iPr_2)_2]$ ligands have been synthesised and used for the deposition of thin films. $[M((SeP^iPr_2)N)_2]$ (M = Cd, Zn) have been synthesised by deprotonation of the N-H moiety with a base to form anionic complexes which are subsequently reacted with the appropriate metal chloride. A new cadmium compound $[MeCd\{(SeP^iPr_2)_2N\}]$ has also been synthesised by the comproportionation of Me_2Cd and $[Cd((SeP^iPr_2)_2N)_2]$

Mixed alklyl/dialkylselenophosphorylamide compounds of indium and gallium have been synthesised by reacting group 13 metal alkyls with $[NH(SeP^iPr_2)_2]$. These compounds have been used for the growth of metal selenide thin films by Low-Pressure Metal-Organic Chemical Vapour Deposition (LP-MOCVD) and Aerosol-Assisted Chemical Vapour Deposition (AA-CVD). The crystallinity of deposited materials has been determined by X-ray powder diffraction and further characterised by scanning electron microscopy, energy dispersive X-ray analysis, X-ray photoelectron spectroscopy and UV-Vis spectroscopy.

Declaration

I hereby declare that no portion of this thesis has been submitted in support of an application for another degree or qualification of the University of Manchester or any other University or Institute of Learning.

Mohammad Afzaal

Copyright

Acknowledgements

First of all, I would like to thank my supervisor Prof. Paul O'Brien for giving me the opportunity to work in his group. His advice and support have been invaluable over the past three years.

I would also like to all my friends in Manchester. Special thanks to David Smyth-Boyle, Jin-Ho Park, and Azad Malik (for introducing me to those horrible bubbler things and tasteless kebabs). I would also like to thank Kuvi, John (proof reading), Nigel, Ombretta, Steve, Dan, Ange, DC, Rufus and Leon. This research could not have been possible without the help of Peter Kenway, Ian Brough, Judith Shacklton, Jim Raftery and Madeline Helliwell. I am also indebted to my collaborators Prof. Derek Woollins (St. Andrews University) and Prof. J. J. Vittal (National University of Singapore).

Finally, sincere thanks go to my family (particularly my father and brothers) and friends for all the help in difficult times and for being supportive.

Dedicated to the memory of my mother

April 2003

Abbreviations

AACVD	aerosol-assisted chemical vapour deposition
CVD	chemical vapour deposition
PVD	physical vapour deposition
LPE	liquid phase epitaxy
MBE	molecular beam epitaxy
ALE	atomic layer epitaxy
SCCM	standard cubic centimetres per minute
MOCVD	metal-organic chemical vapour deposition
AP-MOCVD	atmospheric pressure metal-organic chemical vapour deposition
LP-MOCVD	low-pressure metal-organic chemical vapour deposition
SEM	scanning electron microscope
XRPD	X-ray powder diffraction
EDAX	energy dispersive X-ray analysis
XPS	X-ray photoelectron spectroscopy
AFM	atomic force microscopy
TGA	thermogravimetric analysis
m.p	melting point
IR	infra-red spectroscopy
NMR	nuclear magnetic resonance
mmol	millimole
JCPDS	joint committee of powder diffraction standard
LED	light emitting diode
FT	fourier transform
THF	tetrahydrofuran
ppm	parts per million

Chapter I

Introduction

Summary:

In this chapter, a brief overview of semiconductors and their properties is given. A general discussion of deposition methods including CVD techniques is discussed. In addition, a brief history of III-V and III-VI organometallic compounds is also presented.

1.1 - Introduction

Materials can be categorised into conductors, semiconductors or insulators on the basis of electronic properties. Metals conduct electric current well. On the other hand, insulators do not conduct electric current at all. Semiconductors show intermediate behaviour between these two extremes.

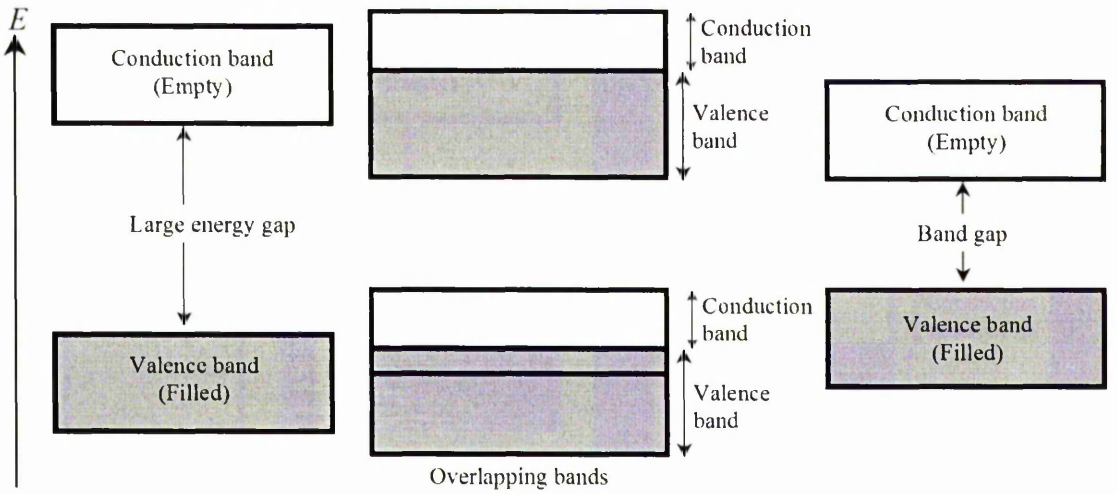

Figure 1.1 shows these different examples; **(a)** an insulator; a completely full valence band is separated by a gap of several electron volts from a completely empty conduction band, and it is energetically unlikely for an electron in the valence band to be promoted to the empty conduction band. **(b)** A conductor; there is a partially filled valence band, and electrons in this band are free to move when an electric field is applied. **(c)** A semiconductor; a completely filled valence band is separated by a small gap or less from an empty conduction band.

At very low temperatures, semiconducting materials are insulators because there is insufficient thermal energy to promote electrons to the conduction band. The energy gap (Eg) between the valence and conduction bands is small *e.g.* 1.14 eV for silicon and only 0.67 eV for germanium, compared to 5 eV or more for many insulators.[1] At room temperature, a substantial number of electrons can gain enough energy to jump the gap to the conduction band, where they are dissociated from their parent atoms and are free to move about the lattice and conductivity in general increases with temperature. For metals, conductivity decreases with temperature, essentially because the scattering of carrier electrons within the material increases with temperature.[2]

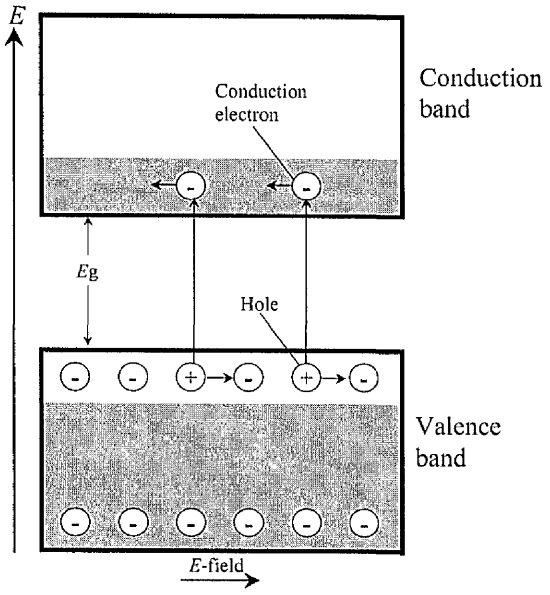

Figure 1.2 Motion of electrons in the conduction band and of holes in the valence band of a semiconductor under the action of an applied electric field E.[3]

An electron in a semiconductor that has been promoted to the empty conduction band is now free and available for electronic conduction. In addition, there is a vacant energy state left in the valence band. The vacant state is called a *hole* and it behaves like a positive charge carrier with the same magnitude of charge as the electron, but of opposite sign. In a pure semiconductor, the number of electrons in the conduction band must equal to the number of holes in the valence band because each electron gives rise to one hole. When an electric field is applied, they move in opposite directions (Fig. 1.2). This is an important property of intrinsic or undoped semiconductors.

An extrinsic semiconductor can be formed from an intrinsic semiconductor by adding impurity atoms to the crystal in a process known as doping. For example, silicon belongs to group IV of the Periodic Table, it has four valence electrons. In the crystal form, each atom shares an electron with a neighbouring atom. In this state it is an intrinsic semiconductor. B, Al, In, Ga all have three electrons in the valence band. When a small proportion of these atoms, (less than 1 in 10^6), is incorporated into the crystal the dopant atom has an insufficient number of electrons to share bonds with the surrounding silicon atoms. One of the silicon atoms has a vacancy for an electron. It creates a hole that contributes to the conduction process at all temperatures. Dopants that create holes in this manner are known as acceptors. This type of extrinsic semiconductor is known as *p*-type as it creates positive charge carriers (Fig. 1.3a). Elements that belong to group V of the periodic table such as As, P, Sb have an extra electron in the valence band. When added as a dopant to intrinsic silicon, the dopant atom contributes an additional electron to the crystal. Dopants that add electrons to the crystal are known as donors and the semiconductor material is said to be *n*-type (Fig. 1.3b).

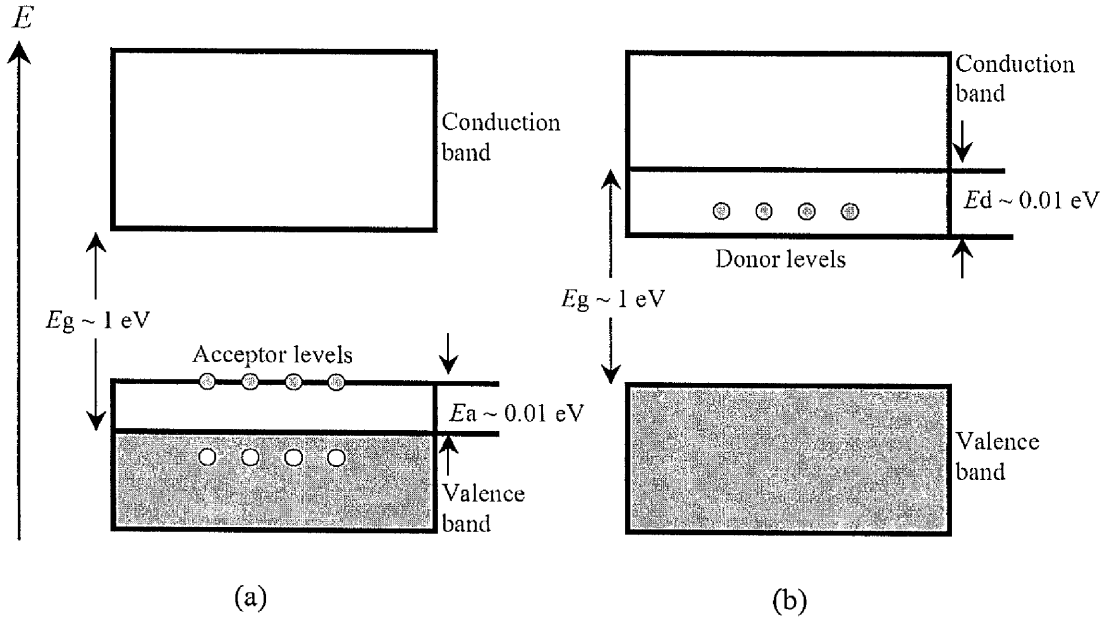

Figure 1.3 Energy band diagrams for (a) *p*-type (b) *n*-type semiconductor.

One of the most fundamental uses of semiconductors, within electronic device technology, is in the construction of *p-n* junctions (Fig. 1.4). A *p-n* junction is a region in which *p*-type and *n*-type semiconductors (*i.e.* opposite polarities) are in contact. A simple *p-n* junction is formed from one material (*e.g.* silicon), doped appropriately to provide the *p*-type and *n*-type conduction layers. These are called homojunctions. As some materials cannot be easily doped to produce both *n*- and *p*-type conductivities, a heterojunction is fabricated between two dissimilar materials *e.g.* CdS(*n*-type)/CdTe(*p*-type) structures in photovoltaic cells. When *p*- and *n*- type semiconductors are placed in contact, the system approaches an equilibrium and charge transfer occurs until the *Fermi* level is constant throughout the material. The carriers will in fact diffuse until there are equal concentrations of carriers on either side of junction. The net effect is the creation of a

depletion region containing no mobile carriers, hence a potential barrier is present before electronic conduction can take place.[4]

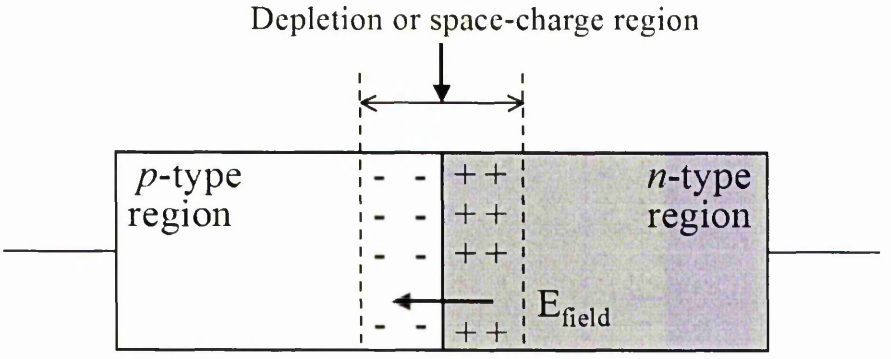

Figure 1.4 Schematic diagram of a *p-n* junction.

When an external battery is connected across a *p-n* junction, the amount of current flow is determined by the polarity of the applied voltage and its effect on the space-charge region. In Fig. 1.5, the positive terminal of the battery is connected to the *n*-type material and the negative terminal to the *p*-type material. The free electrons in the *n*-type material are attracted toward the positive terminal of the battery and away from the junction. At the same time, holes from the *p*-type material are attracted toward the negative terminal of the battery and away from the junction. As a result, the space-charge region at the junction becomes effectively wider, and the potential gradient increases until it approaches the potential of the external battery. Under these conditions, the *p-n* junction is said to be reverse-biased.

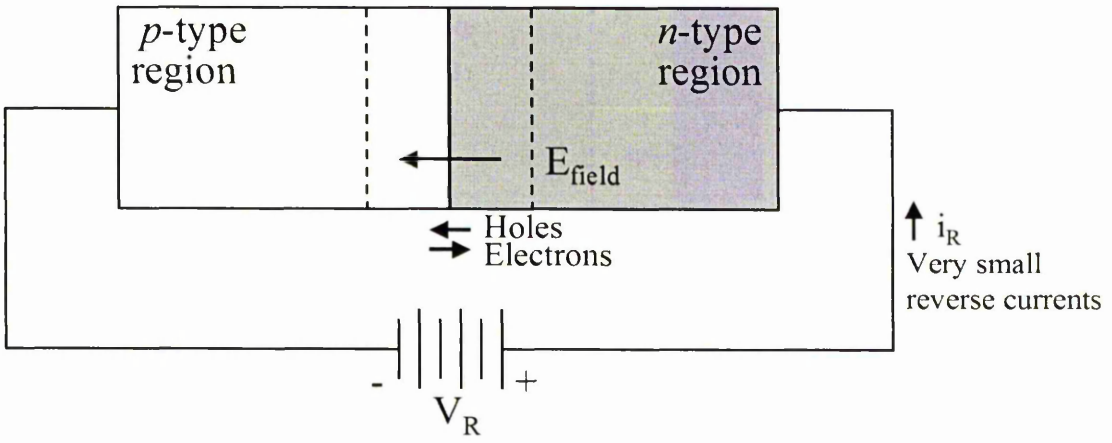

Figure 1.5 Schematic representation of reverse bias.

When the positive terminal of the external battery is connected to the *p*-type material and the negative terminal to the *n*-type material, electrons in the *p*-type near the positive terminal of the battery break their electron-pair bonds and enter the battery, creating new holes. At the same time, electrons from the negative terminal of the battery enter the *n*-type material and diffuse toward the junction. Consequently, the space charge region becomes effectively narrower, and the energy barrier decreases to an insignificant value. Excess electrons from the *n*-type material can penetrate the space charge region, flow across the junction, and move by way of the holes in the *p*-type material toward the positive terminal of the battery. The electron flow continues as long as the external voltage is applied. Under these conditions, the junction is said to be forward-biased (Fig. 1.6).

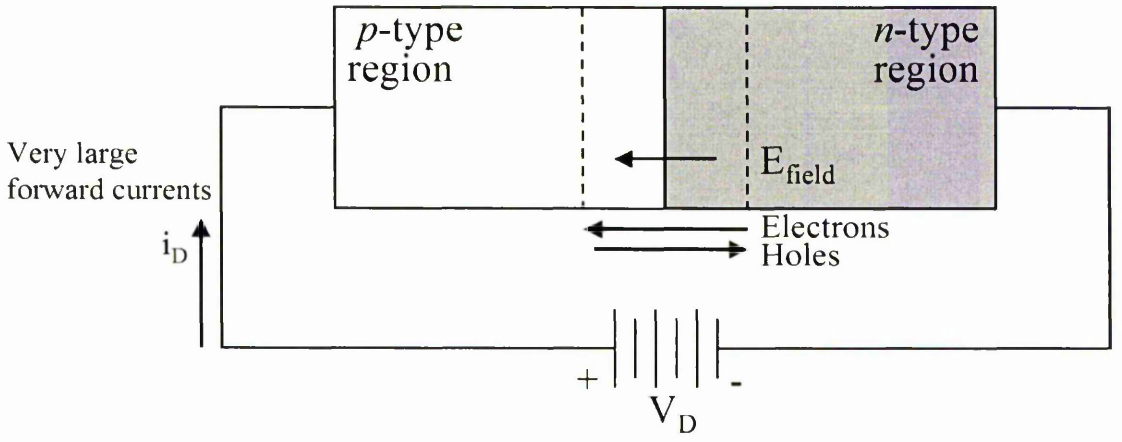

Figure 1.6 Schematic representation of forward bias.

1.2 - Preparation of Semiconductors

A large number of semiconducting materials are produced for a variety of uses in the electronic industry which can be divided into distinct groups, as shown in the table below:

Table 1.1 Physical properties of commonly used semiconducting materials.[2]

Semiconductor	Lattice Parameters (Å)	Band-gap (eV)	Direct/Indirect
IV-IV materials			
Ge	5.646	0.66	Indirect
Si	5.437	1.12	Indirect
II-VI materials			
ZnS	5.420	3.68	Direct
CdS	5.832	2.42	Direct
ZnSe	5.669	2.70	Direct
CdSe	6.050	1.70	Direct
CdTe	6.482	1.56	Direct
III-V materials			
GaP	5.451	2.26	Indirect
GaAs	5.653	1.42	Direct
InP	5.869	1.35	Direct
InAs	6.058	0.36	Direct
AlAs	5.661	2.16	Indirect

The deposition of semiconducting thin films has been performed using numerous techniques on various substrates, mainly belonging to two families, which will be briefly discussed here.

Physical Vapour deposition (PVD)

Chemical Vapour deposition (CVD)

1.2.1 - Physical Vapour Deposition (PVD)

Most metallisation for microelectronics today is preformed by Physical Vapour Deposition (PVD), which includes evaporation and sputtering processes. With both evaporation and sputtering methods, the formation of a layer on a substrate involves three steps: (1) converting a condensed phase material (generally a solid) into the gaseous or vapour phase, (2) transporting the gaseous phase from the source to the substrate surface, followed by (3) nucleation and growth of a new layer.

1.2.2 - Physical Vapour Deposition (PVD) by Evaporation

In PVD by evaporation, the material to be deposited can be heated directly by an electron beam (or laser beam) by directing a stream of high-energy electrons at the target material to create a molten region at the surface and vapourise the material. The evaporated material deposits on a substrate which is maintained at a lower temperature than that of the vapour. In a conventional evaporation process, the material to be deposited is heated under high vacuum conditions (10^{-5} - 10^{-8} Torr).[5] Deposition of alloy films that consist of two or more components can be complicated due to differences in vapour pressures. This makes maintaining stoichiometry of both the target and the deposited films difficult since the target becomes richer in the less volatile species. The

advantages of using the evaporation process are simplicity and reliability, along with high deposition rates and high film purity.

1.2.3 - Physical Vapour Deposition (PVD) by Sputtering

In this technique, the surface atoms of a target material are dislodged by bombardment with energetic ions that are generated in a blow discharge or plasma. The sputtered ions are then ballistically transported to the substrate where they condense to deposit a film. Unlike evaporation, sputtering processes are very well controlled and are generally applicable to all materials: metals, semiconductors and alloys.[6] The deposition of alloys by sputtering is also possible because the composition of the film is locked to the composition of the target.[5]

1.2.4 - Chemical Vapour Deposition (CVD)

CVD is a method in which a volatile molecular species (often metal containing) is transported into the reactor that contains substrates where the molecular species adsorbs and reacts to deposit a film of a particular material (Fig. 1.7).[5]

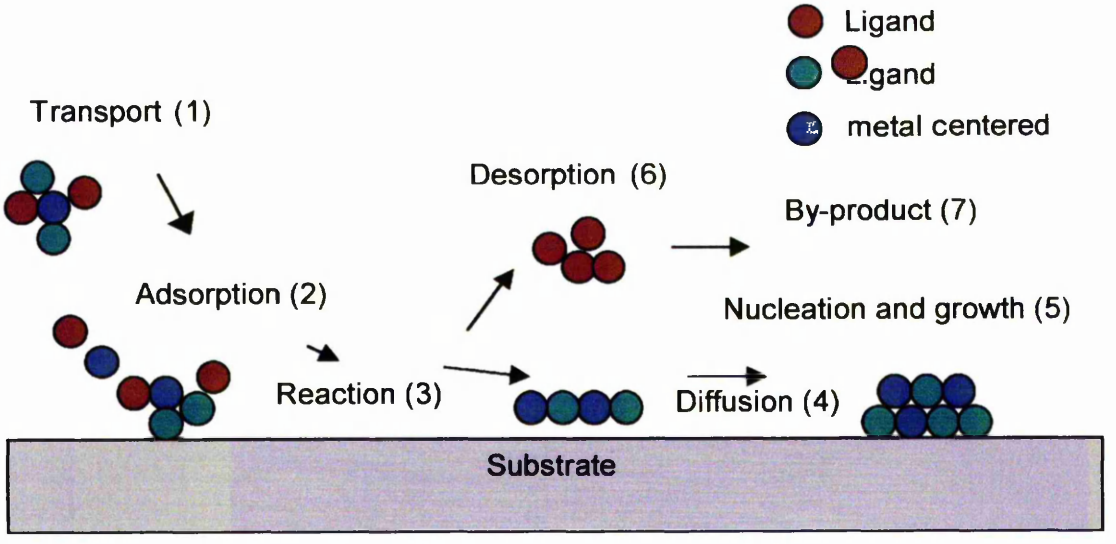

Figure 1.7 Schematic diagram of the CVD process.

However, CVD is a broad term that incorporates a variety of more specific processes, such as MOCVD which refers to CVD using a metal-organic (MO) compound. In general, most reactions involve hazardous toxic vapour phase precursors which are undertaken at low-pressure (LP) from a safety perspective. Additionally, the enhancement of kinetic steps often occurs at low-pressure in the CVD system. This approach depends on the sublimation of precursors with or without a carrier gas.[7] The main advantages of conventional MOCVD are the availability of precursors with sufficient volatility and stability, as well as adequate purity and the need to obtain high vapour pressures of hazardous precursors.

An alternative technique is aerosol-assisted CVD (AA-CVD), which involves the generation of aerosol droplets of precursor solution using a piezoelectric modulator. The droplets are swept into a preheated zone by a carrier gas (N_2 or Ar) where both solvent and precursor are vapourized just before entering into the reactor deposition zone (Fig. 1.8). In contrast, LP-MOCVD and/or conventional CVD rely on the delivery of the precursor at its equilibrium vapour pressure at the source temperature. AACVD is an example of a family of assisted CVD techniques; liquid injection CVD and spray pyrolysis.

In general, aerosol delivery systems are suitable techniques where the precursor is thermally unstable and would decompose if heated for a period of time in order to elevate the vapour pressure. It is also a useful technique for multicomponent systems as several precursors can be dissolved in the same solution and the relative delivery rates are defined by composition.[7]

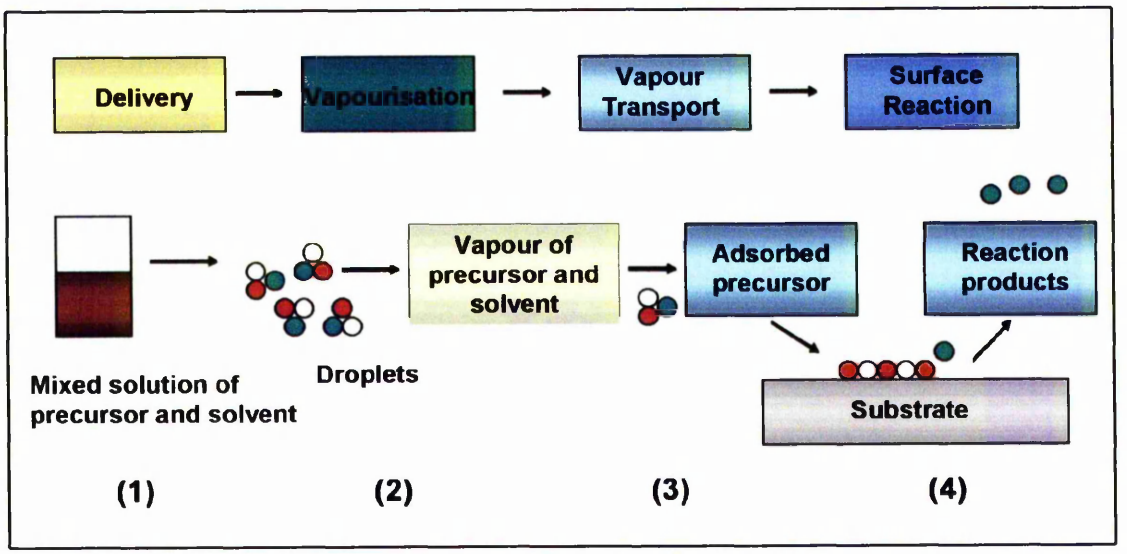

Figure 1.8 Schematic representation of the AACVD process.

1.3 - Other CVD Related Processes

1.3.1 - Liquid Phase Epitaxy (LPE)

LPE is one of the earliest techniques used to produce epitaxial films and closely resembles CVD (Fig. 1.9). In this technique, elemental or compound reservoirs are held at their melting point temperatures. The deposition substrate is passed over the melt and a film is allowed to solidify from solution. LPE has typically been limited to growth of thick, high-purity epitaxial layers. Epitaxial refers to growth of crystallographically orientated film on a single-crystal substrate with similar lattice constants. The lattice dimensions of substrate and film must be similar in order to minimise structural defects in the material, *e.g.* ZnS (lattice constant = 5.42 Å) could be grown epitaxially on silicon (5.43 Å) whereas the same growth will be much more difficult on GaAs (5.653 Å).[8]

When a material is grown epitaxially on a substrate of the same material, such as Si on

Si, the process is termed homoepitaxy. On the other hand, if the layer and substrate are of different materials, such as $Al_xGa_{1-x}As$ on GaAs, the process is termed heteroepitaxy.[5]

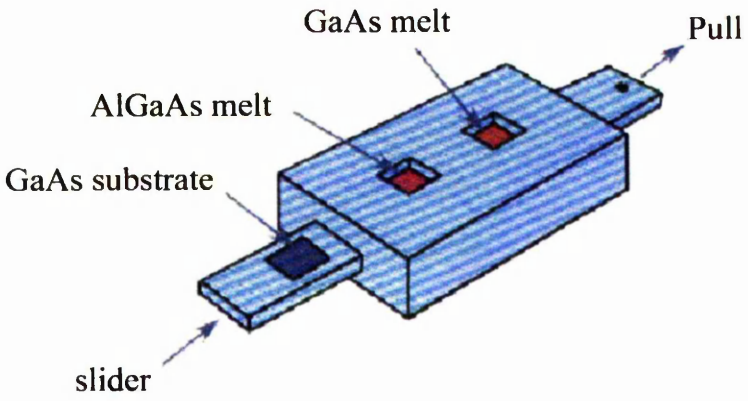

Figure 1.9 Typical vapour phase epitaxy (VPE) system.[9]

1.3.2 - Molecular Beam Epitaxy (MBE)

MBE is a non-CVD epitaxial process, which uses an evaporation method.[5] MBE relies on the elemental sources, which are independently evaporated at a controlled rate in the reaction chamber. The precursor reacts with the heated substrate to give epitaxial film growth. MBE is usually carried out under ultra-high-vacuum conditions (10^{-10} Torr) with low growth rates, where the growth of material occurs by one atomic layer at a time. Film with high purity and very complex layered structures can be deposited (nanostructures) with a precise control of doping of the deposited layers. The low processing temperature with MBE is also important for microelectronic production. If organometallic precursors are employed, the technique is often called metal-organic molecular beam epitaxy.[8]

1.3.3 - Atomic Layer Epitaxy (ALE)

Suntola and Anston first reported the preparation of semiconductor thin films using ALE.[10] ALE means that one layer of each compound is deposited on the surface of the substrate at a time. This is accompanied by sequentially introducing the source gases

containing group III and V precursors into the reactor. At each step, self-limiting adsorption takes place because the group III molecule (or its dissociation product) chemisorbs only to active sites on the substrate until all sites are occupied. The group V molecule then reacts in a site-selective manner with the group III centres, which leads to self limiting adsorption.[2,11,12] In the appropriate temperature and under ideal conditions, this sequence results in film deposition one atomic layer at a time and greater control of stoichiometry. The major advantages of ALE are in the growth of very uniform thin layers. The ALE growth rate is typically limited by the time required for switching from one precursor to other which usually requires several seconds. Consequently, a growth rate of a few atomic layers per minute is obtained by ALE compared to growth rates of several atomic layers per second for a conventional MOCVD process. A number of different materials have been successfully grown by ALE including oxides, ceramics and superconductors.[13]

1.4 - Conventional Precursors

The origin of molecular-precursor chemistry for compound semiconductor materials is found in the pioneering MOCVD studies of Manasevit that showed how metal alkyl compounds could be employed as sources for Group III elements in the CVD process.[14,15] In conventional MOCVD system, the precursors are generally highly volatile materials such as metal alkyls or hydrides. These compounds have several disadvantages, the metal alkyls are highly pyrophoric, the majority of the hydrides gases are of considerable toxicity. These concerns have resulted in the development of organometallic precursors where a metal has been made volatile by bonding it to organic ligands that could replace hazardous and toxic precursors.

Many properties of thin films depend on the phase deposited which includes; crystallographic orientation, degree of crystallinity, composition and impurity concentration.[16] The shape of precursor is very significant because the nature of molecular species at the surface may affect morphology and could affect the structure of the film deposited. When conformal films are required, there must be significant mobility of the species at the surface for the deposition of dense films. The following properties should be considered when selecting a suitable CVD precursor;

- The precursors must have significant vapour pressure and should preferably be air stable. During the decomposition in the reactor, the reaction should be facile and lead to a minimum incorporation of impurities (*e.g.*, carbon) associated with the precursor.
- The purity of the precursor is essential in order to avoid incorporation of extraneous elements, especially those that are electrically active. These

can arise during precursor synthesis (*e.g.*, halides from alkyl halides in dimethylzinc) or be incorporated into the material from the decomposition of the precursor (*e.g.*, carbon).

- Toxicity should be minimised by a suitable choice of compound.

1.5 - Single-Source Molecular Precursors

Semiconductor thin films can be prepared *via* a number of deposition techniques using metal-organic chemical vapour deposition (MOCVD). However, there are restrictions imposed by the precursors on the use of this method, with regards to toxicity or pyrophoricity of metal alkyl and hydride complexes, the tendency for unwanted side reactions and the relative difficulty and importance of obtaining pure compounds.

Thin films can also be grown using single-source precursors which comprise all the elements to be deposited in one molecule. There are a number of advantages associated with single-source molecular precursors, for which they may be considered to be more useful than standard metal alkyl and metal hydride as dual-sources; these include;

- Air and moisture stability.
- Low toxicity.
- Homogenous pre-reaction is limited as there is only a single molecule in the supply stream.
- Stoichiometry of metal atom to chalcogenide (pnictides) atom is governed by design of the organometallic complex.
- Impurity incorporation onto the films may be controlled by ligand design.
- A high degree of association may allow successful low temperature growth.
- The phase of the material grown can be controlled by the core structure of the precursor molecule.

The main disadvantages of single-source precursors derive from their high molecular weights and ensuing generally low volatilities. However, the development of MOCVD under vacuum or ultra-high vaccum means this is no longer a real drawback. Liquid delivery systems are proven alternative delivery modes.[9]

1.6 - Group III-V Compounds: A Historical Perspective

In the 1960s, Coates *et al.* synthesised compounds of the type $[R_2M(\mu\text{-}ER)]_2$ (M = In, Ga; E = P, As, P; R = alkyl, aryl).[17,18] The importance of such compounds was not realised until 30 years later, when it was noted that such compounds might be effective single-source precursors for the growth of III-V materials. A number of groups have studied such compounds for the preparation of many direct and indirect band gap III-V semiconductor materials including: GaAs, InAs, InP, GaP and AlAs.[19-23] The idea behind the use of such compounds is that the group III and group V atoms are found with a known stoichiometry within the complex, and that the M-E bonds are strong enough to remain intact upon heating, where other bonds in the complex are broken to leave organic by-products that are easily removed from the growth system (Table 1.2).

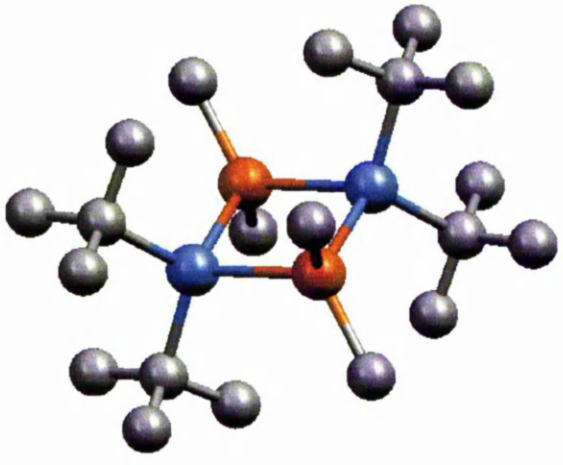

Figure 1.10 Molecular structure of $[Me_2GaAs^tBu_2]_2$.

Table 1.2 Examples of various studied III-V single-source precursors.

Compounds	References
(1:1 stoichiometry)	
$[Me_2GaPMe_2]_n$	18
$[Me_2GaPEt_2]_3$	18
$[Me_2GaAsPh_2]_2$	17
$[Cl_2GaAs(CH_2SiMe_3)_2]_3$	21
$[Cl_2GaSb^tBu_2]_3$	23
$[Me_2InPMe_2]_3$	18
$[(Me_3SiCH_2)_2InPPh_2]_2$	24
$[Me_2InAsPh_2]_2$	17
(1:2 stoichiometry)	
$[ClIn(Sb^tBu_2)_2]_2$	25
$[BrGa\{As(CH_2SiMe_3)_2\}_2]_2$	26
(1:3 stoichiometry)	
$Ga(As^tBu_2)_3$	27
$In(P^tBu_2)_3$	28
(Other stoichiometries)	
$[Li(thf)_4]Ga(AsPh_2)_4]$	29
$[Li(thf)_4]In(PPh_2)_4]$	29
$[(thf)Br_2Ga]_3As$	30

The original method used by Coates to prepare single-source precursors for III-V materials involves alkane elimination reactions between a metal alkyl and dialkylpnictohydride as shown in equation 1.[17,18] Cowley and Jones[27,28] have reported the reaction of a group III metal trichloride with one equivalent of a lithiated dialkylpnictide and two equivalents of a lithium alkyl, yielding a III-V complex, along with the formation of lithium chloride (equation 2). These reactions were quite successful where the alkyl substituents were not bulky, but for large R groups, a silyl halide elimination route was preferred (equation 3).[21,23]

$$Me_3M + R_2EH \rightarrow 1/n(Me_2MER_2)n + CH_4 \qquad \textbf{(Equation 1)}$$

$$2GaCl_3 + 2^tBuELi + 4RLi \rightarrow [R_2Ga(E^tBu_2)]_2 + 6LiCl \qquad \textbf{(Equation 2)}$$

$$GaCl_3 + 3Me_3SiSb^tBu_2 \rightarrow [Cl_2GaSb^tBu_2]_3 + 3Me_3SiCl \qquad \textbf{(Equation 3)}$$

Above mentioned authors also have reported the growth of epitaxial GaAs films from $[Me_2GaAs^tBu_2]_2$ and $[Et_2GaAs^tBu_2]_2$.[31,32] Single-crystal epitaxial films were only obtained at low pressures (5×10^{-6} Torr). Epitaxial layers, which were highly doped with carbon acceptors were obtained from $[Me_2GaAs^tBu_2]_2$ at temperatures of 475 – 550 °C (Fig. 1.10). Polycrystalline films were obtained at low temperatures, and no growth was observed below 423 °C. Epitaxial films were obtained from $[Et_2GaAs^tBu_2]_2$ over the temperature range 400 – 525 °C. The films deposited from $[Et_2GaAs^tBu_2]_2$ were inhomogenous and highly contaminated with carbon. The Ga-C bond was found to play a key role in the quality of the films and in the film growth rate; epitaxial films were grown

on GaAs substrates when the substrate temperature was high enough to effect complete removal of the Ga-alkyl ligands.[32] In an attempt to minimise carbon incorporation, by eliminating Ga-C bonds, and to provide an excess of As to react with Ga atoms during film growth, an alternative single-source precursor [$Ga(As^tBu_2)_3$] with a 1:3 stoichiometry has been employed.[33] Epitaxial films were grown from the precursor on (100) GaAs in a chemical beam epitaxy system. It has been determined that tert-butyl ligands in [$Ga(As^tBu_2)_3$] react by β–hydride elimination process, yielding isobutene and AsH. In [$Me_2GaAs^tBu_2]_2$, the methyl ligands appear to desorb rather than react with surface hydride to produce methane.[33]

In 1991, *Wells et al.* have reported the synthesis of $[Ga_2(AsP)Cl_3]_n$[34] and its use as a single-source precursor for the preparation of gallium arsenide phosphide (GaAsP) films.[35] On thermolysis, the resulting material had the stoichiometry $GaAs_xP_y$ ($0.9 \geq x, y \geq 0.6$). The XRPD and XPS analyses of the deposited films confirmed the stoichiometry of ternary materials instead of a mixture of GaAs and GaP.

Group 13 nitrides are another important area of III-V chemistry. The conventional method involves the reaction of a metal alkyl with ammonia at elevated temperatures of 900 °C.[9] At such high temperatures, there is a reduction in film quality which can be overcome by the use of single-source precursors.

Cowley et al. prepared hexagonal gallium nitride (GaN) films by LP-MOCVD at deposition temperatures of 450 - 650 °C on a variety of substrates using $[Me_2GaN_3]_n$. The azide compound was prepared from Me_2GaCl and NaN_3. The band gap of the films was found to be *ca.* 3.33 eV, which varied with the growth temperature.[36]

The *bis*-azide gallium compound, $(N_3)_2Ga[(CH_2)_3NMe_2]$ has also been utilised for the preparation of GaN films by LP- or AP-MOCVD on sapphire substrates.[37] These films were found to be amorphous below 550 °C, however, the crystallinity of films improved with an increase in deposition temperature (up to 750 °C). At 750 °C, epitaxial growth was observed with the material having a band gap of 3.45 eV. Recently, the same group has synthesised Lewis acid/base adducts $[X_3MN(SnMe_3)_3]$ (X = Cl, Br; M = Al, Ga, In) and $[Cl_2MeMN(SnMe_3)_3]$ (M= Al, Ga) by reacting 1:1 adducts of MX_3 and MCl_2Me with $N(SnMe_3)_3$ and their potential as single-source precursors for the Group 13 nitride materials.[38]

Other examples for the growth of GaN films include $[HClGaN_3]_4$ and $(H_2GaN_3)_n$.[39] $[HClGaN_3]_4$ was prepared by the reaction of LiN_3 and $HGaCl_2$, while $(H_2GaN_3)_n$ was prepared by the reaction of 2GaCl with LiN_3. Both complexes have been used for the growth of high quality GaN films under ultra-high vaccum conditions.

1.7 - Group III-VI Compounds: A Historical Perspective

The chemistry of Group 13 metals containing chalcogenides has been the focus of much research because of their potential as single-source precursors for group III metal sufide, selenide and telluride films. These compounds are highly diverse, with a number of different stoichiometries observed for materials combining group III (Al, Ga, In and Tl) and group VI (S, Se and Te) elements (Table 1.3).[7] Several structural types are found for these compounds including a defect wurzite structure for Ga_2E_3, a defect spinel for In_2E_3 and layered structures for compounds of stoichiometry ME (Fig. 1.11).[40,41] This review can be related to work presented in Chapter 4. In addition to the simple binary compounds, there are important ternary and quaternary phases such as $CuInE_2$ and $CuIn_{1-x}Ga_xE_2$ (E = S or Se).

Table 1.3 Stoichiometries, structures and electronic properties of some chalcogenides of binary and ternary materials (E_{dir} = direct band gap, E_{opt} = optical band gap).[7,42]

Material	Crystal type	Band gap/eV (*T*/*K*)
GaS	Hexagonal	E_{dir} 3.05 (77)
α-Ga_2S_3	Monoclinic	E_{opt} 3.42 (77)
δ-GaSe	Hexagonal	E_{dir} 2.02 (300)
β-Ga_2Se_3	Monoclinic	E_{dir} 2.1-2.2 (77)
GaTe	Monoclinic	E_{dir} 1.69 (295)
InS	Orthorhombic	E_{dir} 2.45 (290)
β-In_2S_3	Tetragonal	E_{dir} 2.03 (300)
γ-In_2S_3	Hexagonal	E_{opt} 1.88 (300)
$CuInS_2$	Tetragonal	E_{dir} 1.53 (300)
$CuInSe_2$	Tetragonal	E_{dir} 1.04-1.27 (77)
$CuGaS_2$	Tetragonal	E_{dir} 2.43 (300)

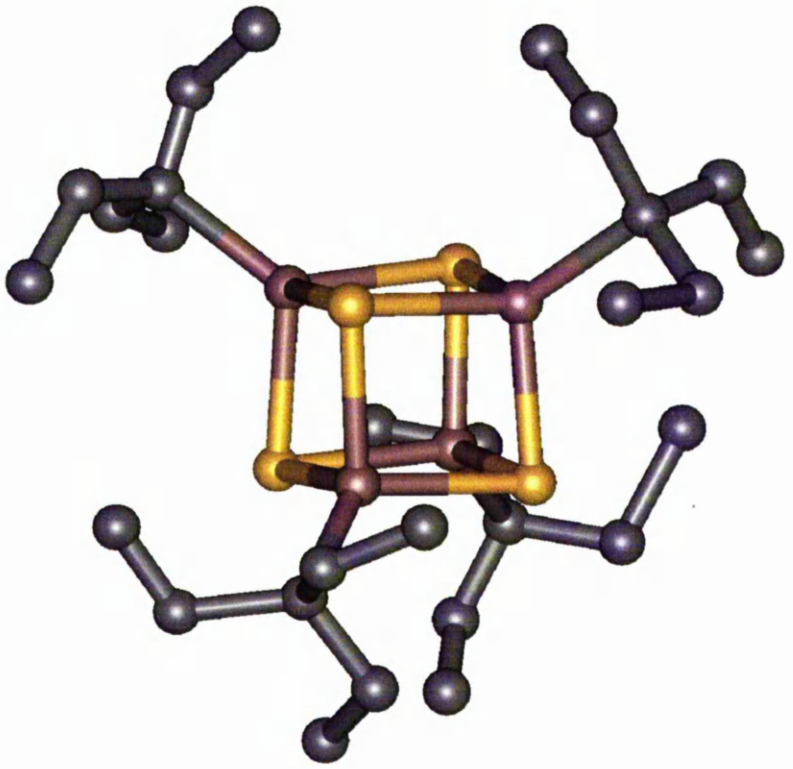

Figure 1.11 Crystal Structure of $[Ga(CEt_3)(\mu_3\text{-}S)]_4$.

The first example of a III-VI compound was a dialkylaluminium thiolate complex, $[AlMe_2(SMe)]$ which has been synthesised by direct reaction of Me_3Al and MeSH.[43] Later, Coates and co-workers have reported a number of dialkylmetal thiolate complexes *e.g.* $[GaMe_2(SMe)]$, $[InMe_2(SMe)]$ and $[TlMe_2(SMe)]$.[44,45] These compounds were easily prepared by the alkane elimination reaction of the metal trialkyl and the alkylthiol. Coates also observed the donor properties of oxygen, sulfur, selenium and tellurium to group III metal alkyls.[46] The same group also described the preparation of several Group III dithiophosphinate complexes of the form $[MMe_2(S_2PMe_2)]$ (M = Al, Ga, In).[47] A series of thiolate-type complexes have been prepared, incorporating halogen atoms,[48] aryl moieties[49] and alkylsilyl substituents.[50]

Weidlein *et al.* have prepared a number of complexes containing metal-sulfur interactions such as dialkyldithioacetate complexes $[MR_2(S_2CMe)]$ (M = Al, Ga, In; R = Me, Et)[51] and thiocarboxylate complexes $[MMe_2(OSCMe)]$.[52] Hausen prepared the analogous diethylindium thiocarboxylate complex, which is different from earlier reported complexes as the indium centre was found to be five co-ordinate as opposed to the four co-ordinate geometry observed in Weidlein's complexes.[53]

A series of group III metal *tris*dialkyldithiocarbamate, compounds, of the form $[M(S_2CNR_2)_3]$ (M = Ga, In; R = Me, Et) have been prepared by the reaction of a metal trihalide and sodium dialkyldithiocarbamate salt.[54] The sodium salt had been prepared by the direct reaction of a secondary amine with sodium hydroxide with the insertion of CS_2 into the metal-nitrogen bond. Later, mixed-alkyl indium dithiocarbamates, $[(R)_2In(S_2CNMe_2)]$ (R = Me, Et) were reported by a salt elimination reaction of a dialkylindium acetate and sodium dimethyldithiocarbamate.[55] An alternative method to prepare mixed-alkyl group III dialkyldithiocarbamates was reported in connection with the thallium derivative, $[(Me)_2Tl(S_2CNMe_2)]$, which was prepared by the insertion of CS_2 into the dialkylmetal alkylamide.[56] A number of mixed alkyl-indium and gallium diethyldithiocarbamate complexes, $[(R)_2In(S_2CNEt_2)]$ (R = Me, Et, Np) (Fig. 1.12) have also been reported by Haggata *et al.*[57] $[(Me)_2In(S_2CNEt_2)]$ was initially prepared *via* the reaction of Me_3In and $[Zn(S_2CNEt_2)_2]$, in attempts to prepare a bimetal species and it was found to be a monomeric solid. Better defined-syntheses involved either stoichimetric amounts of Me_3In and $[In(S_2CNEt_2)_3]$ or the reaction of sodium diethyldithiocarbamate salt with Me_2InCl or metal trialkyl. Other related compounds include the preparation of monothiocarbamato complexes (*e.g.*, $[In(SOCNEt_2)_3]$ and $[Et_2In(SOCNEt_2)]_n$)[58] and

dithiophosphinato complexes (*e.g.*, $[In(S_2PR_2)_3]$ (M = Me,[59] Ph,[59] ^{i}Bu[60]) and $[Ga(S_2PR_2)_3]$ (R = ^{i}Bu,[60] Me,[61])). It has been determined that $[M(S_2P^{i}Bu_2)_3]$ (M = Ga, In) show variable coordination modes because indium is found to be six-coordinate,

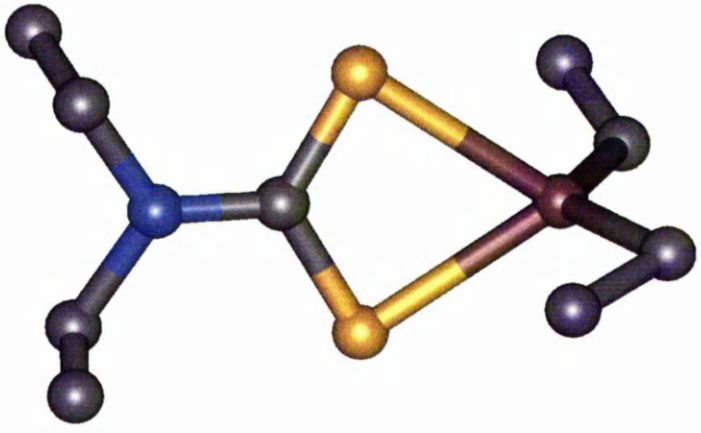

Figure 1.12 Crystal structure of $[(Et)_2In(S_2CNEt_2)]$.[57]

whereas gallium is four-coordinate, being bound to only one chelating and two pendent diisobutyldithiophosphinate ligands in a distorted tetrahedral geometry.

Hoffman and co-workers have reported adducts prepared by the reaction of gallium aryls with aryl thiols giving $[Ph_2GaSPh]_2$,[62] halogeno gallium aryls with alkyl thiols giving $[PhXGaSEt]_2$ (X = Cl, Br, I)[63] and halogeno gallium and indium alkyls with chalcogenols giving $^{i}Pr(Br)GaSC_2H_5$[64] and $^{i}Pr(X)InSC_2H_5$ (X = Br, I)[65] respectively. The same authors also reported the sulfur bridged dihalides, $[X_2GaSR]_2$ (X = Br, I; R = Me, Et, Pr, Ph), synthesised *via* the reaction of gallium halides and lead bis(thiolates).[66]

References

1. S. M. Sze, *Physics of Semiconductor Devices, 2nd ed.*, Wiley, New York, **1981**, 848.
2. A. C. Jones, P. O'Brien, *CVD of Compound Semiconductors*, VCH, Weinheim, **1997**, 4-7.
3. P. A. Cox, *The Electronic Structure and Chemistry of Solids*, Oxford University, **1991**, 23.
4. R. Eisberg, R. Resnick, *Quantum Physics of Atoms, Molecules, solids, Nuclei and Particles, 2nd Ed.*, Wiley, **1985**, 443.
5. L. V. Interrante, M. J. Hampden-Smith, *Chemistry of Advanced Materials, An Overview*, Wiley-VCH. **1998**, 176.
6. S. M. Sze, *VLSI Technology, 2nd edition*, McGraw-Hill, New York, **1988**.
7. M. R. Lazell, P. O'Brien, D. J. Otway, J.-H. Park, *J. Chem. Soc., Dalton Trans.*, **2000**, 4479.
8. G. A. Horley, *Ph.D Thesis*, Imperial College London, **1999**.
9. W. S. Rees, Jr., *CVD of Nonmetals*, VCH, Weinheim, **1997**, 12-261.
10. T. Suntola and J, Anston, U.S. Patent 4 058 430, **1977**.
11. B. Y. Maa, P. D. Dapkus, *Appl. Phys. Lett.*, **1991**, *58*, 2261.
12. J. R. Creighton, *Surface Science*, **1990**, *234*, 287.
13. L. Niinisto, M. Leskela, *Thin Solid Films*, **1993**, *130*, 228.
14. H. M. Manasevit, *Appl. Phys. Lett.*, **1968**, *12*, 156.
15. H. M. Manasevit, W. I. Simpson, *J. Electrochem. Soc.*, **1969**, *116*, 1725.

16. M. R. Lazell, P. O'Brien, D. J. Otway, J.-H. Park, *J. Chem. Soc., Dalton Trans.*, **2000**, 4479.

17. G. E. Coates, J. Graham, *J. Chem. Soc.*, **1963**, 233.

18. O. T. Beachely, G. E. Coates, *J. Chem. Soc.*, **1965**, 3241.

19. D. A. Andrews, G. T. Davis, D. C. Bradley, M. M. Faktor, D. M. Frigo, E. A. D. White, *Semicond. Sci. Techno.*, **1988**, *3*, 1053.

20. K. A. Aitchison, J. D. J. Backer-Dirks, D. C. Bradley, M. M. Faktor, D. M. Frigo, M. B. Hursthouse, B. Hussain, R. L. Short, *J. Organomet. Chem.*, **1989**, *366*, 11.

21. C. G. Pitt, A. P. Purdy, K. T. Higa, R. L. Wells, *Organometallics*, **1986**, *5*, 1266.

22. F. Maury, G. Constant, *Polyhedron*, **1984**, *3*, 581.

23. A. H. Cowley, R. A. Jones, K. B. Kidd, C. M. Nunn, D. L. Westmoreland, *J. Organomet. Chem.*, **1988**, *341*, C1.

24. O. T. Beachley, J. P. Kopasz, H. Zhang, W. E. Hunter, J. L. Atwood, *J. Organomet. Chem.*, **1989**, *325*, 69.

25. A. R. Barrons, A. H. Cowley, R. A. Jones, C. M. Nunn, D. L. Westmoreland, *Polyhedron*, **1988**, *7*, 77.

26. A. P. Purdy, C. G. Pitt, A. T. McPhail, R. L. Wells, *Organometallics*, **1987**, *5*, 2099.

27. A. M. Arif, B. L. Benac, A. H. Cowley, R. L. Geerts, R. A. Jones, K. B. Kidd, J. M. Power, S. T. Schwab, *J. Chem. Soc., Chem. Commun.*, **1986**, 1543.

28. A. M. Arif, B. L. Benac, A. H. Cowley, R. A. Jones, K. B. Kidd, C. M. Nunn, *New. J. Chem.*, **1988**, *12*, 533.

29. C. J. Carrano, A. H. Cowley, D. M. Gioalando, R. A. Jones, C. M. Nunn, J. M. Power, *Inorg. Chem.*, **1988**, *27*, 2709.

30. R. L. Wells, S. Shaffieezad, A. T. McPhail, C. G. Pitt, *J. Chem. Soc., Chem. Commun.*, **1987**, 1823.

31. J. E. Miller, J. G. Ekerdt, *Chem. Mater.*, **1992**, *4*, 7.

32. J. E. Miller, J. G. Ekerdt, *Chem. Mater.*, **1994**, *6*, 343.

33. J. G. Ekerdt, Y. M. Sun, M. S. Jackson, V. Lakhotia, K. A. Pacheco, S. U. Koschmieder, A. H. Cowley, R. A. Jones, *J. Cryst. Growth*, **1992**, *124*, 158.

34. R. L. Wells, R. B. Hallock, A. T. MacPhail, C. G. Pitt, J. D. Johansen, *Chem. Mater.*, **1991**, *3*, 381.

35. S. R. Aubuchon, M. S. Lube, R. L. Wells, *Chem. Vap. Deposition*, **1995**, *1*, 28.

36. V. Lakhotia, D. A. Neumayer, A. H. Cowley, R. A. Jones, J. G. Ekerdt, *Chem. Mater.*, **1995**, *7*, 546.

37. A. Miehr, O. Ambacher, W. Riegar, T. Metzger, E. Born, R. A. Fischer, *Chem. Vap. Deposition*, **1996**, *2*, 51.

38. Q. M. Cheng, O. Stark, F. Stowasser, A. Wohlfart, R. A. Fischer, *J. Mater. Chem.*, **2002**, *12*, 2470.

39. J. McMurran, J. Kouvetakis, D. C. Nesting, D. J. Smith, J. L. Hubbard, *J. Am. Chem. Soc.*, **1998**, *120*, 5233.

40. N. N. Greenwood, A. Earnshaw, *Chemistry of the Elements*, Pergamon press, Oxford, **1984**, Ch 7, 286.

41. L. I. Man, R. M. Imanov, S. A. Semiletov, *Sov. Phys. Crystallogr.*, **1976**, *21*, 335.

42. O. Madelung, R. Poerschke, *Semiconductors: other than Group IV Elements and III-V Compounds*, Springer-Verlag, Berlin, **1992**.

43. H. C. Brown, N. R. Davidson, *J. Am. Chem. Soc.*, **1942**, *64*, 316.

44. G. E. Coates, P. Hayter, *J. Chem. Soc.*, **1953**, 2519.

45. G. E. Coates, R. A. Whitcombe, *J. Chem. Soc.*, **1956**, 3351.

46. G. E. Coates, *J. Chem. Soc.*, **1951**, 2003.

47. G. E. Coates, S. D. Mukherjee, *J. Chem. Soc.*, **1964**, 1295.

48. G. G. Hoffmanm, *Chem. Ber.*, **1985**, *118*, 1655.

49. H. Tada, R. Okawara, *J. Organomet. Chem.*, **1971**, *28*, 21.

50. N. S. Vyazankia, M. N. Bochkarev, A. I. Cherov, *J. Organomet. Chem.*, **1971**, *27*, 175.

51. J. Weidlein, *Z. Anorg. Allg. Chem.*, **1971**, *386*, 129.

52. J. Weidlein, *J. Organomet. Chem.*, **1971**, *32*, 181.

53. H. D. Hausen, H. J. Gruder, *J. Organomet. Chem.*, **1973**, *57*, 243.

54. K. Dymock, G. J. Palenik, J. Slezak, C. L. Raston, A. H. White, *J. Chem. Soc., Dalton Trans.*, **1976**, 28.

55. T. Maeda, R. Okawara, *J. Organomet. Chem.*, **1972**, *39*, 1972.

56. B. Walther, R. Mahrwald, C. Jahn, W. Klar, *Z. Anorg. Allg. Chem.*, **1976**, *423*, 144.

57. S. W. Haggata, J. C. Knowles, M. A. Malik, M. Motevalli, P. O'Brien, *Chem. Mater.*, **1995**, *7*, 716.

58. G. A. Horley, M. Chunggaze, P. O'Brien, A. J. P. White, D. J. Williams, *J. Chem. Soc., Dalton Trans.*, **1998**, 4205.

59. J. Zukerman-Schpector, I. Haiduc, C. Silvestru, R. Cea-Olivares, *Polyhedron*, **1995**, *14*, 3087.

60. J.-H. Park, P. O'Brien, A. J. P. White, D. J. Williams, *Inorg. Chem.*, **2001**, *40*, 3629.

61. C. L. Christopher, A. Hynes, A. R. Barron, I. Haiduc, C. Silvestru, *Polyhedron*, **1996**, *15*, 391.

62. G. G. Hoffman, C. Burschka, *J. Organomet. Chem.*, **1984**, *267*, 229.

63. G. G. Hoffman, C. Burschka, *Z. Anorg. Allg. Chem.*, **1985**, *523*, 121.

64. G. G. Hoffman, R. Fischer, *Inorg. Chem.*, **1989**, *28*, 4165.

65. G. G. Hoffman, R. Faist, *J. Organomet. Chem.*, **1990**, *391*, 1.

66. G. G. Hoffman, *Chem. Ber.*, **1985**, *118*, 1655.

Chapter II

I-III-VI Materials

Summary:

Air-stable bimetallic compounds, $[(Ph_3P)_2AgIn(SCOR)_4]$ (R = Me, Ph) have been used to deposit $AgIn_5S_8$ films by AACVD between 350 – 450 °C. Tetragonal $CuME_2$ (M = In, Ga; E = S, Se) films have been grown by AACVD process using dual-source precursors, $[Cu(E_2CNMe^nHex)_2]$ and $[M(E_2CNMe^nHex)_3]$ (E = S, Se; M = In, Ga). As-deposited films showed a preferred orientation along the (112) plane regardless of growth temperatures.

2.1 - Introduction

Ternary metal chalcogenides I-III-VI_2 (I = Cu, Ag; III = In, Ga; VI = S, Se) have been the focus of recent research due to their use in radiation hard, solar cells. They also have a significant fabrication advantage over III-V semiconductors for solar cell applications, since polycrystalline films may be used, as opposed to epitaxial crystal films.[1]

A number of novel single-source precursors for the deposition of $CuInE_2$ (E = S, Se) have been synthesized and used to deposit thin films by various MOCVD processes. In an early study, Nomura *et al.* reported the deposition of $CuInS_2$ films on glass substrates using an equimolar mixture of [$^{i}Bu_2InS^{n}Pr$] and [$Cu(S_2CN^{n}Bu_2)_2$] dissolved in *p*-xylene.[2] The direct reaction of [$^{n}Bu_2InS^{i}Pr$] with [$Cu(S_2CN^{i}Pr_2)_2$] was shown to yield binuclear complex of the form [$^{n}Bu_2In(S^{i}Pr)Cu(S_2CN^{i}Pr_2)$] from which stoichiometric $CuInS_2$ films were grown by solution pyrolysis at 350 °C.[3] Various hetero-binuclear complexes [$(Ph_3P)_2Cu(\mu\text{-}ER)_2In(ER)_2$] (E = S, Se; R = Et, ^{i}Bu) have been prepared and pyrolysis studies revealed that the selenium derivative could be converted into $CuInSe_2$ at 400 – 450 °C.[4] In continuing such work, Hepp and co-workers were able to deposit $CuInS_2$ films using [$(Ph_3P)_2Cu(\mu\text{-}SEt)_2In(SEt)_2$] below 400 °C by spray MOCVD.[5] Recently, two liquid compounds, [$(^{n}Bu_3P)_2Cu(SR)_2In(SR)_2$] (R = Et, ^{n}Pr) have been used to deposit $CuInS_2$ thin films.[6,7] High quality $CuInS_2$ films have been reported on a copper coated silicon substrate using vapours from $(Et_3NH)[In(SC(O)Ph)_4]$. However, nickel coated silicon substrates lead to deposition of crystalline In_2S_3 thin films.[8]

There are very few reports on the deposition of $CuGaS_2$ films using metal-organic precursors. Buhro *et al.* reported the only known example of single-source precursor for

$CuGaS_2$ films based on [$^nBu_2CuGa(SEt)_4$] used in spray CVD process.[9] High quality epitaxial layers of $CuGaS_2$ films on GaAs (100) and GaP (100) have been deposited by LP-MOVPE using cyclopentadienylcoppertriethylphosphine, tri-propylgallium and ditertiallybutyl sulfide as organometallic precursors.[10]

The possibility of using single-source precursors for silver indium sulfide materials has been so far unexplored. Both $AgInS_2$ and $AgIn_5S_8$ are found to be semi-conducting. Thin films of these materials have been obtained by spray pyrolysis[11,12] which also deposit Ag_2S.[11] Various metal monothiocarboxylate compounds have been used as single-source precursors for metal sulfides.[13-15] The first section of this chapter describes the growth of thin films by AACVD using bimetallic thiocarboxylate compounds, [$(Ph_3P)_2AgIn(SCOR)_4$] (R = Me, Ph) and [$(Ph_3P)CuIn(SC\{O\}Ph)_4$].

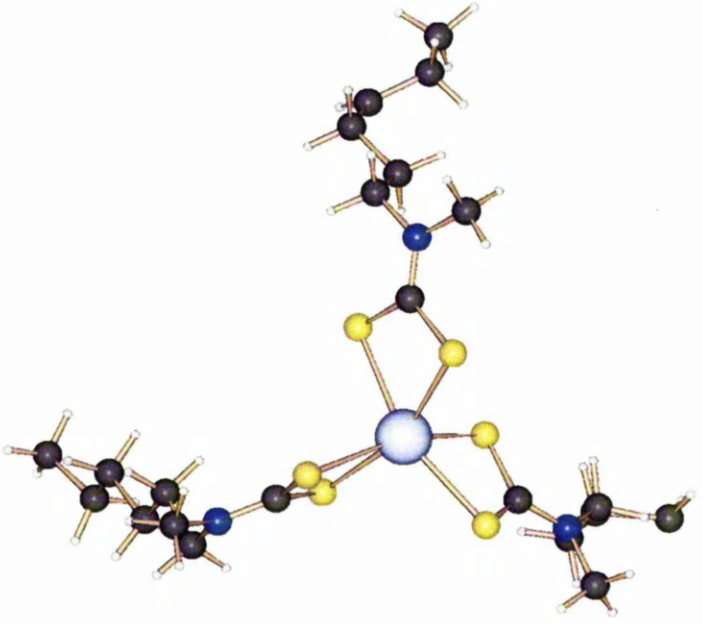

Figure 2.1 X-ray single crystal structure of [$In(S_2CNMe^nHex)_3$].

Over the years, O'Brien *et al.* have synthesised a range of dithio- and diseleno-carbamato complexes of various metals and used them to deposit a wide range of semiconductor materials.[16-18] One particularly successful modification to the sulfur/selenium containing ligands has been to develop compounds in which the parent amine is asymmetrically substituted and involves a bulky or extended alkyl substituent (Fig. 2.1).[19,20] Compounds with these ligands are air stable and sufficiently volatile for the deposition of thin films of materials such as Cu_2E, In_2E_3, Ga_2E_3, ZnE and CdE (E = S; Se).[21,22] Success with the binary parents has lead to deposition of ternary phases (chalcopyrite) of $CuInE_2$ (E = S, Se) by LP-MOCVD (Fig. 2.2).[23,24] The second section of this chapter concerns the growth of $CuInS_2$, $CuInSe_2$ and $CuGaS_2$ films by AACVD process using dual-source metal-organic precursors.

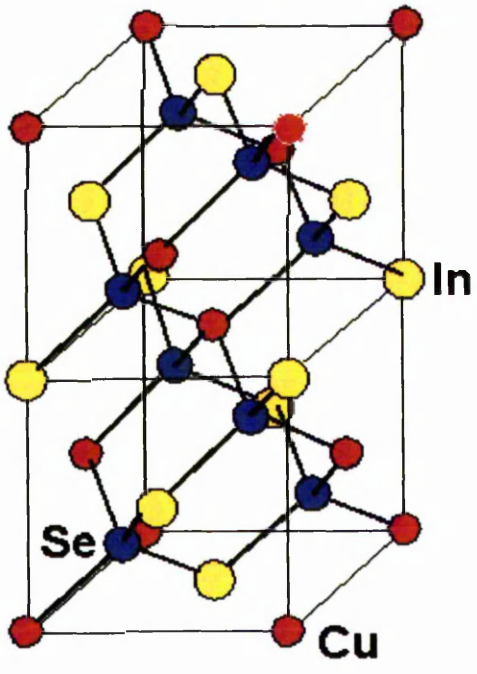

Figure 2.2 Crystalline chalcopyrite structure of $CuInSe_2$.

2.2 - Deposition of Silver Indium Sulfide Thin Films

Silver indium sulfide thin films were deposited by AACVD using the single-source precursors: $[(Ph_3P)_2AgIn(SC\{O\}Me)_4]$ and $[(Ph_3P)_2AgIn(SC\{O\}Ph)_4]$. The synthesis involves the reactions of *bis*-triphenylphosphinesilver salts with the indium salts followed by the addition of the sodium thiocarboxylate. The reactions yield pure compounds and are fairly air-stable for a period of time. The reactions are summarized below.[25]

$$(Ph_3P)_2AgCl + InCl_3.4H_2O + 4NaSC\{O\}R \rightarrow$$

$$[(Ph_3P)_2AgIn(SC\{O\}R)_4] + 4NaCl + 4H_2O$$

(R = Me, Ph)

The crystal structure of $[(Ph_3P)_2AgIn(SC\{O\}Ph)_4]$ is shown in Fig. 2.3, in which the Ag(I) centre has distorted tetrahedral geometry with a P_2AgS_2 core while In(III) adopts distorted octahedral geometry with two terminal $PhC\{O\}S^-$ anions chelating to In(III).[26]

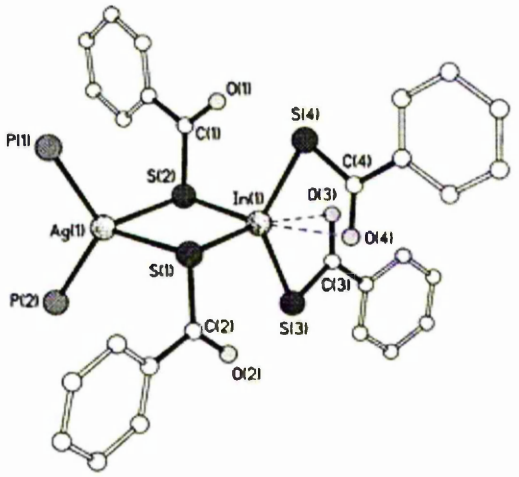

Figure 2.3 X-ray single crystal structure of $[(Ph_3P)_2AgIn(SC\{O\}Ph)_4]$.[25]

The work was carried out in collaboration with Professor J. J. Vittal and his group (National University of Singapore, Singapore).

The usefulness of both compounds as single-source precursors for ternary metal sulfide materials was investigated by thermogravimetric and pyrolysis experiments. The TGA curves of both compounds are shown in Fig. 2.4. The decomposition occurs in unresolved multiple steps in the temperature range 132 – 315 °C for the methyl compound and 175 – 328 °C for the phenyl compound. X-ray powder diffraction (XRPD) patterns of the final residues obtained from the pyrolysis of the compounds indicated the formation of orthorhombic $AgInS_2$.

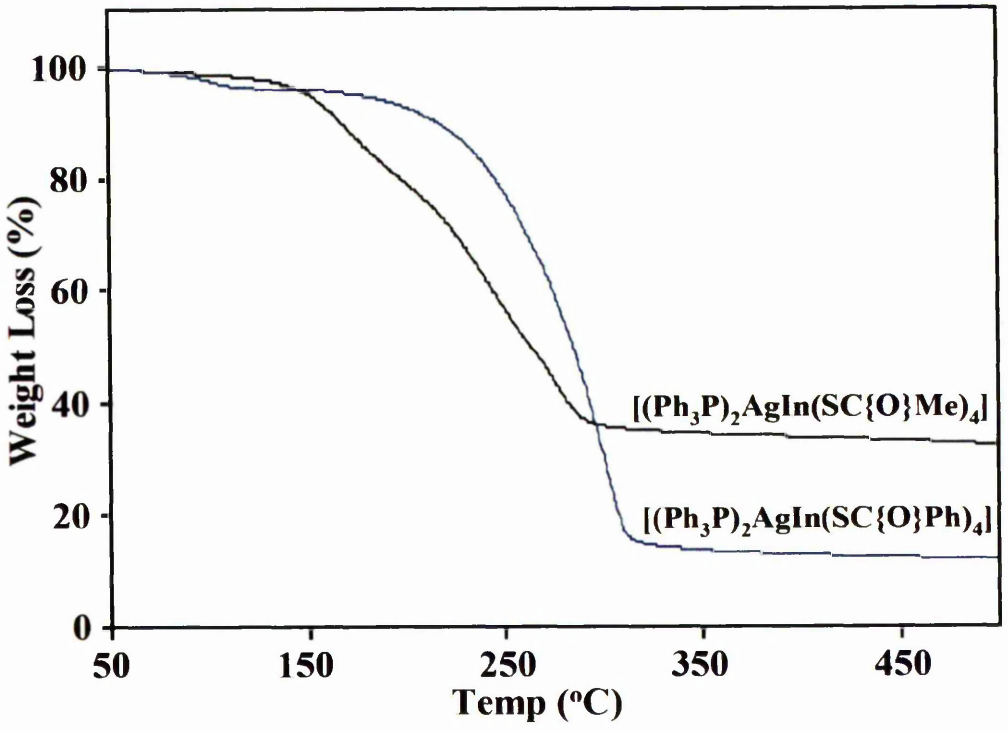

Figure 2.4 TGA analyses of $[(Ph_3P)_2AgIn(SC\{O\}R)_4]$ (R = Me, Ph).

The deposition studies were carried out on glass substrates by dissolving *ca.* 0.25g of precursor in 30 ml of toluene under a dynamic argon flow rate of 180 sccm for 2 hours. Deposited films were specular and adherent (Scotch-tape test) with a dark red colour at high temperatures (400 and 450 °C) and slightly red at low temperature (350

°C). The XRPD studies show that the films prepared from compounds $[(Ph_3P)_2AgIn(SC\{O\}R)_4]$ (R = Me, Ph) are composed of cubic $AgIn_5S_8$ (JCPDS 25-1329) with a preferred orientation along the (311) plane. The XRPD patterns of the films grown from $[(Ph_3P)_2AgIn(SC\{O\}Me)_4]$ (Fig. 2.5) show the (111) and (222) planes are noticeably enhanced with increasing growth temperature and intensities of peaks from the (511) and (440) planes are also reversed.

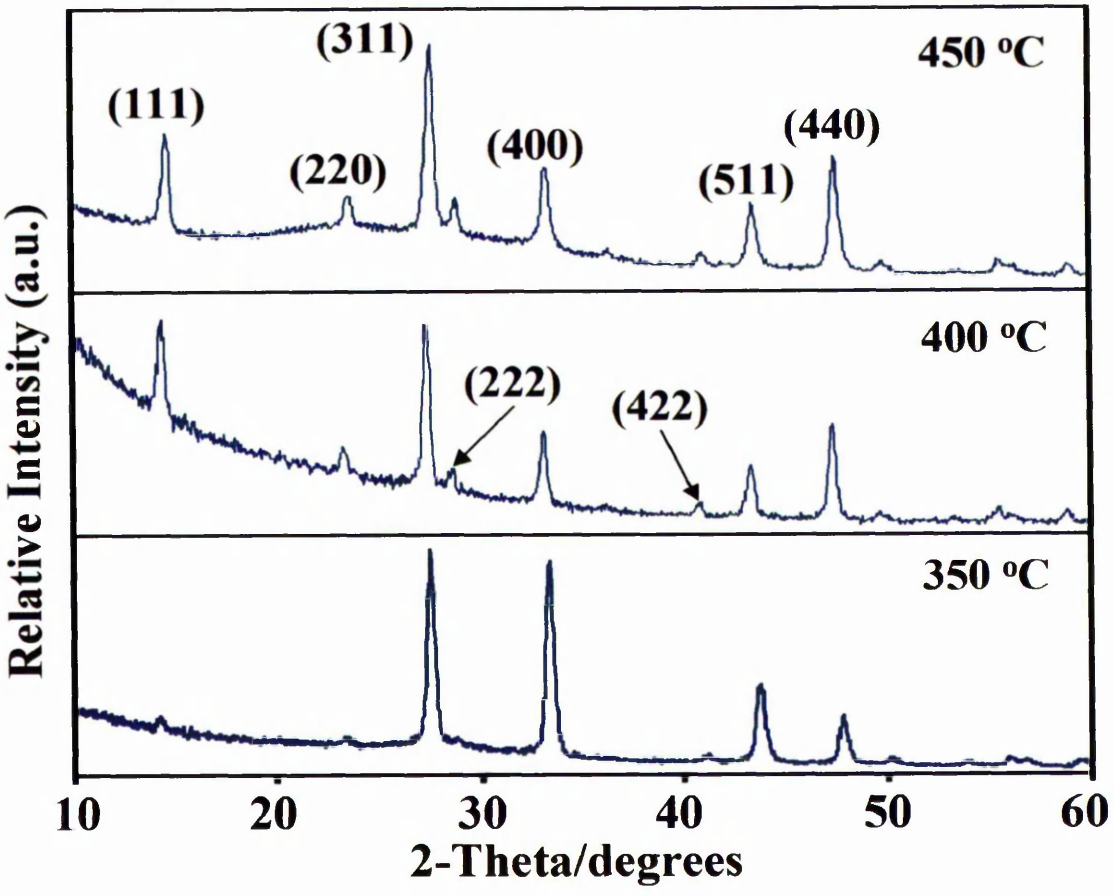

Figure 2.5 XRPD patterns of $AgIn_5S_8$ films deposited from $[(Ph_3P)_2AgIn(SC\{O\}Me)_4]$.

Similarly, XRPD studies of $AgIn_5S_8$ obtained from compound $[(Ph_3P)_2AgIn(SC\{O\}Ph)_4]$ showed similar patterns and no indication of enhancement of peak intensities was observed (Fig. 2.6).

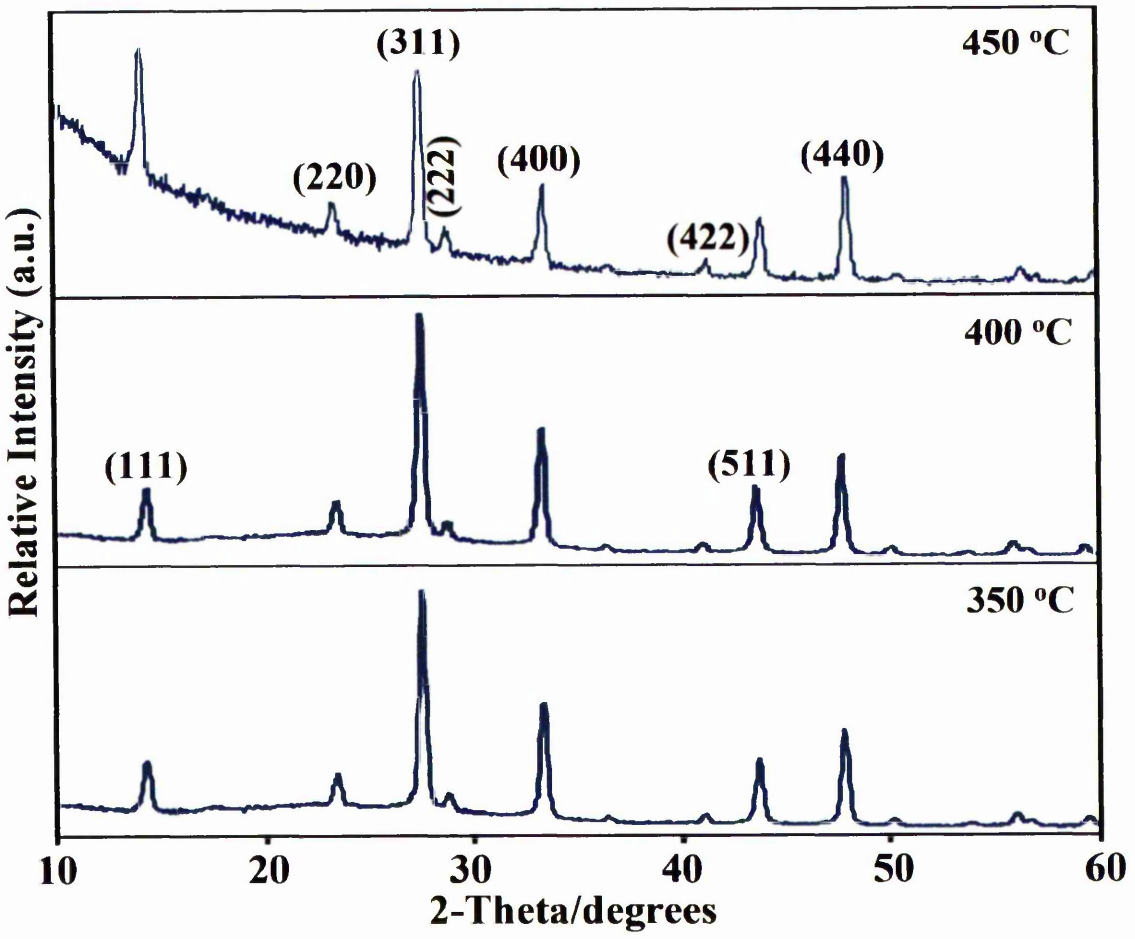

Figure 2.6 XRPD patterns of $AgIn_5S_8$ films deposited from $[(Ph_3P)_2AgIn(SC\{O\}Ph)_4]$.

The scanning electron microscopy (SEM) images of the films deposited from compound $[(Ph_3P)_2AgIn(SC\{O\}Me)_4]$ show changes in the morphologies of films as a function of growth temperatures (Fig. 2.7). The morphology of the films grown on glass at 450 °C consists of thin plate-like particles, perpendicularly laid down onto the substrate with random orientation, and similar morphology was also found in the films grown on Si (100) substrate at same temperature. However, with decreasing growth the temperature to 400 or 350 °C, the morphology becomes more dense and no plate-like particles are formed [Figs. 2.7(a); 2.7(b)]. Growth rate and average particle size of the films grown at 400 °C are *ca.* 0.3 $\mu m\ h^{-1}$ and *ca.* 0.5 μm, respectively, and at 350 °C are 0.2 $\mu m\ h^{-1}$ and *ca.* 0.3 μm.

Morphologies of films grown from $[(Ph_3P)_2AgIn(SC\{O\}Ph)_4]$ are quite different from those grown from methyl analogue. Films obtained at a growth temperature 350 °C revealed a relatively dense morphology and a smaller particle size than those prepared from higher growth temperatures (*ca.* 100 – 300 nm) (Fig. 2.8). Particles on glass substrates grown at 450 °C [Fig. 2.8(c)] have trigonal habits consisting of several layers. However, on changing the substrate from glass to Si(100), the formation of particles lead to rice-like morphology instead of triangular shapes. Growth rates obtained from the cross-section views are *ca.* 0.2 $\mu m\ h^{-1}$ at 350 °C, 0.5 $\mu m\ h^{-1}$ at 400 °C and 0.6 $\mu m\ h^{-1}$ at 450 °C after 2 hours of growth.

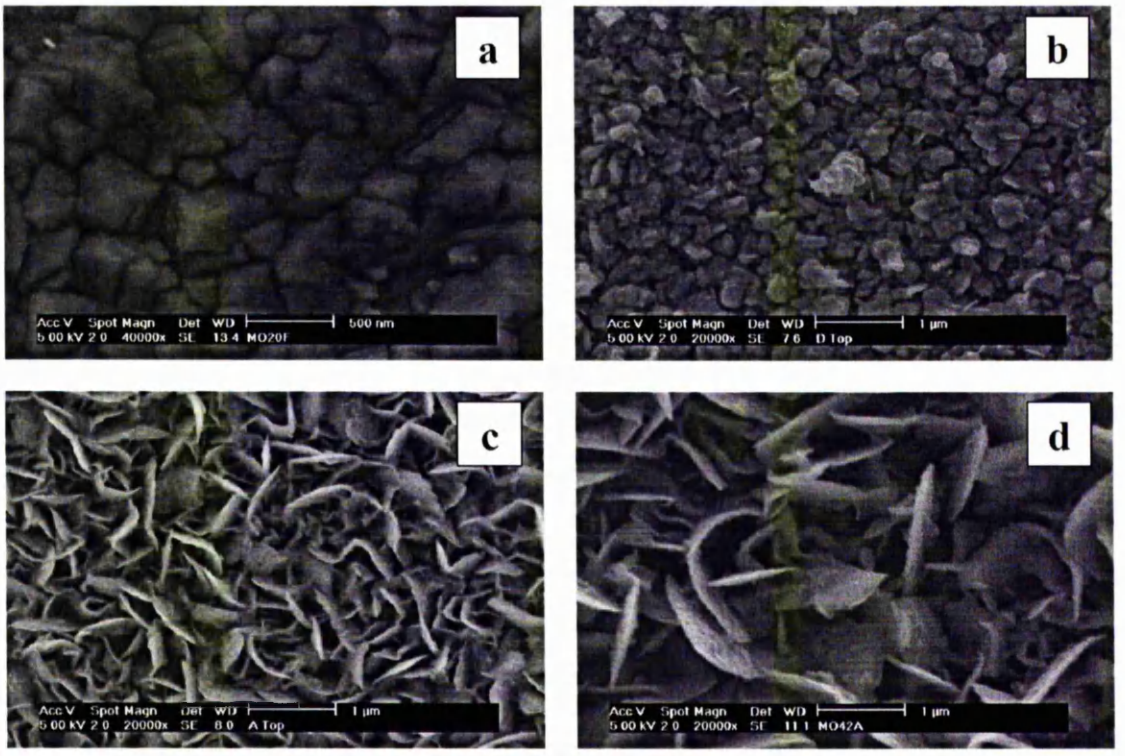

Figure 2.7 SEM images of $AgIn_5S_8$ films grown from $[(Ph_3P)_2AgIn(SC\{O\}Me)_4]$ at (a) 350 °C, (b) 400 °C, (c) 450 °C on glass and (d) 450 °C on Si(100).

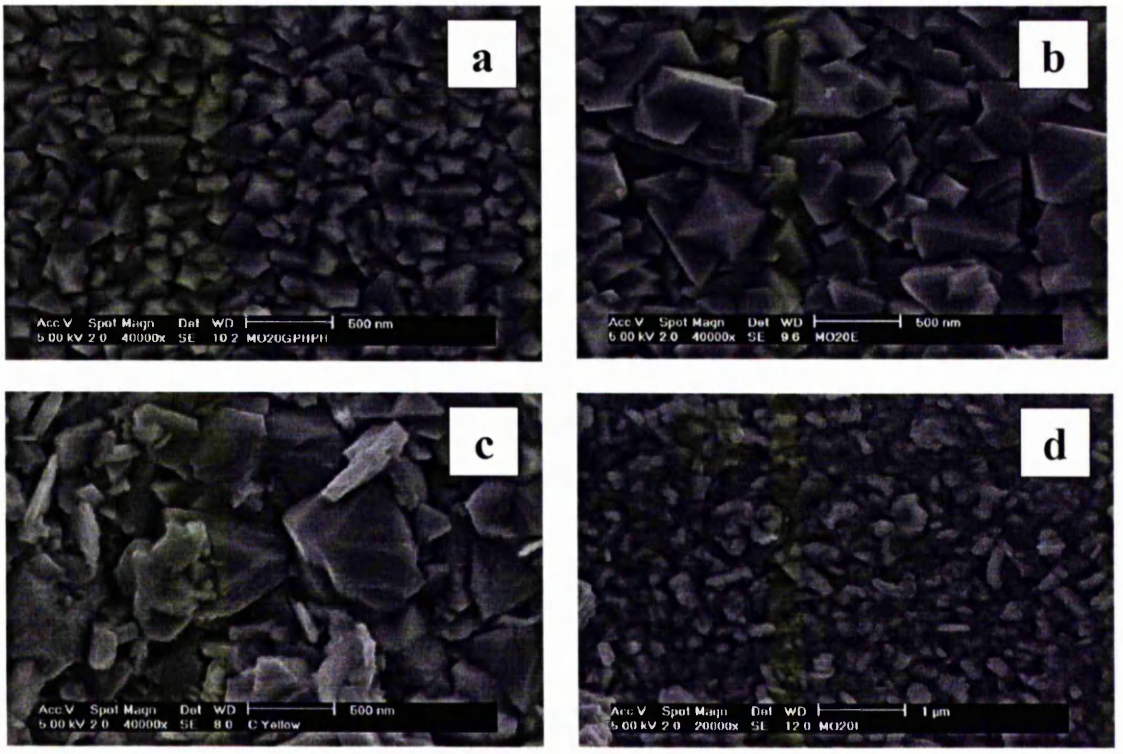

Figure 2.8 SEM images of $AgIn_5S_8$ films grown from $[(Ph_3P)_2AgIn(SC\{O\}Ph)_4]$ at (a) 350 °C, (b) 400 °C, (c) 450 °C on glass and (d) 450 °C on Si(100).

2.3 - Deposition of Indium Sulfide Thin Films

Attempts to deposit $CuInS_2$ films were made using $[(Ph_3P)CuIn(SC\{O\}Ph)_4]$ as a single-source precursor by AACVD. Deposition studies were carried out on glass substrates for 2 hours by dissolving *ca*. 0.25 g of precursor in 30 ml of toluene with an argon flow rate of 180 sccm. The synthesis of the compound involves the reaction of *bis*-triphenylphosphinecopper(I) nitrate with the $[SCOPh]^-$ anion as shown below;

$$(Ph_3P)_2Cu(NO_3) + InCl_3 + 4NaSC\{O\}Ph \rightarrow$$

$$[(Ph_3P)CuIn(SC\{O\}Ph)_4] + NaNO_3 + 3NaCl + PPh_3$$

The TGA and pyrolysis studies indicated that the precursor decomposes to predominantly bulk tetragonal $CuInS_2$.[25] AACVD experiments yielded dark yellow films which were deposited at growth temperatures of 350 – 450 °C after 2 hours of growth. The XRPD studies indicate that β-In_2S_3 (JCPDS 25-0390) has been deposited. Fig. 2.9 indicates the XRPD pattern of β-In_2S_3 film grown on glass at 450 °C and broad peaks indicate that the crystallinity of the particles is relatively poor and preferred orientation along the (311) plane is found. There were no differences on using different solvents such as THF or toluene. Nomura *et al.* reported the growth of $CuIn_5S_8$ films from a bimetallic complex [BuIn(S^iPr)Cu($S_2CN^iPr_2$)] by LP-MOCVD.[27] In their study, a higher growth temperature (450 °C) resulted in films β-In_2S_3, whereas at lower growth temperatures the films consisted of $CuIn_5S_8$.

The SEM studies on the In_2S_3 films show that the particles are randomly orientated on the glass substrate (Fig. 2.10) with *ca.* 1.5 μm h^{-1} growth rate. There was no evidence for copper peaks in the EDAX spectra but in some cases small traces of copper were observed (*ca.* < 1 %). This observation suggests that there was a pre-reaction between the precursor and the solvents used in this study during the CVD process. ESI-MS of the compound showed no molecular ion peak, however, signals due to $[In(SC\{O\}Ph)_4]^-$, $[(PPh_3)_2Cu]^+$, $[(PPh_3)_3Cu]^+$ were present. This indicates the dissociation of the compound in the solution. Such processes are common among phosphine adducts of coinage metal salts and have been substantiated by various techniques including NMR, molecular weight determinations and conductivity measurements.[28-31]

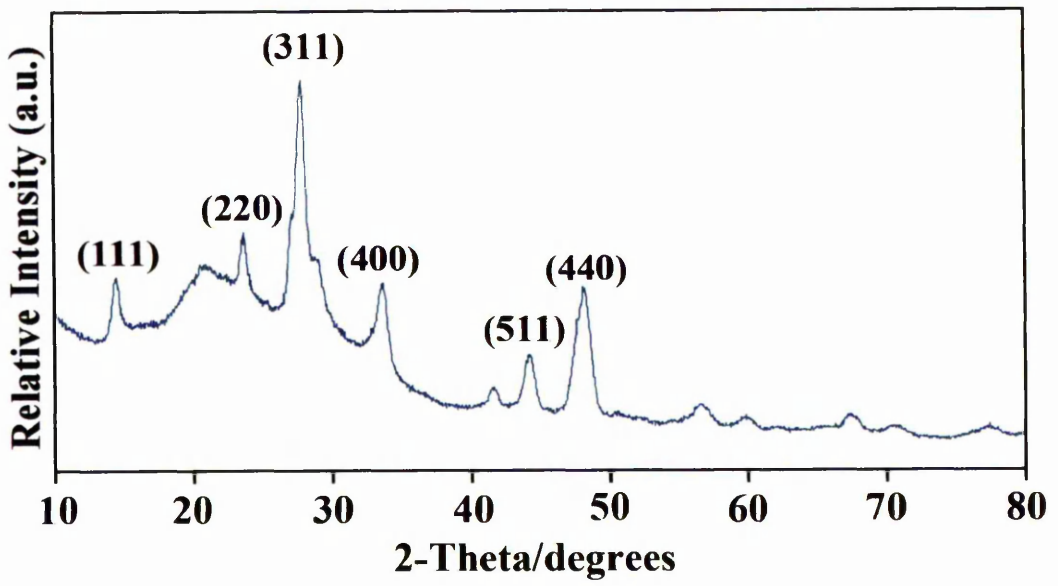

Figure 2.9 XRPD pattern of In_2S_3 deposited from $[(Ph_3P)_2CuIn(SC\{O\}Ph)_4]$ at 450 °C.

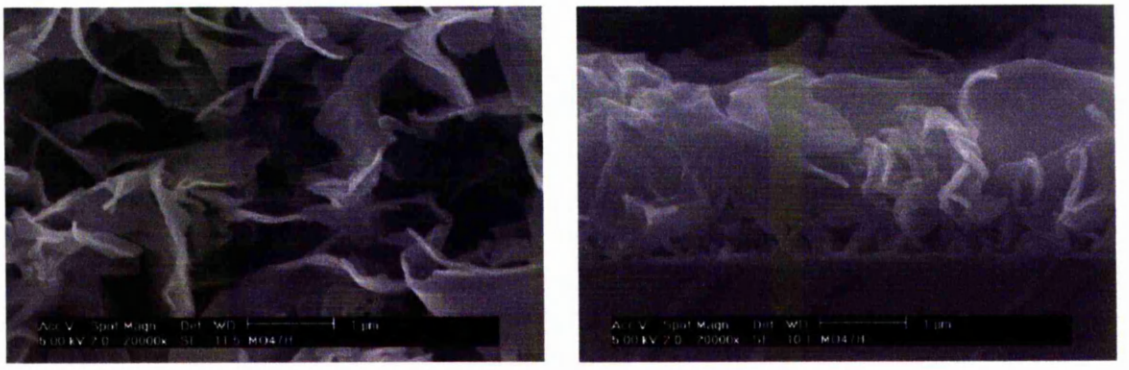

Figure 2.10 SEM images of In_2S_3 film deposited at 450 °C.

X-ray photoelectron spectroscopy (XPS) was also employed to determine photoelectron binding energies of elements comprising the films grown from $[(Ph_3P)CuIn(SC\{O\}Ph)_4]$ in toluene at 450 °C after 2 hours of growth. Figs. 2.11 and 2.12 show In 3*d* and S 2*p* peaks observed before etching and after one hour of etching. The peaks obtained before and after etching were not significantly different in terms of their binding energies and intensities. Indium 3*d* peaks were found at 451.5 eV (In $3d_{5/2}$) and 458.6 eV (In $3d_{3/2}$) before etching and 451.3 eV (In $3d_{5/2}$) and 458.2 eV (In $3d_{3/2}$).

Sulfur 2*p* peaks were found at 163.9 eV in both cases. Relative atomic percentages of indium and sulfur were slightly varied on etching treatment (2:3.66 before etching and 2:3.29 after etching).

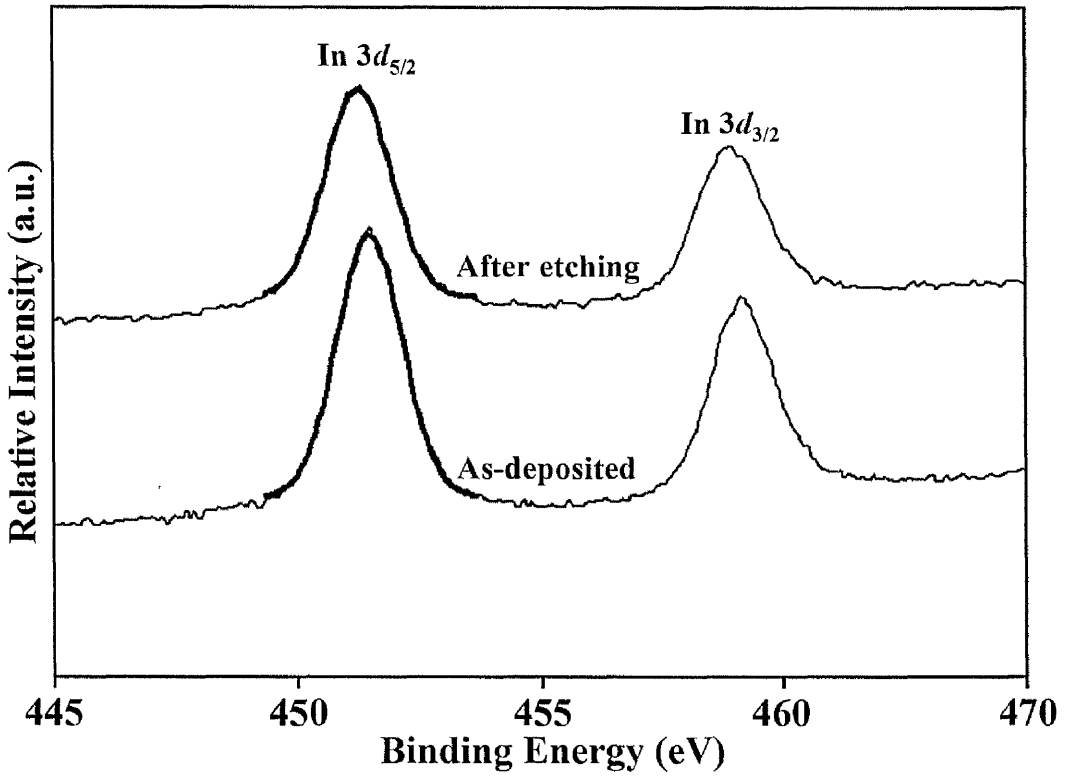

Figure 2.11 XPS spectra of In 3*d* peaks of β-In_2S_3 film as-deposited and after 1 hour of etching.

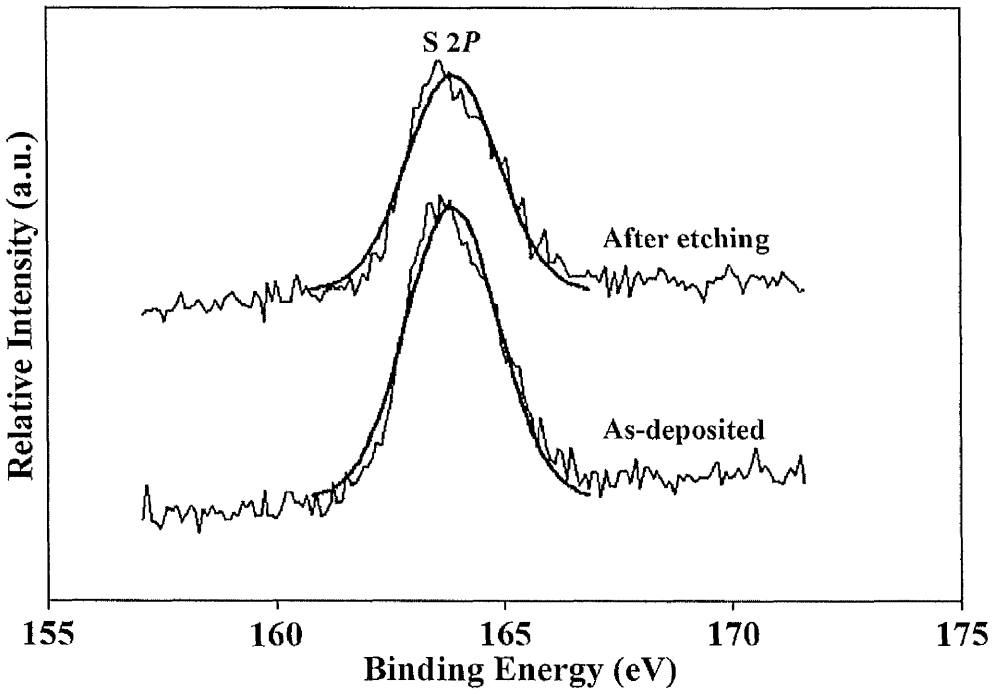

Figure 2.12 XPS spectra of S 2*p* peaks of β-In_2S_3 film as-deposited and after 1 hour of etching.

In this part of the chapter, $CuInS_2$, $CuInSe_2$ and $CuGaS_2$ films have been deposited using organometallic precursors, $M[(S/Se)_2CNMe^nHex]_n$ (M = Cu, In, Ga; n = 2, 3) by AACVD on glass substrates. The syntheses of these compounds have been described in the experimental section.

2.4 - Deposition of Copper Indium Sulfide Thin Films

Initially, stoichiometric amounts of a mixture of compounds $[Cu(S_2CNMe^nHex)_2]$ and $[In(S_2CNMe^nHex)_3]$ were used to deposit copper indium sulfide films between 350 – 450 °C. The precursors were dissolved in 30 ml toluene and the argon flow rate was 180 sccm. Deposited films were black and adherent to the glass substrates. It is interesting to note that employing AACVD process can reduce the minimum deposition temperature for growth of $CuInS_2$ to 350 °C. The XRPD analyses showed that tetragonal $CuInS_2$ films (JCPDS 27-0159) had been deposited with a preferred orientation along the (112) plane regardless of growth temperatures (Fig. 2.13).

SEM analysis of the as-deposited $CuInS_2$ films on glass indicates slightly different features, in terms of morphology, compared to those grown by LP-MOCVD.[24] Films grown at 450 °C show that the particles are formed as randomly orientated flakes *ca.* 0.2 μm thick [Fig. 2.14(b)] as compared to the relatively thick width (*ca.* 1 μm) crystallites grown by LP-MOCVD.[24] Also, the shape of particles are very similar to those prepared on fused silica using $[(Ph_3P)_2CuIn(SEt)_4]$ by spray CVD.[5] After 2 hours of growth, films were found to be *ca.* 1 μm thick with 0.5 μm h^{-1}. At lower growth temperatures (350 °C), a mixture of morphologies can be seen. Particles' size is found to be between 0.5 – 1.6 μm [Fig. 2.14(a)]. The EDAX analyses confirm that the

stoichiometry of films is *ca.* 1:1:2 (Fig. 2.15). Un-assigned peaks are reflections from glass substrates.

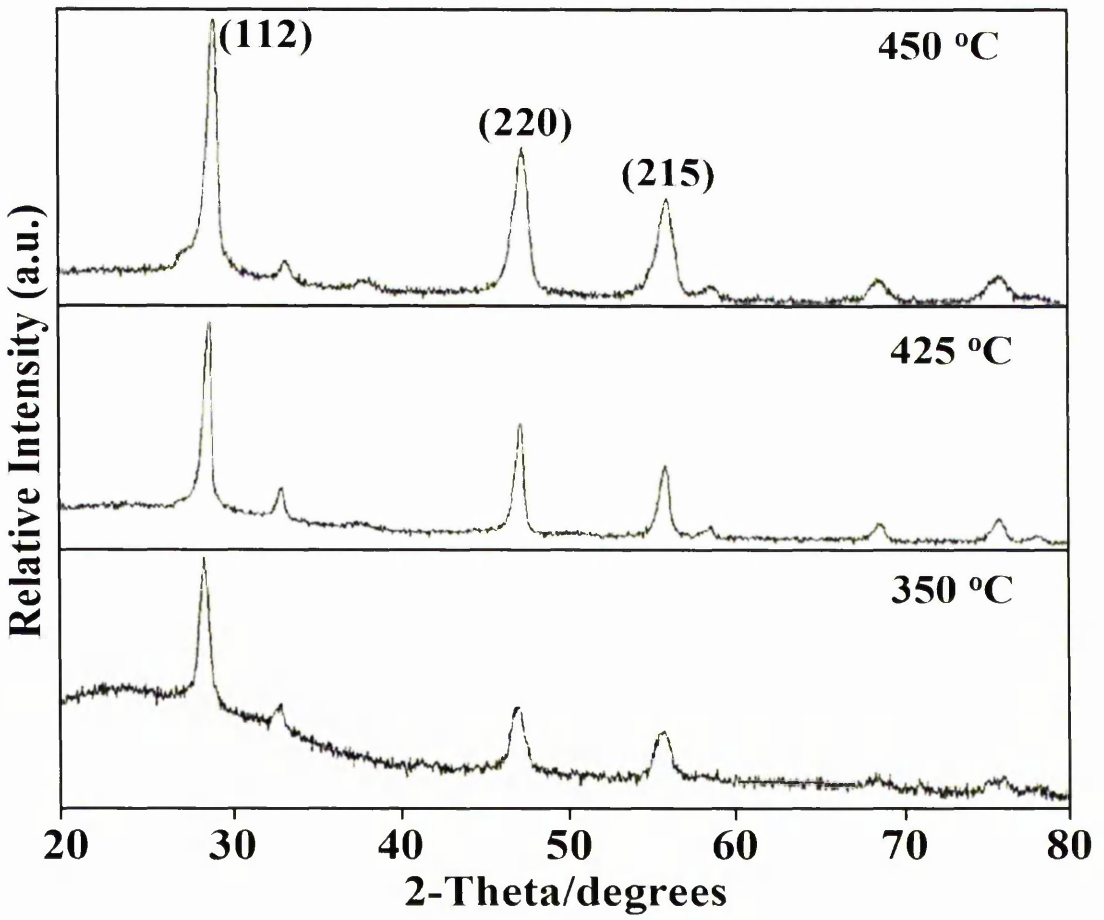

Figure 2.13 XRPD patterns of $CuInS_2$ films deposited at different growth temperatures.

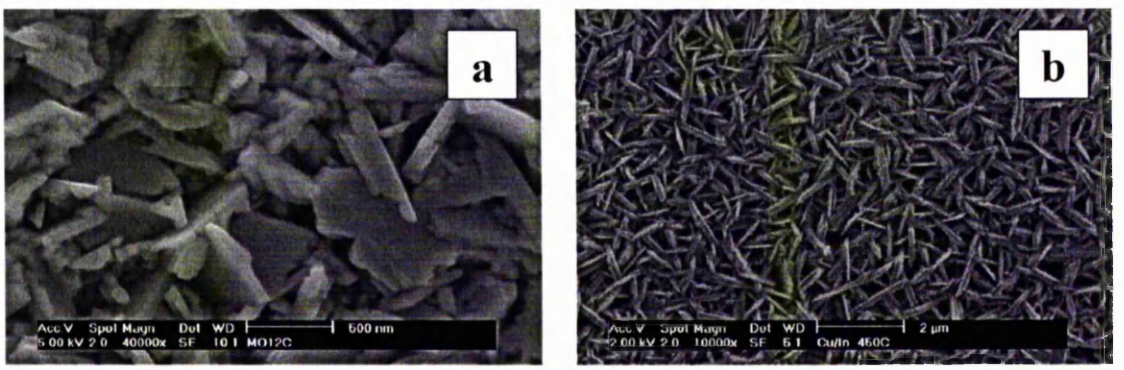

Figure 2.14 SEM images of $CuInS_2$ films deposited at (a) 350 °C and (b) 450 °C.

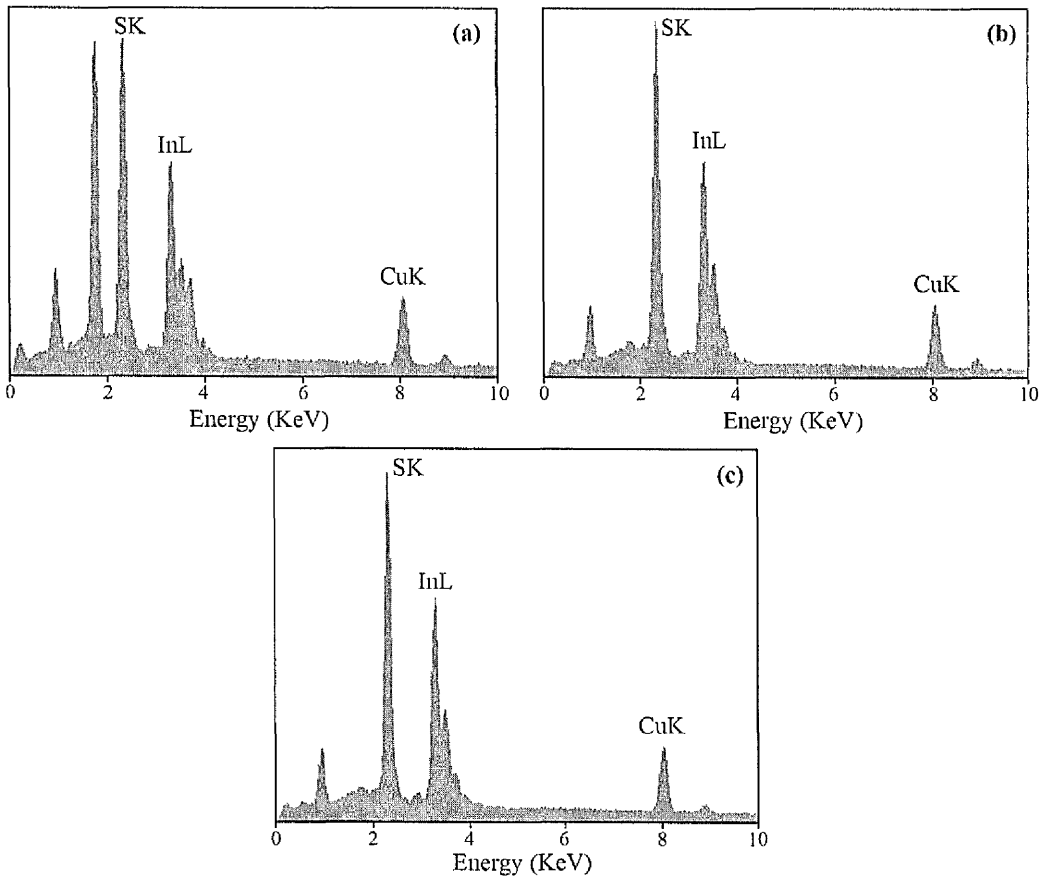

Figure 2.15 EDAX analyses of $CuInS_2$ films deposited (a) 350 °C, (b) 400 °C and (c) 450 °C.

The band gap value for $CuInS_2$ was found to be *ca.* 1.46 eV (Fig. 2.16), which is in good agreement with the previously reported value of 1.5 eV for the optical band gap of $CuInS_2$.[31]

Various ratios of copper and indium precursors were also utilized in order to investigate stoichiometric change of $CuInS_2$ films (Fig. 2.17). The XRPD patterns of as-deposited films grown with different ratios showed that there were no traces of any by-products such as indium sulfide or copper sulfide and indicate no effect on stoichiometry of $CuInS_2$, in contrast to the LP-MOCVD work.[24] Siemer and co-workers[29] have

demonstrated that devices prepared from preferred (112) orientated $CuInS_2$ films have better performance than photovoltaic devices fabricated from other films, since (112) orientated films have a low resistance.

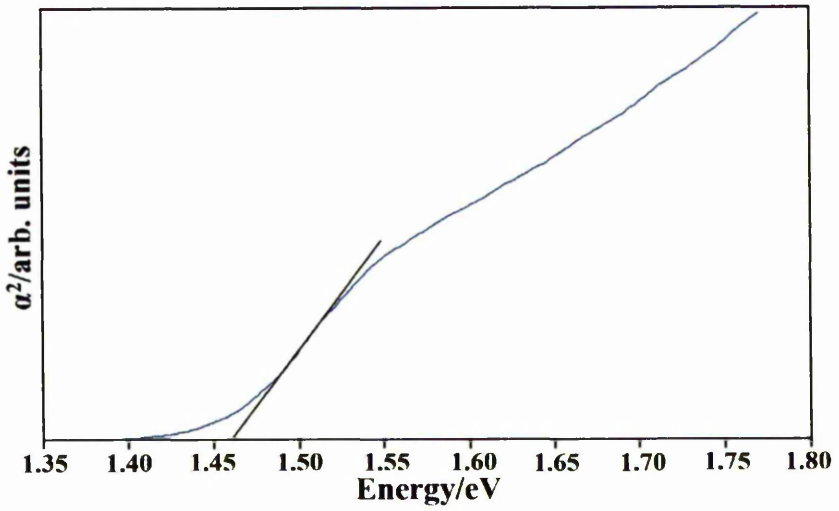

Figure 2.16 UV/Vis spectrum of a $CuInS_2$ film.

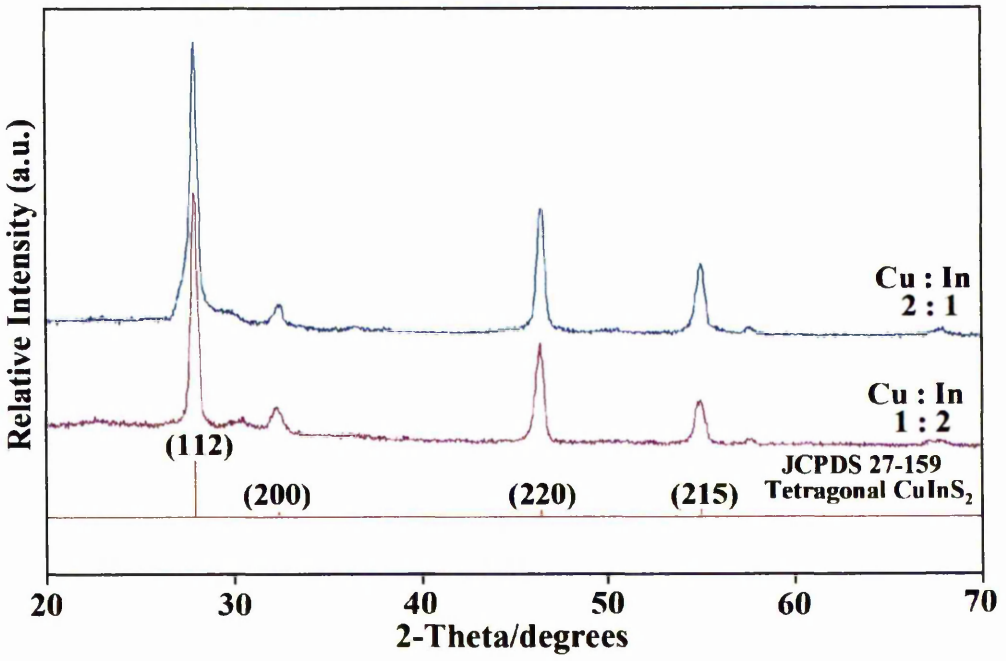

Figure 2.17 XRPD patterns of tetragonal $CuInS_2$ films deposited at 450 °C using different ratios of $[Cu(S_2CNMe^nHex)_2]$ and $[In(S_2CNMe^nHex)_3]$.

2.5 - Deposition of Copper Indium Selenide Thin Films

Copper indium selenide thin films were deposited using $[Cu(Se_2CNMe^nHex)_2]$ and $[In(Se_2CNMe^nHex)_3]$ in 1:1 molar ratios dissolved in 30 ml toluene. Films were grown at 425 – 475 °C with a dynamic argon flow rate (180 sccm) for 2 hours. Deposited films were black and non-adherent to the substrates. The XRPD analyses (Fig. 2.18) suggest that as-deposited films crystallize in the tetragonal phase with a preferred orientation along the (112) direction in all cases (JCPDS 40-1487).

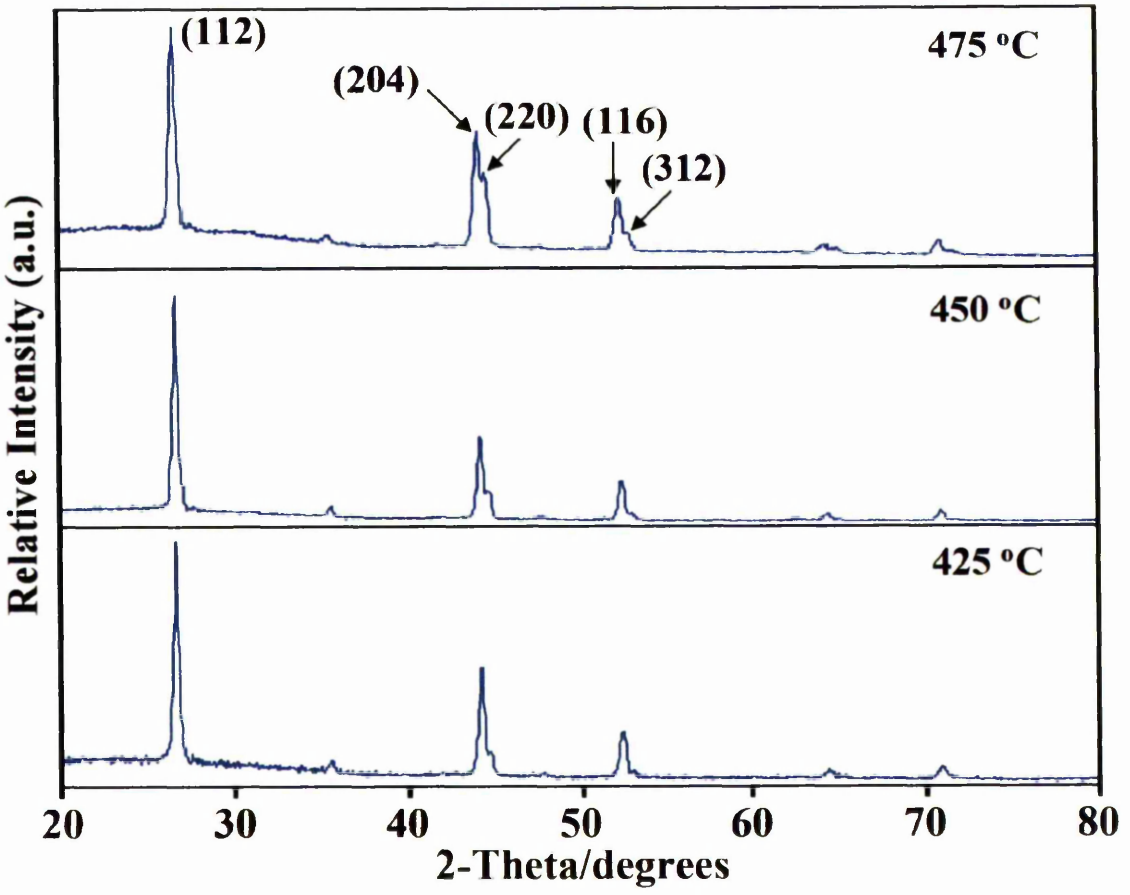

Figure 2.18 XRPD patterns of $CuInSe_2$ films deposited at different growth temperatures.

The SEM images of the films (Fig. 2.19) show that the deposited materials are not homogenous and consist of several different shapes of particles with a poor substrate coverage at a lower growth temperature (425 °C). These findings are consistent with the LP-MOCVD study of $CuInSe_2$ which also reported chalcopyrite structure.[32] EDAX analyses (Fig. 2.20) of as-deposited films confirms the formation of copper rich films *ca.* 27 – 29 %.

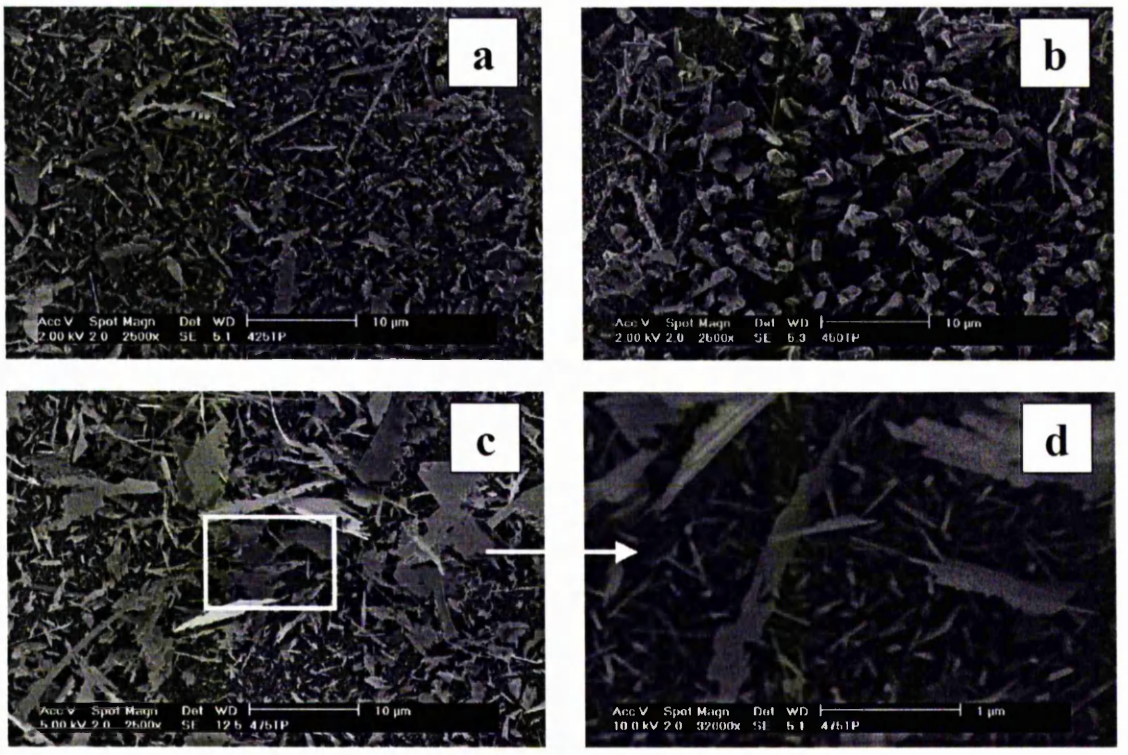

Figure 2.19 SEM images of $CuInSe_2$ films deposited at (a) 425 °C, (b) 450 °C, (c) and (d) 475 °C.

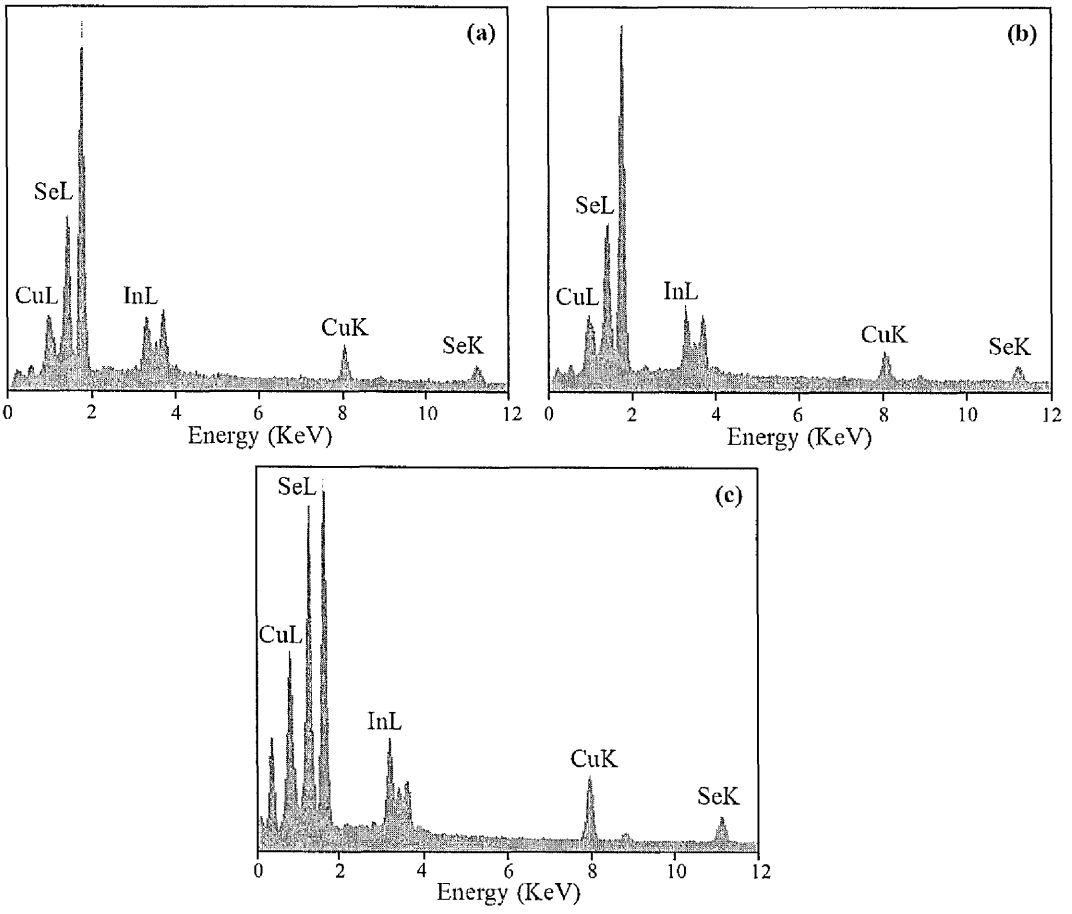

Figure 2.20 EDAX analyses of $CuInSe_2$ films deposited (a) 425 °C, (b) 450 °C and (c) 475 °C.

2.6 - Deposition of Copper Gallium Sulfide Thin Films

Stoichiometric amounts of $[Cu(S_2CNMe^nHex)_2]$ and $[Ga(S_2CNMe^nHex)_3]$ were dissolved in 30 ml toluene. Deposition of films was carried out for 2 hours between 350 – 450 °C under a dynamic flow of argon (flow rate = 180 sccm).

The XRPD patterns (Fig. 2.21) show that as-deposited $CuGaS_2$ films by AACVD had chalcopyrite structure with a preferred orientation along the (112) direction (JCPDS 27-0279). It is also conclusive that at high growth temperatures, the crystallinity of deposited films is improved, indicated by the sharpness of peaks. At lower growth

temperature (350 °C), the XRPD pattern exhibits weak reflections indicating poor crystallinity. Similar results were obtained for the films grown at reduced argon flow rate (120 sccm).

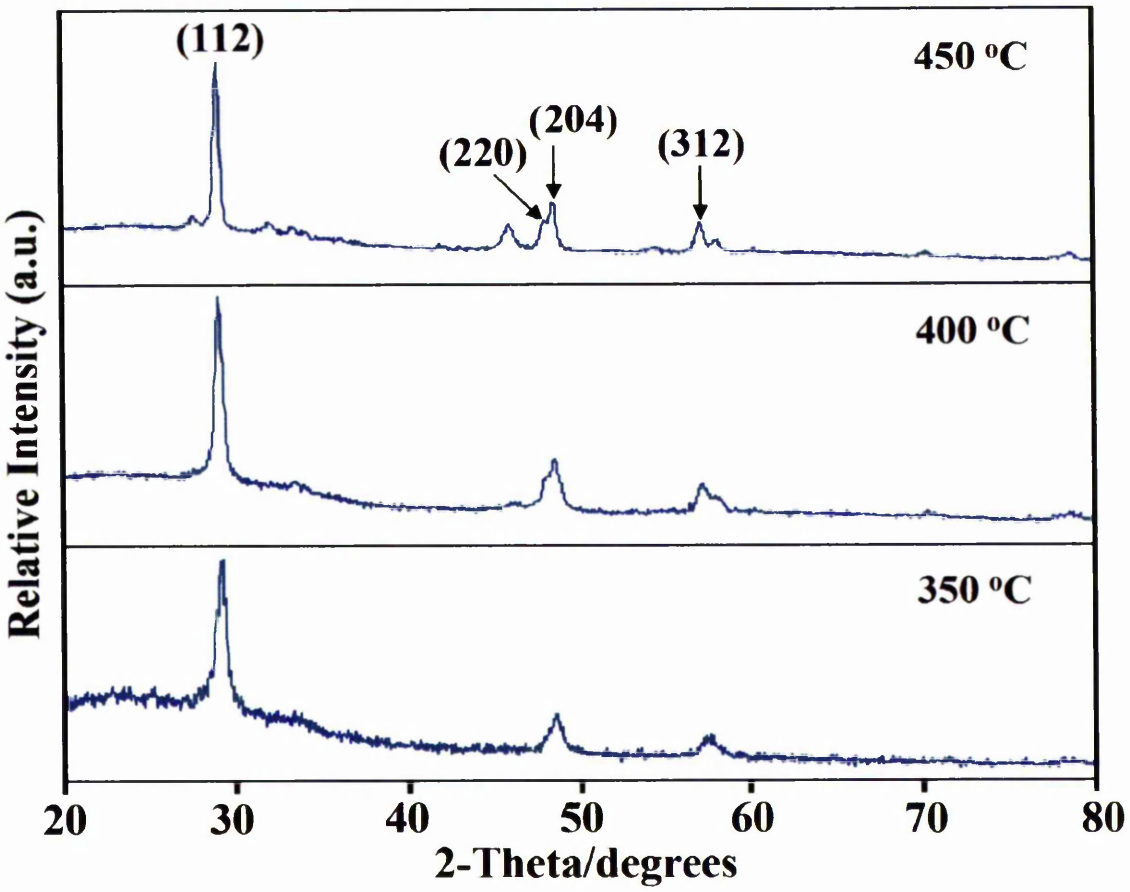

Figure 2.21 XRPD patterns of $CuGaS_2$ films deposited at different growth temperatures.

The SEM analyses (Fig. 2.22) show that the morphology of the films consists of clusters of randomly orientated platelets perpendicular to the surface (180 sccm/flow rate). Growth rates are *ca.* 500 nm h^{-1} at 350 °C and 1 μm h^{-1} at 450 °C. EDAX analyses of the films show Cu (30 %), Ga (24 %) and S (46 %). However, when the flow rate of argon is reduced to 120 sccm, the clusters formed tended to be denser but some individual platelets can also be seen (Fig. 2.22). In 2 hour growth at 450 °C, films with

ca. 1.5 μm thickness were deposited on the glass substrates (growth rate, *ca.* 0.75 μm h^{-1}). EDAX elemental atomic percent for $CuGaS_2$ films (Fig. 2.23) was found out to be 29 %, 23 % and 48 % respectively. Un-assigned peaks are due to amorphous glass substrates.

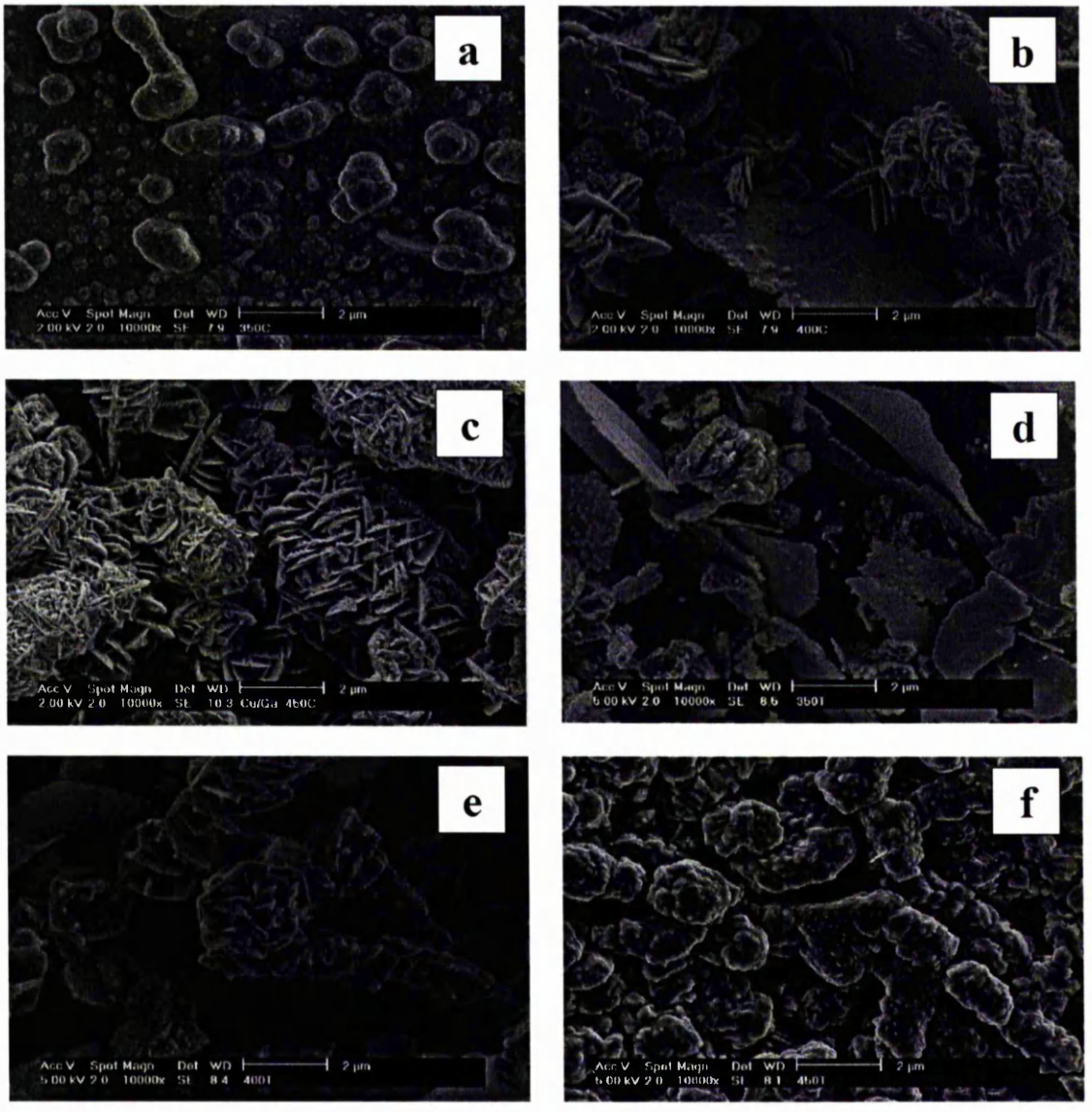

Figure 2.22 SEM images of $CuGaS_2$ films grown on glass at (a) 350 °C, (b) 400 °C and (c) 450 °C (argon flow rate = 180 sccm); (d) 350 °C, (e) 400 °C and (f) 450 °C (argon flow rate = 120 sccm).

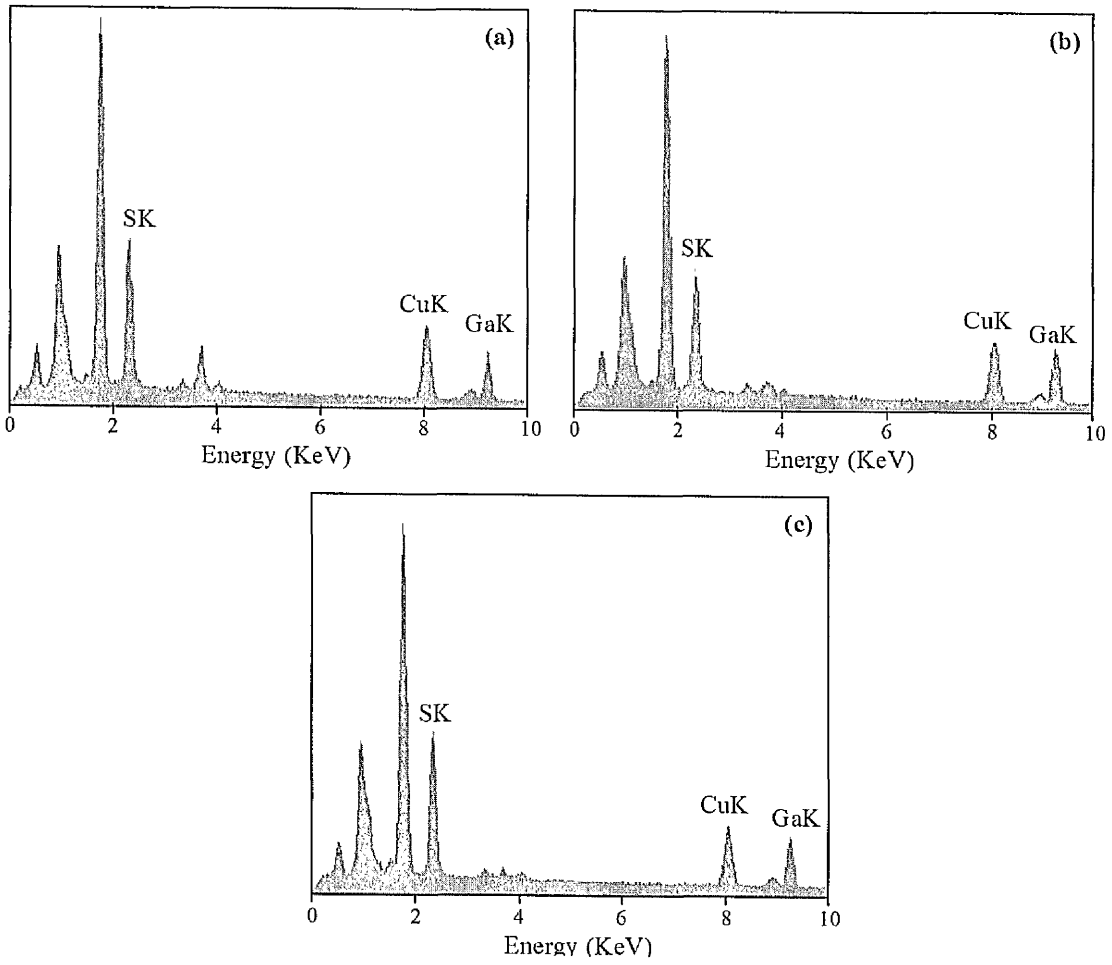

Figure 2.23 EDAX analyses of $CuGaS_2$ films deposited (a) 350 °C, (b) 400 °C and (c) 450 °C.

2.7 - Conclusions

Bimetallic compounds $[(Ph_3P)_2AgIn(SC\{O\}R)_4]$ (R = Me, Ph) have proved to be effective air-stable single-source precursors for the deposition of silver indium sulfide films by AACVD method. XRPD of the final residue obtained from pyrolysis of the compounds indicates the formation of orthorhombic $AgInS_2$. XRPD of the as-deposited films indicates the growth of $AgIn_5S_8$ films with a preferred orientation along the (311) plane. Similarly, TGA and pyrolysis studies of $[(Ph_3P)CuIn(SC\{O\}Ph)_4]$ show that the precursor decomposes to predominantly bulk tetragonal $CuInS_2$. However, AACVD studies of the precursor illustrate the growth of only β-In_2S_3. It has been predicated that the complex dissociates in the solution, because the molecular ion peak was absent from the ESI-MS of the compound, whilst signals due to various fragments were detected.

$CuInS_2$, $CuInSe_2$ and $CuGaS_2$ films also have been prepared by AACVD using air-stable $M[(S/Se)_2CNMe^nHex]_n$ (M = Cu, In, Ga; n = 2, 3) as dual-source precursors on glass substrates. The XRPD studies show that all the as-deposited films have chalcopyrite structure with a preferred orientation along the (112) plane regardless of growth temperatures (Table 2.1).

	$CuInS_2$				$CuInSe_2$				$CuGaS_2$			
hkl	**JCPDS 25-0159**	**450 °C**	**400 °C**	**350 °C**	**JCPDS 40-1487**	**475 °C**	**450 °C**	**425 °C**	**JCPDS 25-0279**	**450 °C**	**400 °C**	**350 °C**
112	3.19	3.19	3.19	3.19	3.35	3.34	3.33	3.35	3.06	3.07	3.07	3.05
200	2.76	2.76	2.76	2.75	2.89	N/A	N/A	N/A	2.67	2.69	2.68	N/A
211	2.41	2.41	2.46	2.45	2.53	2.52	2.51	2.52	N/A	N/A	N/A	N/A
204	1.96	1.95	1.95	1.95	2.05	2.04	2.04	2.05	1.87	1.87	1.89	1.87
220	1.95	N/A	N/A	N/A	2.04	2.03	2.02	N/A	1.89	1.90	1.90	N/A
116	1.67	1.66	1.68	1.66	1.75	1.74	1.74	1.74	1.59	1.61	1.61	1.60

Table 2.1 Comparison of *hkl* values of chalcopyrite thin films.

References

1. C. C. Landry, J. Lockwood, A. R. Barron, *Chem. Mater.*, **1995**, *7*, 699.
2. R. Nomura, K. Kanaya, H. Matsuda, *Chem. Lett.*, **1988**, *11*, 1849.
3. R. Nomura, Y. Seki, H. Matsuda, *J. Mater. Chem.*, **1992**, *2*, 765.
4. W. Hirpo, S. Dhingra, A. C. Sutorik, M. G. Kanatzidis, *J. Am. Chem. Soc.*, **1993**, *115*, 1597.
5. J. A. Hollingsworth, A. F. Hepp, W. E. Buhro, *Chem. Vap. Deposition*, **1999**, *5*, 105.
6. K. K. Banger, J. Cowen, A. F. Hepp, *Chem. Mater.*, **2001**, *13*, 3827.
7. K. K. Banger, J. D. Harris, J. Cowen, A. F. Hepp, *Thin Solid Films*, **2002**, *403-404*, 390.
8. M. Lin, K. P. Loh, T. C. Deivaraj, J. J. Vittal, *J. Chem. Soc., Chem. Commun.*, **2002**, 1400.
9. K. K. Banger, J. A. Hollingworth, J. D. Harris, J. Cowen, W. E. Buhro, A. F. Hepp, *Appl. Organometal. Chem.*, **2002**, *16*, 617.
10. S. Chichibu, S. Shirakata, *J. Appl. Phys.*, **2000**, *87*, 3793.
11. M. Ortega-López, A. Morales-Acevedo, O. Solorza-Feria, *Thin Solid Films*, **2001**, *385*, 120.
12. M. Gorska, R. Beaulieu, J. J. Loferski, B. Roessler, *Thin Solid Films*, **1980**, *67*, 341.
13. G. Shang, M. J. Hampden-Smith, E. N. Duesler, *J. Chem. Soc., Chem. Commun.*, **1996**, 1733.

14. M. D. Nyman, M. J. Hampden-Smith, E. N. Duesler, *Inorg. Chem.*, **1997**, *36*, 2218.

15. M. D. Nyman, K. Jenkin, M. J. Hampden-Smith, T. T. Kodas, E. N. Duesler, A. L. Rheingold, M. L. Liable-Sands, *Chem. Mater.*, **1998**, *10*, 914.

16. M. Kemmler, M. R. Lazell, P. O'Brien, D. J. Otway, J.-H. Park, J. R. Walsh, *J. Mater. Sci., Mater. Elec.*, **2002**, *13*, 531.

17. M. B. Hursthouse, M. A. Malik, M. Motevalli, P. O'Brien, *J. Mater. Chem.*, **1992**, *2*, 949.

18. P. O'Brien, D. J. Otway, J. R. Walsh, *Thin Solid Films*, **1998**, *315*, 57.

19. M. Motevalli, P. O'Brien, J. R. Walsh, I. M. Watson, *Polyhedron*, **1996**, *15*, 2801.

20. P. O'Brien, J. R. Walsh, I. M. Waston, L. Hart, S. R. P. Silva, *J. Cryst. Growth*, **1996**, *167*, 133.

21. S. W. Haggata, M. A. Malik, M. Motevalli, P. O'Brien, J. C. Knowles, *Chem. Mater.*, **1995**, *7*, 716.

22. M. R. Lazell, P. O'Brien, D. J. Otway, J.-H. Park, *Chem. Mater.*, **1999**, *11*, 3430.

23. J. McAleese, P. O'Brien, D. J. Otway, *Chem. Vap. Deposition*, **1998**, *4*, 94.

24. M. Kemmler, M. R. Lazell, P. O'Brien, D. J. Otway, *Mat. Res. Soc. Symp. Pro.*, **2002**, *692*, 215.

25. T. C. Deivaraj, J.-H. Park, M. Afzaal, P. O'Brien, J. J. Vittal, *Chem. Mater.*, **2003**, *15*, 2383.

26. T. C. Deivaraj, J.-H. Park, M. Afzaal, P. O'Brien, J. J. Vittal, *J. Chem. Soc., Chem. Commun.*, **2001**, 2304.

27. R. Nomura, Y. Seki, H. Matsuda, *Thin Soild Films*, **1992**, *209*, 145.

28. P. F. Barron, J. C. Dyason, P. C. Healy, L. M. Engelhardt, B. W. Skelton, A. H. White, *J. Chem. Soc., Dalton Trans.*, **1986**, 1965.

29. H. Nakajima, K. Matsumoto, K. Tanaka, T. Tanaka, *Inorg. Nucl. Chem.*, **1975**, *37*, 2463.

30. J. R. Black, W. Levason, M. D. Spicer, M. Webster, *J. Chem. Soc., Dalton Trans.*, **1993**, 3129.

31. O. Madelung, *Semiconductors Others Than Group IV Elements and III-V Compounds*, Springer-Verlag, Berlin Heidelberg, **1992**, 57.

32. K. Siemer, J. Klaer, I. Luck, D. Bräunig, *IEEE Photovol. Proc.*, **2000**, *22*, 630.

Chapter III

Cadmium and Zinc Chalcogenide Materials

Summary:

The compounds $[Cd((SePR_2)_2N)_2]$, $[MeCd\{(SeP^iPr_2)_2N\}]_2$ and $[Zn((SePR_2)_2N)_2]$ (R = Ph, ^{i}Pr) have been synthesized, characterized and used as single-source precursors for the growth of cadmium selenide and zinc selenide films by LP-MOCVD. Good quality films were deposited on glass substrates at temperatures between 400 – 525 °C. The deposited films were characterized by XRPD, SEM, EDAX and XPS.

3.1 – Introduction

The direct nature of the band gaps in II-VI materials makes them suitable for use in devices, such as blue/blue-green laser diodes,[1-3] which could lead to high-density optical storage systems.[4-6] Cadmium chalcogenides are also useful materials in solid-state polycrystalline solar cells, field effect transistors, sensors and transducers.[7,8]

Probably, the earliest work on the growth of II-VI thin films, using what might be termed single-source precursor, was on CdS films grown from thiourea compounds; $Cd(H_2O)[SC(NH_2)_2]_2Cl_2$[9] and $Cd[SC(NH_2)_2]_2Cl_2$[10] under spray-pyrolysis conditions. Phosphorus-containing molecules such as $Cd[(CH_3)_2PS_2]_2$,[11] $Cd[(C_2H_5)_2PS_2]_2$,[12] and $M[(^tBu)_2P(E)NR]_2$ (M = Zn(II), Cd(II); E = Se, Te; R = ^{i}Pr, C_6H_{11})[13] have been used to grow thin films LP-MOCVD. The telluro-derivatives are among the few such compounds available for depositing cadmium and zinc tellurides. The solid-state chemistry of group 12 metal chalcogenolates shows the formation of involatile, polymeric compounds.[14] Arnold and co-workers have used sterically bulky tellurolate and selenolate ligands to prevent polymerization and have deposited a range of chalcogenides using bulky silicon precursors of general formula $[MESi(SiCH_3)_3]_2$ (M = Zn(II), Cd(II), Hg(II); E = S, Se, Te).[15,16] Bochmann *et al.* extended this chemistry further by producing a range of precursors based on 2,4,6-tri-*tert*-butylphenylchalcogenolate, which have been used to deposit thin films of the metal sulfides and selenides in low-pressure growth experiments.[7,8,17]

Dialkyldichalcogenocarbamates of the group 12 metals have been the precursors most employed in the MOCVD preparation of II-VI thin films. Various groups have studied simple $[M(S_2CNEt_2)_2]$ (M = Cd(II), Zn(II)) complexes and deposited CdS or ZnS

films by various deposition techniques,[18-20] whilst the use of metal diethyldiselenocarbamates to deposit ZnSe and CdSe on glass substrates resulted in the deposition of elemental selenium.[21] Asymmetrical substituents as in $[M(E_2CNMe^nHex)]_2$ [M = Cd(II), Zn(II); E = S, Se) (Fig. 3.1) originally introduced in the molecule in order to increase volatility and have been successfully used to deposit II-VI films by LP-MOCVD. An investigation into the reaction mechanisms was carried out by gas chromatography mass spectroscopy (GC-MS) and electron impact mass spectroscopy (EI-MS). In the compounds with methyl(^{n}hexyl) and related substituents, the formation of diethyl diselenide is hindered and as a result the deposition of selenium during growth is inhibited.[21]

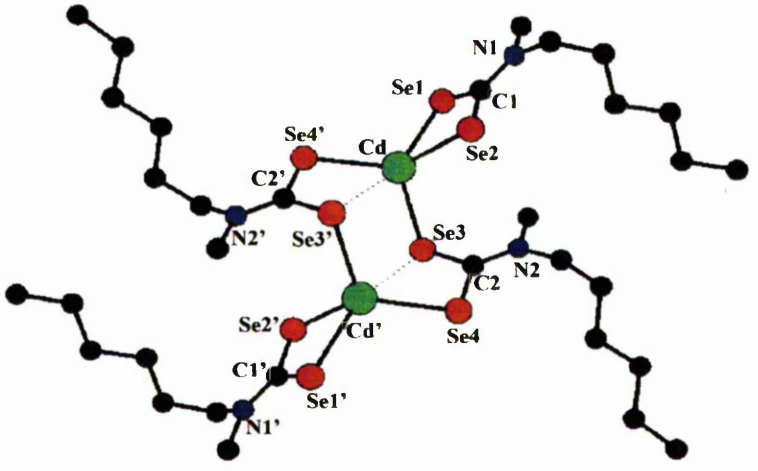

Figure 3.1 X-ray single crystal structure of $[Cd(SeCNMe^nHex)_2]_2$.

Another approach has been to associate the dialkyldichalcogenocarbamato ligand with an alkyl ligand. O'Brien *et al.* have reported the growth of II-VI thin films on glass substrates using mixed alkyl complexes of zinc and cadmium, such as $[RZn(S_2CNEt_2)]_2$ (R = Me,[22] Me_3C, Me_3CCH_2[23]), $[MeCd(Se_2CNEt_2)]_2$, and $[MeZn_{0.5}Cd_{0.5}(Se_2CNEt_2)]_2$.[24]

Hampden-Smith and co-workers have reported the growth of ZnS and CdS films by AACVD using single-source precursors based on monothiocarboxylates; $Zn(SOCCH_3)_2(tmeda)$ and $Cd(SOCCH_3)_2(tmeda)$ (tmeda = *N,N,N,N*-tetramethylethylenediamine) which are monomeric in the solid state with the metal ions in a distorted tetrahedral coordination environment.[25]

The work discussed in this chapter concerns the preparation and characterisation of $[Cd((SePR_2)_2N)_2]$, $[MeCd\{(SeP^iPr_2)_2N\}]_2$ and $[Zn((SePR_2)_2N)_2]$ (R = Ph, ^{i}Pr) and the deposition of cadmium/zinc selenide thin films from such precursors by LP-MOCVD. X-ray single crystal structures of $[MeCd\{(SeP^iPr_2)_2N\}]_2$ and $[Zn((SePR_2)_2N)_2]$ (R = Ph, ^{i}Pr) are also reported and discussed.

3.2 - Synthesis of Precursors

Cadmium and zinc complexes of imino-*bis*(di-isopropylphosphine chalcogenide) ligands, $[M((EP^iPr_2)_2N)_2]$ (M = Zn(II), Cd(II); E = S, Se) have been prepared by the reaction of the sodium salt of $[NH(EP^iPr_2)_2]$ (E = S, Se) with the appropriate group 12 metal salt in methanol. The synthesis of ligands $[NH(EPR_2)_2]$ (E = S, Se; R = Ph, ^{i}Pr) were carried out according to the reported methods.[26,27] The method involves the reaction of R_2PCl (R = Ph, ^{i}Pr) with $NH(SiMe_3)_2$ giving R_2PNHPR_2 (R = Ph, ^{i}Pr) (not isolated) which are oxidized with sulfur/selenium to give $NH(EPR_2)_2$ (E = S, Se; R = Ph, ^{i}Pr). These reactions have many advantages over conventional routes using metal carbonates.[27] High yields are obtained particularly for selenium complexes with reactions occurring efficiently at room temperatures in anhydrous methanol. A mixed-alkyl

The work was carried out in collaboration with Professor Derek Woollins and his group (St. Andrews University, UK).

complex, $[MeCd\{(SeP^iPr_2)_2N\}]_2$ was prepared by the comproportionation of Me_2Cd and $[Cd((SeP^iPr_2)_2N)_2]$ in anhydrous toluene. Similar attempts to synthesise mixed-alkyl zinc complexes by comproportionation reactions were unsuccessful.

3.3 - X-ray Single Crystal Structures

Crystals of the compound $[MeCd\{(SeP^iPr_2)_2N\}]_2$ were obtained from a toluene solution at low temperature and solid state structure of the compound have been determined by single-crystal X-ray diffraction technique. A summary of refinement parameters is given in Table 3.1 and selected interatomic distances and bond angles are presented in Table 3.2. The structure of compound shown in Fig. 3.2 consists of dimeric molecular units; each diselenoimidodiphosphinate chelates to one cadmium atom and bridges to the next. Each cadmium is four-coordinate and bound to three selenium atoms and one carbon. The structure resembles the dimeric structure of *bis*(diethyldiselenocarbamato)cadmium(II) but with the alkyl group replacing the chelating-only carbamato group as in ($NpCdSe_2CNEt_2$) and in ($MeCdS_2CNEt_2$).[22,28] The Cd-Se bond lengths are in the range Cd(1)-Se(1) 2.672(3) to Cd(1)-Se(2a) 2.934(2) Å, which are slightly longer than the parent cadmium compound 2.622(2)-2.636(2) Å.[27] The bite angle Se(1)-Cd(1)-Se(2) 109.61(10)° is less acute than the Se-Cd-Se angle in $[Cd((SeP^iPr_2)_2N)_2]$ (111.32 (6)°).[27] The Cd-C bond length (2.156 Å) is close to those observed in other cadmium alkyls.[22,28,29]

Crystals of $[Zn((SePPh_2)_2N)_2]$ were obtained by slow diffusion of hexane into a chloroform solution. During attempts to synthesize the mixed-alkyl zinc complex by a comproportionation reaction between dimethylzinc and $[Zn((SeP^iPr_2)_2N)_2]$, the

serendipitous formation of $[Zn((SeP^{i}Pr_2)_2N)_2]$ crystals from toluene solution occurred. A summary of refinement parameters of both compounds is given in Table 3.3 and selected interatomic distances and bond angles are presented in Tables 3.4 and 3.5.

X-ray single crystal structures of $[Zn((SePR_2)_2N)_2]$ (R = Ph, ^{i}Pr) shown in Figs. 3.3 and 3.4 show that the zinc atoms are co-ordinated to the selenium atoms through two bidentate ligands forming six-membered chelate rings. The tetrahedral geometries around the zinc atoms are distorted which is reflected in the Se-Zn-Se angles which range from 103.85(9) to 115.93(6)° for $[Zn((SePPh_2)_2N)_2]$ and 106.36(3) to 114.07(3)° for $[Zn((SeP^{i}Pr_2)_2N)_2]$. There is no significant difference in the Zn-Se bond lengths of $[Zn((SePR_2)_2N)_2]$ (R = Ph, ^{i}Pr). The Zn-Se bond lengths are in the range of 2.458(9) to 2.467(9) Å which are slightly larger than Zn-S bond lengths (2.350(11) to 2.359(11) Å). Similarly, Se-Zn-Se bite angles are also greater than the bite angles of S-Zn-S (111.84(4) – 112.81 (4)°).[30] Shortening of the P-N bonds and the subsequent extended P-Se bonds relative to free ligand, indicates an increase in delocalization of electrons within the architecture due to deprotonation.[26]

Table 3.1 Crystal data and structure refinement parameters of $[MeCd\{(SeP^iPr_2)_2N\}]_2$.

Compound	$[MeCd\{(SeP^iPr_2)_2N\}]_2$
emprical formula	$C_{26}H_{62}Cd_2N_2P_4Se_4$
formula weight	1067.30
temperature (K)	160(2)
crystal size (mm^3)	0.45 × 0.35 × 0.10
wavelength (Å)	0.71073
crystal system	Triclinic
Space group	$P\bar{1}$
a (Å)	a = 9.625(8)
b (Å)	b = 10.143(9)
c (Å)	c = 11.180(9)
α (°)	α = 103.44(8)
β (°)	β = 80.97 (9)
γ (°)	γ = 111.88(9)
volume ($Å^3$)	982.1(14)
Z	1
$density_{calcd}$ ($mg\ m^{-3}$)	1.805
abs. coeff., (mm^{-1})	4.971
F(000)	524
θ range (°)	1.88 to 24. 98
reflections collected	3715
independent reflections	3449 [R(int) = 0.0149]
max., min. transmission	0.6363 and 0.2132
data/restraints/pars.	3449/0/181
goodness-of-fit on F^2	1.038
R1, *w*R2 [$I>2\sigma(I)$]	R1 = 0.0283, wR2 = 0.0705
R1, *w*R2 (all data)	R1 = 0.0409, wR2 = 0.0745
diff. peak and hole ($e.Å^{-3}$)	0.951 and -1.260

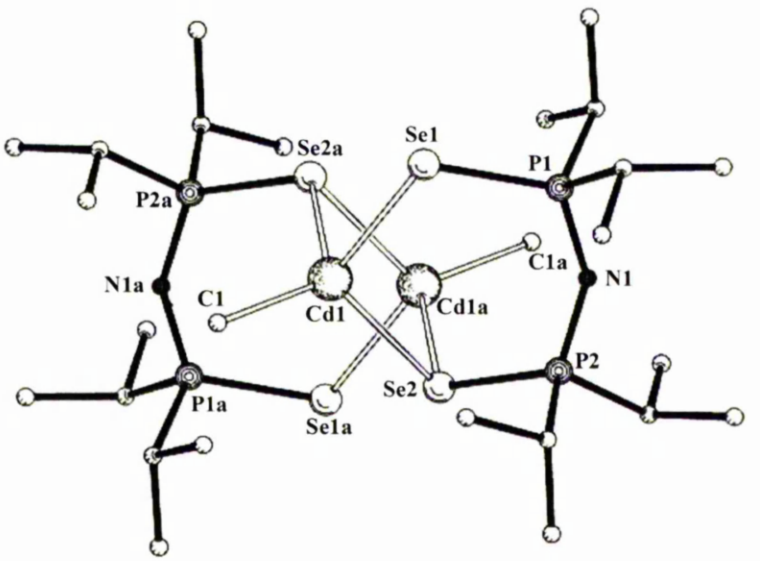

Figure 3.2 X-ray single crystal structure of $[MeCd\{(SeP^{i}Pr_2)_2N\}]_2$.

Table 3.2 Selected interatomic distances (Å) and angles (°) for $[MeCd\{(SeP^{i}Pr_2)_2N\}]_2$.

Cd(1)-C(1)	2.156(5)	Cd(1)-Se(2a)	2.934(2)
Cd(1)-Se(1)	2.672(3)	Se(1)-P(1)	2.171(3)
Cd(1)-Se(2)	2.703(3)	Se(2)-P(2)	2.210(3)
C(1)-Cd(1)-Se(1)	112.48(15)	Se(1)-Cd(1)-Se(2a)	96.86(8)
C(1)-Cd(1)-Se(2)	122.56(15)	Se(2)-Cd(1)-Se(2a)	89.68(8)
Se(1)-Cd(1)-Se(2)	109.61(10)	P(1)-Se(1)-Cd(1)	106.62(10)
C(1)-Cd(1)-Se(2a)	121.19(14)	P(2)-Se(2)-Cd(1)	100.01(9)

Table 3.3 Crystal data and structure refinement parameters of $[Zn((SePPh_2)_2N)_2]$ and $[Zn((SeP^iPr_2)_2N)_2]$.

Compound	$[Zn((SePPh_2)_2N)_2]$	$[Zn((SeP^iPr_2)_2N)_2]$
empirical formula	$C_{48}H_{40}N_2P_4Se_4Zn$	$C_{24}H_{56}N_2P_4Se_4Zn$
formula weight	1149.91	877.70
temperature (K)	433(2)	160(2)
crystal size (mm^3)	0.57 × 0.45 × 0.35	0.45 × 0.13 × 0.10
wavelength (Å)	0.71073	0.71073
crystal system	Triclinic	Triclinic
space group	$P\bar{1}$	$P\bar{1}$
a (Å)	13.727(7)	9.348(2)
b (Å)	13.809(5)	12.880(3)
c (Å)	14.3120(16)	16.389(4)
α (°)	82.74(9)	100.95(2)
β (°)	66.36(6)	102.02(2)
γ (°)	70.13(4)	69.94(2)
volume ($Å^3$)	2337.2(15)	1794.5(7)
Z	2	2
$density_{calcd}$ ($mg\ m^{-3}$)	1.6314	1.625
abs. coeff., (mm^{-1})	3.813	4.936
F(000)	1136	880
θ range (°)	1.55 to 25.10	1.28 to 24.98
reflections collected	8661	6877
independent reflections	8661	6313
max., min. transmission	0.3488 and 0.2178	0.6381 and 0.2148
data/restraints/pars.	8661/0/4392	6313/0/332
goodness-of-fit on F^2	0.982	0.873
R1, *w*R2 [$I>2\sigma(I)$]	0.0596, 0.1763	0.0297, 0.0745
R1, *w*R2 (all data)	0.0787, 0.1963	0.0592, 0.0866
diff. peak and hole ($e.Å^{-3}$)	1.939 and -3.706	0.545 and -0.482

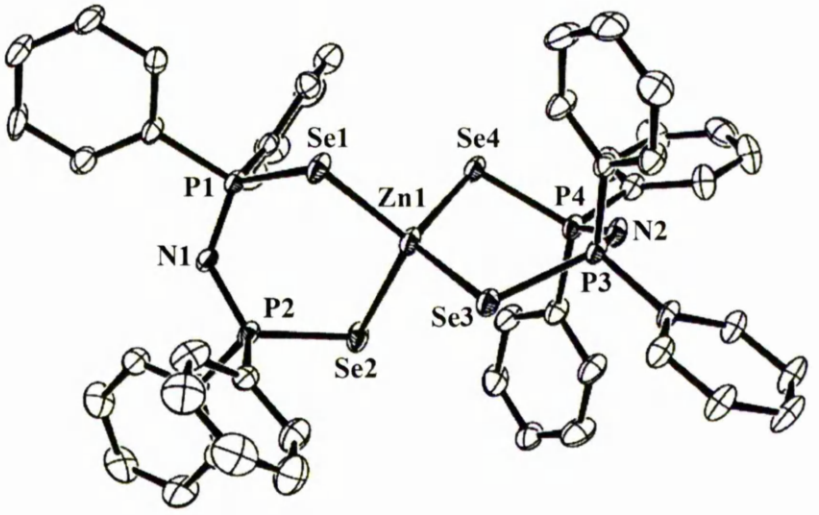

Figure 3.3 X-ray single crystal structure of $[Zn((SePPh_2)_2N)_2]$.

Table 3.4 Selected interatomic distances (Å) and angles (°) for of $[Zn((SePPh_2)_2N)_2]$.

Zn(1)-Se(3)	2.459(3)	Se(1)-P(1)	2.171(3)
Zn(1)-Se(4)	2.475(15)	Se(2)-P(2)	2.179(2)
Zn(1)-Se(1)	2.482(14)	Se(3)-P(3)	2.186(2)
Zn(1)-Se(2)	2.484(19)	Se(4)-P(4)	2.187(2)
Se(3)-Zn(1)-Se(4)	115.93(6)	Se(1)-Zn(1)-Se(2)	114.71(5)
Se(3)-Zn(1)-Se(1)	103.85(9)	P(1)-Se(1)-Zn(1)	94.11(7)
Se(4)-Zn(1)-Se(1)	111.35(8)	P(2)-Se(2)-Zn(1)	97.46(7)
Se(3)-Zn(1)-Se(2)	115.03(9)	P(3)-Se(3)-Zn(1)	102.22(7)
Se(4)-Zn(1)-Se(2)	106.10(9)	P(4)-Se(4)-Zn(1)	94.80(8)

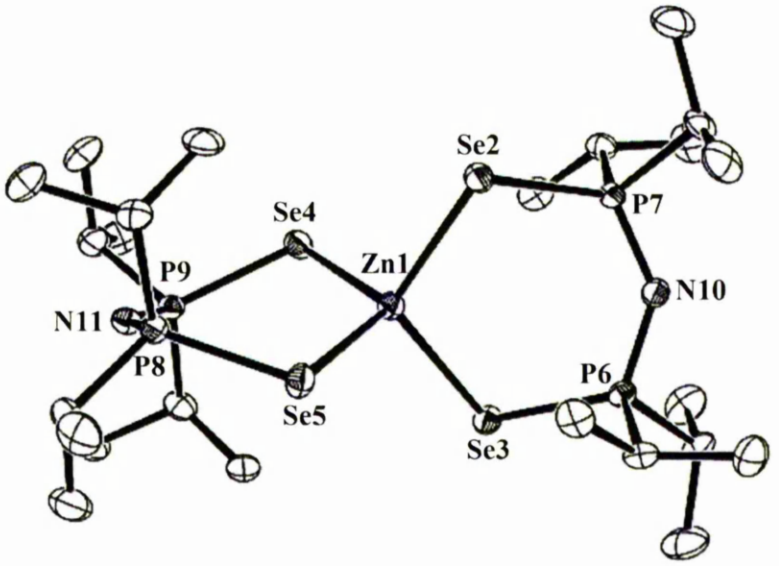

Figure 3.4 X-ray single crystal structure of $[Zn((SeP^{i}Pr_2)_2N)_2]$.

Table 3.5 Selected interatomic distances (Å) and angles (°) for of $[Zn((SeP^{i}Pr_2)_2N)_2]$.

Zn(1)-Se(2)	2.458(9)	Se(2)-P(7)	2.177(13)
Zn(1)-Se(5)	2.458(9)	Se(3)-P(6)	2.179(13)
Zn(1)-Se(4)	2.459(8)	Se(4)-P(9)	2.189(13)
Zn(1)-Se(3)	2.467(9)	Se(5)-P(8)	2.183(13)
Se(2)-Zn(1)-Se(5)	107.31(3)	Se(4)-Zn(1)-Se(3)	109.29(3)
Se(2)-Zn(1)-Se(4)	106.55(3)	P(7)-Se(2)-Zn(1)	103.30(4)
Se(5)-Zn(1)-Se(4)	114.07(3)	P(6)-Se(3)-Zn(1)	103.01(4)
Se(2)-Zn(1)-Se(3)	114.07(3)	P(9)-Se(4)-Zn(1)	102.83(4)
Se(5)-Zn(1)-Se(3)	106.36(3)	P(8)-Se(5)-Zn(1)	103.67(4)

3.4 - Deposition of Cadmium Selenide Thin Films

Cadmium selenide thin films were deposited using the following single-source precursors: $[Cd((SePPh_2)_2N)_2]$, $[Cd((SeP^iPr_2)_2N)_2]$ and $[MeCd\{(SeP^iPr_2)_2N\}]_2$. The volatility characteristics of the precursors were determined by thermogravimetric analyses (TGA) at atmospheric pressure and are shown in Fig. 3.5.

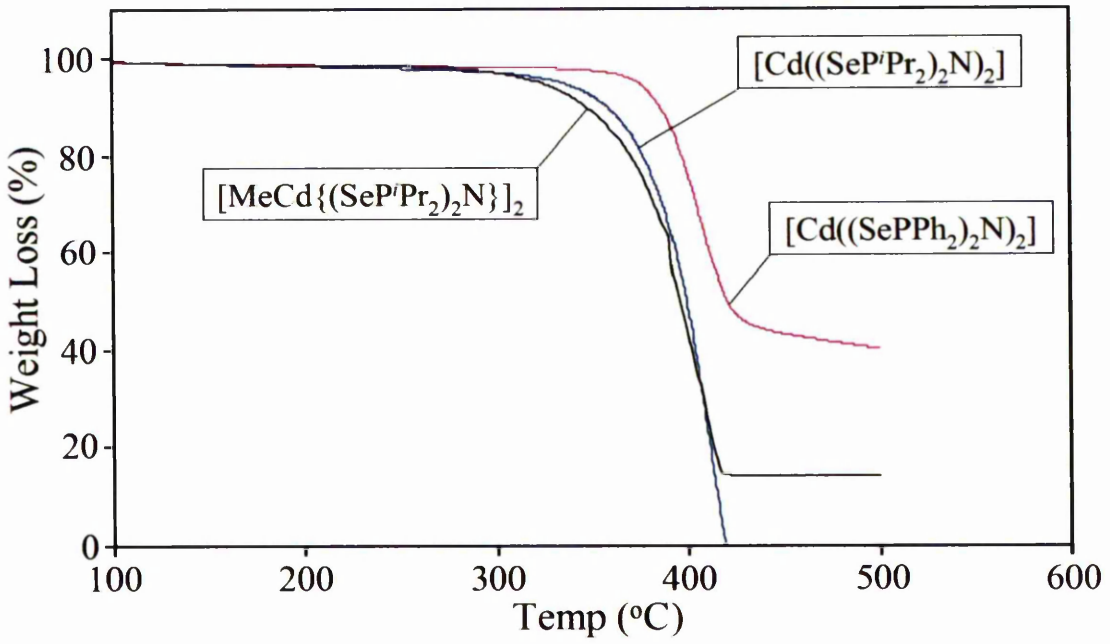

Figure 3.5 TGA analyses of cadmium compounds.

It can be seen that $[Cd((SeP^iPr_2)_2N)_2]$ sublimes cleanly between 332 – 420 °C without any residue which makes it a suitable single-source precursor for MOCVD studies, whereas the phenyl analogue begins to evaporate at higher temperature *ca.* 370 – 440 °C. $[MeCd\{(SeP^iPr_2)_2N\}]_2$ sublimes between 275 – 410 °C leaving *ca.* 14 % residue. The XRPD of the final residue obtained from pyrolysis of the compound indicated predominantly bulk hexagonal CdSe.

Deposition of cadmium selenide thin films was carried out by LP-MOCVD on glass substrates for 1 hour with *ca.* 200 mg of precursor used for each growth experiment. Table 3.6 shows experimental details for growing cadmium selenide thin films by LP-MOCVD.

Table 3.6 The experimental details of LP-MOCVD deposited films.

Precursor	Growth Temp (°C)	Source Temp (°C)	Description
$[Cd((SePPh_2)_2N)_2]$	475	375	No deposition observed
	500	375	Black, adherent non-uniform
	525	375	Black and adherent
$[Cd((SeP^iPr_2)_2N)_2]$	425	325	No deposition
	450	325	Very little deposition
	475	325	Black and adherent
	500	325	Black and adherent
$[MeCd[(SeP^iPr_2)_2N\}]_2$	400	285	No deposition observed
	425	285	Black, adherent and uniform
	450	285	Black, adherent and uniform
	475	285	Non-adherent, powdery and black

Table 3.7 shows X-ray results including *d*-spacing and relative intensities for cadmium selenide films grown from $[Cd((SePR_2)_2N)_2]$ (R = Ph, ^{i}Pr) and $[MeCd\{(SeP^iPr_2)_2N\}]_2$. It shows that the deposited films are consistent with hexagonal CdSe (JCPDS 08-0459).

Table 3.7 *d*-spacing and intensity profiles for hexagonal CdSe films.

	$[Cd((SePPh_2)_2N)_2]$		$[Cd((SeP^iPr_2)_2N)_2]$		$[MeCd\{(SeP^iPr_2)_2N\}]_2$	
JCPDS (08-0459) *d* (hkl) (%)	500 °C *d* (%)	525 °C *d* (%)	475 °C *d* (%)	500 °C *d* (%)	425 °C *d* (%)	450 °C *d* (%)
3.72 (100) (100)	3.72 (62)	3.73 (38)	3.72 (100)	3.72 (100)	N/A	3.71 (32)
3.51 (002) (70)	3.51 (100)	3.51 (21)	3.50 (12)	N/A	3.49 (100)	3.50 (100)
3.29 (101) (75)	3.29 (42)	3.29 (100)	3.28 (15)	3.28 (22)	N/A	3.29 (59)
2.55 (102) (35)	2.56 (18)	2.55 (26)	2.54 (3)	2.54 (1)	2.54 (1)	2.56 (29)
2.15 (110) (85)	2.15 (41)	2.15 (39)	2.14 (36)	2.15 (77)	N/A	2.15 (20)
1.98 (103) (70)	1.98 (45)	1.98 (55)	1.97 (5)	1.96 (1)	1.98 (6)	1.98 (44)

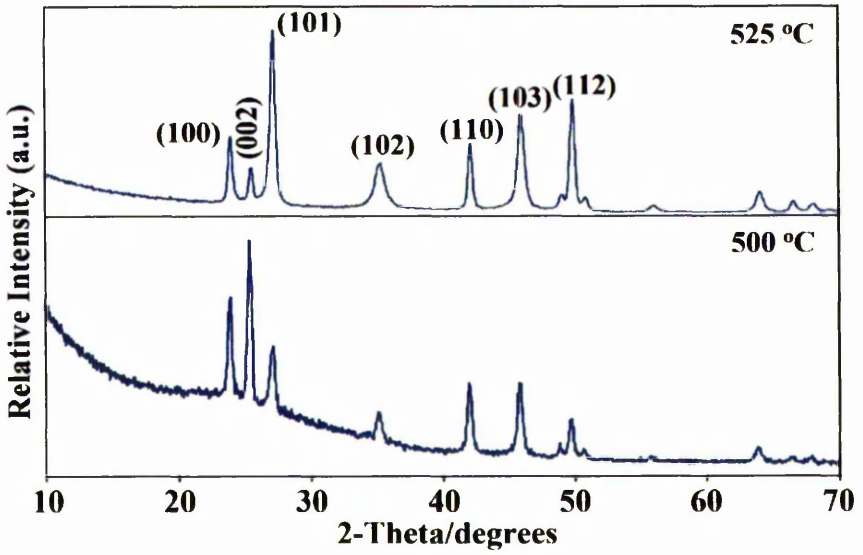

Figure 3.6 XRPD patterns of CdSe films deposited from $[Cd((SePPh_2)_2N)_2]$.

The XRPD patterns of films deposited from $[Cd((SePPh_2)_2N)_2]$ (Fig. 3.6) showed different preferred orientations [(002) *vs.* (101)] at 500 and 525 °C respectively. In contrast, CdSe films deposited from isopropyl moiety (Fig. 3.7) showed a different preferred orientation of (100). The growth of films was also observed at lower growth temperatures due to an increase in volatility between the phenyl- and the isopropyl-substituted diselenoimidodiphoshanto complex. The film deposited at 500 °C was slightly more orientated than the film grown at 475 °C, indicated by the absence of the (002) plane at 25.5° 2θ.

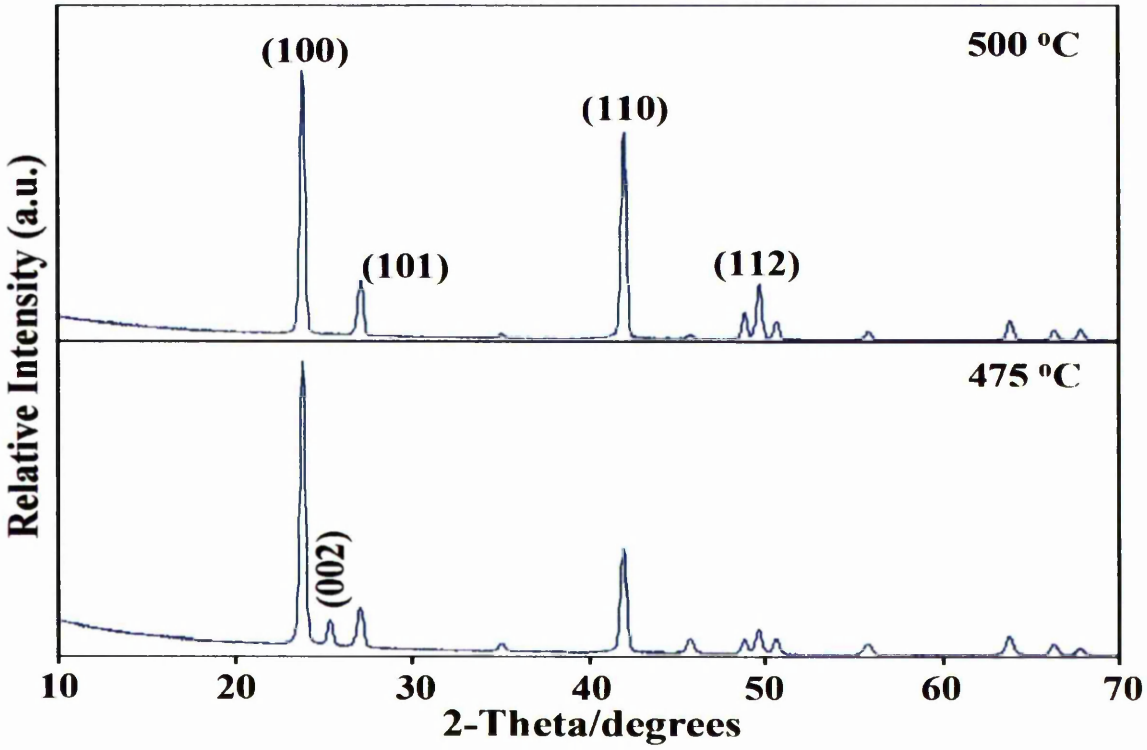

Figure 3.7 XRPD patterns of CdSe films deposited from $[Cd((SeP^iPr_2)_2N)_2]$.

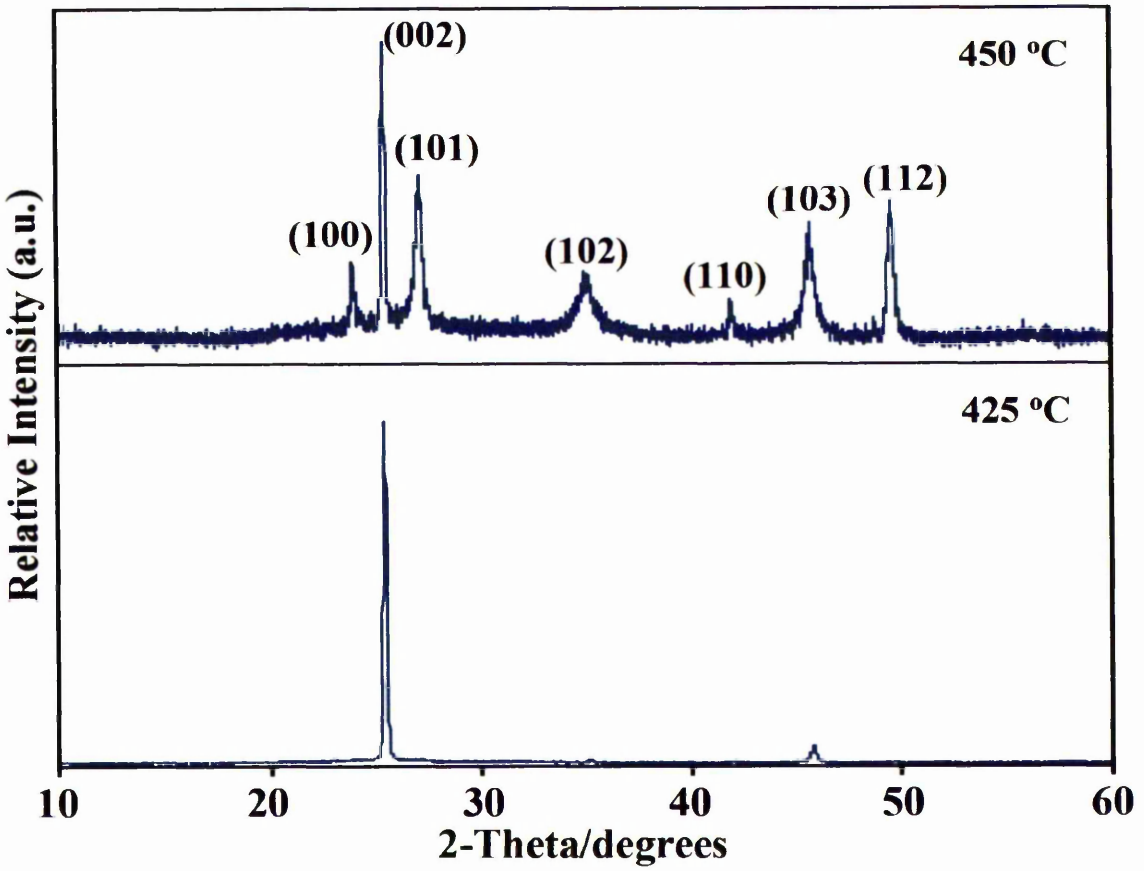

Figure 3.8 XRPD patterns of CdSe films deposited from $[MeCd\{(SeP^iPr_2)_2N\}]_2$.

The XPRD patterns of CdSe films deposited from the dimeric complex, $[MeCd\{(SeP^iPr_2)_2N\}]_2$ (Fig. 3.8) showed that a lower growth temperature (425 °C) results in a highly orientated polycrystalline film, in contrast to results obtained at a higher deposition temperature (450 °C). The film deposited at 475 °C was found to be amorphous as confirmed by XRPD.

3.5 - SEM and EDAX Studies of Cadmium Selenide Films

The SEM studies show that the morphologies of the as-deposited CdSe films depend on the growth temperatures. For example, film deposited at 525 °C from $[Cd((SePPh_2)_2N)_2]$ indicate a dense morphology and the surface displays clusters of platelets fused together giving a rice-like morphology. Cluster size was found to be *ca.* 1 μm. SEM image of the side profile of the film shows that the film is *ca.* 1 μm in thickness, thus giving a growth rate of *ca.* 1 $\mu m\ h^{-1}$ (Fig. 3.9).

The SEM analyses show that the film grown at 500 °C from $[Cd((SeP^iPr_2)_2N)_2]$ consists of randomly oriented platelets (*ca.* 1 µm in size) with a growth rate of *ca.* 3 µm h^{-1} (Fig. 3.10). Similar morphology is also observed for the films grown at 475 °C, although a lower growth rate of 1.75 $\mu m\ h^{-1}$ is observed. CdSe films grown from $[Cd((SeP^iPr_2)_2N)_2]$ exhibited a high degree of crystallinity hence indicating larger particle size and high deposition rate in comparison to CdSe films deposited from its phenyl analogue.

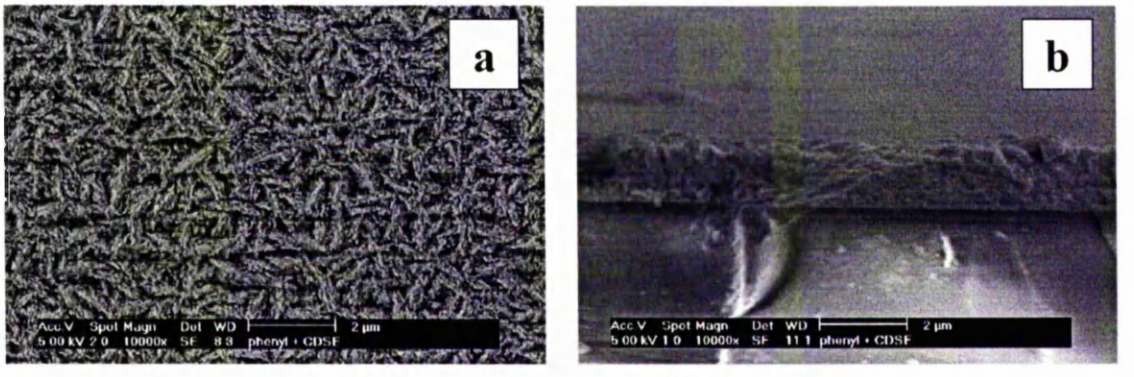

Figure 3.9 SEM images of CdSe films grown from $[Cd((SePPh_2)_2N)_2]$ at 525 °C; (a) top view, (b) cross-sectional view.

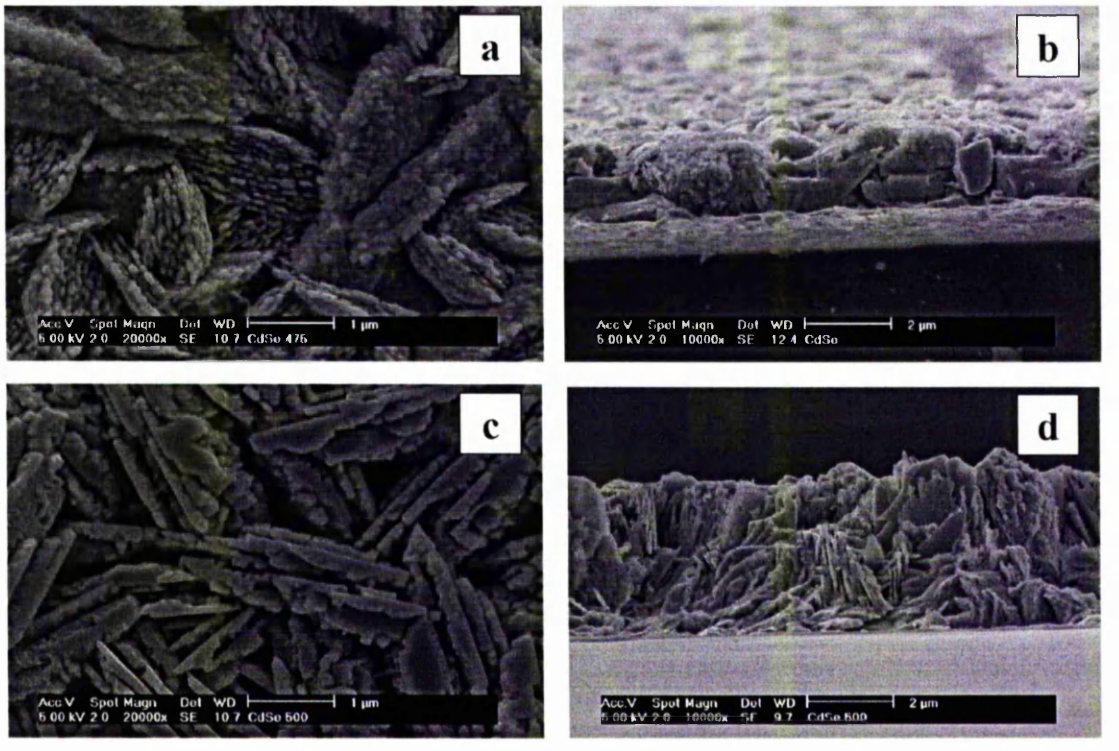

Figure 3.10 SEM images of CdSe films grown from $[Cd((SeP^{i}Pr_2)_2N)_2]$ (a) and (b) 475 °C; (c) and (d) 500 °C.

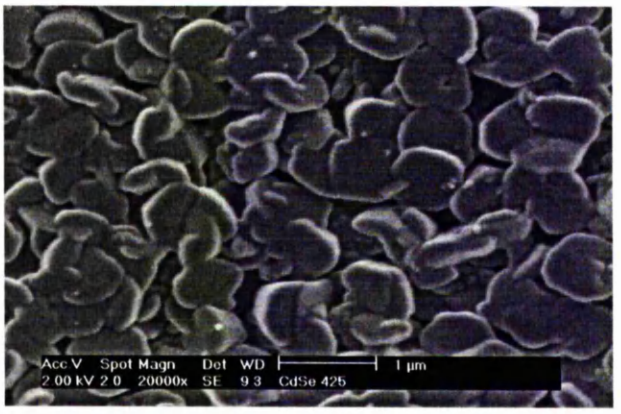

(a)

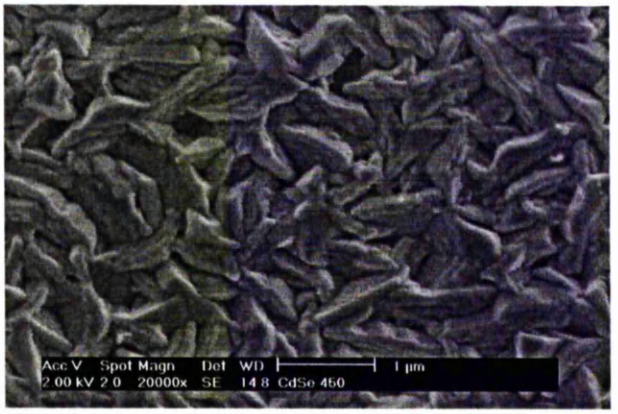

(b)

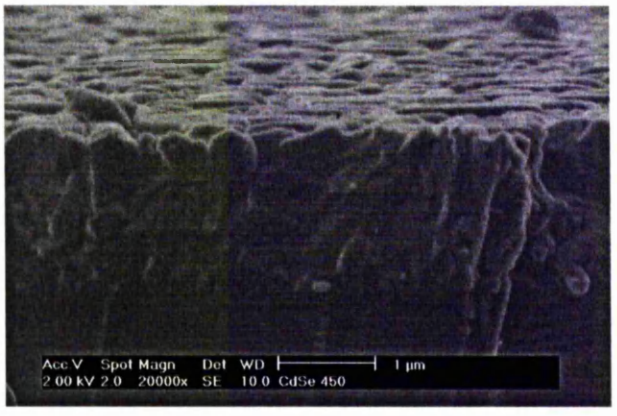

(c)

Figure 3.11 SEM images of CdSe films deposited from $[MeCd\{(SeP^{i}Pr_2)_2N\}]_2$ at (a) 425 ^{o}C, (b) 450 ^{o}C (top view) and (c) 450 ^{o}C (cross-sectional view).

The SEM studies of films deposited from $[MeCd\{(SeP^{i}Pr_2)_2N\}]_2$ indicate how the morphology of films changes with the growth temperature (Fig. 3.11). The morphology of the film grown at 425 °C consists of randomly orientated platelets. At 450 °C, the film shows randomly orientated flakes and the growth rate is found to be *ca.* 1.2 μm h^{-1}. The AFM analysis of the film deposited at 425 °C confirms hexagonal features of the film (Fig. 3.12).

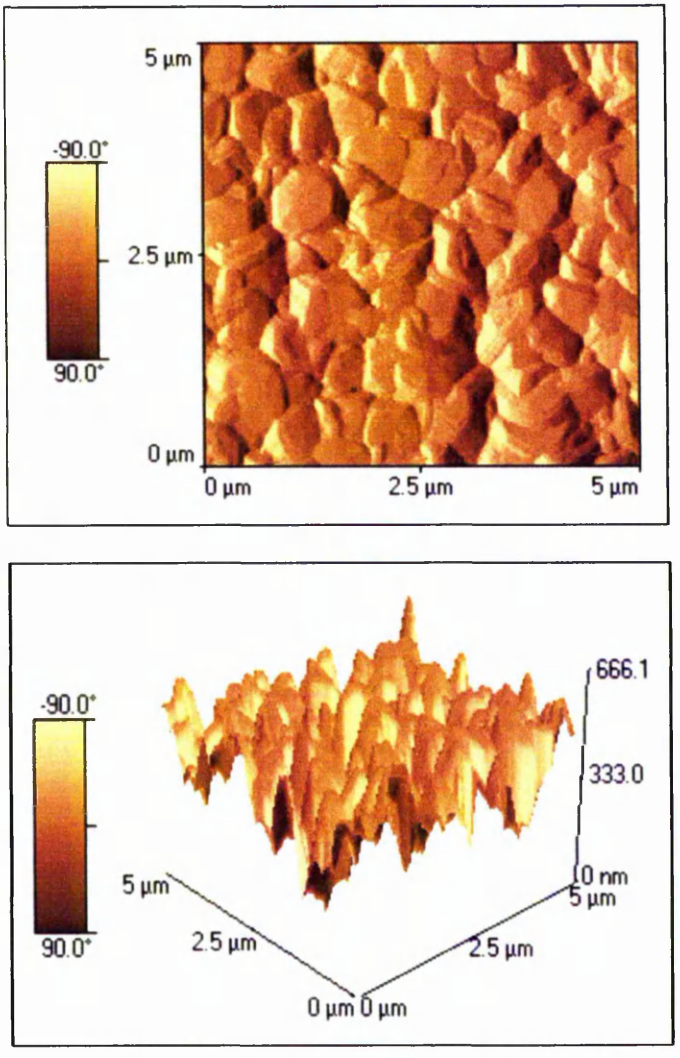

Figure 3.12 AFM images of CdSe films deposited on glass from $[MeCd\{(SeP^{i}Pr_2)_2N\}]_2$ at 425 °C.

The EDAX analyses of films grown from the complex, $[Cd((SePPh_2)_2N)_2]$ confirms the 1:1 stoichiometry of cadmium and selenium, but 1 % of phosphorus was also detected which was incorporated during the decomposition of the precursor [Fig. 3.13(a)]. Signals attributed to silicon and sodium were also evident and originated from the glass substrates. The EDAX analyses of films prepared from $[Cd((SeP^iPr_2)_2N)_2]$ at 500 °C indicate that the films are slightly selenium rich with 54 % and cadmium 46 % [Fig. 3.13(b)]. Un-assigned peaks are due to glass substrates. No phosphorus contamination was detected in the films. Similarly, EDAX analysis of films deposited at 425 °C from $[MeCd\{(SeP^iPr_2)_2N\}]_2$ also indicated the formation of selenium rich films (52 %) and cadmium (48 %).

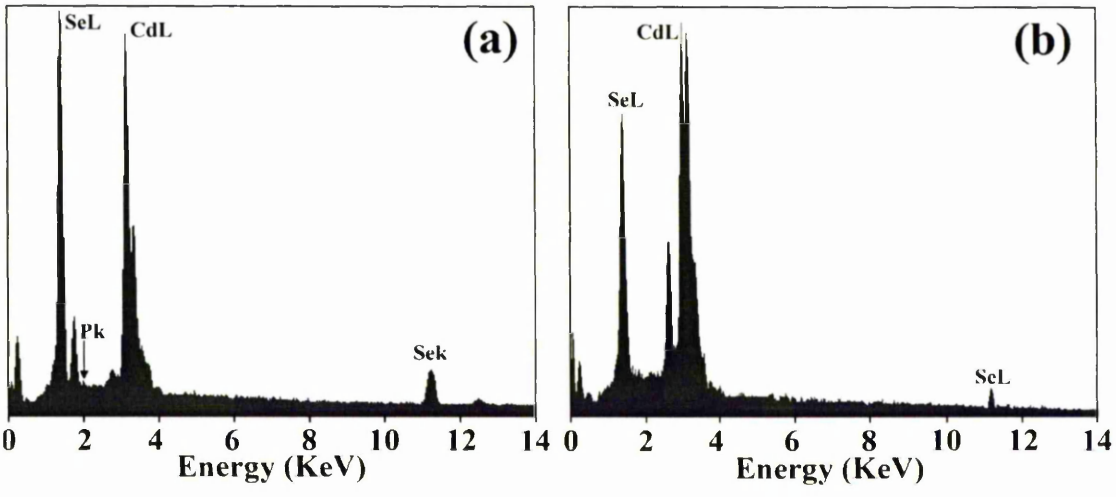

Figure 3.13 EDAX analysis of (a) $[Cd((SePPh_2)_2N)_2]$ and (b) $[Cd((SeP^iPr_2)_2N)_2]$.

X-ray photoelectron spectroscopy (XPS) was also employed to determine the photoelectron binding energies of the elements comprising the films grown at 425 °C from mixed-alkyl cadmium complex. Survey scans before and after ion etching process showed that the spectrum of the sample before etching is found to be a typical oxidized surface as indicated by the O 1s core-level signal, which vanished after the etching

process. The carbon peak was also minimized after etching. Figs. 3.14 and 3.15 show the high-resolution spectra of Cd and Se regions of the film. The peaks obtained before and after etching are not significantly different in terms of their binding energies and intensities. In the case of Cd, the Cd $3d_{5/2}$ peak ranged from 408.8 to 406.6 eV. In the Se case, the Se $3d_{5/2}$ peak ranged from 51.9 to 55.6 eV. Relative atomic percentages of cadmium and sulfur were found to be slightly variable depending on etching treatment (1:1.09 before etching and 1.04:1 after etching). No phosphorus contamination was detected in the film.

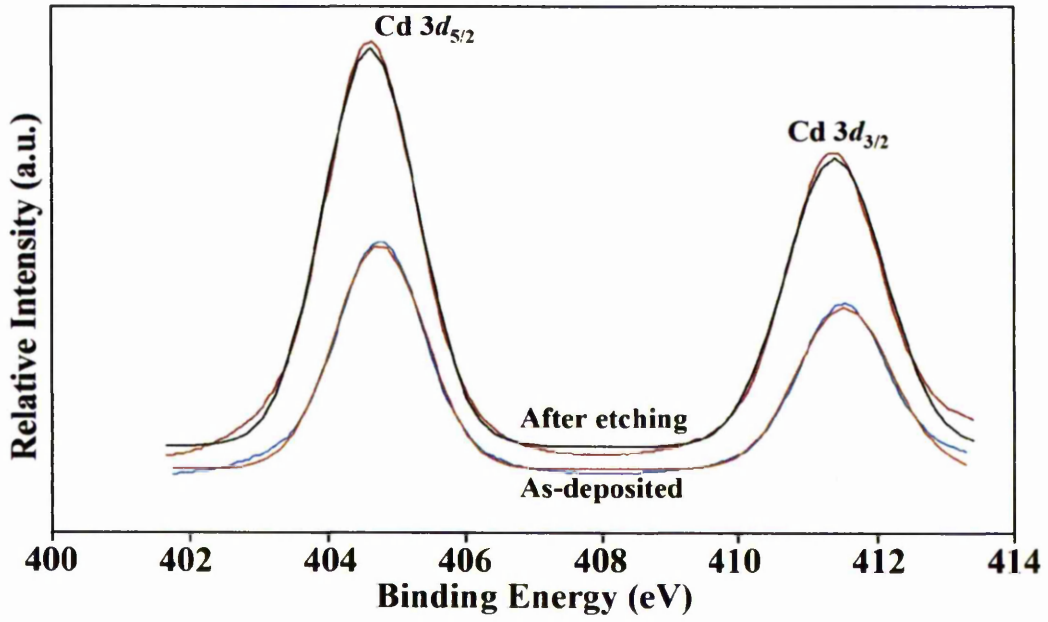

Figure 3.14 XPS spectrum of Cd 3*d* peaks of a CdSe film.

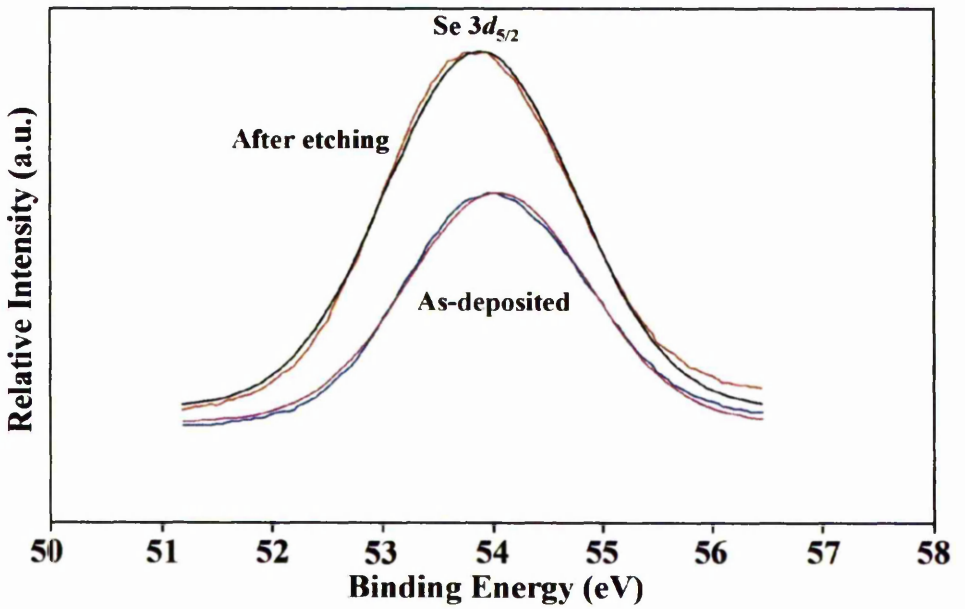

Figure 3.15 XPS spectrum of Se 3*d* peaks of a CdSe film.

3.6 - Deposition of Zinc Selenide Thin Films

Deposition of zinc selenide thin films was carried out using $[Zn((SePR_2)_2N)_2]$ (R = Ph, ^{i}Pr) as single-source precursors. Deposition of thin films was carried out by LP-MOCVD on glass substrates for one hour with *ca.* 200 mg of precursor used for each growth experiment. The volatility characteristics of the precursors were studied by TGA at atmospheric pressure which showed that $[Zn((SeP^iPr_2)_2N)_2]$ decomposes cleanly without any residues between 250 – 366.2 °C, whereas the phenyl analogue decomposes at higher temperature. Both zinc complexes decompose in the same manner to those observed for the cadmium complexes, $[Cd((SePR_2)_2N)_2]$ (R = Ph, ^{i}Pr).

Zinc selenide thin films were deposited at growth temperatures of 500 and 525 °C from $[Zn((SePPh_2)_2N)_2]$ maintaining precursor temperature at 375 °C. Attempts to deposit ZnSe films from $[Zn((SeP^iPr_2)_2N)_2]$ were made over a range of substrate temperatures (400 – 500 °C) but the optimum growth temperature appeared to be between 425 – 450 °C with precursor temperature at 275 °C. The-deposited films were dark orange, transparent and well-adherent to the glass substrate (Scotch - tape test).

Table 3.8 *d*-spacing and intensity profiles for hexagonal ZnSe on the glass substrates from $[Zn((SePPh_2)_2N)_2]$and $[Zn((SeP^iPr_2)_2N)_2]$.

	$[Zn((SePPh_2)_2N)_2]$		$[Zn((SeP^iPr_2)_2N)_2]$	
JCPDS (15-0105)	500 °C	525 °C	425 °C	450 °C
d (hkl) (%)	*d* (%)	*d* (%)	*d* (%)	*d* (%)
3.43 (100) (100)	3.48 (55)	3.47 (48)	3.45 (100)	3.45 (97)
3.25 (002) (90)	3.28 (100)	3.29 (100)	3.29 (91)	3.28 (91)
3.05 (101) (70)	3.07 (28)	3.08 (27)	N/A	3.07 (33)
2.00 (110) (100)	2.01 (41)	2.01 (29)	2.00 (36)	2.00 (100)
1.70 (112) (70)	1.71 (30)	1.71 (19)	1.71 (23)	1.85 (13)
1.35 (203) (60)	1.36 (1)	1.36 (2)	N/A	1.71 (42)

Table 3.8 shows X-ray results indicating *d*-spacing and relative intensities for zinc selenide films grown from $[Zn((SePPh_2)_2N)_2]$ and $[Zn((SeP^iPr_2)_2N)_2]$. The values are indexed to hexagonal ZnSe films (JCPDS 15-0105). Films deposited from $[Zn((SeP^iPr_2)_2N)_2]$ show a preferred orientation along the (002) plane (Figs. 3.16 and 3.17). The crystallinity of ZnSe films deposited from $[Zn((SeP^iPr_2)_2N)_2]$ also depends on the growth temperatures. At higher growth temperature (450 °C), the crystallinity of the deposited film is significantly improved as indicated by the sharpness of XRPD pattern. Similarly, zinc selenocarbamate complexes, $[MeZnSe_2CNEt_2]_2$ and $[EtZnSe_2CNEt_2]_2$ also lead to deposition of hexagonal ZnSe thin films.[31] However, $[Zn(Se_2CNMe^nHex)_2]$ gave cubic ZnSe with a preferred (111) orientation.[32]

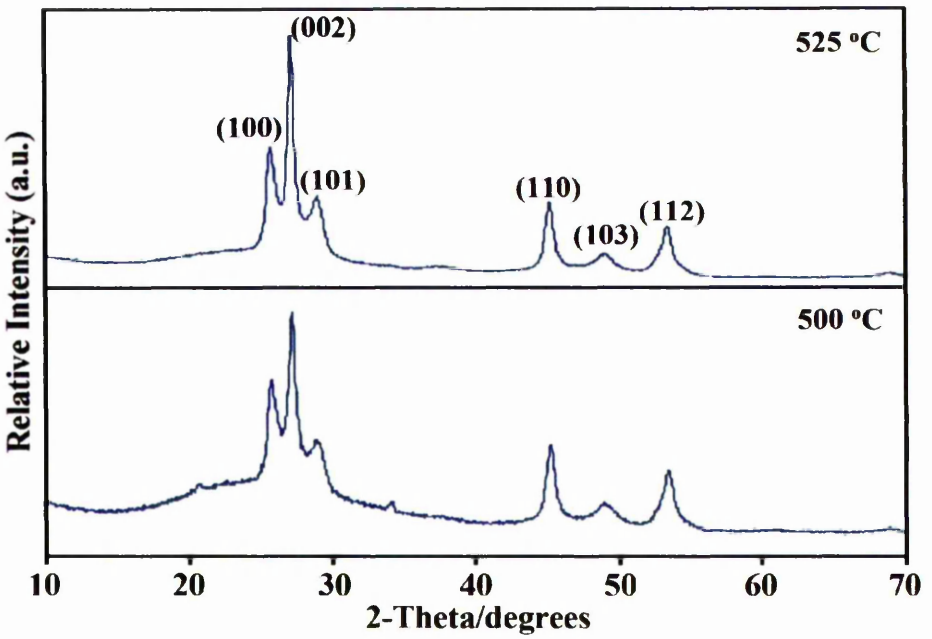

Figure 3.16 XRPD patterns of ZnSe films deposited from $[Zn((SePPh_2)_2N)_2]$.

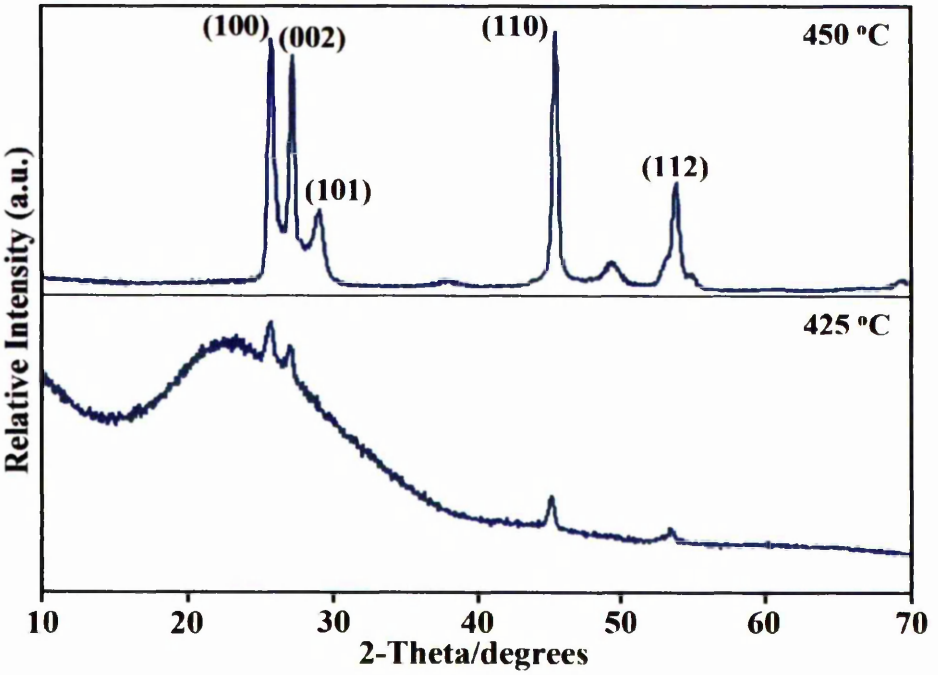

Figure 3.17 XRPD patterns of ZnSe films deposited from $[Zn((SeP^iPr_2)_2N)_2]$.

The SEM analysis (Fig. 3.18) of ZnSe film grown at 525 °C from $[Zn((SePPh_2)_2N)_2]$ shows that the film has a featureless nanocrystalline morphology on the glass substrate and is fully dense. In 1 hour of growth, a film *ca.* 1.2 μm thick was deposited. However, the formation of hillock was also found on the ZnSe layer, possibly due to slight variation of deposition temperature or different thermal expansion between ZnSe and glass substrate. At 500 °C, the film exhibited a poor morphology.

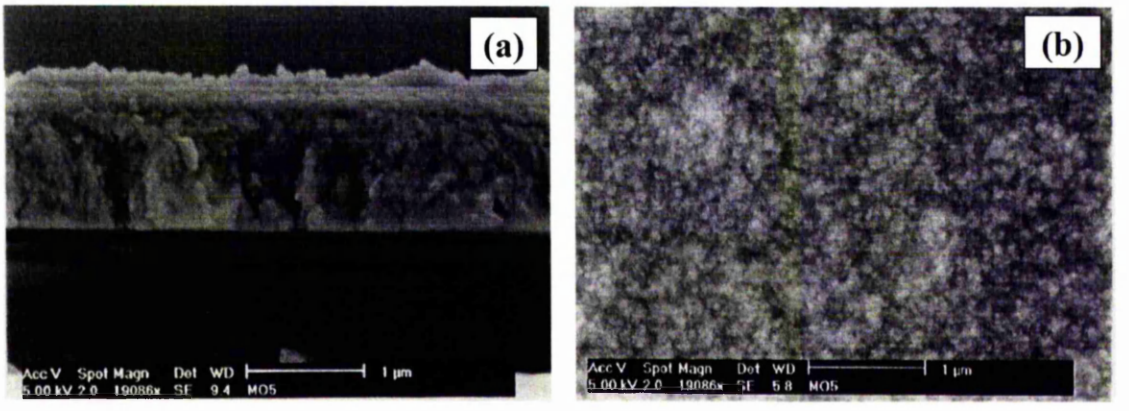

Figure 3.18 SEM images of ZnSe films from $[Zn((SePPh_2)_2N)_2]$ at 525 °C; (a) cross-sectional view and (b) top view.

The SEM micrographs for the film deposited from $[Zn((SeP^iPr_2)_2N)_2]$ at 450 °C on glass consists of well-defined, randomly orientated particles, with an average size of *ca.* 0.5 μm (Fig. 3.19). In 1 hour growth, film with *ca.* 2 μm thickness has been deposited. In contrast, film deposited at 425 °C had platelike morphologies with the plates laid down horizontally with respect to the glass surface.

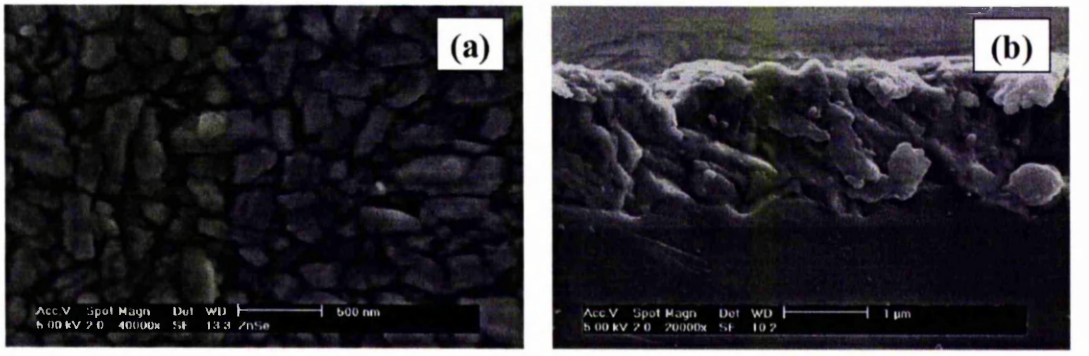

Figure 3.19 SEM images of ZnSe films from $[Zn((SeP^{i}Pr_2)_2N)_2]$ at 450 °C; (a) cross-sectional view and (b) top view.

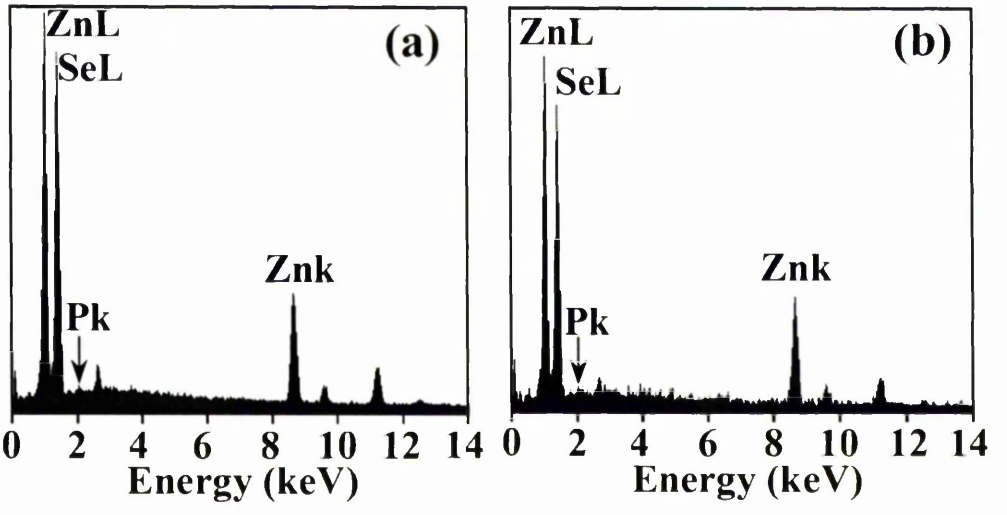

Figure 3.20 EDAX spectra of ZnSe films from (a) $[Zn((SePPh_2)_2N)_2]$and (a) $[Zn((SeP^{i}Pr_2)_2N)_2]$ on glass substrates.

The EDAX analyses of ZnSe films deposited from $[Zn((SePR_2)_2N)_2]$ (R = Ph, ^{i}Pr) (Fig. 3.20) confirm that as-deposited ZnSe films are close to stoichiometric ZnSe. However, traces of phosphorus (*ca.* 2 %) were also detected in both cases. Unassigned peaks are due to reflections from the glass substrate.

The band gaps of as-deposited CdSe and ZnSe thin films have been determined by direct band gap method (Figs. 3.21 and 3.22). Extrapolation of the linear region of the

absorption profile provided values of 1.73 eV for CdSe and 2.62 eV for ZnSe which are similar to the literature values.[33]

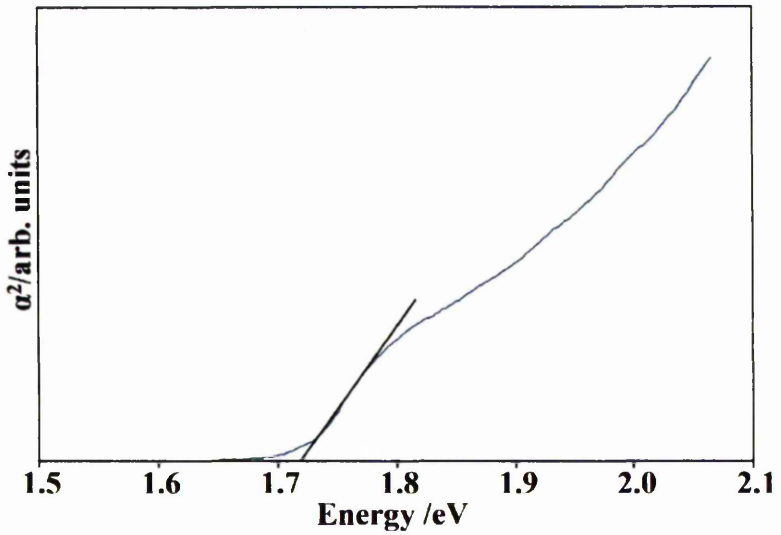

Figure 3.21 UV/Vis spectrum CdSe film deposited from $[Cd((SeP^{i}Pr_2)_2N)_2]$.

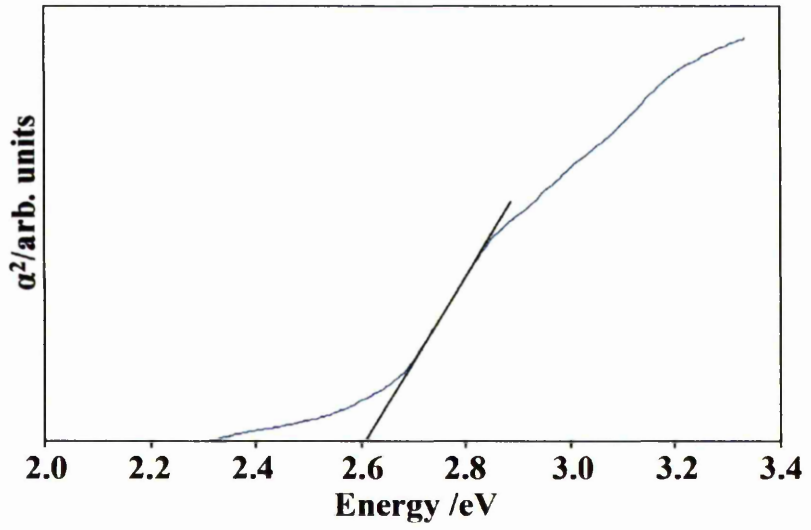

Figure 3.22 UV/Vis spectrum ZnSe film deposited from $[Zn((SeP^{i}Pr_2)_2N)_2]$.

3.7 – Conclusions

$[M((SePR_2)_2N)_2]$ (M = Cd(II), Zn(II); R = Ph, ^{i}Pr) have been synthesized and used as single-source precursor for the deposition of CdSe and ZnSe films by LP-MOCVD. X-ray single crystal structures of $[Zn((SePR_2)_2N)_2]$ (R = Ph, ^{i}Pr) indicated distorted tetrahedral geometry around the zinc atoms. The XRPD analyses of all the as-deposited materials indicate the growth of hexagonal films regardless of growth temperatures. Mixed-alkyl cadmium compound, $[MeCd\{(SeP^iPr_2)_2N\}]_2$ also has been synthesized and its X-ray single structure determined. This complex proved to be suitable for the growth of CdSe films at comparatively low temperatures.

References

1. D. Bruce, D. O'Hare, *Inorganic Materials,* Wiley, London, **1997**, 523.
2. I. G. Dance, R. G. Garbutt, D. C. Craig, M. L. Scudder, *Inorg. Chem.*, **1987**, *26*, 3732.
3. I. G. Dance, R. G. Garbutt, D. C. Craig, M. L. Scudder, *Inorg. Chem.*, **1987**, *26*, 4057.
4. I. G. Dance, R. G. Garbutt, M. L. Scudder, *Inorg. Chem.*, **1990**, *29*, 1571.
5. M. B. Hursthouse, O. F. Z. Khan, M. Mazid, M. Motevalli, P. O'Brien, *Polyhedron*, **1990**, *9*, 541.
6. F. Z. Khan, P. O'Brien, *Polyhedron*, **1991**, *10*, 325.
7. M. Bochmann, K. J. Webb, M. Harman, M. B. Hursthouse, *Angew. Chem. Int., Ed. Engl.,* **1990**, *29*, 638.
8. M. Bochmann, K. J. Webb, M. B. Hursthouse, M. Mazid, *J. Chem. Soc., Dalton Trans.,* **1991**, 2317.
9. V. N. Semyonow, E. M. Averbach, L. A. Michalyeva, *Zh. Neorg. Khim.*, **1979**, *24*, 911.
10. M. Krunks, E. Mellikov, E. Sork, *Thin Solid Films*, **1986**, *145*, 105.
11. Y. Takahashi, R. Yuki, M. Sugiura, S. Motojima, K. Sugiyama, *J. Cryst. Growth*, **1980**, *50*, 491.
12. M. A. H. Evans, J. O. Williams, *Thin Solid Films*, **1982**, *87*, L1.
13. G. C. Bwembya, X. Song. M. Bochmann, *Chem. Vap. Deposition*, **1995**, *1*, 78.
14. A. N. Gleizes, *Chem. Vap. Deposition*, **2000**, *6*, 155.

15. B. O. Dabbousi, P. J. Bonasia, J. Arnold, *J. Am. Chem. Soc.*, **1991**, *113*, 3186.

16. P. J. Bonasia, J. Arnold, *Inorg. Chem.*, **1992**, *31*, 2508.

17. M. Bochmann, K. J. Webb, *J. Chem. Soc., Dalton Trans.*, **1991**, 2325.

18. R. Nomura, T. Murai, T. Toyosaki, H. Matsuda, *Thin Solid Films*, **1995**, *271*, 4.

19. M. B. Hursthouse, M. A. Malik, M. Motevalli, P. O'Brien, *Polyhedron*, **1992**, *11*, 45.

20. M. Motevalli, P. O'Brien, J. R. Walsh, I. M. Watson, *Polyhedron*, **1996**, *15*, 2801.

21. M. Chunggaze, M. A. Malik, P. O'Brien, *J. Mater. Chem.*, **1999**, *10*, 2433.

22. M. B. Hursthouse, M. A. Malik, M. Motevalli, P. O'Brien, *Organometallics*, **1991**, *10*, 730.

23. M. A. Malik, M. Motevalli, J. R. Walsh, P. O'Brien, *Organometallics*, **1992**, *11*, 3136.

24. M. B. Hursthouse, M. A. Malik, M. Motevalli, P. O'Brien, *J. Mater. Chem.*, **1992**, *2*, 949.

25. M. Nyman, M. J. Hampden-Smith, E. Duesler, *Chem. Vap. Deposition*, **1996**, *2*, 171.

26. V. Garcia-Montalvo, J. Novosad, P. Kilian, J. D. Woollins, A. M. Z. Slwain, P. G. Y. Garcia, M. Lopez-Cardoso, G. Espinosa-Perez, R. Cea-Olivares, *J. Chem. Soc., Dalton Trans.*, **1997**, 1025.

27. D. Cupertino, D. J. Birdsall, A. M. Z. Slawin, J. D. Woollins, *Inorg. Chem. Acta,* **1999**, *290*, 1.

28. I. Abrahams, M. A. Malik, M. Motevalli, P. O'Brien, *J. Organomet. Chem.*, **1994**, *465*, 73.

29. M. J. Henderson, R. Papasergio, C. L. Raston, A. H. White, M. F. Lappert, *J. Chem. Soc., Chem. Commun.*, **1986**, 672; G. W. Bushnell, S. R. Stobart, *Can. J. Chem.*, **1980**, *58*, 672.

30. D. Cupertino, R. Keyte, A. M. Z. Slawin, D. J. Williams, J. D. Woollins, *Inorg. Chem.*, **1996**, *35*, 2695.

31. M. A. Malik, P. O'Brien. *Chem. Mater.*, **1991**, *3*, 999.

32. M. Chunggaze, J. McAleese, P. O'Brien, D. J. Otway, *J. Chem. Soc., Chem. Commun.*, **1998**, 833.

33. J. I. Pankove, *Optical processes in semiconductors*, Dover Publications Inc., New York, **1970**, 1327.

Chapter IV

Gallium and Indium Chalcogenide Materials

Summary:

The syntheses and characterisations of the mixed alkyl/dialkylselenophosphorylamides, $[Me_2Ga(SeP^iPr_2)_2N]$ and $[R_2In(SeP^iPr_2)_2N]$ (R = Me, Et) are reported together with the X-ray single crystal structures of $[Me_2M(SeP^iPr_2)_2N]$ (M = Ga (III) or In (III)) which have Se_2C_2 coordination at the metal centers. These compounds have been used as single-source precursors for the deposition of metal (Ga, In) selenide films on glass substrates by MOCVD processes.

4.1 - Introduction

Thin films of III-VI materials are potential alternatives to II-VI materials in optoelectronic and photovoltaic devices,[1,2] and also have a potential application as passivating layers for III-V devices.[3] In addition, there are also important and related ternary and quaternary phases such as $CuInE_2$ and $CuIn_{1-x}Ga_xE_2$ (E = S, Se) with uses in solar cells.[1]

The first attempts to grow III-VI materials were reported by Nomura and co-workers who proposed the alkylindium chalcogenides [$In^iBu_2(S^nPr)$] and [$In^nBu_2(S^nPr)$], which are both liquid at room temperature, as single-source precursors for the deposition of indium sulfide.[4] They deposited β-In_2S_3 thin films from [$In^nBu_2(S^nPr)$] by LP-MOCVD at 300 – 400 °C on Si(100) and quartz substrates.[5] Gysling *et al.* prepared indium selenide films on GaAs(100) by spray-assisted MOCVD using a toluene solution of either [$In(SePh)_3$] or [$In\ Me_2(SePh)$].[6] Different phases of InSe were grown at different substrate temperatures, with a cubic phase observed at deposition temperatures between 310 – 365 °C. Pyrolysis of [$In(SePh)_3$] gave hexagonal films of In_2Se_3 at 470 – 530 °C. A new selenium rich cubic phase, In_2Se_3 has been grown using $In[SeC(SiMe_3)_3]_3$ as the precursor.[7]

Barron *et al.* have suggested that molecular design can play an important and direct role in determining the nature of thin films deposited from single-source precursors. Using cubane-type *tert*-butylgallium sulfide [^{t}BuGaS]$_4$ (Fig. 4.1) in an atmospheric pressure MOCVD experiment, a new metastable cubic GaS film is deposited on both KBr and GaAs and on the latter a degree of epitaxial growth is observed.[8] The films have a high band gap (Eg > 3.0 eV) and are highly insulating (> 2×10^9 Ω cm).

They also used the dimeric thiolato complex, $[Ga^tBu_2(S^tBu)]_2$, to deposit poorly crystalline hexagonal films of GaS.[9] They suggested that the formation of cubic GaS is influenced by the cubic nature of the core of $[^t BuGaS]_4$ precursor which is maintained throughout deposition (Fig. 4.1).

The hypothesis that molecular structure can influence the phase morphology of as-deposited films was further investigated with the analogous cubane selenide and telluride precursors $[GaR\text{-}(\mu_3\text{-}E)]_4$ (E = Se, Te; R = CMe_3, $CEtMe_2$, CEt_2Me, Et_3C).[10,11] Hexagonal phases of GaSe and GaTe were deposited by AP-MOCVD and LP-MOCVD, respectively. A similar decomposition pathway for selenium and tellurium compounds is predicted as for $[^t BuGaS]_4$.[12] Indium chalcogenide cubane structures have also been reported with $[^t BuInSe]_4$ yielding only indium metal films by LP-MOCVD.[13] By contrast, $[(Me_2EtC)InSe]_4$ deposited hexagonal InSe by LP-MOCVD between 290 – 350 °C.[14]

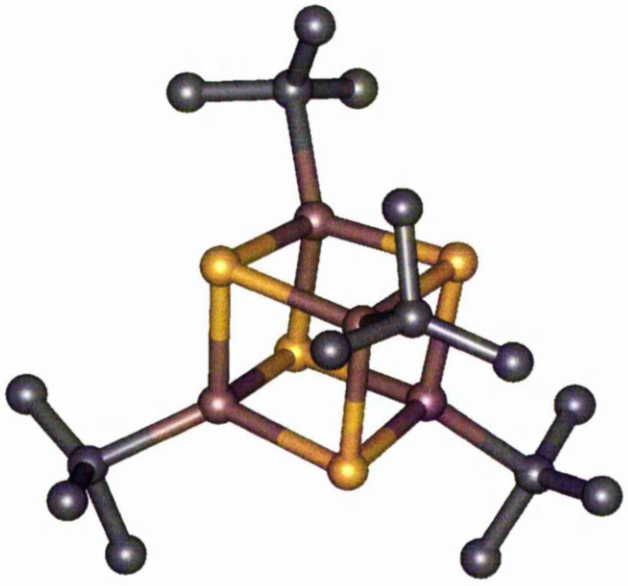

Figure 4.1 X-ray single crystal structure of $[^t BuGaS]_4$.[12]

O'Brien and co-workers have deposited III-VI thin films from alkyl metal dithiocarbamates,[15] and dialkyldichalcogenocarbamates.[16,17] Indium sulfide thin films have been deposited on GaAs(100) substrates by LP-MOCVD using $[R_2In(S_2CNEt_2)]$ (R = Me, Et, Np), which are air-sensitive compounds. However, the gallium precursor $[Me_2Ga(S_2CNEt_2)]$ proved to be less effective for the growth of gallium sulfide thin films. Complexes of indium $[In(E_2CN(Me)R)_3]$ (E = S, Se; R = ^{n}Bu, ^{n}Hex)[16,17] have also been used to grow indium sulfide/selenide thin films. In a similar way, α-Ga_2S_3 thin films have been deposited on GaAs(100) at 500 °C by LP-MOCVD using $[Ga(S_2CNMe^nHex)_3]$.[18]

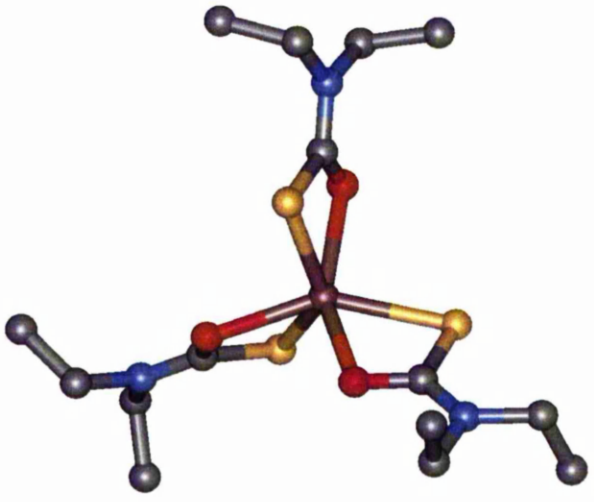

Figure 4.2 X-ray single crystal structure of $[In(SOCNEt_2)_3]$.[22]

Other reports of single-source precursors for group 13 chalcogenides have been based on dithiocarbonates, monothiocarbamates and monothiocarboxylates.[19] Bessergenev *et al.* have reported the growth of cubic α-In_2S_3 materials on glass substrates by LP-MOCVD using $[In(S_2CO^iPr)_3]$.[20] Examples of monothiocarbamates include $[In(SOCNEt_2)_3]$,[21] $[In(SOCN^iPr_2)_3]$[22] and $[Ga(SOCNEt_2)_3]$.[23] β-In_2S_3 thin films have been

produced from $[In(SOCNEt_2)_3]$ (Fig. 4.2) and $[In(SOCN^iPr_2)_3]$ on glass substrates by LP-MOCVD, with the isopropyl complex being more volatile. $[Ga(SOCNEt_2)_3]$ led to formation of cubic GaS films which are similar to films grown by Barron and co-workers.[12] Gallium thiocarboxylate compounds such as $[Ga(SCOMe)_2(CH_3)$-(dmp)] and $[GaMe(SCOMe)_2(dmp)]$ (dmp = 3,5-dimethylpyridine)[24] and an indium ionic complex,[25] $[Hdmp]^+[In(SCOCH_3)_4]^-$ have been used in AACVD experiments to deposit α-Ga_2S_3 and β-In_2S_3 films. This study is notable mainly as the deposited films were prepared below 300 °C.

In the present work, the syntheses of $[R_2In(SeP^iPr_2)_2N]$ (R = Me, Et) and $[Me_2Ga(SeP^iPr_2)_2N]$ have been carried out and solid-state structures of $[Me_2M(SeP^iPr_2)_2N]$ (M = In(III), Ga(III)) are reported. Furthermore, the growth of gallium selenide and indium selenide thin films from synthesized compounds by LP-MOCVD and AACVD are also discussed.

4.2 - Synthesis of Precursors

The compounds $[R_2In(SeP^iPr_2)_2N]$ (R = Me, Et) and $[Me_2Ga(SeP^iPr_2)_2N]$ have been prepared using 1:1 stoichiometric amounts of $[NH(SeP^iPr_2)_2]$ and group 13 metal alkyls in anhydrous toluene. The synthesis of $[NH(SeP^iPr_2)_2]$ has been described in experimental section. The acidic nature of the amino proton in the ligand makes it a good candidate for alkane elimination reactions towards group 13 metal alkyls. All the compounds are soluble in common organic solvents and are fairly stable but were stored under nitrogen at 5 °C to avoid any decomposition.

The first indication of complexation of ligand through alkane elimination is observed by the absence of N-H resonance in ^1H NMR at 3.10 ppm. For

$[Me_2In(SeP^iPr_2)_2N]$, the methyl resonance is found at *ca.* $\delta = 0.47$ ppm which is similar to the methyl resonance observed for the gallium complex (*ca.* $\delta = 0.60$ ppm). The compound, $[Et_2In(SeP^iPr_2)_2N]$ shows a quartet at $\delta = 1.25$ ppm and triplet at $\delta = 1.65$ ppm, as expected for the equivalent ethyl groups (Fig. 4.3). The EI-MS spectra of all the compounds show a molecular ion peak relating to the molecular mass of the compound. All the compounds gave satisfactory elemental analyses.

The TGA of $[Me_2Ga(SeP^iPr_2)_2N]$ shows that the precursor sublimes in one step between 175 – 400 °C leaving *ca.* 35 wt % final residue at atmospheric pressure. The brown colored residue obtained from the pyrolysis of the compound was analyzed by XRPD, however the pattern was not definative. The broad peaks in the pattern could be tentatively cubic Ga_2Se_3. The EDAX analysis was also consistent with the comparative Ga_2Se_3. The TGA of $[Me_2In(SeP^iPr_2)_2N]$ (Fig. 4.4) reveals that the precursor has one step decomposition mechanism (*ca.* 185 – 376 °C). However, in the study of $[Et_2In(SeP^iPr_2)_2N]$ (Fig. 4.5) there is a defined 43 % weight loss between 197 – 305 °C and again a 18 % mass loss between 350 – 417 °C. This result is evidence for the decomposition of the complex *via* a two-step mechanism, involving the loss of $[(P^iPr_2)_2N]$ moiety at temperature between 150 and 218 °C at atmosphere pressure. The XRPD pattern of the black colored final residue (*ca.* 18 wt %) obtained from pyrolysis of the compound indicated the formation of γ-In_2Se_3.

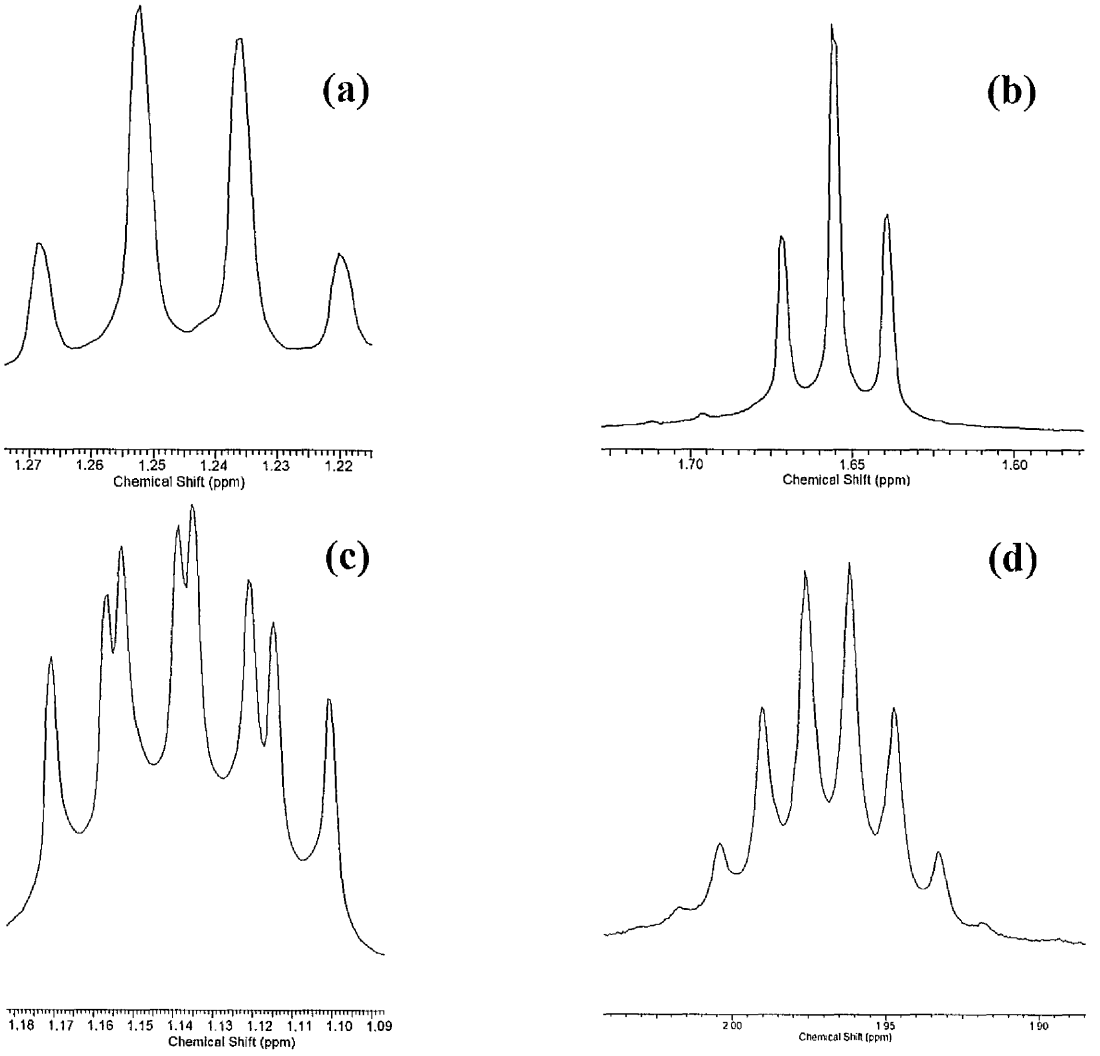

Figure 4.3 ^{1}H NMR spectra of $[Et_2In(SeP^{i}Pr_2)_2N]$ (a) CH_3-C*H*$_2$ (b) CH_2-C*H*$_3$ (c) C-C*H*$_3$ and (d) C-*H*.

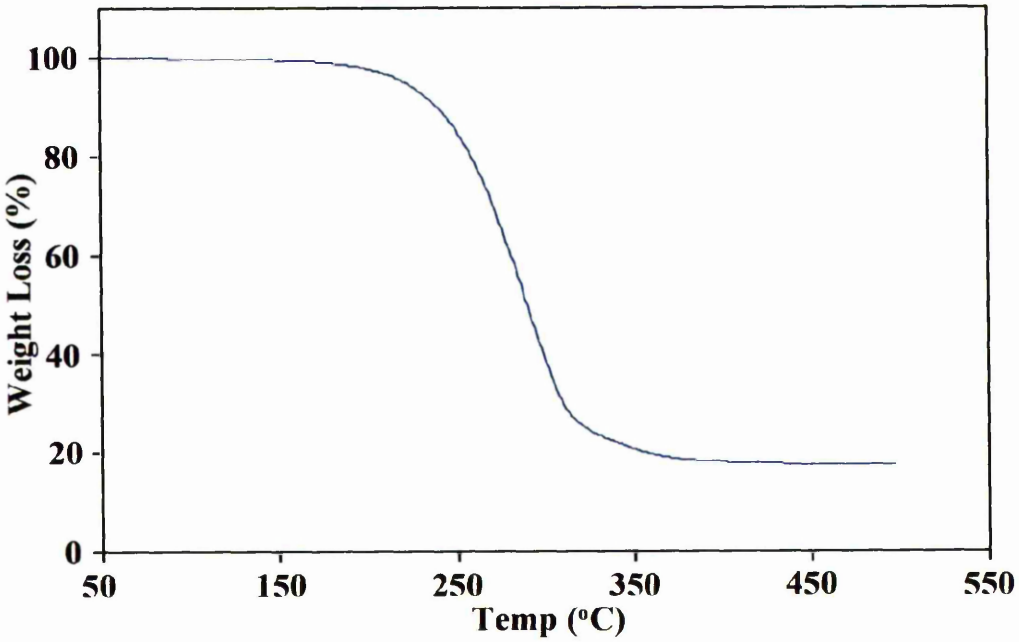

Figure 4.4 TGA profile of $[Me_2In(SeP^iPr_2)_2N]$.

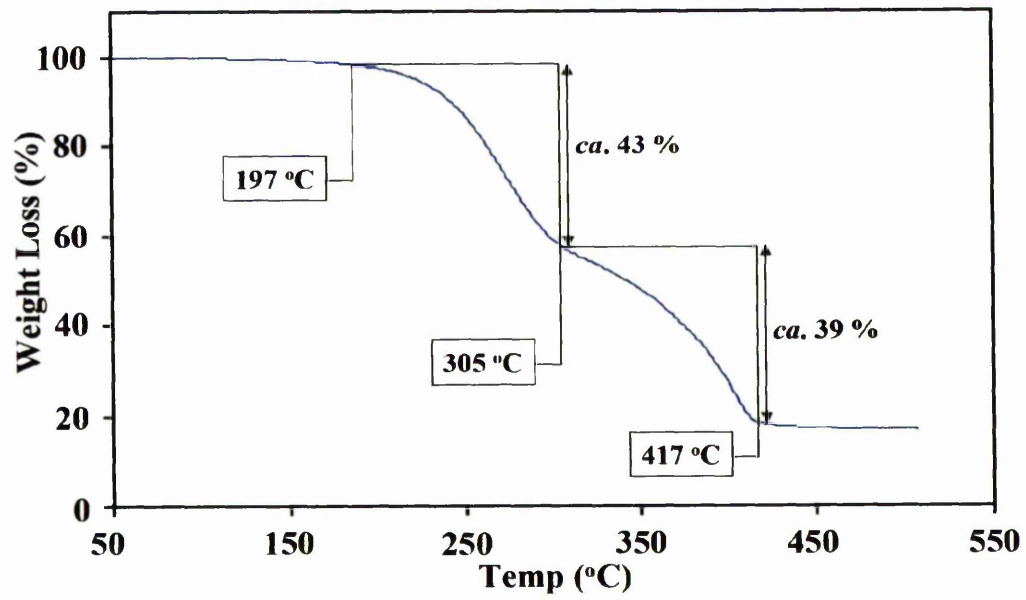

Figure 4.5 TGA profile of $[Et_2In(SeP^iPr_2)_2N]$.

Table 4.1 Crystal data and structure refinement parameters of $[Me_2Ga(SeP^iPr_2)_2N]$ and $[Me_2In(SeP^iPr_2)_2N]$.

Compound	$[Me_2Ga(SeP^iPr_2)_2N]$	$[Me_2In(SeP^iPr_2)_2N]$
empirical formula	$C_{14}H_{34}NP_2Se_2Ga$	$C_{14}H_{34}NP_2Se_2In$
formula weight	506	551.10
temperature (K)	100(2)	100(2)
crystal size (mm^3)	0.7 × 0.5 × 0.5	0.2 × 0.2 × 0.2
wavelength (Å)	0.71073	0.71073
crystal system	Monoclinic	Monoclinic
space group	$P2_1/n$	$P2_1/n$
a (Å)	13.989(2)	14.6027(14)
b (Å)	10.4987(18)	17.9871(18)
c (Å)	14.254(2)	16.5824(16)
α (°)	90	90
β (°)	94.094	99.774(2)
γ (°)	90	90
volume ($Å^3$)	2088.1(6)	4292.3(7)
Z	4	8
$density_{calcd}$ ($mg\ m^{-3}$)	1.610	1.706
abs. coeff., (mm^{-1})	4.950	4.636
F(000)	1016	2176
θ range (°)	1.97 to 28.52	1.68 to 26.38
reflections collected	17046	33762
independent reflections	4931	8734
max., min. transmission	0.1910 and 0.1292	0.457 and 0.457
data/restraints/pars.	4931/0/191	8734/0/381
goodness-of-fit on F^2	1.035	1.001
R1, *w*R2 [$I>2\sigma(I)$]	0.0267, 0.0690	0.00387, 0.0957
R1, *w*R2 (all data)	0.0306, 0.0710	0.0498, 0.1025
diff. peak and hole ($e.Å^{-3}$)	1.205 and -0.557	1.351 and -2.070

4.3 - X-ray Single Crystal Structures

Crystals of $[Me_2Ga(SeP^iPr_2)_2N]$ were obtained from hexane at -25 °C. The crystal structure of the compound is shown in Fig. 4.6 and selected bond lengths and angles are summarised in Table 4.2. The structure of the compound shows a dimethylgallium moiety coordinated to the imidophosphineselenate ligand in a distorted tetrahedral geometry. The Ga-Se bond lengths are (2.490(5) and 2.504(5) Å) which are comparable to those reported for $[Et_2Ga(SePPh_2)_2N]$ (2.514(10) and 2.535(10) Å)[26] and $[Cp^*Ga(\mu_3\text{-}Se)]_4$ (ranging between 2.445 – 2.499 Å).[27] The complex $[Tp(Bu^t)_2]GaSe$ synthesised by Parkin and Kuchta has the shortest known Ga-Se bond lengths which are consistent with multiple bond character (2.214(1) Å).[28] The bite angle of Se(2)-Ga(1)-Se(1) is 108.947(11)° which is similar to the reported value.[26] The structure of the compound has smaller C-Ga-C angle (120.14(10)°) in comparison to the angle observed for $[Et_2Ga(SePPh_2)_2N]$ (125.5(4)°).[26] Shortening of the P-N bonds to (1.588(18) and 1.593(17) Å) and the subsequently extended P-Se bonds (2.192(6) and 2.193(6) Å) relative to free ligand, indicates an increase in delocalisation within the structure due to deprotonation.[29]

Crystals of $[Me_2In(SeP^iPr_2)_2N]$ were obtained from toluene undisturbed for a period of time at low temperature. The asymmetric unit of the crystal structure contains 2 similar molecules and molecule 1 is illustrated in Fig. 4.7. As a result, indium compound contains 8 molecules in a unit cell whereas gallium compound has only 4 molecules (Figs. 4.8 and 4.9). The indium compound is isostructural with the gallium analogue (Fig. 4.6). Similarly, the indium atom is in a distorted tetrahedral coordination environment, with the Se(2)-In(1)-Se(1) angle being smaller than C(13)-In(1)-C(14) angle as a

consequence of the imidophosphineselenate chelate ring (Table 4.3). The bite angle of Se-In-Se (107.417(16)°) is considerably greater than the bite observed in a *tris*-chelate compound, $In[(SePPh_2)_2N]_3$ (95.549 °) due to the greater steric requirements of three ligands around a six-coordinate metal centre comparison to $[Me_2In(SeP^iPr_2)_2N]$, that is four coordinate.[30] The C(13)-In(1)-C(14) angle is (125.00(17)°) which is similar to the value (123(1)°) reported for $[Bu_2^tIn(\mu\text{-}SeBu^t)]_2$.[31] The In-Se bond lengths (2.675(5) and 2.684(5) Å) are shorter than $[In(SePPh_2)_2N]_3$ (average 2.75 Å),[30] [(2,4,6-trimethylphenyl)$_2$In(μ-SePh)]$_2$ (average 2.732 Å),[32] and $[(Me_3CCH_2)_2In(\mu\text{-}SePh)]_2$ (average 2.743 Å).[33] In comparison with $[Me_2Ga(SeP^iPr_2)_2N]$, the indium compound shows longer metal-selenium bonds, as expected due to the larger size of indium.

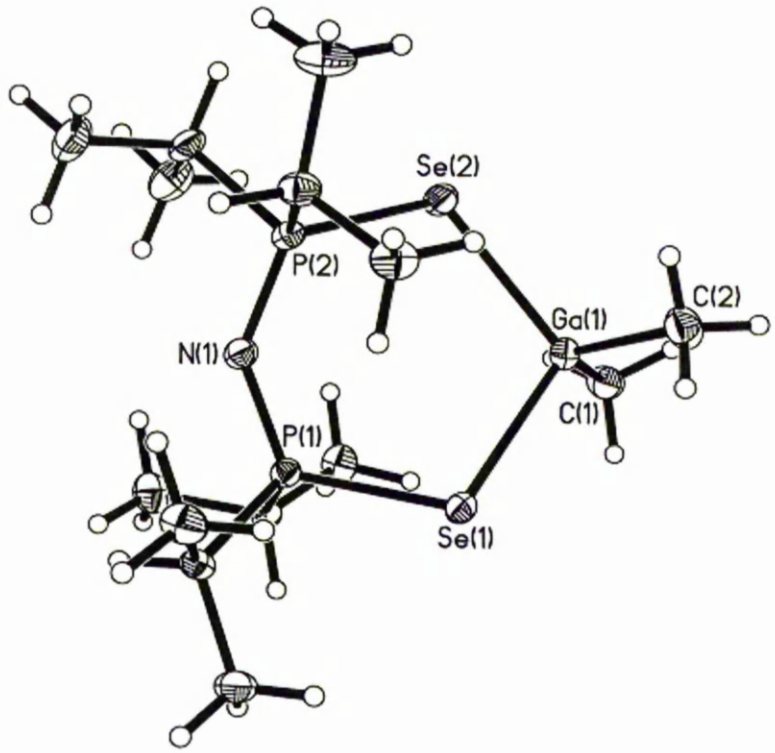

Figure 4.6 X-ray single crystal structure of $[Me_2Ga(SeP^iPr_2)_2N]$.

Table 4.2 Selected interatomic distances (Å) and angles (°) for of $[Me_2Ga(SeP^iPr_2)_2N]$.

Ga(1)-C (1)	1.979(2)	C(2)-Ga(1)-C(1)	120.14(10)
Ga(1)-C(2)	1.970(2)	C(2)-Ga(1)-Se(2)	110.39(7)
Ga(1)-Se(1)	2.504(5)	C(1)-Ga(1)-Se(2)	104.58(7)
Ga(1)-Se(2)	2.490(5)	C(2)-Ga(1)-Se(1)	100.21(7)
Se(1)-P(1)	2.193(6)	C(1)-Ga(1)-Se(1)	112.36(6)
Se(2)-P(2)	2.192(6)	Se(2)-Ga(1)-Se(1)	108.947(11)
N(1)-P(1)	1.593(17)	P(1)-Se(1)-Ga(1)	106.054(17)
N(1)-P(2)	1.588(18)	P(2)-Se(2)-Ga(1)	105.831(19)

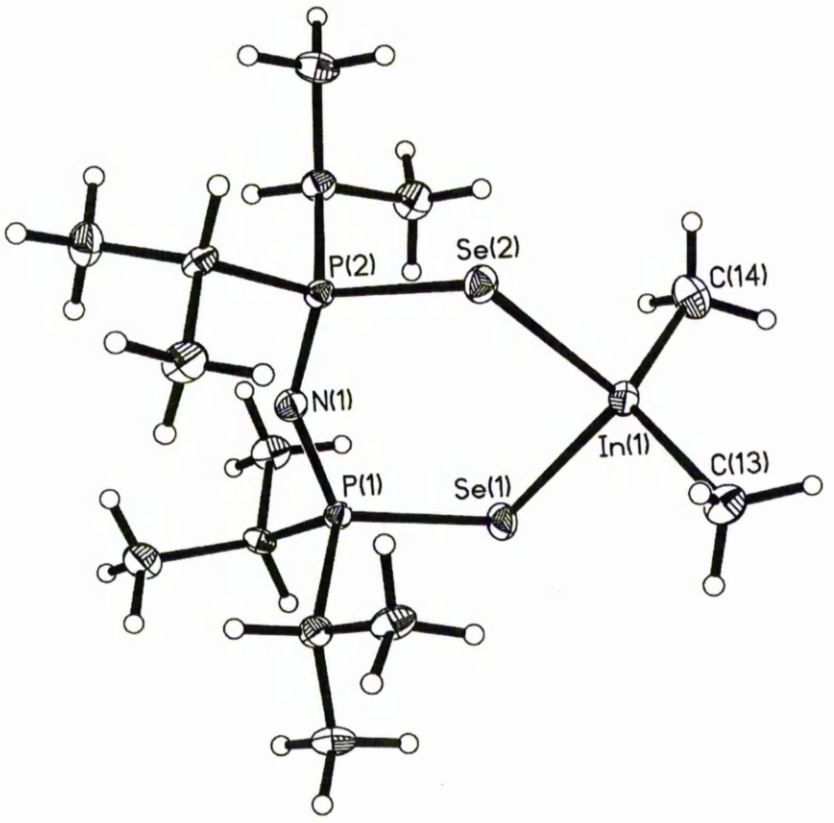

Figure 4.7 X-ray single crystal structure of $[Me_2In(SeP^iPr_2)_2N]$.

Table 4.3 Selected interatomic distances (Å) and angles (°) for of $[Me_2In(SeP^iPr_2)_2N]$.

In(1)-C(13)	1.979(2)	C(13)-In(1)-C(14)	125.00(17)
In(1)-C(14)	1.970(2)	C(13)-In(1)-Se(2)	101.67(13)
In(1)-Se(1)	2.504(5)	C(14)-In(1)-Se(2)	112.22(12)
In(1)-Se(2)	2.490 (5)	C(13)-In(1)-Se(1)	109.41(12)
Se(1)-P(1)	2.193(6)	C(14)-In(1)-Se(1)	100.32(12)
Se(2)-P(2)	2.192(6)	Se(2)-In(1)-Se(1)	107.417(16)
N(1)-P(1)	1.593(17)	P(1)-Se(1)-In(1)	104.77(3)
N(1)-P(2)	1.588(18)	P(2)-Se(2)-In(1)	104.28(3)

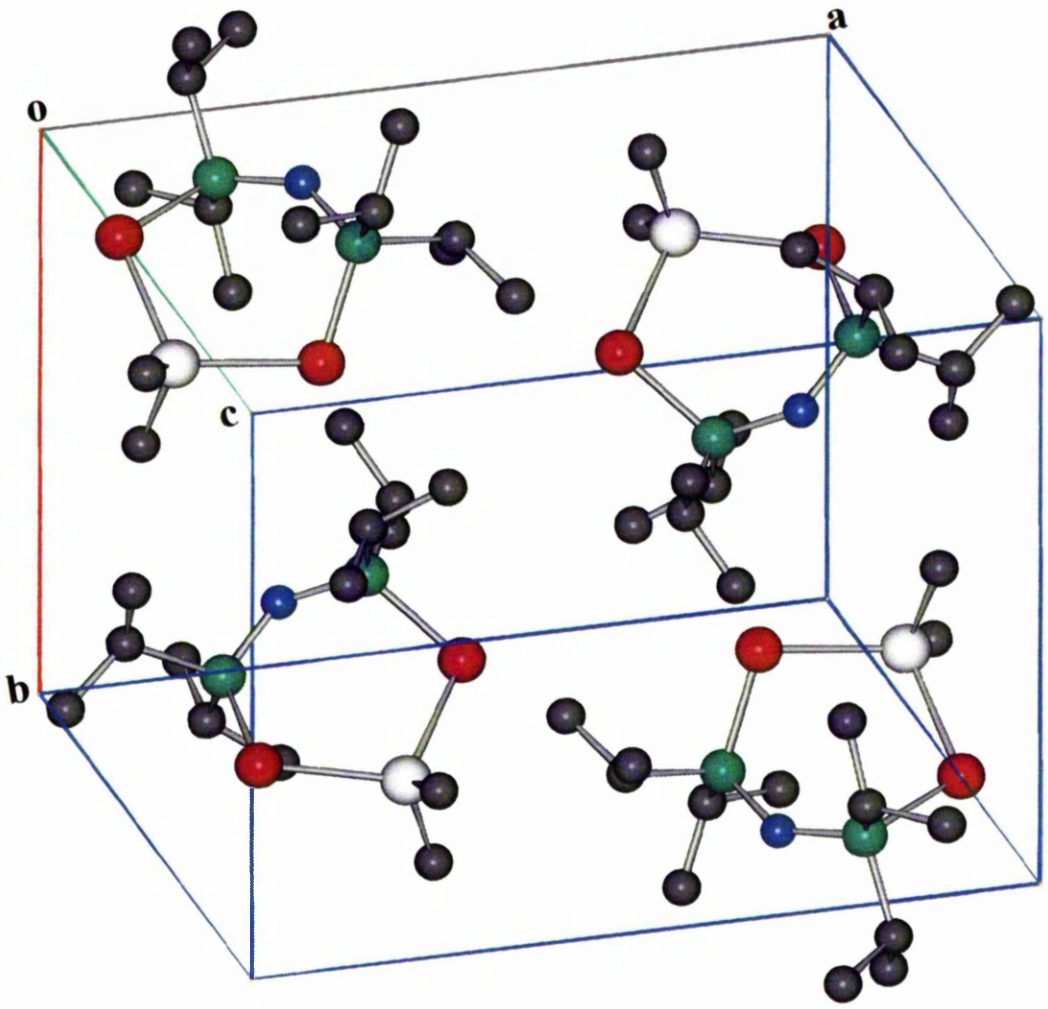

Figure 4.8 The molecular packing diagram of $[Me_2Ga(SeP^iPr_2)_2N]$.

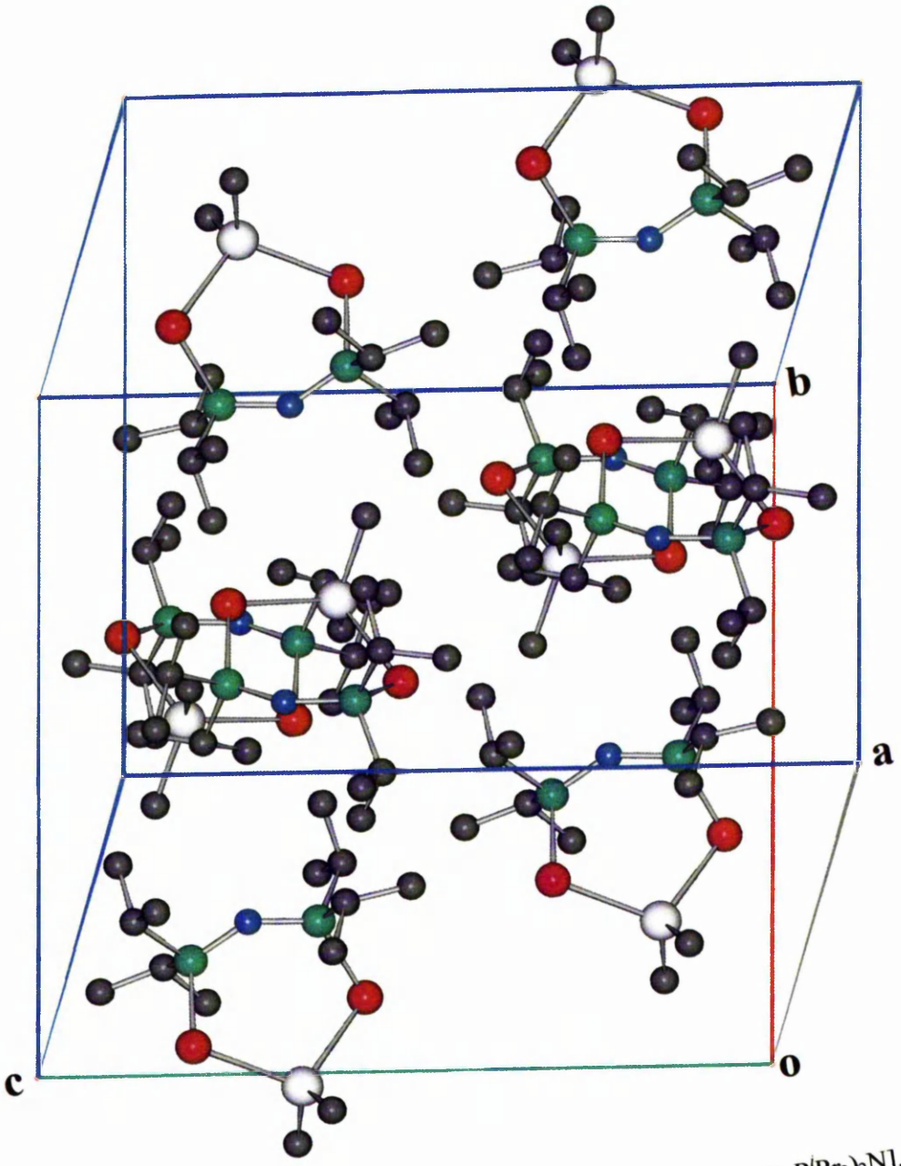

Figure 4.9 The molecular packing diagram of $[Me_2In(SeP^iPr_2)_2N]$.

4.4 - Cubic Ga_2Se_3 Films from $[Me_2Ga(SeP^iPr_2)_2N]$

Gallium selenide thin films were grown by AACVD and LP-MOCVD using $[Me_2Ga(SeP^iPr_2)_2N]$ as a single source precursor. Deposition of films by AACVD was attempted on glass substrates over a range of deposition temperatures (400 – 475 °C) with *ca.* 150 mg of precursor in 20 ml toluene. The deposition studies were carried out under a dynamic argon flow rate of 120 sccm for 2 hours. However, growth of films was only observed at higher growth temperatures (450 and 475 °C). As-deposited films were dark brown, non-uniform and non-adherent to the glass substrates.

The XRPD patterns of films grown by AACVD are shown in Fig. 4.10. The patterns are consistent with the formation of cubic Ga_2Se_3 (JCPDS 05-724) with a preferred orientation along the (111) direction. The film deposited at 450 °C produced broad peaks, indicating small particle sizes, but at higher deposition temperature the peaks sharpened. In contrast, Ga_2Se_3 films deposited from a cubane complex, $[Cp^*Ga(\mu_3\text{-}Se)]_4$ showed relatively broad XRPD pattern even after annealing the film at 500 °C.[26] However, when similar cubane complexes, $[(R)Ga(\mu_3\text{-}Se)]_4$ (R = CMe_3, $CEtMe_2$ and CEt_2Me) where cyclopentadienyl derivative is replaced by alkyl groups were used, they resulted in deposition of GaSe films between 325 – 370 °C.[10]

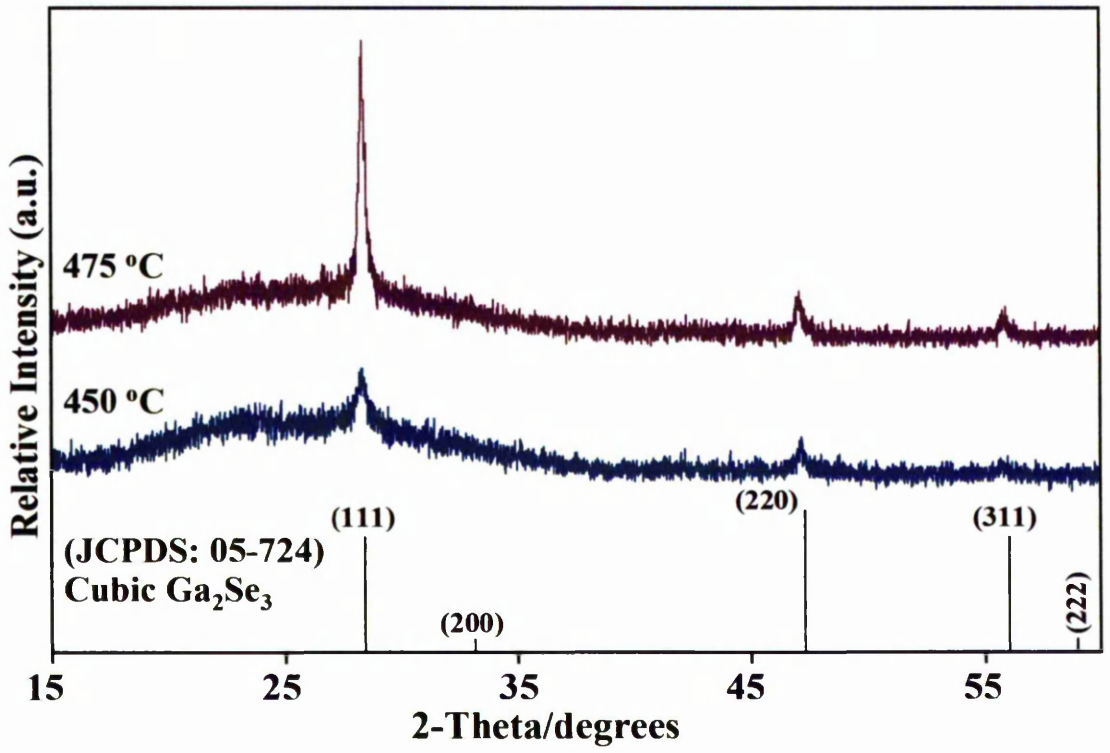

Figure 4.10 XRPD patterns of Ga_2Se_3 films deposited by AACVD.

A SEM image of the film deposited at 450 °C shows that the surface consists of randomly oriented and poorly defined particles, *ca.* 0.75 μm in thickness [Fig. 4.11(a)]. In contrast, the film grown at 475 °C consists of thin plate-like particles, laid down perpendicularly onto the substrate with random orientation [Fig. 4.11(b)]. The growth rate at 475 °C is *ca.* 0.75 μm h^{-1}. EDAX analyses (Fig. 4.12) of the grown films at random sites showed that a gallium-to-selenium ratio is close to 2:3. There was no phosphorus contamination detected in the films. Un-assigned peaks are due to reflections from amorphous glass substrates.

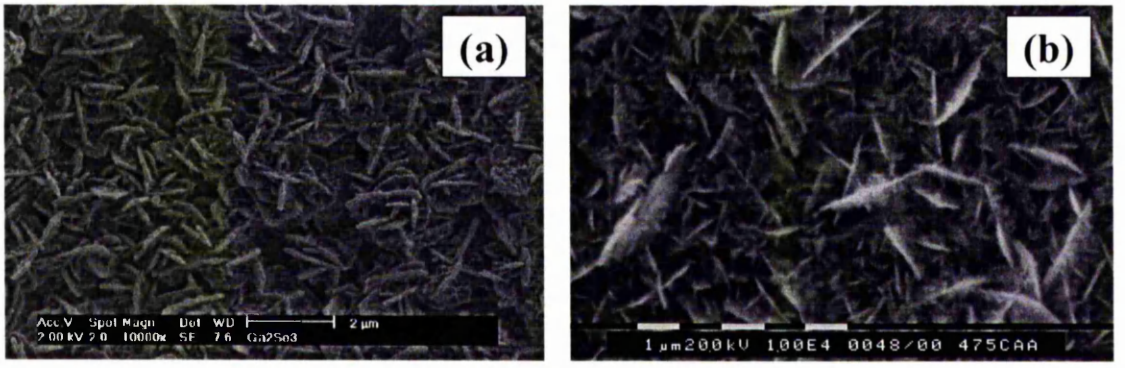

Figure 4.11 SEM images of Ga_2Se_3 films deposited by AACVD at (a) 450 °C, (b) 475 °C.

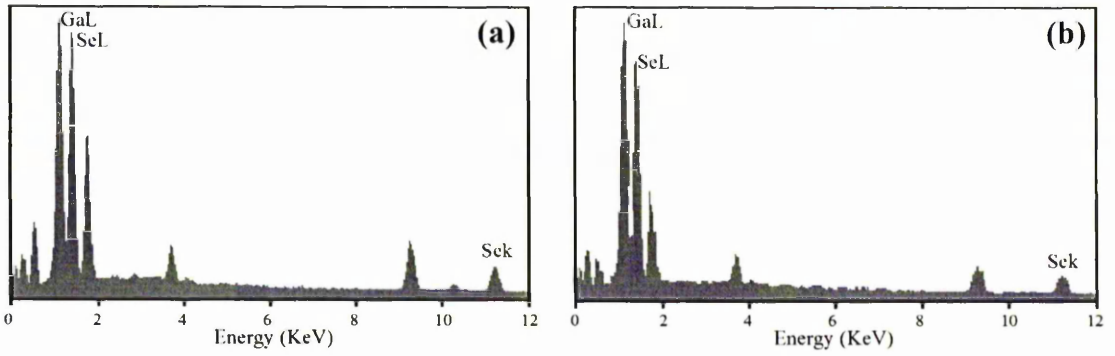

Figure 4.12 EDAX analysis of Ga_2Se_3 films deposited by AACVD at (a) 450 °C and (b) 475 °C.

As an alternative, deposition was also attempted by LP-MOCVD on glass substrates for 1 hour using *ca.* 150 mg of precursor . Deposition was attempted over a range of substrate temperatures (400 - 500 °C), whilst the precursor temperature was maintained at 185 °C. Little or no deposition was observed below 450 °C. The films obtained were yellow and transparent at 450 °C, light-red at higher temperatures, and adherent to the glass substrate surface (Scotch-tape test).

The XRPD analyses show that the films are cubic Ga_2Se_3 at all growth temperatures with a preferred orientation along the (111) plane (Table 4.4). The XRPD patterns indicate that the crystallinity of deposited films is dependent on the growth temperatures (Fig. 4.13). Deposition carried out at 450 °C yielded relatively poorly crystalline Ga_2Se_3 film, whilst higher deposition temperature results in improved crystallinity. In comparison with Ga_2Se_3 films grown by AACVD, LP-MOCVD yields Ga_2Se_3 with improved crystallinity as indicated by XRPD.

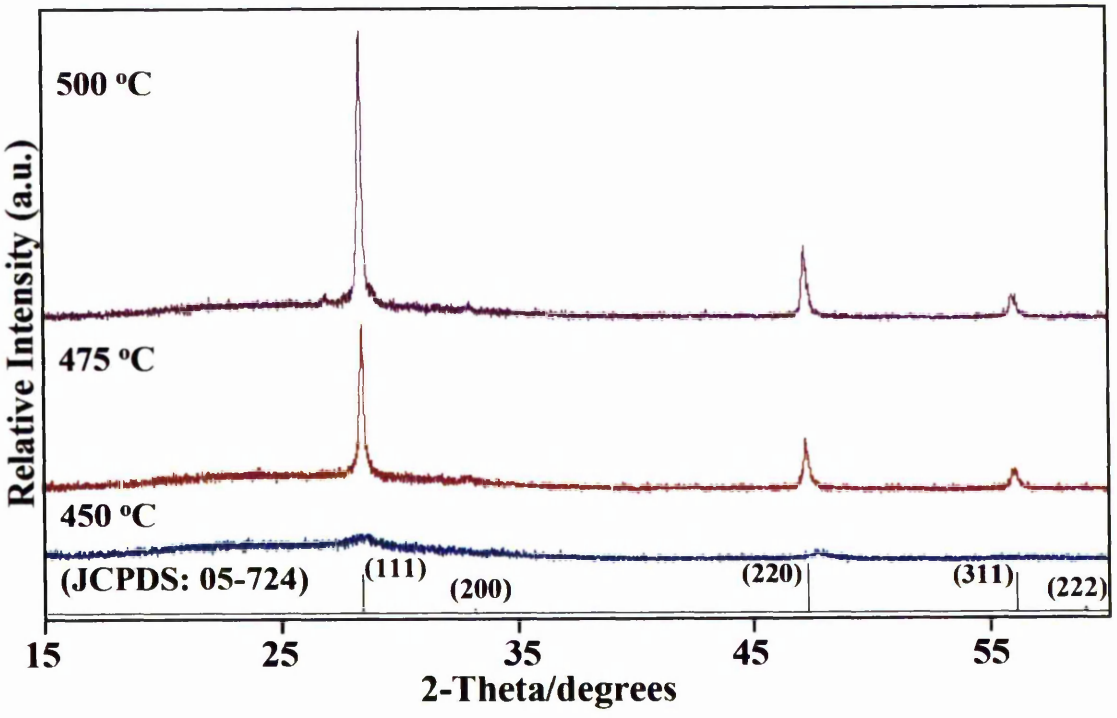

Figure 4.13 XRPD patterns of Ga_2Se_3 films deposited by LP-MOCVD.

Table 4.4 *d*-spacing and intensity profiles for cubic Ga_2Se_3 films on the glass substrates from $[Me_2Ga(SeP^iPr_2)_2N]$.

	AACVD		LP-MOCVD		
JCPDS (05-724) *d* (hkl) (%)	450 °C *d* (%)	475 °C *d* (%)	450 °C *d* (%)	475 °C *d* (%)	500 °C *d* (%)
3.14 (111) (80)	3.15 (100)	3.14 (100)	3.12 (100)	3.14 (100)	3.14 (100)
2.70 (200) (10)	N/A	N/A	N/A	N/A	2.71 (10)
1.92 (220) (100)	1.92 (75)	1.93 (22)	1.91 (54)	1.92 (34)	1.92 (11)
1.64 (311) (80)	1.65 (68)	1.64 (18)	N/A	1.64 (16)	2.7 (27)

Figure 4.14 shows SEM micrographs of the deposited films at different growth temperatures. The film deposited at 450 °C has featureless nanocrystalline morphology and poor coverage is also observed [Fig. 4.14(a)]. At higher growth temperatures (475 and 500 °C), dense morphology is evident and particles have irregular shapes [Figs. 4.14(b); 4.14(c)]. The growth rate at 500 °C is *ca.* 1.25 $\mu m\ h^{-1}$. Morphologies of Ga_2Se_3 films deposited by LP-MOCVD improved significantly whereas, Ga_2Se_3 films deposited by AACVD were poor and non-uniform. In comparison with Ga_2Se_3 films grown by AACVD, EDAX analysis of the film deposited at 500 °C shows that the film is slightly selenium rich with 64% and gallium 36%. No phosphorus was detected in the films.

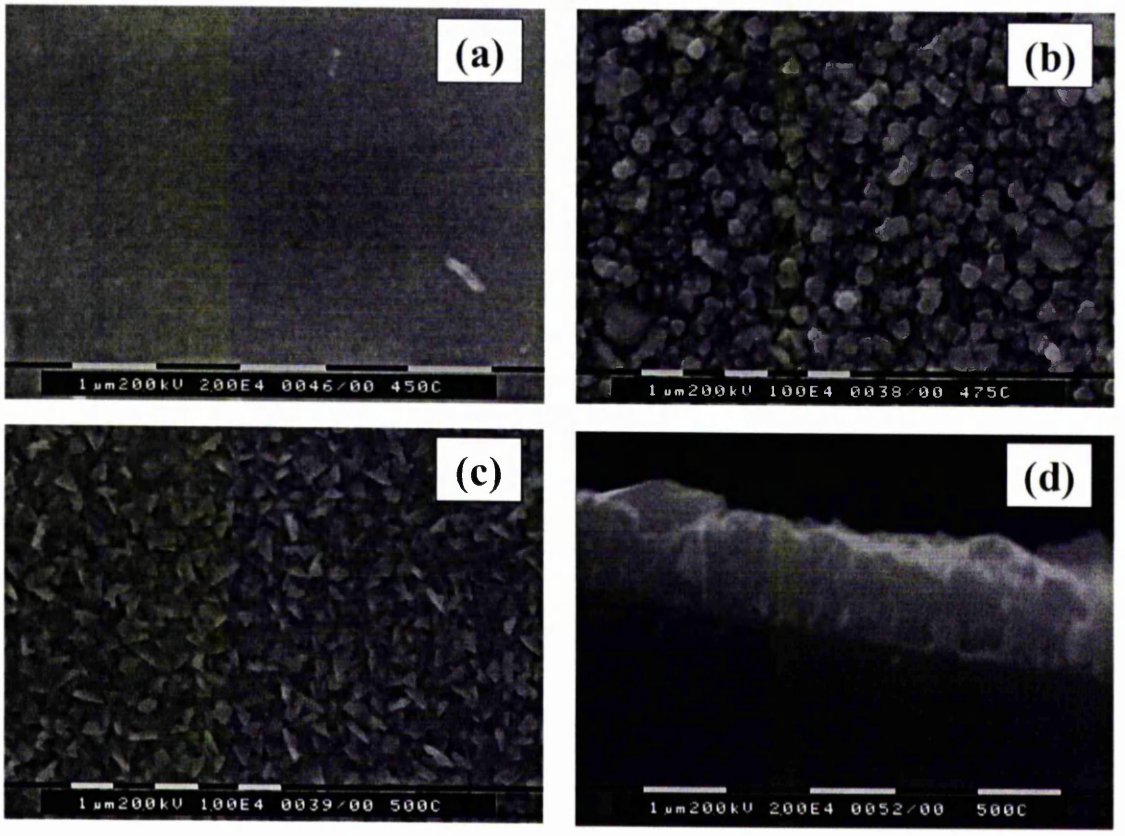

Figure 4.14 SEM images of Ga_2Se_3 films deposited by LP-MOCVD at (a) 450 °C, (b) 475 °C, (c) and (d) 500 °C.

4.5 - Description of In_2Se_3 Films Grown by AACVD

Indium selenide films were deposited from $[Me_2In(SeP^iPr_2)_2N]$ and $[Et_2In(SeP^iPr_2)_2N]$ by AACVD on amorphous glass substrates. The experimental details are given in Table 4.5. Films were grown for 2 hours by dissolving *ca.* 150 mg of precursor in 20 ml toluene using a dynamic argon flow of 120 sccm.

Table 4.5 Experimental details for growing indium selenide films.

Precursor	Growth Temp. (°C)	Description
$[Me_2In(SeP^iPr_2)_2N]$	475	Thick, black and uniform film
	450	Black, non-uniform film
	425	Black, non-uniform film
	400	Slightly coated film
	375	Very poor thin film
	350	No deposition
$[Et_2In(SeP^iPr_2)_2N]$	475	Black, uniform film
	450	Black, non-uniform film
	425	Grey, non-uniform film
	400	Grey colour film

4.6 - Results and Discussion

4.6.1 - Growth of Indium Selenide Films from $[Me_2In(SeP^iPr_2)_2N]$

Indium selenide films were deposited using $[Me_2In(SeP^iPr_2)_2N]$ as a single source precursor at substrate temperatures of 375 – 475 °C. At higher deposition temperatures (450 – 475 °C), deposited films were black and fairly adherent to the glass substrate surface.

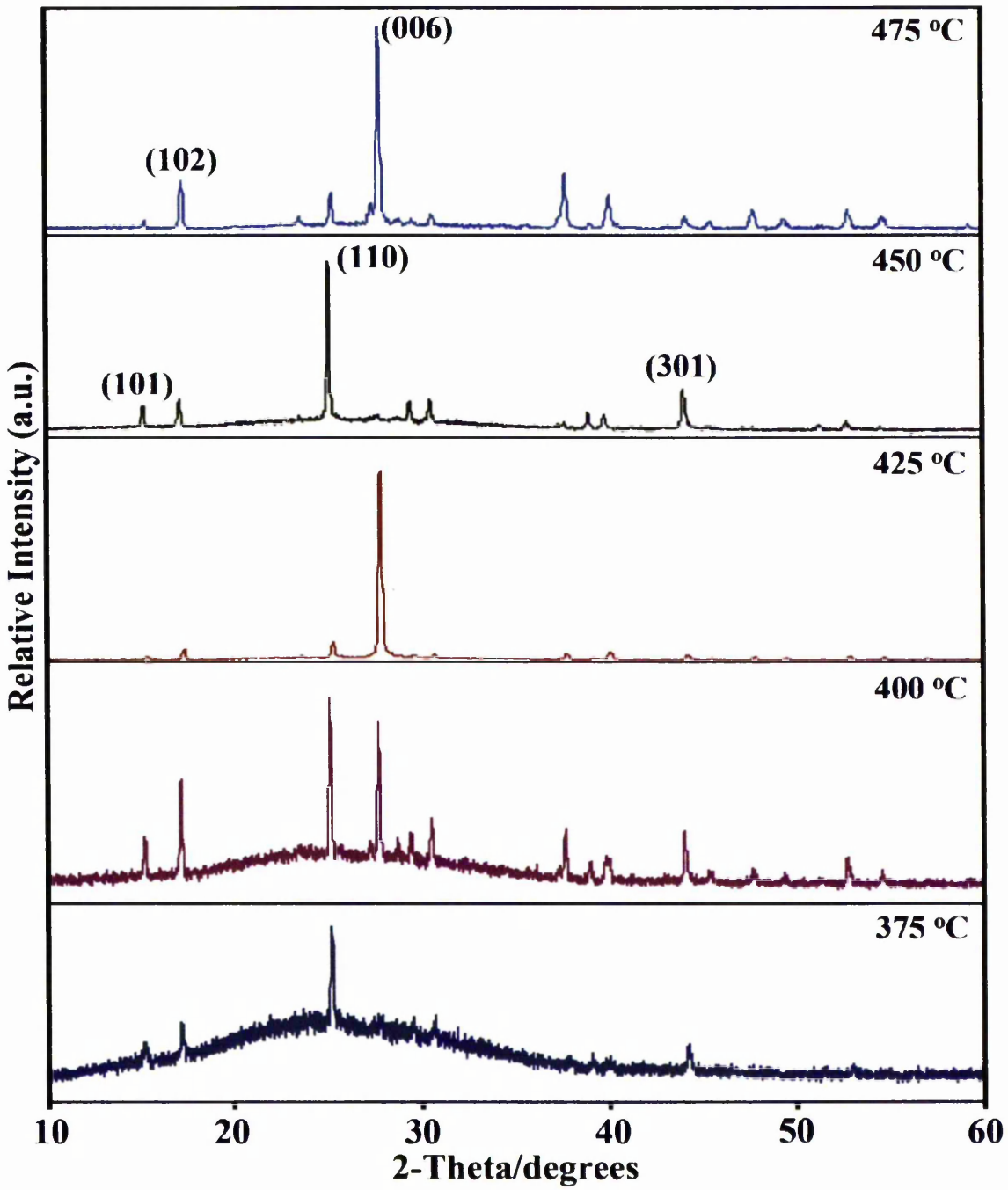

Figure 4.15 XRPD patterns of γ-In_2Se_3 films deposited from $[Me_2In(SeP^iPr_2)_2N]$ at different growth temperatures.

Table 4.6 *d*-spacing and intensity profiles for hexagonal In_2Se_3 films on the glass substrates from $[Me_2In(SeP^iPr_2)_2N]$.

JCPDS (40-1407) *d* (hkl) (%)	375 °C *d* (%)	400 °C *d* (%)	425 °C *d* (%)	450 °C *d* (%)	475 °C *d* (%)
5.88 (101) (21)	5.82 (34)	5.86 (32)	5.85 (2)	5.84 (16)	5.82 (7)
5.21 (102) (51)	5.18 (46)	5.19 (60)	5.17 (6)	5.19 (22)	5.14 (25)
3.56 (110) (77)	3.53 (100)	3.55 (100)	3.53 (10)	3.55 (100)	3.53 (15)
3.23 (006) (81)	3.20 (50)	3.22 (88)	3.20 (100)	3.22 (13)	3.25 (100)
3.12 (113) (25)	N/A	3.11 (32)	3.09 (3)	N/A	3.10 (8)
2.94 (202) (48)	2.91 (49)	2.93 (41)	2.91 (4)	2.93 (21)	2.92 (7)
2.39 (116) (70)	2.38 (26)	2.39 (36)	2.38 (4)	2.39 (9)	2.38 (29)
2.32 (211) (41)	2.30 (28)	2.30 (21)	2.39 (1)	2.31 (14)	2.30 (7)

The XRPD analysis shows that hexagonal γ-In_2Se_3 (JCPDS 40-1407) films have been deposited onto glass substrates at growth temperatures of 375 – 475 °C (Table 4.6). Films grown at 375, 400 and 450 °C show a preferred orientation along the (110) plane whilst films deposited at 475 and 425 °C have a preferred orientation along the (006) plane (Fig. 4.15). At lower deposition temperature (375 °C), the degree of crystallinity of the as-deposited film is reduced, indicated by the intensity of XRPD pattern. In contrast, hexagonal β-In_2Se_3 thin films have been reported using the single-source precursor $[In(SeC(SiMe_3)_3]_3$.[7] It is interesting to note that γ-In_2Se_3 is generally stable at high temperature (> 650 °C).[27]

The SEM studies indicate that the morphology of the films changes depending on the growth temperature (Fig. 4.16). The films grown at 425 and 475 °C have globular

morphologies. Platelet crystals are evident at 450 °C. At lower growth temperatures of 375 and 400 °C, the growth of indium selenide is very slow, with a poor coverage on the substrate after 2 hours of growth. At 475 °C, film with *ca.* 1.5 μm thickness was deposited.

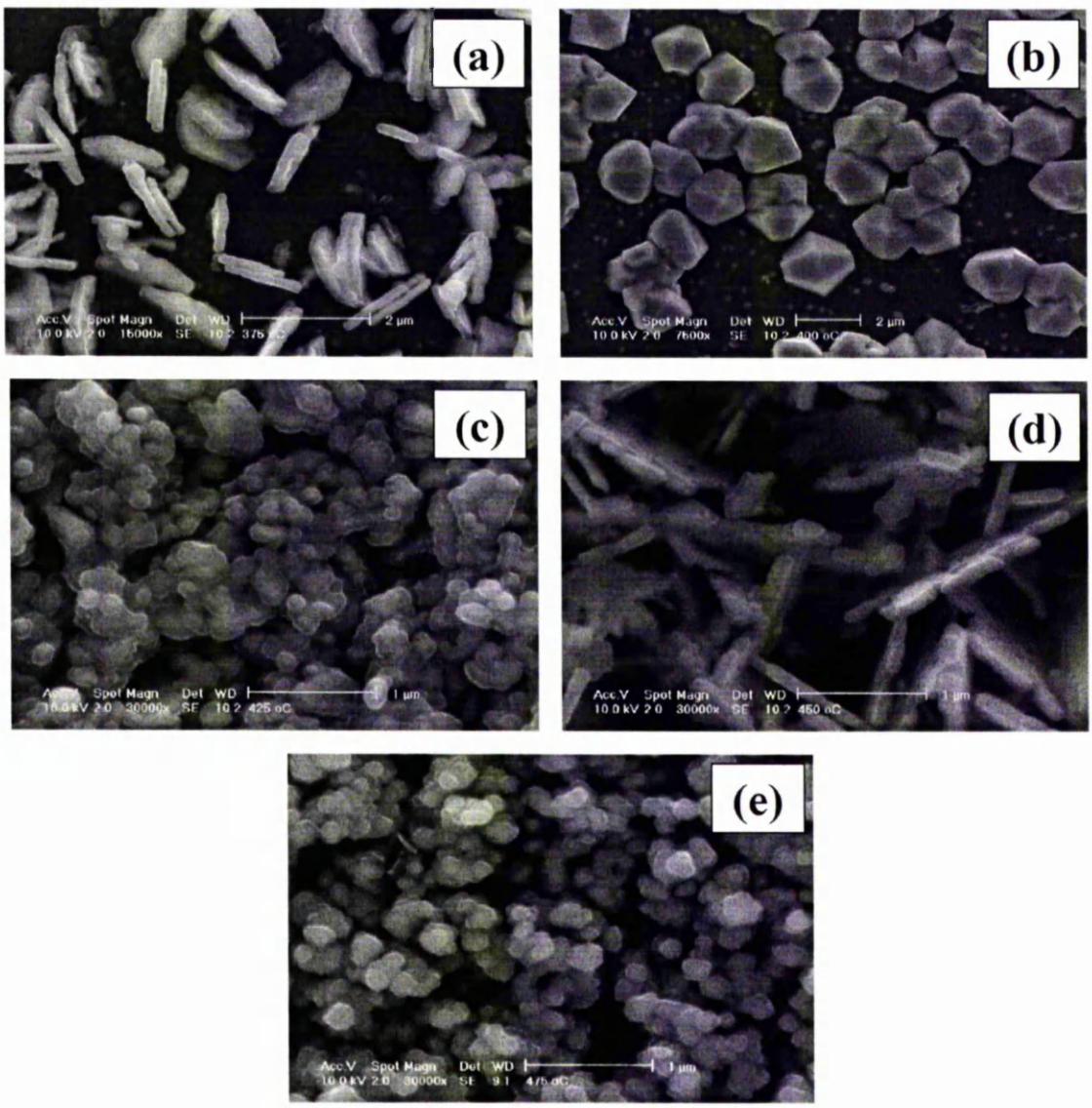

Figure 4.16 SEM images of In_2Se_3 films deposited from $[Me_2In(SeP^iPr_2)_2N]$ at (a) 375 °C, (b) 400 °C, (c) 425 °C, (d) 450 °C and (e) 475 °C.

The EDAX analyses (Fig. 4.17) confirm that the stoichiometry of In_2Se_3 films is close to 2:3. There was no phosphorous contamination detected in the films. Un-assigned peaks are due to amorphous glass substrates. Table 4.7 summarises the percentage values obtained for indium and selenium at different growth temperatures.

Table 4.7 EDAX analyses of indium selenide films deposited at different temperatures.

Dep Temp (°C)	Indium (atomic %)	Selenide (atomic %)
375	40	60
400	41	59
425	39	61
450	41	59
475	38	62

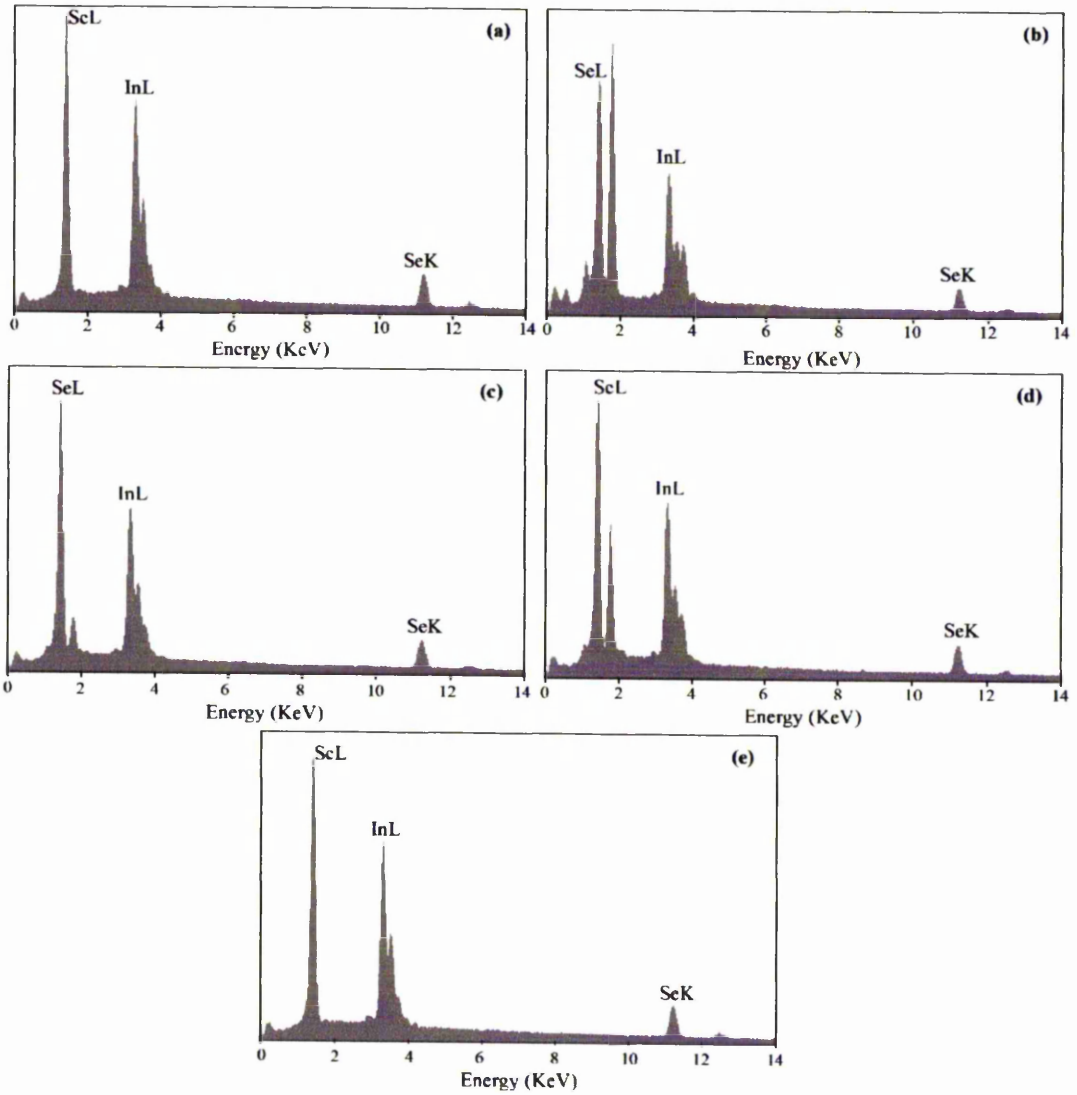

Figure 4.17 EDAX analyses of In_2Se_3 films deposited from $[Me_2In(SeP^iPr_2)_2N]$ at (a) 375 °C, (b) 400 °C, (c) 425 °C, (d) 450 °C and (e) 475 °C.

4.6.2 - Growth of Indium Selenide Films from $[Et_2In(SeP^iPr_2)_2N]$

Deposition of indium selenide films from $[Et_2In(SeP^iPr_2)_2N]$ were attempted at substrates temperatures of 400 – 475 °C with *ca.* 150 mg of the precursor used for each experiment. Little or no film growth was observed at substrate temperatures below 400 °C. As-deposited films were black and fairly adherent to the glass substrate surface.

The XRPD studies indicate that the hexagonal γ-In_2Se_3 phase (JCPDS 40-1407) has been grown with a preferred orientation along the (006) plane except for the film deposited at 475 °C which showed a preferred orientation along the (110) plane (Fig. 4.18). In contrast, the film deposited from the methyl analogue at 475 °C shows a preferred orientation of (006).

Fig. 4.19 shows the SEM micrographs of the various changes observed at different growth temperatures, which are different from films grown from methyl moiety. The films deposited at 425 and 450 °C have similar morphologies with columnar aggregates. As deposition temperature decreases to 400 °C, morphology consists of anhedral grains. At 475 °C, the surface consists of randomly oriented platelets. The thickness of films obtained from the cross-sectional views were found to be *ca.* 0.5 μm at 400 °C, 1.5 μm at 425 °C and 1 μm at 450 °C on glass substrates after 2 hours of growth. The EDAX analysis (Fig. 4.20) shows that the indium to selenium ratio is close to 2:3 for the film grown at 450 °C but a small trace of phosphorous (< 1%) was also found, which was incorporated during the decomposition of the precursor.

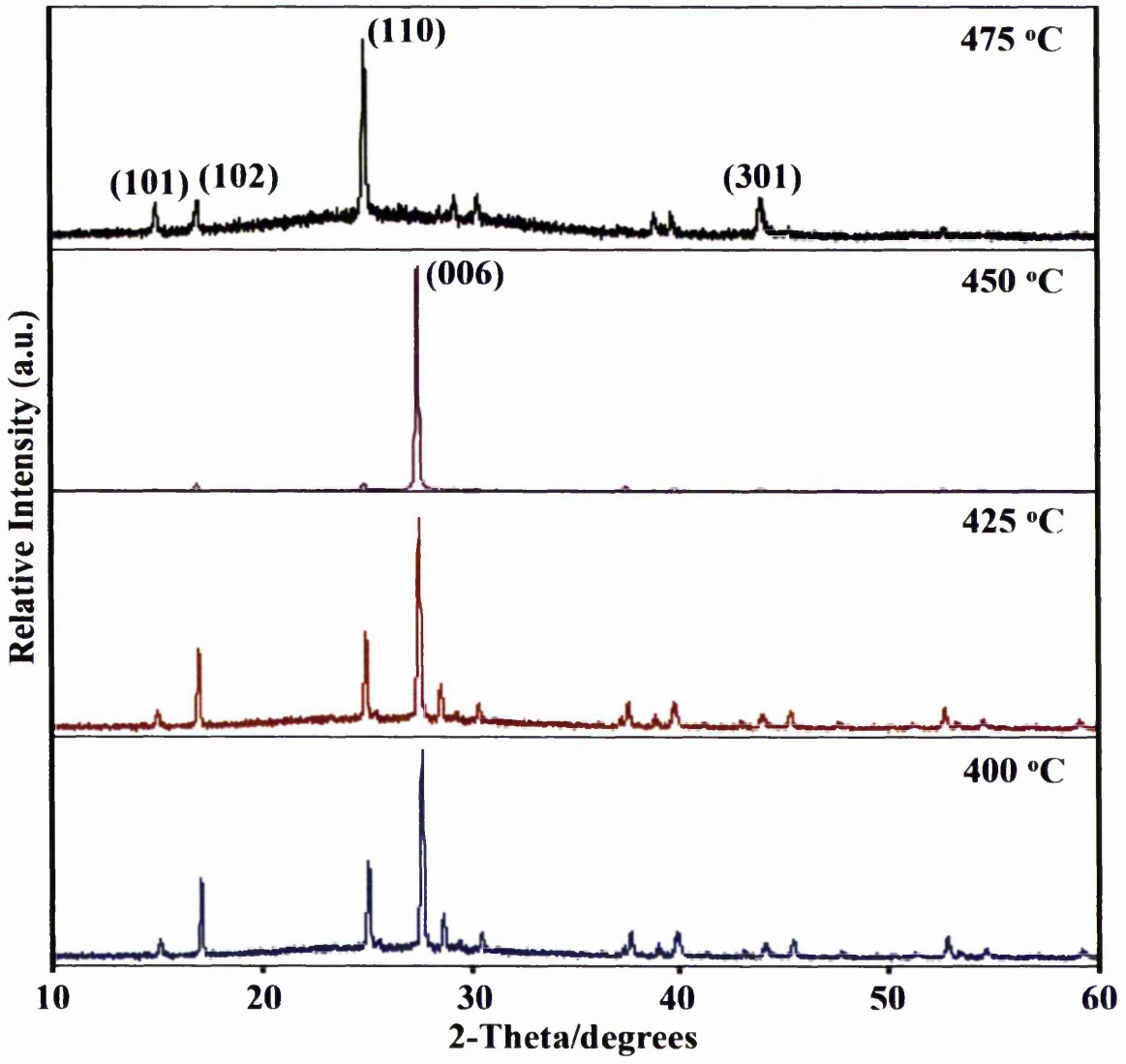

Figure 4.18 XRPD patterns of γ-In_2Se_3 films deposited from $[Et_2In(SeP^iPr_2)_2N]$ at different growth temperatures.

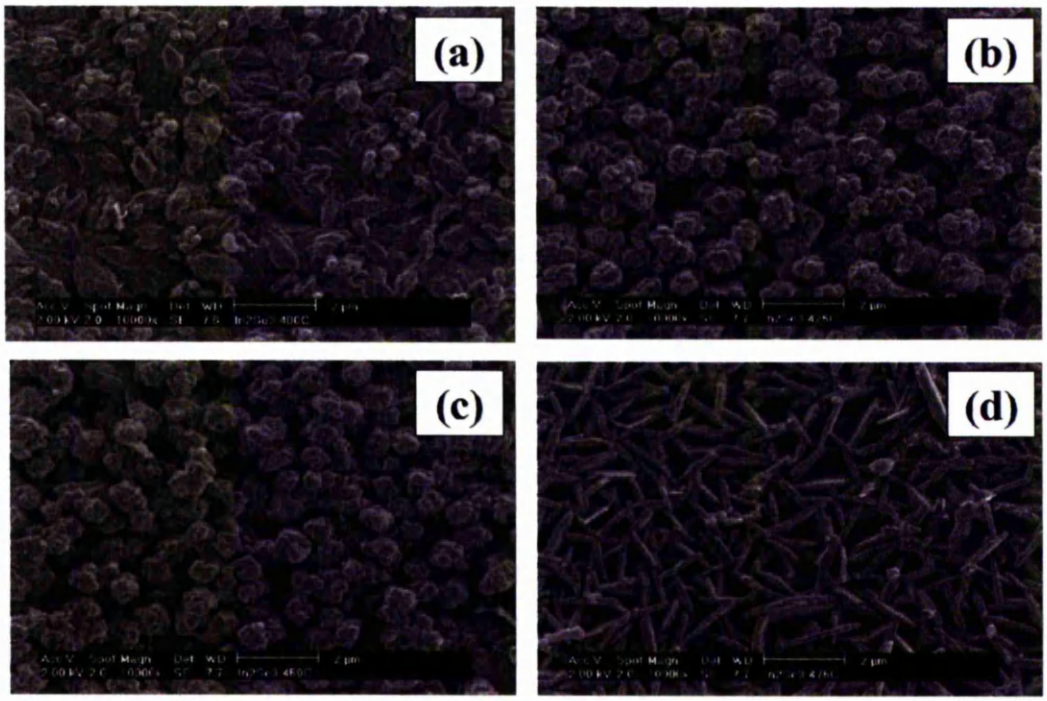

Figure 4.19 SEM images of γ-In_2Se_3 films deposited from $[Et_2In(SeP^iPr_2)_2N]$ at (a) 400 °C, (b) 425 °C, (c) 450 °C and (d) 475 °C.

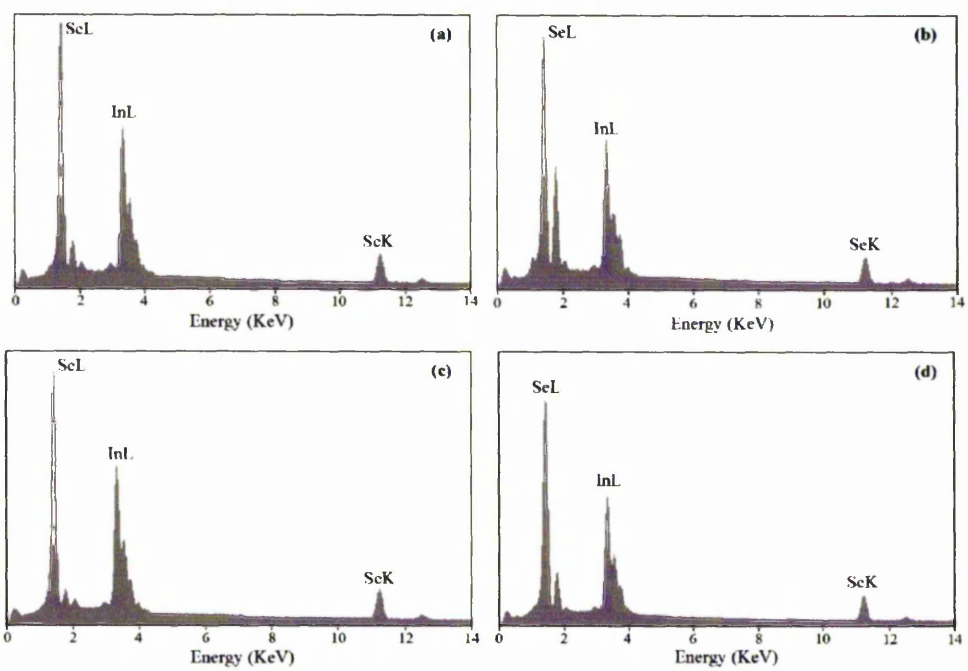

Figure 4.20 EDAX analyses of In_2Se_3 films deposited from $[Et_2In(SeP^iPr_2)_2N]$ at (a) 400 °C, (b) 425 °C, (c) 450 °C and (d) 475 °C.

4.7 – Conclusions

$[Me_2Ga(SeP^iPr_2)_2N]$ and $[R_2In(SeP^iPr_2)_2N]$ (R = Me, Et) have been synthesised and used as single-source precursors for the growth of gallium selenide and indium selenide films. X-ray single crystal structures of $[Me_2M(SeP^iPr_2)_2N]$ (M = Ga or In) show distorted tetrahedral geometry at the metal centres. The XRPD studies show that cubic Ga_2Se_3 and hexagonal γ-In_2Se_3 films have been deposited on glass substrates. These selenium-ligands are relatively easy to prepare from elemental selenium and obviate the need for the use of noxious CSe_2 as used in preparing diselenocarbamates.

References

1. M. R. Lazell, P. O'Brien, D. J. Otway, J.-H. Park, *J. Chem. Soc., Dalton Trans.*, **2000**, 4479.
2. O. Madelung, R. Poerschke, *Semiconductor: other than Group IV Elements and III-V Compounds*, Springer-Verlag: Berlin, 1992.
3. W. E. Rees Jr, *CVD of Nonmetals*, VCH: New York, 1996.
4. R. Nomura, S.-J. Inzawa, K. Kanaya, H. Matsuda, *Appl. Organomet. Chem.*, **1989**, *3*, 195.
5. R. Nomura, K. Konishi, H. Matsuda, *Thin Solid Films,* **1989**, *3*, 195.
6. H. J. Gysling, A. A. Wernberg, F. N. Blanton, *Chem. Mater.*, **1992**, *4*, 900.
7. J. Cheon, J. Arnold, K.-M. Ku, E. D. Bourret, *Chem. Mater.*, **1995**, *7*, 2273.
8. A. N. MacInnes, M. B. Power, A. R. Barron, *Chem. Mater.*, **1992**, *4*, 11.
9. A. N. MacInnes, M. B. Power, A. R. Barron, *Chem. Mater.*, **1993**, *5*, 1344.
10. E. G. Gillan, A. R. Barron, *Chem. Mater.*, **1997**, *9*, 3037.
11. E. G. Gillan, S. G. Bott, A. R. Barron, *Chem. Mater.*, **1997**, *9*, 796.
12. P. Pernot, A. R. Barron, *Chem. Vap. Deposition*, **1995**, *1*, 75.
13. S. L. Stoll, S. G. Bott, A. R. Barron, *J. Chem. Soc., Dalton Trans.*, **1997**, 1315.
14. S. L. Stoll, A. R. Barron, *Chem. Mater.*, **1998**, *10*, 650.
15. S. W. Haggata, M. A. Malik, M. Motevalli, P. O'Brien, J. C. Knowles, *Chem. Mater.*, **1995**, *7*, 716.
16. P. O'Brien, D. J. Otway, J. R. Walsh, *Chem. Vap. Deposition*, **1997**, *3*, 227.
17. P. O'Brien, D. J. Otway, J. R. Walsh, *Thin Solid Films*, **1998**, *315*, 57.
18. M. R. Lazell, P. O'Brien, D. J. Otway, J.-H. Park, *Chem. Mater.*, **1999**, *11*, 3430.

19. A. N. Gleizes, *Chem. Vap. Deposition*, **2000**, *6*, 155.

20. V. G. Bessergenev, E. N. Ivanova, Y. A. kovalevskaya, S. A. Gromilov, V. N. Kirichenko, S. V. Larionov, *Inorg. Mater.*, **1996**, *32*, 592.

21. G. A. Horley, M. Chunggaze, P. O'Brien, A. J. P. White, D. J. Williams, *J. Chem. Soc., Dalton Trans.*, **1998**, 315.

22. G. A. Horley, P. O'Brien, J.-H. Park, A. J. P. White, D. J. Williams, *J. Mater. Chem.*, **1999**, *9*, 1289.

23. G. A. Horley, M. R. Lazell, P. O'Brien, *Chem. Vap. Deposition*, **1999**, *5*, 203.

24. G. Shang, M. J. Hampden-Smith, E. N. Duesler, *J. Chem. Soc., Chem. Commun.*, **1996**, 1733.

25. G. Shang, K. Kunze, M. J. Hampden-Smith, E. N. Duesler, *Chem. Vap. Deposition*, **1996**, *2*, 242.

26. M. À. Munoz-Hernández, A. Singer, D. A. Atwood, R. Cea-Olivares, *J. Organomet. Chem.*, **1998**, *571*, 15.

27. S. Schultz, E. G. Gillian, J. L. Ross, M. L. Rogers, R. D. Rogers, A. R. Barron, *Organometallics,* **1996**, *15*, 4880.

28. M. C. Kuchta, G. Parkin, *Inorg. Chem.*, **1997**, *36*, 2492.

29. D. Cupertino, D. J. Birdsall, A. M. Z. Slawin, J. D. Woollins, *Inorg. Chim. Acta*, **1999**, *290*, 1.

30. R. Cea-Olivares, V. Garcia-Montalvo, J. Novosad, J. D. Woollins, R. A. Toscano, G. Espinosa-Pèrez, *Chem. Ber.*, **1996**, *129*, 919.

31. S. L. Stoll, S. G. Bott, A. R. Barron, *J. Chem. Soc., Dalton Trans.*, **1997**, 1315.

32. H. Rahbarnoohi, R. Kumar, M. J. Heeg, J. P. Oliver, *Organomatallics*, **1995**, *14*, 3869.

33. O. T. Beachely Jr, J. C. Lee Jr, H. J. Gysling, S.-H. L. Chao, M. R. Churchill, C. H. Lake, *Organometallics*, **1992**, *11*, 3144.

Chapter V

Experimental

5.1 - Chemicals

Indium (III) chloride (Aldrich); Gallium (III) chloride (Aldrich); Copper (I) chloride (Aldrich); *N*-methylhexylamine (96%, Aldrich); Sodium hydroxide (Aldrich); Toluene (BDH); Methanol (BDH); Selenium (Aldrich); 1,1,1,3,3,3-Hexamethyldisilazane (Aldrich); Diisopropylchlorophosphine (Aldrich); Diethyl ether (Aldrich); Chloroform (Aldrich); Cadmium (II) chloride (Aldrich); Zinc (II) chloride (Aldrich); Benzene (Aldrich); Hexane (BDH); Carbon disulfide (BDH); Dichloromethane (BDH); Tetrahydrofuran (BDH); Dimethylcadmium (Epichem); Dimethylzinc (Epichem); Trimethylindium (Epichem); Triethylindium (Epichem); Trimethylgallium (Epichem); $[(Ph_3P)_2AgIn(SC\{O\}R)_4]$ (R = Me or Ph)[1] and $[(Ph_3P)_2CuM(SC\{O\}Ph)_4]$[2] (Prof. J. J. Vittal, Chemistry department, National University of Singapore, Singapore).

5.2 - Handling of Air-Sensitive Compounds

The synthetic procedures were carried out in an inert atmosphere using a double manifold Schlenk-line, attached to an Edwards E2M8 vacuum pump, and a dry nitrogen cylinder. All flasks were evacuated then purged with nitrogen at least three times prior to use, with external heat applied where deemed necessary. Solid air-sensitive compounds were handled inside a glove box under an atmosphere of dry nitrogen. Liquid air-sensitive chemical were transferred to schlenk type flasks either by cannula or using syringes. Dry solvents were used throughout the syntheses, either distilled over standard drying agents (Na/benzophenone, CaH_2 *etc.*) or purchased, and stored in flasks over molecular sieves. Deuterated solvents for NMR measurements were frozen at liquid nitrogen temperature, degassed under vacuum and then flushed with nitrogen. After

repeating this procedure three times, the deuterated solvents were stored under nitrogen over molecular sieves.

5.3 – Syntheses of CSe_2

CSe_2 is a very toxic and evil-smelling liquid and extreme care must be observed during the preparation and manipulation. All experimental procedures must be carried out in a fume hood and under nitrogen. The synthesis of CSe_2 was carried out using an adaptation of the method of Henriksen and Kristiansen.[3] Selenium powder (*ca.* 30 g) was reacted with CH_2Cl_2 vapour at a high temperature (575 °C) under nitrogen for 3 - 4 hours. CH_2Cl_2 was removed at atmospheric pressure and CSe_2 was obtained after distillation of the crude product under vacuum (Schlenck line) into a liquid nitrogen trap. The product was stored in a refrigerator at *ca.* -20 °C.

5.4 - Single-Source Precursors

A series of single source precursors has been synthesised characterised and used to grow thin films on various substrates. The crystal structures of various precursors have also been determined by X-ray single crystal crystallography. Bimetallic thiocarboxylate precursors; $[(Ph_3P)_2AgIn(SC\{O\}R)_4]$ (R = Me or Ph)[1] and $[(Ph_3P)_2CuM(SC\{O\}Ph)_4]$[2] were synthesised and donated by Prof. J. J. Vittal's group (Chemistry department, National University of Singapore, Singapore).

5.4.1 - [Cu($S_2CNMe^nHex)_2$]

Carbon disulfide (3.96 ml, 66 mmol) was added dropwise *via* a dropping funnel sodium hydroxide (2.64 g, 66 mmol) and N-methylhexylamine (10 ml, 66 mmol) in methanol (80 ml) at 0 °C. The yellow colour solution obtained was immediately added to copper chloride (5.26 g, 33 mmol) dissolved in water to give a black precipitate, which was filtered and dried under vacuum. The crude product was recrystallised from toluene at room temperature to give [$Cu(S_2CNMeHex)_2$]. Yield 64 %, m.p. 48 °C, Elemental analysis: $C_{16}H_{32}S_4N_2Cu$ Calculated: C 43.29, H: 7.2, N: 6.05 %. Found: C: 42.76, H: 6.97, N: 6.05 %. EI-MS: m/z 444 [M^+], 253 [$CuS_2CNCH_3C_6H_{13}$], 117 [S_2CNCH_2CH], 116 [S_2CNCH_2C].

5.4.2 - [Cu($Se_2CNMe^nHex)_2$]

Carbon diselenide (2.4 g, 7.06 mmol) in 1,4-dioxane (100 ml) was slowly added *via* a dropping funnel to a stirred solution of sodium hydroxide (0.56 g, 7 mmol) and *N*-methylhexylamine (2 ml, 7.06 mmol) at -10 °C. The resultant solution was filtered and immediately added to a solution of copper chloride (0.94 g, 3.53 mmol) to give a black precipitate. The precipitate was then filtered and dried under vaccum. The solid product was recrystallised from toluene at room temperature to give [$Cu(Se_2CNMeHex)_2$]. Yield 70 %, Elemental analysis: $C_{16}H_{32}Se_4N_2Cu$ Calculated: C: 30.45, H: 5.07, N: 4.44 %. Found: C: 30.84, H: 5.65, N: 4.45%. EI-MS: m/z 288 [$CuSe_2CNCH_3CH_2C$], 300 [$CuSe_2CNCCH_2CH_2CH$], 314 [$CuSe_2CNCHCH_2CH_2CH_2C$].

5.4.3 - [In(S_2CNMe^{n}Hex)$_3$]

Carbon disulfide (3.96 ml, 66 mmol) was added dropwise *via* a dropping funnel to sodium hydroxide (2.64 g, 66 mmol) and N-methylhexylamine (10 ml, 66 mmol) stirring vigorously in methanol (80 ml) at 0 °C. The yellow coloured solution obtained was immediately added to indium chloride (4.8 g, 21mmol mmol) dissolved in water to give a white precipitate, which was filtered and dried under vacuum. The crude product was recrystallised from toluene at room temperature to give [In(S_2CNMeHex)$_3$]. Yield 67 %, m. p. 100 °C, Elemental analysis: $C_{24}H_{48}N_3S_6In$ Calculated: C: 42.02, H: 6.91, N: 5.88 %. Found: C: 42.27, H: 6.73, N: 6.01 %. ^{1}H NMR (δ, C_6D_6, 300 MHz): 0.86 (t, 9H, -$NCH_2CH_2CH_2CH_2CH_2\mathit{CH_3}$), 1.18 (m, 18H, -$CH_2CH_2\mathit{CH_2CH_2CH_2}CH_3$), 1.38 (m, 6H, -$NCH_2\mathit{CH_2}CH_2CH_2CH_2CH_3$), 2.8 (s, 9H, -$N\mathit{CH_3}$), 3.3 (t, 6H, -$N\mathit{CH_2}CH_2CH_2CH_2CH_2CH_3$).

5.4.4 - [In(Se_2CNMe^{n}Hex)$_3$]

Carbon diselenide (1.85 g, 1.08 mmol) in 1,4-dioxane (75 ml) was slowly added *via* a dropping funnel to a stirred solution of sodium hydroxide (0.217 g, 1 mmol) and *N*-methylhexylamine (0.8 ml, 7.06 mmol) in methanol (100 ml) at -10 °C. The resultant orange solution was filtered and immediately added to a solution of indium chloride (0.4 g, 0.36 mmol) in water (50 ml) to give a yellow precipitate. The precipitate was then filtered and dried under vaccum. The solid product was recrystallised from toluene at room temperature to give [In(Se_2CNMeHex)$_3$]. Yield 57 %, Elemental analysis: $C_{24}H_{48}N_3Se_6In$ Calculated: C: 29.81, H: 4.96, N: 4.35 %. Found: C: 30.83, H: 4.97, N: 4.40 %. ^{1}H NMR (δ, C_6D_6, 300 MHz): 0.55 (t, 9H, -$NCH_2CH_2CH_2CH_2CH_2\mathit{CH_3}$), 0.77

(m, 18H, -$CH_2CH_2CH_2CH_2CH_2CH_3$), 1.00 (m, 6H, -$NCH_2CH_2CH_2CH_2CH_2CH_3$), 2.4 (s, 9H, -$NCH_3$), 2.9 (t, 6H, -$NCH_2CH_2CH_2CH_2CH_2CH_3$).

5.4.5 - [$Ga(S_2CNMe^nHex)_3$]

Carbon disulfide (3.96 ml, 66 mmol) was added dropwise *via* a dropping funnel sodium hydroxide (2.64 g, 66 mmol) and N-methylhexylamine (10 ml, 66 mmol) in methanol (80 ml) at 0 °C. Gallium chloride (14.66 ml) in hexane solution (1.5 M) was slowly added to the solution *via* an equilibrating funnel to give a white solid, which was was filtered and dried under vacuum. The solid product was recrystallised from toluene at room temperature to give [$Ga(S_2CNMeHex)_3$]. Yield 68 %, m. p. 85 °C, Elemental analysis: $C_{24}H_{48}N_3S_6Ga$ Calculated: C: 44.99, H: 7.55, N: 6.56 % Found: C: 44.78, H: 8.14, N: 6.58 %. ^1H NMR (δ, C_6D_6, 300 MHz): 0.92 (t, 9H, $NCH_2CH_2CH_2CH_2CH_2CH_3$), 1.18 (m, 18H, -$CH_2CH_2CH_2CH_2CH_2CH_3$), 1.40 (m, 6H, -$NCH_2CH_2CH_2CH_2CH_2CH_3$), 2.8 (s, 9H, -$NCH3$), 3.4 (t, 6H, -$NCH_2CH_2CH_2CH_2CH_2CH_3$).

5.4.6 - [$NH(SeP^iPr_2)_2$]

A solution of diisopropylchlorophosphine (72 g , 0.472 mol) in anhydrous toluene (100 ml) was added dropwise over 45 minutes to a stirred solution of 1,1,1,3,3,3-hexamethyldisilazane (38.07 g , 0.236 mol) in anhydrous toluene (150 ml) at 60 °C. The reaction was stirred at 60 - 70 °C for 4 hours and cooled to room temperature. Selenium powder (37.27 g , 0.472 mol) was added and the suspension heated at reflux for 12 hours. The resulting orange homogeneous solution was concentrated to *ca.* 100 ml and cooled at O °C for 12 hours. The resulting white precipitate was recovered and washed

with diethyl ether (100 ml) and cold toluene (100 ml). Recrystallisation from chloroform/hexane. Yield 71 %, m. p. 171-173 °C, Elemental analysis: $C_{12}H_{29}NP_2Se_2$ Calculated: C: 35.39, H: 7.18, N: 3.44, P: 15.28 % Found: C: 35.31, H: 7.26, N: 3.49, P: 15.10 %. ^{1}H NMR (δ, $CDCl_3$, 300 MHz): 1.3 (m, 24H, $8CH_3$-R), 2.75 (m, 4H, 4R-CH), 3.1 (s, 1H, N-H). ^{31}P NMR (δ, $CDCl_3$, 400 MHz): 90.829. FT-IR: 1385, 3209 (N-H), 907, 879 (P-N-P), 489 (P-Se) cm^{-1}. EI-MS: *m/z* 408 ($M + H^+$).

5.4.7- $[Cd((SeP^iPr_2)_2N)_2]$

Sodium methoxide (1.09 g, 19.7 mmol) was added to a stirred solution of $NH(SeP^iPr_2)_2$ (6 g, 19.16 mmol) in anhydrous methanol (100 ml) and stirred for 10 minutes at room temperature. $CdCl_2$ (1.76 g, 9.56 mmol) was added to the resulting solution and white precipitate was formed immediately. The suspension was furthur stirred for 2 - 3 hours and it was filtered and dried under vaccum. The compound was recrystallised from toluene. Yield 85 %, m. p. 161-163 °C, Elemental analysis: $C_{24}H_{56}N_2P_4Se_4Cd$ Calculated: C: 31.16, H: 6.10, N: 3.03, P: 13.39 %. Found: C: 31.33, H: 6.15, N: 2.98, P: 13.53 %. ^{1}H NMR (δ, $CDCl_3$, 300 MHz): 1.15 (m, 48H, $16CH_3$-R), 2.1 (m, 8H, 8R-CH). ^{31}P NMR (δ, $CDCl_3$, 400 MHz): 57.10. FT-IR: 1226, 763 (P-N-P), 425 (P-Se) cm^{-1}. EI-MS: *m/z* 926 ($M + H^+$).

5.4.8 - $[MeCd\{(SeP^iPr_2)_2N\}]_2$

A solution of cadmium imino-bis(diisopropylphosphine selenide) (2.4 g, 2.59 mmol) in dry toluene (~ 50 ml) was stirred with dimethylcadmium (0.38 g, 2.59 mmol) at room temperature for 1 hour. After removal of solvent under vacuum, a yellow coloured

solid was obtained. Some of this product was recrystallised in toluene to give clear crystals. Yield 87 %, m. p. 191 °C, Elemental analysis: $C_{26}H_{62}N_2P_4Se_4Cd_2$ Calculated: C: 29.28, H: 5.81, N: 2.63 %. Found: C: 30.40, H: 6.12, N: 2.84 %. ^{1}H NMR (δ, $CDCl_3$, 300 MHz): 0.10 [s, 6H, Cd-CH_3), 0.8 (m, 48H, 16CH_3-R), 1.5 (m, 8H, 8R-CH). ^{31}P NMR (δ, $CDCl_3$, 400 MHz): 54.76. FT-IR: 671 (Cd-C), 1227, 754 (P-N-P).

5.4.9 - [Zn((SeP^{i}Pr$_2$)$_2$N)$_2$]

Sodium methoxide (0.56 g, 9.82 mmol) was added to a stirred solution of **1** (4.00 g , 9.82 mmol) in anhydrous methanol (100 ml). The resulting pink solution was stirred at room temperature for 10 minutes. Zinc chloride (0.68 g, 4.91 mmol) was added yielding an immediate off white precipitate. The suspension was stirred at room temperature for 2 hours. The recovered solid was washed with methanol (100 ml) and dried under vacuum. The product was recrystallised from chloroform/methanol. Yield 87 %, m. p. 171-173 °C, Elemental analysis: $C_{24}H_{56}N_2P_4Se_4Zn$ Calculated: C: 32.83, H: 6.43, N: 3.19, P: 14.11 %. Found: C: 33.02, H: 6.61, N: 3.12, P: 14.18 %. ^{1}H NMR (δ, $CDCl_3$, 300 MHz): 1.2 (m, 48H, 16CH_3-R), 2.0 (m, 8H, 8R-CH). ^{31}P NMR (δ, $CDCl_3$, 400 MHz): 57.20. FT-IR: 1228, 762 (P-N-P), 427 (P-Se) cm^{-1}. EI-MS: *m/z* 878 (M + H$^+$).

5.4.10 - [Me$_2$Ga(SeP^{i}Pr$_2$)$_2$N]

The compound was prepared by the addition of Me_3Ga (0.75 g, 6.54 mmol) in toluene (25 ml) to a stirred solution of NH(SeP^{i}Pr$_2$)$_2$ (2.7 g, 6.55 mmol) in toluene. Removal of solvent and volatiles *in vacuo* led to a viscous liquid which was crystallised by adding hexane. Yield 84 %, m.p. 61 °C. Elemental analysis: $C_{14}H_{34}N_1P_2Se_2Ga$

Calculated: C, 33.23, H, 6.77, N, 2.77, P, 12.24 %. Found: C, 32.75, H, 6.85, N, 2.77, P, 11.86 %. ^{1}H NMR (δ, C_6D_6, 300 MHz): 0.60 (s, 6H, Ga-CH_3], 1.1 [m, 24H, C-CH_3], 1.95 [m, 4H, C-H]; ^{31}P NMR (δ, C_6D_6, 400 MHz): 57.43 [m]. FT-IR: 515, 569 (Ga-C), 1223 (P-N-P) cm^{-1}. EI-MS: *m/z* 507 (M + H$^+$), 491 (MeGa(SeP^{i}Pr$_2$)$_2$N)$^+$.

5.4.11 - [Et$_2$In(SeP^{i}Pr$_2$)$_2$N]

This preparation is as for [Me$_2$Ga(SeP^{i}Pr$_2$)$_2$N], except that the reaction involved the following quantities. NH(SeP^{i}Pr$_2$)$_2$ (1.5 g, 3.68 mmol), triethylindium (0.75 g, 3.67mmol). Recrystallisation was carried out from toluene. Yield 76%, m.p. 62 - 64 °C. Elemental analysis: $C_{16}H_{38}N_1P_2Se_2In$ Calculated: C, 33.18, H, 6.61, N, 2.42, P, 10.70 %. Found: C, 33.54, H, 6.81, N, 2.41, P, 10.71 %. ^{1}H NMR (δ, C_6D_6, 300 MHz): 1.1 (m, 24H, C-CH_3], 1.25 [q, 4H, In-CH_2], 1.65 [6H, t, C-CH_3], 1.9 [4H, m, C-H]; ^{31}P NMR (δ, C_6D_6, 400 MHz): 58.45 [m]. FT-IR: 513, 569 (In-C), 1231 (P-N-P) cm^{-1}. EI-MS: *m/z* 579 (M + H$^+$), 549 (EtIn(SeP^{i}Pr$_2$)$_2$N)$^+$.

5.4.12 - [Me$_2$In(SeP^{i}Pr$_2$)$_2$N]

Trimethylindium (0.43 g, 2.69 mmol) was sublimed into a flask into which was added dry toluene (40 ml), and then NH(SeP^{i}Pr$_2$)$_2$ (1.1 g, 2.69 mmol) while the flask was held at -196 °C. After addition, the flask was slowly brought to room temperature, and a fierce reaction was observed as the experiment commenced. The reactants were stirred for 30 mins, at which point the volatiles were removed *in vacuo* to yield a white powder. Yield 75%, m.p. 57 °C. Elemental analysis: $C_{14}H_{34}N_1P_2Se_2In$ Calculated: C, 30.53, H, 6.17, N, 2.54 %. Found: C, 29.07, H, 5.98, N, 2.44 %. ^{1}H NMR (δ, C_6D_6, 300 MHz): 0.47

(s, 6H, In-CH_3], 1.1 [m, 24H, C-CH_3], 1.90 [4H, m, C-H]; ^{31}P NMR (δ, C_6D_6, 400 MHz): 58.22 [m]. FT-IR: 512 (In-C), 1229 (P-N-P) cm^{-1}. EI-MS: *m/z* 551 ($M + H^+$), 535 $(MeIn(SeP^iPr_2)_2N)^+$.

5.5 - Chemical Vapour Deposition (CVD) Methods

5.5-1 - Aerosol-Assisted Chemical Vapour Deposition (AACVD)

The AACVD kit was set up as in Fig. 5.1. The carrier gas flow rate was controlled by Platon flow gauges. The solution in the flask is placed in a water bath above the piezoelectric modulator of a humidifier, where aerosol droplets are generated and transferred by the carrier gas into a hot-wall zone. Then both the solvent and the precursor evaporate and the precursor vapour reaches the heated substrate surface where thermally induced reactions and film deposition take place. This homemade aerosol-assisted chemical vapour deposition kit consists of a two-neck flask, a PIFCO ultrasonic humidifier (Model No. 1077) and a CARBOLITE furnace.

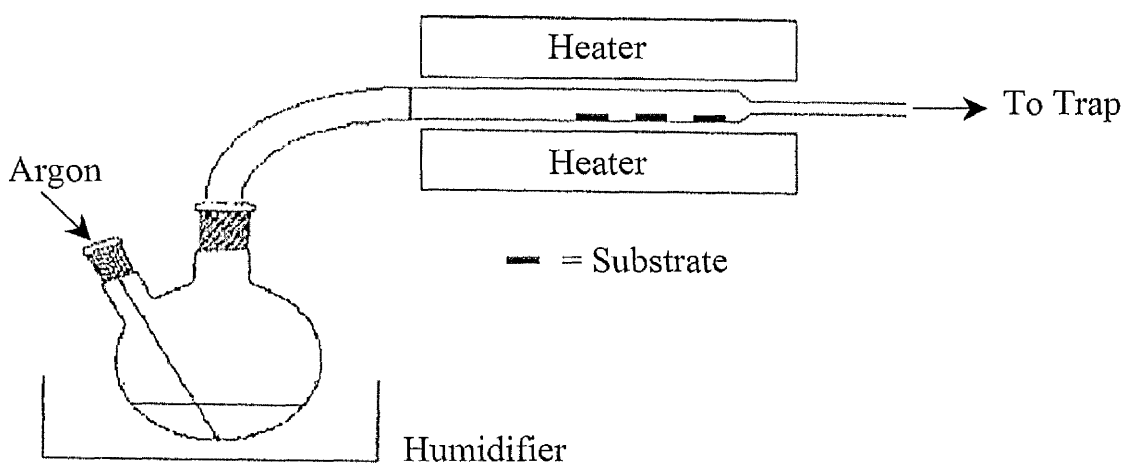

Figure 5.1 Schematic diagram of an aerosol-assisted CVD kit.

5.5.2 - Low-Pressure Metal-Organic Chemical Vapour Deposition (LP-MOCVD)

Deposition of thin films was also carried out in a home-made LP-MOCVD reactor (Fig. 5.2). A graphite susceptor held substrates (dimensions 10 × 15 mm) which were heated by a tungsten halogen lamp and a thermocouple monitored the temperature of the susceptor. The pressure in the reactor was kept at 10^{-2} Torr throughout CVD experiments.

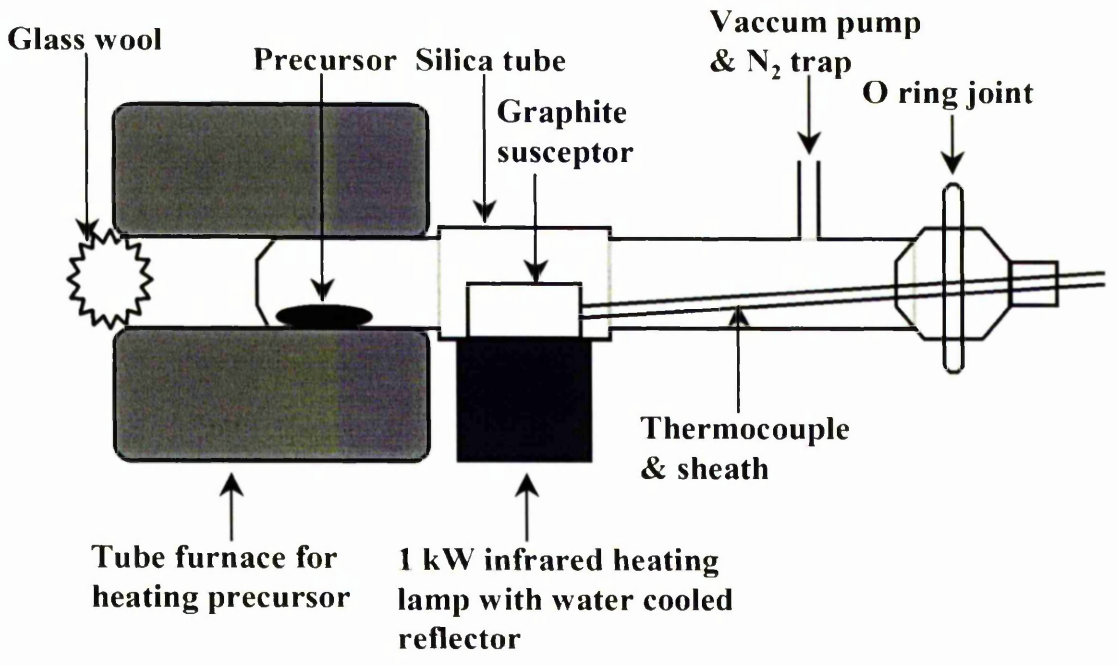

Figure 5.2 Schematic diagram of a cold-wall LP-MOCVD reactor.

5.6 - Substrates

The cleaning process of substrates used for CVD experiments includes removing unwanted impurities and residues. A standard procedure for cleaning glass substrates can be as follows;

- Glass slides were degreased in trichloroethylene and placed in acetone to remove organic residues.
- Substrates were rinsed in deionised water.
- The substrates were placed in 50 % nitric acid for 30 mins and a further 10 mins ultrasonication in deionised water.
- Finally rinsed in deionised water and air-dried.

Single crystalline substrates were rinsed in ethanol (HPLC) grade, rinsed in deionised water and then air-dried.

5.7 - Pyrolysis Experiments

The pyrolysis experiment was performed in a quartz glass reactor using a heating furnace. The sample was heated to 475 °C under a constant flow of argon.

5.8 - Characterisation Methods

5.8.1 - Characterisation of Compounds

NMR spectra were carried out using a Bruker AM-500 FT, Bruker AC300 FT-NMR Spectrometers, as C_6D_6 or $CdCl_3$. Infrared spectra were recorded on a Specac single reflectance ATR instrument. Mass spectra were recorded on a Kratos concept 1S instrument. Melting points were recorded on a Gallenkamp melting point apparatus and are uncorrected. TGA measurements were carried out by a Seiko SSC/S200 model with a heating rate of 10 °C min^{-1} under nitrogen.

5.8.2 - UV-Vis Spectroscopy (UV-Vis)

A Heλios-Beta Thermospectronic spectrophotometer was used to carry out the optical measurements. For a direct band gap material with parabolic bands, α is related to the bandgap energy Eg by

$$\alpha = C(h\nu - Eg)^{1/2}$$

Where C is a constant. The linear dependence of α^2 *vs.* $h\nu$ is indicative of direct bandgap materials.

5.8.3 - X-ray Powder Diffraction (XRPD)

X-ray Powder diffraction (XRPD) studies were carried out by a Bruker AXS D8 diffractometer using monochromated Cu-K_α radiation. The samples were mounted flat and scanned in a step size of 0.04° with a count rate of 2.5 sec. The diffraction patterns were then compared to the documented patterns in the JCPDS index.

The *d*-spacings were calculated using Bragg's Law:

$$n\lambda = 2dsin\theta$$

Where λ is the wavelength of the radiation used, n is an integer, d is the perpendicular spacing between the lattice planes in the crystal and θ is the complement of the angle of incidence of the X-ray beam.

5.8.4 - Scanning Electron Microscopy (SEM) and Energy-Dispersive Spectroscopy (EDAX)

All samples were coated with carbon, to avoid charging of the sample by the electron beam, using Edward's coating system E306A before scanning electron

microscopy (SEM) was carried out. SEM was carried out using Philip XL30 FEG. Energy dispersive X-ray analysis (EDAX) analyses were preformed using DX4.

5.8.5 - Atomic Force Microscopy (AFM)

The Burleigh instruments Metris-2000 was used in non-contact mode for the AFM measurements.

5.8.6 - X-ray Photoelectron Spectroscopy (XPS)

The XPS measurements were performed in the ultra-high vacuum chamber (base pressure of 10^{-8} Pa) of an ESCA 300 spectrometer using Mg-$K\alpha$ excitation. The energy scale was calibrated using Au and argon ions were used for etching. The energy scale was calibrated using $C1s$ (284.6 eV) as a reference. Samples were etched for 1 hour to remove impurities obtained from the ambient. Furthermore, the peak areas of the element cores are measured and used to calculate the elemental ratios for the deposited films. Elements composition was calculated using the following relationship:

$$Cx = \frac{Ix / Sx}{\sum_{X} Ix / Sx} \times 100\%$$

Where Ix is the area of the peak under the curve for the element x and Sx is the corresponding sensitivity factor.

5.8.7 - Crystallographic Structural Determination

Crystallographic data for $[Zn((SePPh_2)_2N)_2]$, $[Zn((SeP^iPr_2)_2N)_2]$ and $[MeCd\{(SeP^iPr_2)_2N\}]_2$ were collected on a CAD-4 diffractometer and Mo-Kα radiation ($\lambda = 0.71069$ Å) using ω-2θ scan. Crystallographic measurements for $[Me_2Ga(SeP^iPr_2)_2N]$ and $[Me_2In(SeP^iPr_2)_2N]$ were made using graphite monochromated Mo-Kα radiation ($\lambda = 0.71073$Å) on a Bruker APEX diffractometer. The structures were solved by Direct Methods and refined by full-matrix least squares on F^2.[4] All calculations were carried out using the SHELXTL package.[5] All non-hydrogen atoms were refined with anisotropic atomic displacement parameters. Hydrogen atoms were placed in calculated positions, assigned isotropic thermal parameters and allowed to ride on their parent carbon atoms.

References

1. T. C. Deivaraj, J.-H. Park, M. Afzaal, P. O'Brien, J. J. Vittal, *Chem. Mater.*, **2003**, *15*, 2383.
2. T. C. Deivaraj, J.-H. Park, M. Afzaal, P. O'Brien, J. J. Vittal, *J. Chem. Soc., Chem. Commun.*, **2001**, 2304.
3. L. Henrikson and E. S. S. Kristansen, *Int. J. Sulfur Chem, Part A,* **1972**, *2*, 133.
4. G. M. Sheldrick, **1997.** SHELXL97 and SHELXS 97. University of Göttingen, Germany.
5. Bruker **2000** SHELXTL. Version 6.10. Bruker AXS Inc., Madison, Wisconsin, USA.

Summary of Conclusions and Future Work

Semiconductor compounds are important materials in modern materials, used principally in a large number of electronic devices commonly used in day to day basis. The preparation of semiconducting materials often involves the decomposition of organometallic or metal-organic precursors. The research carried out in this thesis concerns the syntheses and characterisation (IR, NMR, TGA and MS) of metal-organic precursors and growth of thin film materials by techniques such as metal-organic low-pressure chemical vapour deposition (LP-MOCVD) and aerosol-assisted chemical vapour deposition (AACVD).

First part of research focuses on materials which have potential applications in solar cells such as $CuInE_2$ (E = S, Se) and $CuGaS_2$. Such materials have been deposited using metal-organic compounds by CVD techniques and characterised by XRPD, SEM/EDAX, and UV. XRPD showed a preferred orientation along the (112) plane regardless of growth temperatures. Attempts to deposited $AgInS_2$ films from bimetallic compounds, $[(Ph_3P)_2AgIn(SCOR)_4]$ (R = Me, Ph) were also attempted using AACVD. However, XRPD showed the presence of $AgIn_5S_8$ films with a preferred orientation of (331) plane.

The second part of research involved the growth of thin films which have potential applications in optoelectronic and photovoltaic devices. For this purpose, $[M((SePR_2)_2N)_2]$ (M = Cd(II), Zn(II); R = Ph, ^{i}Pr) and $[MeCd\{(SeP^iPr_2)_2N\}]_2$ have been synthesized and used as single-source precursors for growth of metal selenide films by LP-MOCVD. X-ray single crystal structures of $[Zn((SePR_2)_2N)_2]$ (R = Ph, ^{i}Pr) show distorted tetrahedral geometry at the zinc atoms. A new mixed-alkyl cadmium complex,

$MeCd\{(SeP^iPr_2)_2N\}]_2$ also has been synthesised by comproportionation of Me_2Cd and $[Cd((SeP^iPr_2)_2N)_2]$ in anhydrous toluene. XRPD of deposited materials confirmed the growth of hexagonal metal selenide films and show different surface morphologies depending on growth temperatures.

Finally, alkane elimination reactions between $[NH(SeP^iPr_2)_2]$ and group 13 metal alkyls have been performed. X-ray single crystal structures of $[Me_2M(SeP^iPr_2)_2N]$ (M = Ga (III) or In (III)) show Se_2C_2 coordination at the metal centres. The synthesised compounds were utilized to produce hexagonal M_2Se_3 (M = In. Ga) materials on glass substrates by LP-MOCVD and AACVD processes.

Semiconductor nanocrystals have attracted much attention in recent years in both fundamental research and technical applications because of their unique size-dependent optical and electronic properties. Future work will concentrate on producing a simple and easily-controllable method to prepare I-III-VI_2 nonocrystals by thermolysing $[(Ph_3P)_2AgIn(SCOR)_4]$ (R = Me, Ph) in hexadecylamine (HDA) or trioctylphosphine oxide (TOPO). These nanocrystals will be further investigated for their applications in devices such as solar cells.

Appendix

Printed Publications

CHEMCOMM Communication
www.rsc.org/chemcomm

Single-source precursors to ternary silver indium sulfide materials

Theivanayagam C. Deivaraj,[a] Jin-Ho Park,[b] Mohammmad Afzaal,[b] Paul O'Brien*[b] and Jagadese J. Vittal*[a]

[a] *Department of Chemistry, 3 Science Drive 3, National University of Singapore, Singapore. E-mail: chmjjv@nus.edu.sg*

[b] *The Manchester Materials Science Centre and Department of Chemistry, The University of Manchester, Oxford Road, Manchester, UK M13 9PL. E-mail: paul.obrien@man.ac.uk*

Received (in Cambridge, UK) 1st August 2001, Accepted 1st October 2001
First published as an Advance Article on the web 24th October 2001

Compounds of type $[(Ph_3P)_2AgIn(SC\{O\}R)_4]$ (R = Me (1), Ph (2)) are excellent single-source precursors for $AgInS_2$ bulk materials by pyrolysis and $AgIn_5S_8$ films by aerosol assisted chemical vapour deposition (AACVD).

In the past two decades chemists have been interested in synthesizing effective molecular precursors for various metal chalcogenides.[1–4] However, the possibility of single-source precursors for silver indium sulfide materials has been unexplored. Both $AgInS_2$ and $AgIn_5S_8$ are known to be semiconducting.[5–8] $AgInS_2$ finds applications as linear and nonlinear optical materials. The band gap of $AgIn_5S_8$ is 1.80 eV (300 K) and has been identified as making it a suitable candidate for photovoltaic solar cell applications.[9] Thin films of these sulfides have been obtained by spray pyrolysis[10,11] which also deposits Ag_2S.[10] Various metal monothiocarboxylates have been used as single-source precursors for metal sulfides.[12–14] Hence we attempted to synthesize bimetallic thiocarboxylate compounds as single-source molecular precursors to silver indium sulfides. Here we report the synthesis and characterization of compounds of the type $[(Ph_3P)_2AgIn(SCOR)_4]$ [R = Me (**1**), Ph (**2**)] along with the results of AACVD experiments.

The compounds were synthesized by reacting $[(Ph_3P)_2AgCl]_2$ and $InCl_3{\cdot}4H_2O$ with four molar equivalents of $Na^+RC\{O\}S^-$.† The structure of compound **2** (as its chloroform solvate) has been determined unequivocally by X-ray crystallography.‡

A view of **2** is shown in Fig. 1. Compound **2** consists of $(Ph_3P)_2Ag$ and $In(SC\{O\}Ph)_2$ units bridged by two $PhC\{O\}S^-$ ligands through μ-*S* bridging. The Ag(I) centre has distorted tetrahedral geometry with a P_2AgS_2 core while In(III) adopts distorted octahedral coordination geometry with two terminal $PhC\{O\}S^-$ anions chelating to In(III). The $AgInS_2$ ring is essentially planar with the two benzoyl groups attached to the S atoms in *anti* fashion.

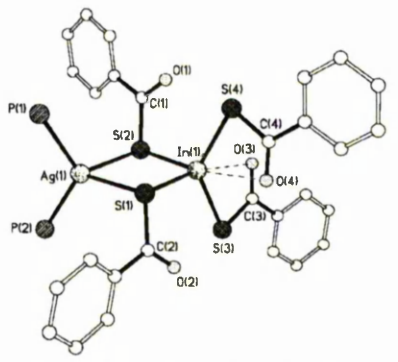

Fig. 1 Molecular structure of compound **2**. All hydrogen atoms and the phenyl rings on the triphenylphosphine ligand have been deleted for clarity. Selected bond distances (Å) and angles (°): Ag(1)–S(1), 2.7032(8); Ag(1)–S(2), 2.7173(8); Ag(1)–P(1), 2.4649(8); Ag(1)–P(2), 2.4573(1); In(1)–S(1), 2.5421(8); In(1)–S(2), 2.5352(2); In(1)–S(3), 2.4594(9); In(1)–S(4), 2.4571(9); In(1)–O(3), 2.672(2); In(1)–O(4), 2.664(3); S(1)–Ag(1)–S(2), 87.20(2), P–Ag(1)–S, 104.47(3)–117.61(3); P(2)–Ag(1)–P(1), 122.44(3); S(2)–In(1)–S(1), 87.20(2); S(3)–In(1)–S(1), 108.76(3); S(4)–In(1)–S(1), 101.05(3); S(3)–In(1)–S(2), 99.53(3); S(4)–In(1)–S(2), 111.23(3); S(4)–In(1)–S(3), 134.75(3); S–In–O, 59.98(6)–170.67(6); In(1)–S(1)–Ag(1), 89.05(2); In(1)–S(2)–Ag(1), 88.88(2).

The residual weights observed for **1** and **2** in thermogravimetric analyses indicate the formation of $AgInS_2$. The decomposition occurs in unresolved multiple steps in the temperature range 132–315 °C for **1** and 175–328 °C for **2**. X-Ray powder diffraction (XRPD) of the final residue obtained from pyrolysis of compounds **1** and **2** indicated the formation of orthorhombic $AgInS_2$, JCPDS: 25-1328 (Fig. 2).§ I-III-VI_2 materials are known to prefer tetragonal structures and hence the formation of the high temperature orthorhombic $AgInS_2$ phase is interesting.[4,15]

However, aerosol assisted chemical vapour deposition (AACVD) of a THF solution of compound **1** yielded $AgIn_5S_8$.¶ Films on glass deposited at 400 and 450 °C from the precursor were found to be transparent and adherent (Scotch tape test) with a dark red colour.

XRPD analysis (step size; 0.04° per 2 s) confirmed that the films were found to be cubic-$AgIn_5S_8$ (JCPDS 25-1329) with a preferred orientation along (311) (Fig. 3). Scanning electron

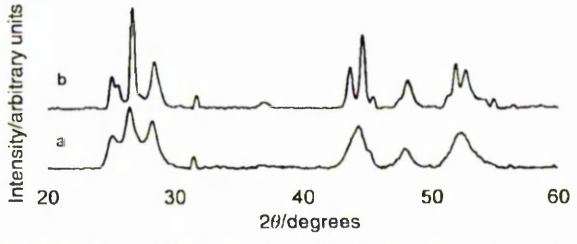

Fig. 2 X-Ray powder diffraction of $AgInS_2$ formed by pyrolysis of compounds (a) **1** and (b) **2**.

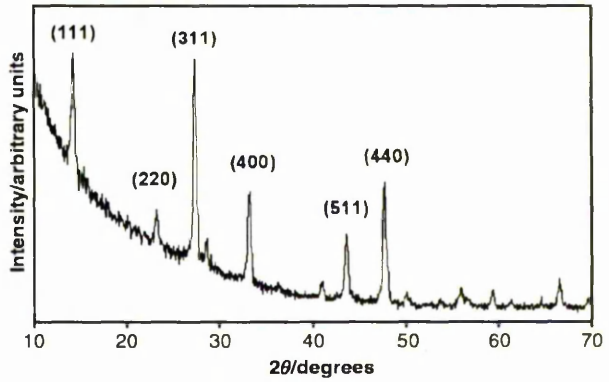

Fig. 3 X-Ray powder diffraction of $AgIn_5S_8$ thin films formed from compound **1**.

 DOI: 10.1039/b106923c

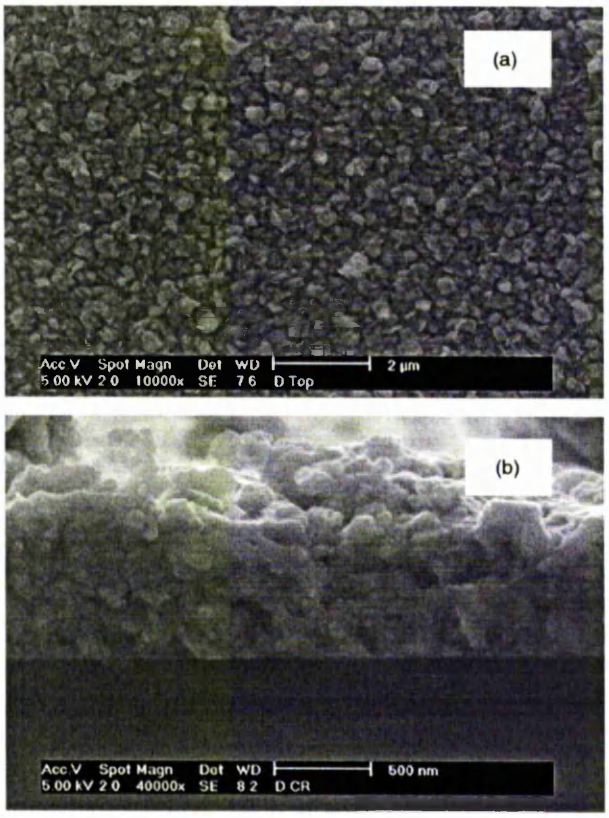

Fig. 4 SEM images of the film on glass grown at 400 °C from compound **1** (a): top view, (b): cross view.

microscopy (SEM) studies showed there is a dramatic change in the morphologies of films grown at 400 and 450 °C. The morphology of films grown at 450 °C consists of thin plate-like particles, perpendicularly laid down onto the substrate with random orientation. However, with decreasing growth temperature from 450 to 400 °C, the morphology was dense and no longer were plate-like particles formed (Fig. 4). Growth rate and average particle size of the films grown at 400 °C were *ca.* 0.3 μm h^{-1} and *ca.* 0.5 μm.

In conclusion, $[(Ph_3P)_2Ag(\mu\text{-}SC\{O\}Me\text{-}S)_2In(SC\{O\}Me)_2]$ (**1**) is shown to be a suitable single-source precursor for the deposition of cubic $AgIn_5S_8$ films on glass substrates by AACVD at 400 and 450 °C. The films grown at 400 °C were dense on a glass substrate. Similar results have also been obtained for **2**.

The significance of the current study is two fold. First of all, we have isolated and characterized bimetallic compounds containing In(III) and Ag(I) for the first time. Secondly, their potential use as single source precursors to silver indium sulfide has been clearly demonstrated. To the best of our knowledge no single-source precursors have been reported for silver indium sulfides previously in the literature. Further studies of novel single-source precursors for the growth of I–III–VI thin films are in hand.

J. J. V. would like to thank the National University of Singapore for a research grant (Grant No. R-143-000-084-112) and P. O. B. thanks EPRSC, UK for support.

Notes and references

† *Synthesis* of **1** and **2**: indium chloride tetrahydrate (0.10 g, 0.34 mmol) dissolved in 12 mL MeOH was added to a CH_2Cl_2 solution (25 mL) of $\{(PPh_3)_2AgCl\}_2$ (0.23 g, 0.17 mmol). To this solution was added NaSC{O}Me prepared *in situ* by mixing 97.5 μL (1.36 mmol) of $CH_3\{O\}CSH$ and 0.031 g (1.36 mmol) of sodium in 15 mL of MeOH. The solvents were removed by a flow of N_2. The product was extracted into 20 mL of CH_2Cl_2, filtered immediately, layered with 40 mL of petroleum ether (bp 35–60 °C) and allowed to stand at 5 °C overnight. The creamy precipitate thus formed was filtered off and washed with petroleum ether (bp 35–60 °C) and Et_2O and dried under vacuum. Yield: 0.37 g (76%). Anal. Calc. for $C_{44}H_{42}O_4S_4P_2AgIn$ (*M* 1047.71): C, 50.44; H, 4.02; S, 12.24. Found: C, 50.52; H, 4.02; S, 12.79%. ^1H NMR ($CDCl_3$): δ 2.24 (s, 12H, CH_3), 7.28–7.41 (m, 30H, $(C_6H_5)_3P$). ^{13}C NMR ($CDCl_3$): δ for thioacetato ligand: 34.1 ($CH_3C\{O\}S$), 206.8 ($MeC\{O\}S$); for the PPh_3: 129.4 (C_3, ^3J(P–C) = 9.8 Hz), 130.8 (C_4), 132.1 (C_1, ^1J(P–C) = 25.1 Hz), 134.1 (C_2, ^2J(P–C) = 16.3 Hz). ^{31}P NMR: δ 8.03. Compound **2** was also obtained by a procedure similar to that described for **1** but $PhC\{O\}SH$ was used instead of $MeC\{O\}SH$. Yield: 79%. Anal. Calc. for $C_{64}H_{50}O_4S_4P_2AgIn$ (*M* 1296.0): C, 59.31; H, 3.89; S, 9.90. Found: C, 58.36; H, 3.80; S, 9.66%. ^{13}C NMR ($CDCl_3$): δ for thiobenzoato ligand: 127.8 ($C_{2/6}$ or $C_{3/5}$), 129.2 ($C_{2/6}$ or $C_{3/5}$), 132.8 (C_4), 138.0 (C_1); for the PPh_3: 128.7 (C_3, ^3J(P–C) = 9.8 Hz), 129.9 (C_4), 132.3 (C_1, ^1J(P–C) = 22.9), 133.7 (C_2, ^2J(P–C) = 16.3). ^{31}P NMR: δ 7.28(s).

‡ *Crystal data* for **2**·$CHCl_3$: triclinic, $P\bar{1}$; a = 12.7284(5); b = 14.3145(6); c = 18.7071(7) Å; α = 90.716(1); β = 99.624(1); γ = 110.728(1)°; V = 3133.4(2) Å^3; Z = 2; D_c = 1.500 g cm^{-3}; R_1 = 0.0486; wR_2 = 0.0802. CCDC reference number 169235. See http://www.rsc.org/suppdata/cc/b1/b106923c/ for crystallographic data in CIF or other electronic format.

§ Pyrolysis experiments were performed in a quartz or Pyrex glass reactor using a horizontal tube furnace. The samples were heated to 300 °C under a dynamic vacuum of *ca.* 0.5 Torr.

¶ Thin films of silver indium sulfide were grown on borosilicate glass slides by AACVD. The growth apparatus consisted of a flask containing the solution with a pipette connected to an argon flow which was used as the propellant and carrier gas. The flask was attached, *via* reinforced tubing, to a silica tube containing the glass substrates, which were heated in a tube furnace. $[(Ph_3P)_2Ag(\mu\text{-}SCOMe)_2In(SCOMe)_2]$ (**1**) (~20 mg) was dissolved in tetrahydrofuran (20 mL) at room temperature, and injected into the growth apparatus, with the substrate at 400 or 450 °C. The system was allowed to run for 1 h, with a constant argon flow rate of 140 sccm (carrying the precursor from flask to substrate), at which point the substrates, thin coatings, were collected.

1 M. Bochmann, *Chem. Vap. Deposition*, 1996, **2**, 85.
2 P. O'Brien and R. Nomura, *J. Mater. Chem.*, 1995, **5**, 1761.
3 A. N. Gleizes, *Chem. Vap. Deposition*, 2000, **6**, 155.
4 M. Lazell, P. O'Brien, D. J. Otway and J. H. Park, *J. Chem. Soc., Dalton Trans.*, 2000, 4479.
5 S. C. Abrahams and J. L. Bernstein, *J. Chem. Phys.*, 1973, **59**, 1625.
6 I. Yonenaga, K. Sumino, E. Niwa and K. Masumoto, *J. Cryst. Growth*, 1996, **167**, 616.
7 A. Usujima, S. Takeuchi, S. Endo and T. Irie, *Jpn. J. Appl. Phys., Part 2*, 1981, **20**, 505.
8 Y. Ueno, Y. Hattori, M. Ito, T. Sugiura and H. Minoura, *Sol. Energy Mater. Sol. Cells*, 1992, **26**, 229.
9 N. M. Gasanly, A. Serpengüzel, A. Aydinli, O. Gürlü and I. Yilmaz, *J. Appl. Phys.*, 1999, **85**, 3198.
10 M. Ortega-López, A. Morales-Acevedo and O. Solorza-Feria, *Thin Solid Films*, 2001, **385**, 120.
11 M. Gorska, R. Beaulieu, J. J. Loferski and B. Roessler, *Thin Solid Films*, 1980, **67**, 341.
12 G. Shang, M. J. Hampden-Smith and E. N. Duesler, *Chem. Commun.*, 1996, 1733.
13 M. D. Nyman, M. J. Hampden-Smith and E. N. Duesler, *Inorg. Chem.*, 1997, **36**, 2218.
14 M. D. Nyman, K. Jenkins, M. J. Hampden-Smith, T. T. Kodas, E. N. Duesler, A. L. Rheingold and M. L. Liable-Sands, *Chem. Mater.*, 1998, **10**, 914.
15 C. C. Landry, J. Lockwood and A. R. Barron, *Chem. Mater.*, 1995, **7**, 699.

Novel Bimetallic Thiocarboxylate Compounds as Single-Source Precursors to Binary and Ternary Metal Sulfide Materials

Theivanayagam C. Deivaraj,[†] Jin-Ho Park,[‡] Mohammad Afzaal,[‡] Paul O'Brien,*[,‡] and Jagadese J. Vittal*[,†]

Department of Chemistry, National University of Singapore, Singapore 117543, and The Manchester Materials Science Centre and Department of Chemistry, The University of Manchester, Oxford Road, Manchester, UK M13 9PL

Received January 28, 2003. Revised Manuscript Received March 24, 2003

The binuclear compounds $[(Ph_3P)CuM(SC\{O\}Ph)_4]$ (M = Ga (**1**) or In (**2**)), $[(Ph_3P)_2AgGa(SC\{O\}Ph)_4]$ (**3**), $[(Ph_3P)_2AgIn(SC\{O\}R)_4]$ (R = Me (**4**) or Ph (**5**)) have been synthesized and characterized. The solid-state structures of compounds **1**–**3** have been determined by X-ray crystallography. Thermogravimetry and pyrolysis studies revealed that these compounds decompose to give the corresponding ternary metal sulfide materials. However, using the aerosol-assisted chemical vapor deposition (AACVD) method, In_2S_3 thin films were obtained from **2** and $AgIn_5S_8$ thin films were obtained from compounds **4** and **5**.

Introduction

Metal sulfides find a wide variety of applications, e.g., in photovoltaics and optoelectronic devices, and hence there has been considerable interest in synthesizing single-source precursors for these materials.[1–4] Such precursors have been considered as attractive sources for bulk materials, thin films, or nanoparticles. Among such materials, $CuInS_2$ with a band gap of 1.53 eV at ambient temperature is considered a good candidate for photovoltaic applications.[5] Solar cells fabricated with thin films of $CuInS_2$ have light-conversion efficiencies of ca. 7%.[6] $CuGaS_2$ has a wide band gap (2.49 eV) and is used in green light emitting diodes.[7] $AgInS_2$, $AgIn_5S_8$, and $AgGaS_2$ are used as linear and nonlinear optical materials.[8,9] Despite these many potential applications for ternary materials such as $MM'S_2$ (M = Cu or Ag and M′ = Ga or In), single-source precursors for these materials are rare. Kanatzidis et al. have prepared and characterized compounds of the general formula $(Ph_3P)_2Cu(\mu\text{-}ER)_2In(ER)_2$ (E = S or Se and R = Et or *iso*-Bu). The single-crystal structures of these compounds have also been reported.[10] These compounds, when subjected to pyrolysis, yielded the corresponding ternary materials. Buhro and co-workers have used $(Ph_3P)_2Cu(\mu\text{-}SEt)_2In(SEt)_2$ to obtain thin films of $CuInS_2$ using spray MOCVD.[11] Nomura et al. have prepared a compound of the formula $[Bu_2In(SPr)Cu(S_2CNPr_2)]$ and used it to deposit thin films of $CuInS_2$.[12] These authors have also reported the deposition of $CuInS_2$ by solution pyrolysis of Bu_2InSPr and $Cu(S_2CNBu_2)_2$.[13] Recently, two liquid compounds, $[(n\text{-}Bu_3P)_2Cu(SR)_2In(SR)_2]$ (R = Et and *n*-Pr) have been successfully used to deposit $CuInS_2$ thin films.[14,15] As a part of our ongoing explorations of metal–thiocarboxylate systems,[16–27] we have now devoted attention to the syntheses of single-source molec-

* For correspondence: paul.obrien@man.ac.uk (P.O.B.) or chmjjv@nus.edu.sg (J.J.V.).
† National University of Singapore.
‡ The University of Manchester.

(1) Bochmann, M. *Chem. Vap. Deposition* **1996**, *2*, 85.
(2) O'Brien, P.; Nomura, R. *J. Mater. Chem.* **1995**, *5*, 1761.
(3) Lazell, M.; O'Brien, P.; Otway, D. J.; Park, J. H. *J. Chem. Soc., Dalton Trans.* **2000**, 4479.
(4) Gleizes, A. N. *Chem. Vap. Deposition* **2000**, *6*, 155.
(5) Thiel, F. A. *J. Electrochem. Soc.* **1982**, *129*, 1570.
(6) Wu, Y. L.; Lin, H. Y.; Sun, C. Y.; Yank, M. H.; Hwang, H. L. *Thin Solid Films* **1989**, *168*, 113.
(7) Oishi, K.; Kobayashi, S.; Ohta, S. I.; Tsuboi, N.; Kaneko, F. *J. Cryst. Growth* **1997**, *177*, 88.
(8) Abrahams, S. C.; Bernstein, J. L. *J. Chem. Phys.* **1973**, *59*, 1625.
(9) Yonenga I.; Sumino, K.; Niwa, E.; Masumoto, K. *J. Cryst. Growth* **1996**, *167*, 616.
(10) Hirpo, W.; Dhingra, S.; Sutorik, A. C.; Kanatzidis, M. G. *J. Am. Chem. Soc.* **1993**, *115*, 1597.
(11) Hollingsworth, J. A.; Hepp, A. F.; Buhro, W. E. *Chem. Vap. Deposition* **1999**, *5*, 105.
(12) Nomura, R.; Seki, Y.; Matsuda, H. *J. Mater. Chem.* **1992**, *2*, 765.
(13) Nomura, R.; Fujii, S.; Kanaya, K.; Matsuda, H. *Polyhedron* **1990**, *9*, 361.
(14) Banger, K. K.; Harris, J. D.; Cowen, J. E.; Hepp, A. F. *Thin Solid Films* **2002**, *403–404*, 390.
(15) Banger, K. K.; Cowen, J.; Hepp, A. F. *Chem. Mater.* **2001**, *13*, 3827.
(16) Vittal, J. J.; Dean, P. A. W. *Inorg. Chem.* **1993**, *32*, 791.
(17) Vittal, J. J.; Dean, P. A. W. *Inorg. Chem.* **1996**, *35*, 3089.
(18) Vittal, J. J.; Dean, P. A. W.; Craig, D. C.; Scudder, M. L. *Inorg. Chem.* **1998**, *37*, 1661.
(19) Devy, R.; Vittal, J. J.; Dean, P. A. W. *Inorg. Chem.* **1998**, *37*, 6939.
(20) Sampanthar, J. T.; Deivaraj, T. C.; Vittal, J. J.; Dean, P. A. W. *J. Chem. Soc., Dalton Trans.* **1999**, 4419.
(21) Sampanthar, J. T.; Vittal, J. J.; Dean, P. A. W. *J. Chem. Soc., Dalton Trans.* **1999**, 3153.
(22) Deivaraj, T. C.; Lai, G. X.; Vittal, J. J. *Inorg. Chem.* **2000**, *39*, 1028.
(23) Deivaraj, T. C.; Dean, P. A. W.; Vittal, J. J. *Inorg. Chem.* **2000**, *39*, 3071.
(24) Deivaraj, T. C.; Vittal, J. J. *J. Chem. Soc., Dalton Trans.* **2001**, 322.
(25) Deivaraj, T. C.; Vittal, J. J. *J. Chem. Soc., Dalton Trans.* **2001**, 329.
(26) Deivaraj, T. C.; Lye, W. H.; Vittal, J. J. *Inorg. Chem.* **2002**, *41*, 3755.
(27) Lin, M.; Loh, K. P.; Deivaraj, T. C.; Vittal, J. J. *Chem. Commun.* **2002**, 1400.

10.1021/cm031027v CCC: $25.00
Published on Web 05/13/2003

ular precursors for I−III−VI materials. A preliminary account of this study has been published earlier.[28] In this paper we report on the synthesis and characterization of compounds of the type $[(Ph_3P)CuM(SC\{O\}Ph)_4]$ (M = Ga (**1**) or In (**2**)), $[(Ph_3P)_2AgGa(SC\{O\}Ph)_4]$ (**3**), and $[(Ph_3P)_2AgIn(SC\{O\}R)_4]$ (R = Me (**4**) or Ph(**5**)), their thermal properties, and results of AACVD experiments.

Experimental Section

General. All materials were obtained commercially and used as received. The solvents were dried by allowing them to stand over 3-Å molecular sieves overnight. The preparations were carried out under nitrogen atmosphere and the yields are reported with respect to the metal salts. The compounds are fairly stable but were stored under nitrogen at 5 °C to avoid any decomposition. The starting material $Ga(NO_3)_3{\cdot}xH_2O$ ($x \approx 3$ by TG analysis) was purchased from Aldrich and $[(Ph_3P)_2Cu(NO_3)]$ was prepared by a literature method.[29] Compounds **4** and **5** were prepared as described earlier.[28]

Synthesis of $[(PPh_3)Cu(\mu\text{-}SC\{O\}Ph\text{-}S)(\mu\text{-}SC\{O\}Ph\text{-}S,O)_2Ga(SC\{O\}Ph)]$ (1). To NaSC{O}Ph formed in situ (by reacting PhC{O}SH (184 μL, 1.56 mmol) and Na (0.04 g, 1.56 mmol) in MeOH (15 mL)), 0.1 g of $Ga(NO_3)_3{\cdot}3H_2O$ (0.32 mmol) in MeOH (10 mL) was added to get a yellow solution and was followed by the addition of $(Ph_3P)_2Cu(NO_3)$ (0.25 g, 0.39 mmol) in CH_2Cl_2 (15 mL). The orange solution thus obtained was stirred and the solvents were removed under a flow of N_2. The product obtained as red oil along with some yellow powder was extracted with CH_2Cl_2 (20 mL), and the resulting red solution was separated and layered with petroleum ether. Reddish yellow crystals were obtained the following day. The crystals of **1** were collected, washed with petroleum ether, and dried under vacuum. Yield 0.27 g (89%); mp 163 °C (decomposition). Anal. Calcd for $C_{46}H_{35}O_4S_4PCuGa$ (mol wt 944.29): C, 58.51; H, 3.74. Found: C, 58.48; H, 3.77. ^{13}C NMR ($CDCl_3$) δ, ppm thiobenzoato ligand: 127.3 ($C_{2/6}$ or $C_{3/5}$), 128.3 ($C_{2/6}$ or $C_{3/5}$), 131.4 (C_4), 138.8 (C_1), 202.9 (Ph*C*OS). PPh_3: 128.6 (C_3, ^3J(P−C) = 8.7 Hz), 129.6 (C_4), 132.9 (C_1, ^1J(P−C) = 27.2 Hz), 133.7 (C_2, ^2J(P−C) = 15.2 Hz). ^{31}P NMR: δ, ppm −1.54 (s). Selected IR data: 1594.9 (w, C=O) and 983.7 (s, C−S) cm^{-1}.

Synthesis of $[(PPh_3)Cu(\mu\text{-}SC\{O\}Ph\text{-}S,O)_2(\mu_2\text{-}SC\{O\}Ph\text{-}S_2,O)In(SC\{O\}Ph)]$ (2). The compound was synthesized using a procedure similar to **1** but $Ga(NO_3)_3{\cdot}3H_2O$ was replaced by $InCl_3{\cdot}4H_2O$. Yield 69%; mp 185 °C (melting with decomposition). Anal. Calcd for $C_{46}H_{35}O_4S_4PCuIn{\cdot}0.5\ CH_2Cl_2$ (mol wt 1031.85): C, 54.13; H, 3.52. Found: C, 54.38; H, 3.74. ^{13}C NMR ($CDCl_3$) δ, ppm thiobenzoato ligand: 127.9 ($C_{2/6}$ or $C_{3/5}$), 129.3 ($C_{2/6}$ or $C_{3/5}$), 133.1 (C_4), 137.7 (C_1), 206.7 (Ph*C*OS). PPh_3: 128.5 (C_3, ^3J(P−C) = 8.7 Hz), 129.6 (C_4), 132.8 (C_1, ^1J(P−C) = 20.0 Hz), 133.7 (C_2, ^2J(P−C) = 14.2 Hz). ^{31}P NMR: δ, ppm −1.57. Selected IR data: 1594.5 (s, C=O), 950.0 (s, C−S) cm^{-1}.

$[(PPh_3)_2Ag(\mu\text{-}SC\{O\}Ph\text{-}S)Ga(SC\{O\}Ph)_3]$ (3). A solution of PPh_3 (0.21 g, 0.78 mmol) in 15 mL of MeCN was added to a solution of $AgNO_3$ (0.07 g, 0.39 mmol) in 10 mL of MeCN and stirred for about 10 min to obtain a precipitate of $(PPh_3)_2AgNO_3$. The solvents were evaporated, and the resulting white solid, dissolved in 20 mL of $CHCl_3$, was added to $Ga(NO_3)_3{\cdot}3H_2O$ (0.1 g, 0.39 mmol) in 12 mL of MeOH. To this solution, C_6H_5COSNa (prepared in situ by reacting C_6H_5COSH (184 μL, 1.56 mmol) with Na (0.036 g, 1.564 mmol) in 15 mL of MeOH) was added. The resulting bright yellow solution was stirred for 30 min and then the solvents were removed by a flow of N_2. The product was extracted with $CHCl_3$ (15 mL) and filtered immediately, and the filtered product was layered with petroleum ether and stored at 5 °C. Colorless crystals of **3** thus obtained were filtered, washed with Et_2O, and dried under vacuum. Yield 0.37 g (76%); mp 167 °C (melting with decomposition). Anal. Calcd for $C_{64}H_{50}O_4S_4P_2AgGa$ (mol wt 1250.9): C, 61.45; H, 4.02. Found: C, 61.87; H, 4.06. ^{13}C NMR ($CDCl_3$) δ, ppm thiobenzoic acid ligand: 127.7 ($C_{2/6}$ or $C_{3/5}$), 128.3 ($C_{2/6}$ or $C_{3/5}$), 131.6 (C_4), 140.6 (C_1), 201.0 (Ph*C*OS). PPh_3: 128.6 (C_3, ^3J(P−C) = 9.8 Hz), 129.7 (C_4), 133.0 (C_1, ^1J(P−C) = 20.7 Hz), 133.8 (C_2, ^2J(P−C) = 16.3 Hz). ^{31}P NMR: δ, ppm 6.53. IR data (cm^{-1}): 1569.4 (s, C=O), 973.8 (w, C−S).

Instruments and Characterization. The $^{13}C\{^1H\}$ and $^{31}P\{^1H\}$ NMR spectra were recorded on a Bruker ACF300 FTNMR spectrometer using TMS as internal and 85% H_3PO_4 as external reference at 25 °C. The IR spectra (KBr pellet) were recorded using a Bio-Rad FTIR spectrometer. The elemental analyses were performed by the microanalytical laboratory of the chemistry department, National University of Singapore. Thermogravimetric analyses were carried out using a SDT 2980 TGA thermal analyzer with a heating rate of 10 °C min^{-1} in N_2 atmosphere using a sample size of 5−10 mg per run. X-ray powder patterns were obtained using a D5005 Bruker AXS X-ray diffractometer. Pyrolysis experiments were carried out in a horizontal tube furnace in a quartz reaction chamber. The quartz reactor was subjected to dynamic vacuum of about 0.5 Torr. The SEM images were obtained from a JEOL JSM-T220A instrument for bulk materials and a Philips XL30 FEG for thin films and EDAX analyses. The XPS measurements were performed in the ultrahigh vacuum chamber (base pressure of 10^{-8} Pa) of an ESCA 300 spectrometer using Mg Kα excitation. The energy scale was calibrated using Au and argon ions were used for etching.

X-ray Crystallography. The diffraction experiments were carried out at 20 °C on a Bruker SMART CCD diffractometer with Mo Kα radiation from a sealed tube. The program SMART[30] was used for collecting frames of data, indexing reflections, and determination of lattice parameters; SAINT[30] was used for integration of the intensity of reflections and scaling. SADABS[31] was used for absorption correction, and SHELXTL[32] was used for space group and structure determination and least-squares refinements on F^2. The relevant crystallographic data and refinement details are shown in Table 1. The phenyl ring of the thiobenzoate anion (C31−C36) in **1** was found to be disordered. Two disorder models with equal occupancies were refined for the same. There are 3.5 $CHCl_3$ solvent molecules present in **3**. All the solvent molecules were disordered and were treated with a soft SADI restraint on C−Cl and Cl··Cl distances. Disorder models were resolved for the $CHCl_3$ molecules. One molecule is disordered over two positions with occupancies of 0.55 and 0.45. Another $CHCl_3$ molecule is disordered over three locations with occupancies of 0.6, 0.25, and 0.15. The half molecule of $CHCl_3$ present in **3** is also disordered over two locations with occupancies of 0.3 and 0.2.

Aerosol-Assisted Chemical Vapor Deposition (AACVD). Approximately 0.25 g of precursor was dissolved in 30 mL of toluene (or THF) in a round-bottomed flask. Six glass substrates (1 × 2 cm) were placed inside the reactor tube. The carrier gas flow rate was controlled by Platon flow gauges. The solution in the flask was placed in a water bath above the piezoelectric modulator of a humidifier in which aerosol droplets were generated and transferred by the carrier gas (N_2, flow rate 180 sccm) into the hot-wall zone. Then both the solvent and the precursor were evaporated, and the precursor vapor reached the heated substrate surface where thermally induced reactions and film deposition took place. This homemade aerosol-assisted chemical vapor deposition kit consisted of a two-necked flask, a PIFCO ultrasonic humidifier (model 1077) and a Carbolite furnace.

(28) Deivaraj, T. C.; Park, J.-H.; Afzaal, M.; O'Brien, P.; Vittal, J. J. *Chem. Commun.* **2001**, 2304.

(29) Kubas, G. J. *Inorg. Synth.* **1970**, *19*, 93.

(30) *SMART & SAINT Software Reference Manuals*, Version 4.0; Siemens Energy & Automation, Inc.: Analytical Instrumentation: Madison, WI, 1996.

(31) Sheldrick, G. M. *SADABS Software for Empirical Absorption Correction*; University of Göttingen: Göttingen, Germany, 2000.

(32) *SHELXTL Reference Manual*, Version 5.1; Bruker Analytical X-ray Systems, Inc.: Madison, WI, 1997.

Table 1. Crystal Data and Structure Refinement for 1–3

	1	2	3
chemical formula	$C_{46}H_{35}CuGaO_4PS_4$	$C_{46}H_{35}CuInO_4PS_4 \cdot 0.5\ CH_2Cl_2$	$C_{64}H_{50}O_4S_4P_2AgGa \cdot 3.5\ CHCl_3$
formula weight	944.21	1031.77	1668.60
temperature, °C	20	20	−50
λ, Å	0.71073	0.71073 Å	0.71073
crystal system	monoclinic	triclinic	triclinic
space group	$P2_1/c$	$P\bar{1}$	$P\bar{1}$
unit cell dimensions			
a, Å	13.0239(2)	10.5914(1)	15.0668(7)
b, Å	9.2656(2)	11.8903(1)	15.3124(7)
c, Å	36.1156(8)	19.6156(3)	18.6217(8)
α, deg	90	74.151(1)	101.240(1)
β, deg	94.320(1)	77.889(1)	113.171(1)
γ, deg	90	77.254(1)	95.551(1)
V, Å^3	4345.8(2)	2288.19(5)	3801.6(3)
Z	4	2	2
ρ, g/cm^3	1.443	1.498	1.458
μ, mm^{-1}	1.381	1.286	1.177
F(000)	1928	1042	1682
θ range, deg	1.86 to 26.37	1.81 to 26.37	2.04 to 25.00
index ranges	$-16 \le h \le 16$	$-13 \le h \le 12$	$-17 \le h \le 17$
	$-11 \le k \le 11$	$-14 \le k \le 13$	$-18 \le k \le 15$
	$-30 \le l \le 45$	$-24 \le l \le 16$	$-17 \le l \le 22$
reflections collected	22503	13171	22382
independent reflections	8684, $R_{int} = 0.0670$	8996, $R_{int} = 0.0272$	13374, $R_{int} = 0.0219$
data/restraints/parameters	8684/0/474	8996/1/542	13374/84/803
GOF on F^2	1.094	1.054	1.028
final R indices ($I > 2\sigma(I)$)	R1 = 0.0858	R1 = 0.0398	R1 = 0.0670
	wR2 = 0.1903	wR2 = 0.1105	wR2 = 0.1989
R indices (all data)	R1 = 0.1327	R1 = 0.0531	R1 = 0.0852
	wR2 = 0.2161	wR2 = 0.1162	wR2 = 0.2124
extinction coefficient		0.0010(3)	
largest difference peak and hole, e·Å^{-3}	1.180 and −0.783	1.081 and −0.656	2.003 and −1.320

Results and Discussion

Synthesis. The compounds $[(Ph_3P)Cu(\mu\text{-}SC\{O\}Ph)_3M(SC\{O\}Ph)]$ (M = Ga(**1**) or In(**2**)) were prepared by reacting bis-triphenylphosphinecopper(I) nitrate with the appropriate $[M(SC\{O\}Ph)_4]^-$ anion as shown below in eq 1. In the resulting bimetallic complexes the copper atoms are bonded to the sulfur centers of the thiobenzoate ligands and only to one PPh_3 unit.

$$(Ph_3P)_2Cu(NO_3) + MX_3 + 4NaSC\{O\}Ph \rightarrow NaNO_3 + 3NaX + PPh_3 + [(Ph_3P)Cu(SC\{O\}Ph)_3M(SC\{O\}Ph)] \quad (M = Ga\ (\mathbf{1});\ In\ (\mathbf{2})) \quad (1)$$

Attempts to isolate the thioacetate analogues of **1** and **2** using a similar synthetic method were unsuccessful. Compounds **1** and **2** were fairly stable, however, they were stored at 5 °C in sample vials purged with nitrogen. From reactions of $(Ph_3P)_2Ag(NO_3)$ with the $[M(SC\{O\}R)_4]^-$ anion, no pure bimetallic compounds could be isolated. Hence, the synthetic route was slightly modified as follows. The bis-triphenylphosphine silver salts were premixed with the corresponding indium or gallium salts followed by the addition of the sodium thiocarboxylate. The reactions are summarized below (eq 2 or 3). These reactions yielded pure **3**–**5**.

$$(Ph_3P)_2Ag(NO_3) + Ga(NO_3)_3 \cdot 3H_2O + 4NaSC\{O\}Ph \rightarrow [(Ph_3P)_2Ag(\mu\text{-}SC\{O\}Ph)Ga(SC\{O\}Ph)_3] + 4NaNO_3 \quad (2)$$

$$(Ph_3P)_2AgCl + InCl_3 \cdot 4H_2O + 4NaSC\{O\}R \rightarrow [(Ph_3P)_2Ag(\mu\text{-}SC\{O\}Ph)In(SC\{O\}R)_3] + 4NaCl \quad (R = Me\ (\mathbf{4});\ Ph\ (\mathbf{5})) \quad (3)$$

However, under similar conditions we were unable to isolate $[(Ph_3P)_2AgGa(SC\{O\}Me)_4]$. Attempts to synthesize **4** and **5** at room temperature led to decomposition of the compounds, hence they were synthesized at 0 °C.

Table 2. Selected Bond Lengths (Å) and Angles (deg) of 1

Bond Lengths			
Cu(1)–S(1)	2.488(2)	Cu(1)–S(2)	2.265(2)
Cu(1)–S(3)	2.266(2)	Cu(1)–P(1)	2.266(2)
Ga(1)–S(1)	2.268(2)	Ga(1)–S(4)	2.240(2)
Ga(1)–O(2)	1.870(5)	Ga(1)–O(3)	1.879(5)
S(1)–C(1)	1.788(8)	S(2)–C(2)	1.666(7)
S(3)–C(3)	1.671(8)	S(4)–C(4)	1.767(8)
O(1)–C(1)	1.222(9)	O(2)–C(2)	1.280(8)
O(3)–C(3)	1.256(8)	O(4)–C(4)	1.229(9)
Bond Angles			
S(2)–Cu(1)–S(1)	107.66(8)	S(3)–Cu(1)–S(1)	102.26(7)
S(2)–Cu(1)–S(3)	119.17(9)	P(1)–Cu(1)–S(1)	113.17(7)
S(2)–Cu(1)–P(1)	105.94(8)	S(3)–Cu(1)–P(1)	108.86(7)
S(4)–Ga(1)–S(1)	117.69(8)	O(2)–Ga(1)–S(1)	121.2(2)
O(3)–Ga(1)–S(1)	113.8(2)	O(2)–Ga(1)–S(4)	99.1(2)
O(3)–Ga(1)–S(4)	102.2(2)	O(2)–Ga(1)–O(3)	99.7(3)
Ga(1)–S(1)–Cu(1)	79.39(6)	C(1)–S(1)–Cu(1)	110.6(3)
C(2)–S(2)–Cu(1)	111.5(3)	C(3)–S(3)–Cu(1)	113.3(2)
C(1)–S(1)–Ga(1)	90.5(3)	C(4)–S(4)–Ga(1)	96.9(3)
C(2)–O(2)–Ga(1)	132.6(5)	C(3)–O(3)–Ga(1)	133.6(5)
O(1)–C(1)–S(1)	118.7(6)	O(2)–C(2)–S(2)	125.8(6)
O(3)–C(3)–S(3)	124.9(5)	O(4)–C(4)–S(4)	120.8(7)

Structure of $[(PPh_3)Cu(\mu\text{-}SC\{O\}Ph\text{-}S)(\mu\text{-}SC\{O\}Ph\text{-}S,O)_2Ga(SC\{O\}Ph)]$ (1). A perspective view of **1** is shown in Figure 1 and selected bond lengths and angles are given in Table 2. In **1**, both the metal atoms, Cu(1) and Ga(1), are present in distorted tetrahedral geometry. The copper atom is bonded to one triphenylphosphine ligand and three sulfur atoms of three thiobenzoato ligands. All three thiobenzoato ligands bridge the two metal centers: two $PhC\{O\}S^-$ anions through a μ_2-*S*,*O*, and the other in a μ_2-*S* fashion. The distorted tetrahedral coordination environment at Ga(1) is made up by a S_2O_2 donor set. The P(1)–Cu(1)

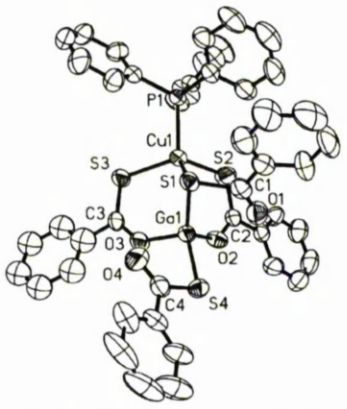

Figure 1. ORTEP diagram (with 50% probability of displacement ellipsoids) showing the molecular structure of **1**. Hydrogen atoms have been omitted for clarity.

distance, (2.266(2) Å) observed in **1** is normal.[22] The Cu(1)−S(1) distance, 2.488(2) Å, is longer than Cu(1)−S(2) and Cu(1)−S(3) (2.265(2) and 2.266(2) Å, respectively) because S(1) is also involved in bonding to the Ga atom. The Cu−S distances from bridging sulfur atoms are expected to be longer than those from nonbridging ligands.[21,22,24] Further, the shortening of C−S and lengthening of C−O distances may be attributed to the delocalization of electrons at the thiocarboxylate groups containing C(2) and C(3) atoms. A similar trend was observed in the other triphenylphosphinecopper thiocarboxylate compounds.[22] The Ga(1)−S(1) and Ga(1)−S(4) distances, 2.268(2) and 2.240(2) Å, respectively, are not equal as expected for the bridging and terminal Ga−S bonds. The Ga(1)−O(2) and Ga(1)−O(3) distances, 1.870(5) and 1.879(5) Å respectively, fall within the range of established Ga−O distances (1.780−2.020 Å) obtained from the Cambridge Structure Database.[33] The Ga(1)−O(1) and Ga(1)−O(4) distances, 2.690(6) and 2.913(7) Å, respectively, are significantly less than the sum of van der Waals radii, 3.4 Å, and represent very weak interactions. Further, the distorted tetrahedral geometry at Ga(1) (99.1−121.2°) appears to support this.

Structure of [(PPh$_3$)Cu(μ-SC{O}Ph-*S,O*)$_2$(μ_2-SC{O}Ph-*S*$_2$,*O*)In(SC{O}Ph)] (2). A view of **2** is shown in Figure 2 and selected bond lengths and angles are given in Table 3. Compound **2** is a bimetallic compound containing copper and indium atoms. Of these, Cu(1) is bonded to one triphenylphosphine ligand and three thiobenzoate anions through their sulfur donor sites forming a tetrahedral $PCuS_3$ core as in **1**. Three thiobenzoate anions bridge the two metal ions through two μ_2-*S,O* and one μ_2-*S*$_2$,*O* bonding modes. The fourth thiobenzoate anion chelates the indium metal atom. The coordination environment about the In(1) atom is thus distorted octahedral with a InO_4S_2 core. The P(1)−Cu(1) distance, 2.283(1) Å, is slightly longer than the corresponding bond distance observed in **1**. The Cu(1)−S(1) and Cu(1)−S(2) distances (2.265(1) and 2.281(1) Å, respectively) are longer than the Cu(1)−S(3) distance (2.470(1) Å) because of different types of bonding modes as explained above for **1**. It was also observed that the

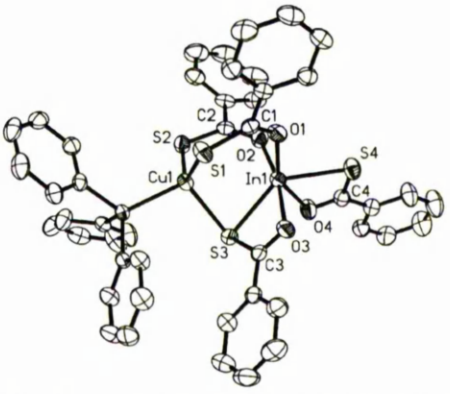

Figure 2. Thermal ellipsoid plot showing a view of **2**. Hydrogen atoms are not shown.

Table 3. Selected Bond Lengths (Å) and Angles (deg) of 2

	Bond Lengths		
Cu(1)−S(1)	2.265(1)	Cu(1)−S(2)	2.281(1)
Cu(1)−S(3)	2.470(1)	Cu(1)−P(1)	2.283(1)
In(1)−S(3)	2.537(1)	In(1)−S(4)	2.503(1)
In(1)−O(1)	2.126(3)	In(1)−O(2)	2.139(3)
In(1)−O(3)	2.372(3)	In(1)−O(4)	2.386(3)
In(1)−Cu(1)	3.068(1)	S(1)−C(1)	1.679(4)
S(2)−C(2)	1.680(4)	S(3)−C(3)	1.762(4)
S(4)−C(4)	1.726(4)	O(1)−C(1)	1.275(4)
O(2)−C(2)	1.273(4)	O(3)−C(3)	1.239(4)
O(4)−C(4)	1.240(4)	In(1)···Cu(1)	3.068(1)
	Bond Angles		
S(1)−Cu(1)−S(2)	118.58(4)	S(1)−Cu(1)−S(3)	114.95(4)
S(2)−Cu(1)−S(3)	104.06(4)	S(1)−Cu(1)−P(1)	109.95(4)
S(2)−Cu(1)−P(1)	106.26(4)	P(1)−Cu(1)−S(3)	101.34(4)
S(4)−In(1)−S(3)	136.62(4)	O(1)−In(1)−S(3	124.76(7)
O(2)−In(1)−S(3)	108.43(7)	O(3)−In(1)−S(3)	63.38(7)
O(4)−In(1)−S(3)	83.97(7)	O(1)−In(1)−S(4)	89.37(7)
O(2)−In(1)−S(4)	96.19(7)	O(3)−In(1)−S(4)	94.86(7)
O(4)−In(1)−S(4)	63.30(7)	O(1)−In(1)−O(2)	89.8(1)
O(1)−In(1)−O(3)	89.4(1)	O(2)−In(1)−O(3)	168.92(9)
O(1)−In(1)−O(4)	150.9(1)	O(2)−In(1)−O(4)	83.9(1)
O(3)−In(1)−O(4)	101.9(1)	C(1)−S(1)−Cu(1)	112.2(1)
C(2)−S(2)−Cu(1)	114.9(1)	C(3)−S(3)−Cu(1)	105.7(1)
Cu(1)−S(3)−In(1)	75.55(3)	C(3)−S(3)−In(1)	80.2(1)
C(4)−S(4)−In(1)	81.1(1)	C(1)−O(1)−In(1)	129.5(2)
C(2)−O(2)−In(1)	130.2(2)	C(3)−O(3)−In(1)	98.4(2)
C(4)−O(4)−In(1)	96.6(2)	O(1)−C(1)−S(1)	124.6(3)
O(2)−C(2)−S(2)	125.5(3)	O(3)−C(3)−S(3)	117.7(3)
O(4)−C(4)−S(4)	119.0(3)		

In(1)−O(1) and In(1)−O(2) distances (2.126(3) and 2.139(3) Å, respectively) are shorter than the In(1)−O(3) and In(1)−O(4) distances (2.372(3) and 2.386(3) Å, respectively). The former In−O distances fall in the upper range of distances observed in a few indium alkoxide compounds, 1.969−2.152 Å.[34] The shorter In−O distance may be attributed to extra negative charges acquired by O(1) and O(2) due to the delocalization of electrons in these thiocarboxylate groups. The lengthening of C−O and shortening of C−S bonds appear to suggest this. On the other hand, the longer In−O distances may be attributed to the weakening of the bond between In(III) and neutral carbonyl oxygen atom as indicated by the C=O distances in Table 3. The thiobenzoato ligands adopt three types of bonding modes: a terminal chelating mode, a bridging mode with the O atoms linked to indium and the S atoms to copper, and a terminal chelating mode with an additional Cu−S bond. The nonbonding distance Cu(1)···

(33) Allen, F. H.; Davies, J. E.; Galloy, J. J.; Johnson, O.; Kennard, O.; Macreae, C. F.; Mitchell, E. M.; Mitchell, G. F.; Smith J. M.; Watson, D. G. *J. Chem. Inf. Comput. Sci.* **1991**, *31*, 187.

(34) Suh, S.; Hoffman, D. M. *J. Am. Chem. Soc.* **2000**, *122*, 9396.

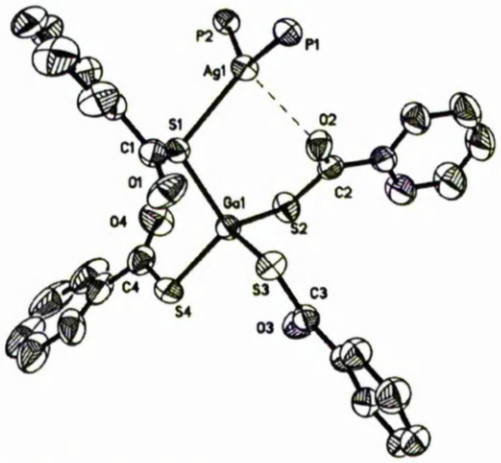

Figure 3. Perspective view of **3**.

Table 4. Selected Bond Lengths (Å) and Angles (deg) of 3

	Bond Lengths		
Ag(1)−S(1)	2.623(2)	Ag(1)−P(1)	2.451(2)
Ag(1)−P(2)	2.455(2)	Ga(1)−S(1)	2.309(2)
Ga(1)−S(2)	2.271(2)	Ga(1)−S(3)	2.273(2)
Ga(1)−S(4)	2.271(2)	S(1)−C(1)	1.778(6)
S(2)−C(2)	1.761(6)	S(3)−C(3)	1.766(6)
S(4)−C(4)	1.761(7)	O(1)−C(1)	1.193(7)
O(2)−C(2)	1.216(7)	O(3)−C(3)	1.198(7)
O(4)−C(4)	1.215(8)		
	Bond Angles		
P(1)−Ag(1)−S(1)	120.86(5)	P(2)−Ag(1)−S(1)	105.66(5)
P(1)−Ag(1)−P(2)	129.14(5)	S(2)−Ga(1)−S(1)	106.21(6)
S(3)−Ga(1)−S(1)	115.00(6)	S(4)−Ga(1)−S(1)	107.10(6)
S(2)−Ga(1)−S(3)	112.99(6)	S(2)−Ga(1)−S(4)	113.00(7)
S(4)−Ga(1)−S(3)	102.55(7)	Ga(1)−S(1)−Ag(1)	109.26(6)
C(1)−S(1)−Ag(1)	99.5(2)	C(1)−S(1)−Ga(1)	104.4(2)
C(2)−S(2)−Ga(1)	97.5(2)	C(3)−S(3)−Ga(1)	97.4(2)
C(4)−S(4)−Ga(1)	101.1(3)	O(1)−C(1)−S(1)	121.6(5)
O(2)−C(2)−S(2)	122.9(5)	O(3)−C(3)−S(3)	123.2(5)
O(4)−C(4)−S(4)	121.9(5)		

In(1), 3.068(1) Å, is shorter than the sum of their van der Waals radii (3.3 Å)[35] as was also observed in $(Ph_3P)_2Cu(\mu\text{-}SEt)_2In(SEt)_2$, $(Ph_3P)_2Cu(\mu\text{-}SeEt)_2In(SeEt)_2$, and $(Ph_3P)_2Cu(\mu\text{-}S(iso\text{-}Bu))_2In(S(iso\text{-}Bu)_2$, which are 3.34, 3.32, and 3.24 Å, respectively.[10] The origin of this bond shortening has not been investigated further. However, the longer Cu−P distance, 2.283(1) Å, as compared to **1** may be a consequence of this Cu··In weak interaction. The In(1) has a highly distorted octahedral environment with S_2O_4 donor set. The In−S distances, 2.537(1) and 2.503(1) Å, are comparable to 2.457(1)−2.542(1) Å observed in **5** which also has highly distorted octahedral geometry at In(III).[28]

Structure of $[(Ph_3P)_2Ag(\mu\text{-}SC\{O\}Ph\text{-}S)Ga(SC\{O\}Ph)_3]$ (3). A perspective view of **3** is shown in Figure 3 and selected bond lengths and angles are listed in Table 4. Compound **3** crystallizes with 3.5 $CHCl_3$ molecules. It consists of one anionic $[Ga(SC\{O\}Ph)_4]$ and a cationic $[(Ph_3P)_2Ag]$ unit. All four thiobenzoate anions are S-bonded to the gallium ion, Ga(1), and hence it has a tetrahedral GaS_4 core. One thiobenzoate anion adopts a sulfur atom, S(1) in its bridging mode to bind Ga(1) and Ag(1). The distance between Ag(1) and O(2), 2.626(3) Å, is far less than the sum of the van der Waals radii (3.2 Å) suggesting that there may be weak interaction between these two atoms in the solid state. However, the sum of the bond angles, 355.66° supports trigonal planar geometry at Ag(1) and a slight deformation of the geometry due to Ag··O close contact. The Ga−S distances in **3** fall in the range 2.271(2)−2.309(2) Å which are comparable to the Ga−S distances observed in $[Et_3NH][Ga(SC\{O\}Ph)_4]$.[36] The Ag(1)−P(1) and Ag(1)−P(2) distances, 2.451(2) and 2.455(2) Å, respectively, are comparable to those observed in **5**.[28] A weak interaction appears to exist between Ga(1) and O(2) (2.626(4) Å) which is significantly lower than the sum of the van der Waals radii of 3.4 Å.

Table 5. Pyrolysis and TGA Results for 1−5

	TG results			
compd	temp range (°C)	residual wt obsd (calcd) (%)	residual wt from pyrolysis[a] (%)	product of decomposition
1	150−327	25.5 (20.9)	20.8	$CuGaS_2$[b]
2	168−350	24.3 (24.5)	24.0	$CuInS_2$[c]
3	185−349	18.9 (19.3)	19.3	$AgGaS_2$[d]
4	132−315	28.4 (27.4)	27.9	$AgInS_2$[e]
5	175−328	23.6 (22.1)	22.1	$AgInS_2$[e]

[a] The samples were heated at 300 °C under a 0.5 Torr pressure for 30 min. [b] Tetragonal $CuGaS_2$ (JCPDS Code 06-0358). [c] Tetragonal $CuInS_2$ (JCPDS Code 27-0159); [d] Tetragonal $AgGaS_2$ (JCPDS 27-0615). [e] Orthorhombic $AgInS_2$ (JCPDS Code 25-1328).

The structures of **1** and **2** exhibit subtle differences in the bonding modes of the thiocarboxylate anion. In **1**, μ_2-*S,O* and μ_2-*S* bonding modes are displayed, whereas in **2**, μ_2-*S,O* and μ_2-S_2,*O* are observed. These changes in bonding modes may be attributed to the change in the size of the metal atoms. The bimetallic compounds of Ag and Ga/In show interesting structural features. In **3**, the metal atoms Ag and Ga are bridged by a thiobenzoate anion through a μ_2-*S* bonding while another thiobenzoate ligand bonded to the gallium metal atom weakly interacts with the silver metal atom through its oxygen donor site. On the other hand, the Ag and In metal centers are bridged by two $PhC\{O\}S^-$ ligands in **5**.[28] Furthermore, the Cu−Ga and Cu−In distances in **1** and **2**, respectively, are shorter than the sums of their van der Waals radii, while the Ag−In distance in **5** is not. The soft Cu atom is always bonded to the soft S donor sites; the harder Ga atoms accept S and O donor centers but its site does allow a coordination number of four in these compounds. The larger In atom achieves a coordination number of six by bonding the thiocarboxylate ions in a chelating mode.

Thermogravimetric and Pyrolysis Studies. The usefulness of **1**−**5** as single-source precursors for ternary sulfide materials was investigated by thermogravimetry and pyrolysis experiments. The TG curves are presented in Figure 4 and the results are tabulated in Table 5. The loss of dichloromethane in **2** was observed in the temperature range 79−111 °C. The observed weight loss, 6.3%, matched well with the calculated value, 6.4%, for the loss of a half molecule of CH_2Cl_2. It is unusual that CH_2Cl_2 is lost at such a high temperature. The elemental analysis of **2** also indicated the presence of half a CH_2Cl_2 molecule per formula unit. This suggests that the CH_2Cl_2 molecules are strongly occluded in **2**. The TG experiment on solvent-free **2** confirmed that the initial weight loss is indeed due to the loss of CH_2Cl_2.

(35) Bondi, A. *J. Phys. Chem.* **1964**, *68*, 441.

(36) Deivaraj, T. C.; Vittal, J. J. Unpublished results.

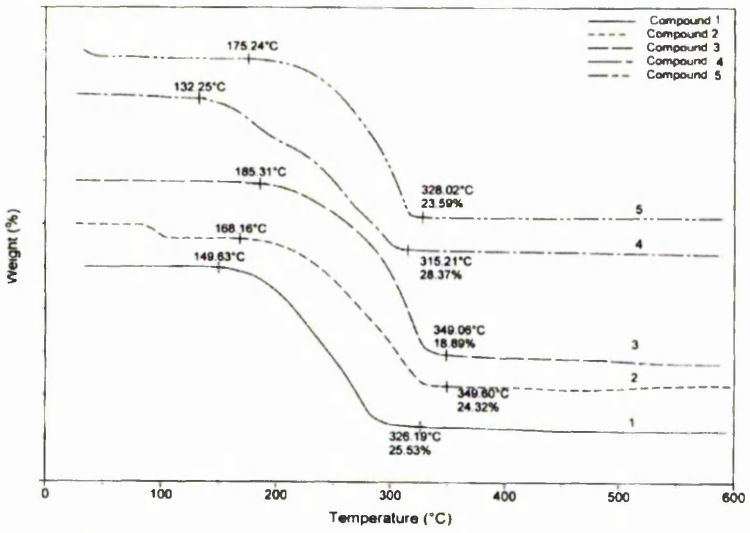

Figure 4. Thermogravimetric curves of **1**−**5**.

TG data reveal that the compounds decompose in the temperature range 150−350 °C in unresolved multiple steps to stable final products, which were found to be the corresponding ternary sulfides. The residual masses for **1**−**5** agree with the formation of the ternary sulfides except for **1** as shown in Table 4. The residue of **1** probably contains some side products of decomposition. On the basis of the thermal decomposition pathway of metal thiocarboxylates discussed by Hampden-Smith[37−41] the decomposition reaction may be described as in eq 4.

$$[(Ph_3P)_xMM'(SC\{O\}R)_4] \rightarrow MM'S_2 + 2RC(O)SC(O)R + xPPh_3 \quad (4)$$

To identify the nature of the ternary materials obtained, all compounds were subjected to pyrolysis at 300 °C at a pressure of 0.5 Torr for 30 min. The ternary materials thus obtained were characterized by X-ray powder diffraction, EDAX, and SEM. The XRPD patterns are shown in Figure 5. The residues obtained from **1** and **2** matched the tetragonal phases of $CuGaS_2$ and $CuInS_2$ (JCPDS database). Pyrolysis of **3** resulted in formation of tetragonal $AgGaS_2$. The X-ray powder diffraction patterns of these residues suggested a high degree of crystallinity. The EDAX profiles of the samples show peaks for all the corresponding elements, as well as peaks for carbon, due to incorporated graphite mesh and oxygen due to aerobic conditions. The copper/gallium/sulfur and copper/indium/sulfur ratios were found to be 1:1.12:1.82 and 1:1.08:1.89, respectively, confirming the stoichiometry of these compounds. The SEM images (Supporting Information) of the ternary materials showed a wide distribution of particle sizes

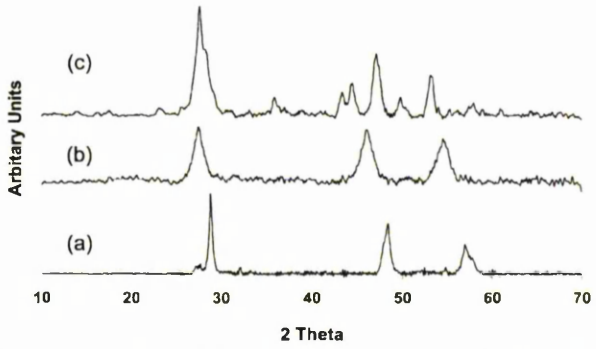

Figure 5. X-ray powder diffraction patterns of (a) $CuGaS_2$ from **1**, (b) $CuInS_2$ from **2**, and (c) $AgGaS_2$ from **3** by pyrolysis.

for the sulfide materials which account for the broad peaks observed in their X-ray powder diffraction patterns. The particle size of the sulfide materials ranges from 5 to 50 μm.

Aerosol-Assisted Chemical Vapor Deposition of [(Ph$_3$P)Cu(SC{O}Ph)$_3$In(SC{O}Ph)]. Attempts to deposit thin films using **2** as a single-source precursor by aerosol-assisted chemical vapor deposition resulted in predominantly β-In_2S_3 materials rather than the expected $CuInS_2$, as was observed from TGA and pyrolysis studies. In most cases, dark yellow β-In_2S_3 films were obtained at growth temperatures of 350−450 °C after 2 h of growth confirmed by XRPD. There were no differences on using different solvents such as THF or toluene. Figure 6 indicates the XRPD pattern of β-In_2S_3 film grown on glass from **2** in toluene at 450 °C after 2 h growth. Broad peaks indicate that crystallinity of the particles is relatively poor and a preferred orientation along the (311) plane is found. Nomura et al. reported the growth of $CuIn_5S_8$ films from BuIn(S^{n}Pr)Cu($S_2CN^nPr_2$) by LP-MOCVD.[42] In their study, a higher growth temperature (450 °C) resulted in films of β-In_2S_3, whereas at lower growth temperatures the films consisted of $CuIn_5S_8$.

XPS was employed to determine photoelectron binding energies of the elements comprising the films grown

(37) Shang, G.; Hampden-Smith, M. J.; Duesler, E. N. *Chem. Commun.* **1996**, 1733.
(38) Shang, G.; Kunze, K.; Hampden-Smith, M. J.; Duesler, E. N. *Chem. Vap. Deposition* **1996**, *2*, 242.
(39) Nyman, M. D.; Hampden-Smith, M. J.; Duesler, E. N. *Chem. Vap. Deposition* **1996**, *2*, 171.
(40) Nyman, M. D.; Jenkins, K.; Hampden-Smith, M. J.; Kodas, T. T.; Duesler, E. N.; Rheingold, A. L.; Liable-Sands, M. L. *Chem. Mater.* **1998**, *10*, 914.
(41) Nyman, M. D.; Hampden-Smith, M. J.; Duesler, E. N. *Inorg. Chem.* **1997**, *36*, 2218.

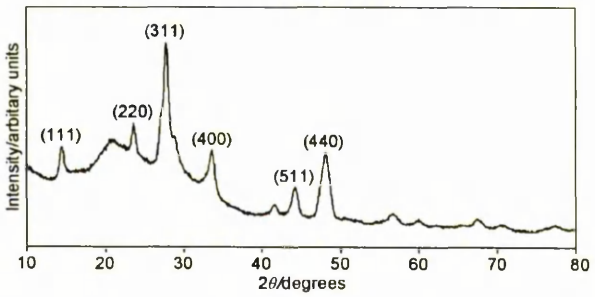

Figure 6. XRPD pattern of a β-In_2S_3 film grown from a solution of compound **2** in toluene at 450 °C by AACVD.

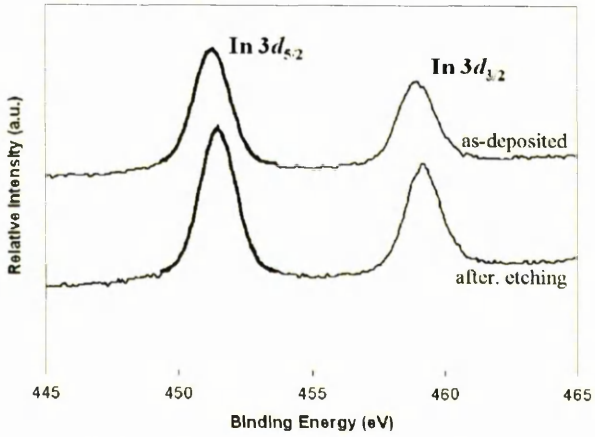

Figure 7. XPS spectra of In 3*d* peaks of a β-In_2S_3 film as-deposited and after 1 h of etching.

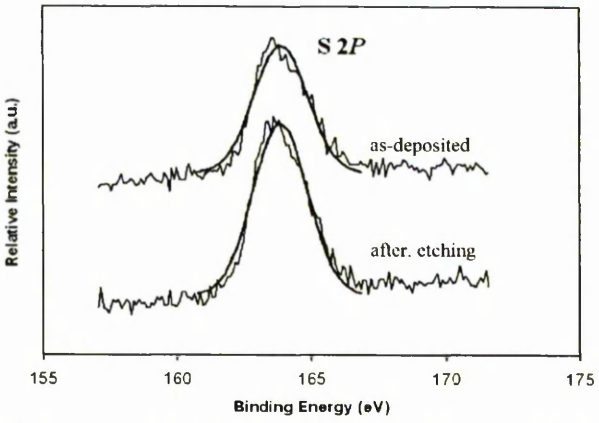

Figure 8. XPS spectra of S 2*s* peaks of a β-In_2S_3 film as-deposited and after 1 h of etching.

from **2** in toluene at 450 °C after 2 h growth. Figures 7 and 8 show In 3*d* and S 2*p* peaks observed before etching and after 1 h of etching. The peaks obtained before and after etching are not significantly different in terms of their binding energies and intensities. Indium 3*d* peaks were found at 451.5 eV (In $3d_{5/2}$) and 458.6 eV (In $3d_{3/2}$) before etching and 451.3 eV (In $3d_{5/2}$) and 458.2 eV (In $3d_{3/2}$) after etching. Sulfur 2*p* peaks were found at 163.9 eV in both cases. Relative atomic

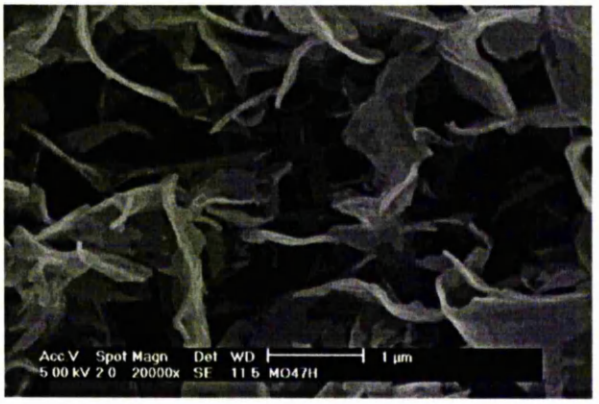

(a)

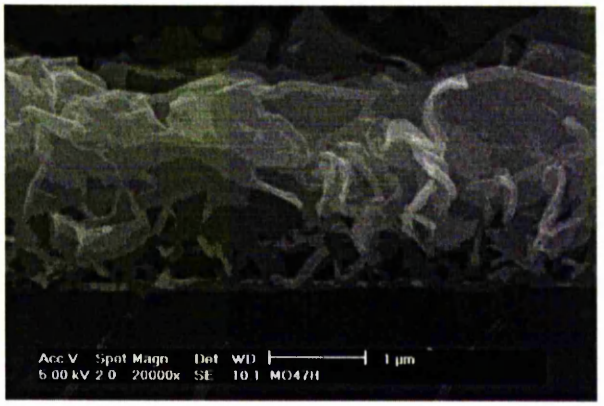

(b)

Figure 9. SEM images of a In_2S_3 film grown from the solution of toluene and compound **2** at 450 °C: (a) top view, (b) cross-section view.

percentages of indium and sulfur were found to be slightly variable depending on etching treatment (2:3.66 before etching and 2:3.29 after etching).

SEM studies on the In_2S_3 films show that the particles are randomly oriented on the glass substrate (Figure 9) with ca. 1.5 μm/h growth rate. There was also no evidence for copper peaks in the EDAX spectra but in some cases small traces of copper were observed (ca. <1%). This observation suggests that there was a pre-reaction between the precursor and the solvents used in this study during the CVD process. ESI-MS of **2** showed no molecular ion peak, however, signals due to $[In(SC\{O\}Ph)_4]^-$, $[(PPh_3)_2Cu]^+$, and $[(PPh_3)_3Cu]^+$ were present. This indicates the dissociation of the compound in the solution. Such processes are common among phosphine adducts of coinage metal salts and have been substantiated by various techniques including NMR, molecular weight determinations, and conductivity measurements.[43-46] Our finding of dissociation, using

(42) Nomura, R.; Seki, Y.; Matsuda, H. *Thin Solid Films* **1992**, *209*, 145.

(43) Muetterties, E. L.; Alegranti, C. W. *J. Am. Chem. Soc.* **1972**, *94*, 6386.

(44) Barron, P. F.; Dyason, J. C.; Healy, P. C.; Engelhardt, L. M.; Skelton, B. W.; White, A. H. *J. Chem. Soc., Dalton Trans.* **1986**, 1965.

(45) Nakajima, H.; Matsumoto, K.; Tanaka, K.; Tanaka, T. *Inorg. Nucl. Chem.* **1975**, *37*, 2463.

(46) Black, J. R.; Levason, W.; Spicer, M. D.; Webster, M. *J. Chem. Soc., Dalton Trans.* **1993**, 3129.

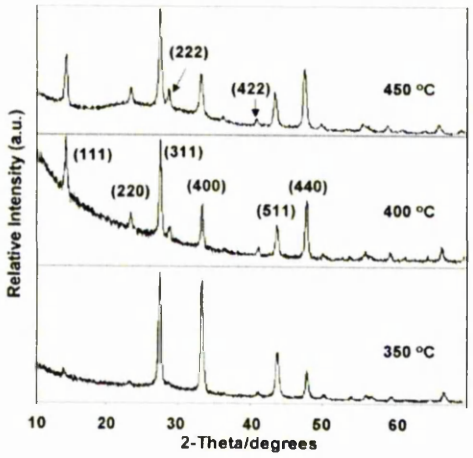

Figure 10. X-ray powder diffraction pattern of $AgIn_5S_8$ thin films formed from **4**.

ESIMS, also concurs with the findings of Henderson et al.[47]

Aerosol-Assisted Chemical Vapor Deposition of $[(Ph_3P)_2Ag(SC\{O\}R)_3In(SC\{O\}R)]$ (R = Me (4); Ph (5)). Aerosol-assisted chemical vapor deposition (AACVD) of THF solution of **4** and **5** yielded $AgIn_5S_8$ films. Films grown on glass at 350, 400, and 450 °C from **4** were transparent and adherent (Scotch tape test) with a dark red color, and films grown at 350 °C were slightly red. XRPD analysis (step size 0.04°/2 s) confirmed that the films prepared from compounds **4** and **5** were found to be cubic-$AgIn_5S_8$ (JCPDS 25-1329) with a preferred orientation along the (311) plane (Figure 10). XRPD patterns of films grown from **4** showed the (111) and (222) planes were noticeably enhanced with increasing growth temperature, and intensities of peaks from the (511) and (440) planes were also reversed. XRPD measurements of films from compound **5** indicate similar patterns but no indication of enhancement of peak intensities was observed in the case of the films grown from **4**.

Scanning electron microscopy (SEM) images (Figure 11) of the $AgIn_5S_8$ films obtained from **4** show the dramatic changes in the morphology of films grown as a function of growth temperatures. The morphology of the films grown on glass at 450 °C (Figure 11c) consists of thin platelike particles, positioned laid down onto the substrate with random orientation, and a similar morphology was also found in the films grown on Si(100) substrates at the same temperature. However, with decreasing the growth temperature to 400 or 350 °C, the morphology becomes more dense and no platelike particles were formed (Figure 11a and b). Growth rate and average particle size of the films grown at 400 °C were ca. 0.3 μm/h and ca. 0.5 μm, respectively, and at 350 °C were ca. 0.2 μm/h and ca. 0.3 μm.

Morphologies of films grown from compound **5** (Figure 12) are quite different from those grown from **4**. Films obtained at a growth temperature of 350 °C revealed a relatively dense morphology and a smaller particle size (ca. 100−300 nm) than those prepared from higher growth temperatures. Particles on glass substrates (Figure 12c) grown at 450 °C have trigonal habits consisting of several layers. However, on changing the substrate from glass to Si(100), the formation of par-

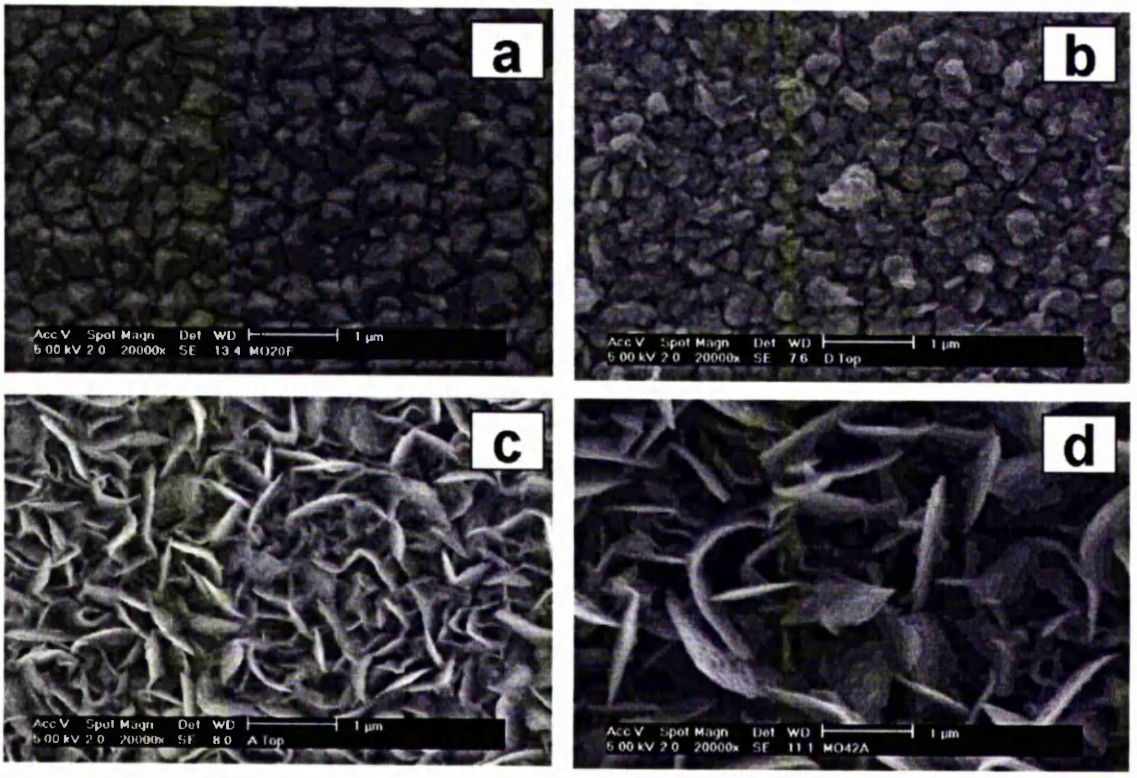

Figure 11. SEM images of $AgIn_5S_8$ films on glass grown from **4**: (a) 350 °C on glass, (b) 400 °C on glass, (c) 450 °C on glass, and (d) 450 °C on Si(100).

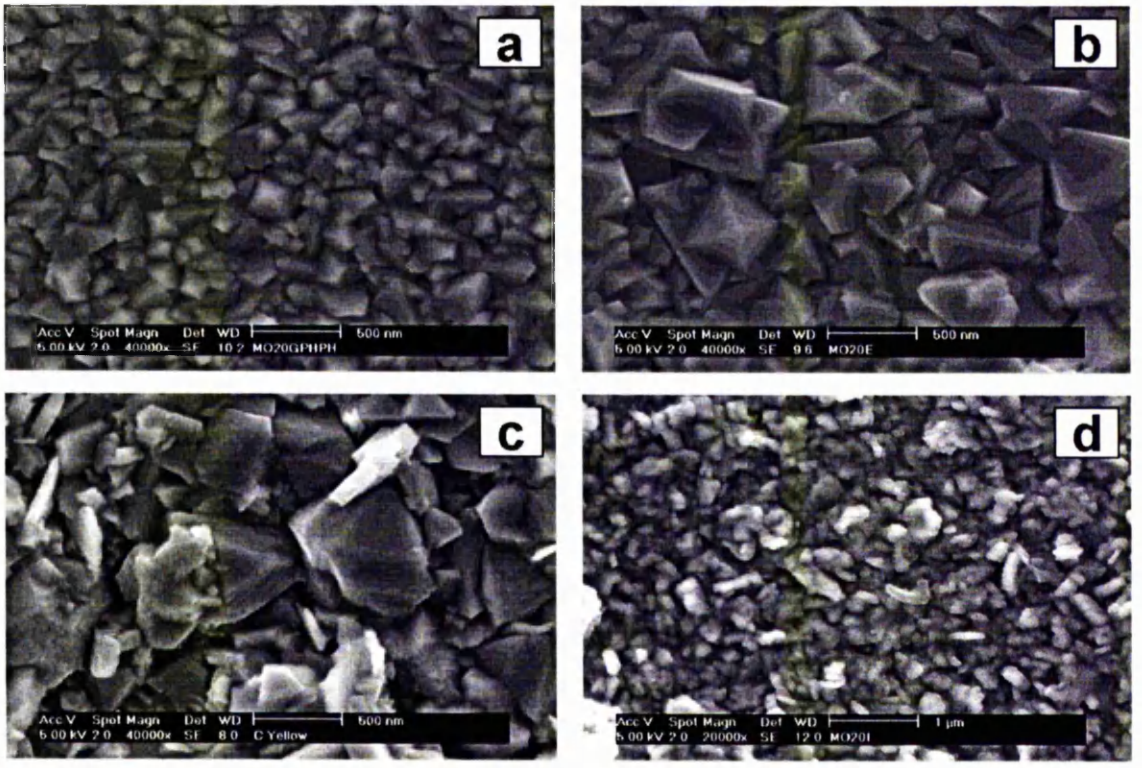

Figure 12. SEM images of $AgIn_5S_8$ films on glass grown from **5**: (a) 350 °C on glass, (b) 400 °C on glass, (c) 450 °C on glass, and (d) 450 °C on Si(100).

ticles leads to rice-like instead of triangular shapes (Figure 12d). Growth rates obtained from cross-section views for the films were found to be ca. 0.2 μm/h at 350 °C, 0.5 μm/h at 400 °C, and 0.6 μm/h at 450 °C on glass substrates after 2 h of growth.

Conclusion

In this paper, we have reported the syntheses and characterization of the compounds $[(Ph_3P)CuM(SC\{O\}Ph)_4]$ (M = Ga (**1**) or In (**2**)) and $[(Ph_3P)_2AgGa(SC\{O\}Ph)_4]$ (**3**). The structures of the three compounds have been determined by X-ray crystallography. Thermogravimetric analyses and pyrolysis studies of **1**−**5** indicate that these compounds decompose to give ternary $MM'S_2$ materials. Compounds **4** and **5** can also be used as precursors for $AgIn_5S_8$ films as was demonstrated by AACVD experiments. These compounds may also have the potential to be used to prepare nanocrystalline sulfides via the single-source molecular precursor route.

Acknowledgment. We thank the National University of Singapore for a grant to J.J.V. (RP-143-000-084-112) and a graduate scholarship to T.C.D. P.O.B. thanks EPRSC, UK for support. J.J.V. thanks the Royal Society of Chemistry for the travel grant to visit Manchester, UK.

Supporting Information Available: SEM micrographs of the pyrolysis products of compounds **1**−**5** (PDF). This material is available free of charge via the Internet at http://pubs.acs.org.

CM031027V

(47) Bonnington, L. S.; Toll, R. K.; Gray, E. J.; Flett, J. I.; Henderson, W. *Inorg. Chim. Acta* **1999**, *290*, 213.

JOURNAL OF Materials CHEMISTRY

The deposition of thin films of $CuME_2$ by CVD techniques (M = In, Ga and E = S, Se)

Jin-Ho Park,[a] Mohammad Afzaal,[a] Michael Kemmler,[a] Paul O'Brien,*[a] David J. Otway,[b] Jim Raftery[a] and John Waters[a]

[a]*The Manchester Materials Science Centre and Department of Chemistry, University of Manchester, Oxford Road, Manchester, UK M13 9PL. E-mail: paul.obrien@man.ac.uk; jin-ho.park@man.ac.uk; Fax: 0161-275-4616; Tel: 0161-275-4652*

[b]*Department of Chemistry, Imperial College of Science, Technology and Medicine, Exhibition Road, London, UK SW7 2AZ*

Received 13th March 2003, Accepted 1st May 2003
First published as an Advance Article on the web 25th June 2003

Thin film(s) of chalcopyrite $CuME_2$ (where M = In or Ga; E = S or Se) have been grown by low-pressure metal-organic chemical vapour deposition (LP-MOCVD) or aerosol-assisted chemical vapour deposition (AACVD) using the precursors $M(E_2CNMe^nHex)_3$ and $Cu(E_2CNMe^nHex)_2$. Films were grown on various substrates between 350–500 °C and characterized by X-ray diffraction, XPS, optical spectroscopy (UV/Vis), EDAX and scanning electron microscopy.

Introduction

Ternary metal chalcogenides I–III–VI_2 (I = Cu; III = In, Ga and VI = S, Se) have been the focus of much recent research due to their use in high efficiency, radiation hard, solar cells. They also have a significant fabrication advantage over III–V semiconductors for solar cell applications, since polycrystalline films may be used, as opposed to epitaxial crystal films.[1]

A number of novel single-source precursors for the deposition of $CuInE_2$ (E = S or Se) have been synthesized and used to deposit thin films by various MOCVD processes. In an early study, Nomura *et al.* reported the deposition of $CuInS_2$ films on glass substrates using an equimolar mixture of $[^tBu_2InSPr]$ and $Cu(S_2CNBu_2)_2$ dissolved in *p*-xylene.[2] The direct reaction of $[^nBuInS^iPr]$ with $Cu(S_2CN^iPr_2)$ was shown to yield a binuclear complex of the form $^nBuIn(S^iPr)Cu(S_2CN^iPr_2)$ from which stoichiometric $CuInS_2$ was grown by solution pyrolysis at 350 °C.[3] Various hetero-binuclear complexes $(Ph_3P)_2Cu(\mu\text{-}ER)_2In(ER)_2$ (E = S, Se; R = Et, ^{t}Bu) have been prepared and pyrolysis studies revealed that the selenium derivative could be converted into $CuInSe_2$ at 400–450 °C.[4] In continuing work, Hepp and co-workers were able to deposit $CuInS_2$ films using $(Ph_3P)_2Cu(\mu\text{-}SEt)_2In(SEt)_2$ below 400 °C by spray MOCVD.[5] Recently, two liquid compounds, $[(^nBu_3P)_2Cu(SR)_2In(SR)_2]$ (R = Et and ^{n}Pr) have been used to deposit $CuInS_2$ thin films.[6,7] High quality $CuInS_2$ has been reported on a copper coated silicon substrate using vapors from $(Et_3NH)[In(SC(O)Ph)_4]$. However, nickel coated silicon substrates lead to deposition of crystalline In_2S_3 thin films.[8]

There are very few reports on the deposition of $CuGaS_2$ films using metal-organic precursors. Buhro *et al.* reported the first known example of a single-source precursor for $CuGaS_2$ films based on $[\{^nBu\}_2CuGa(SEt)_x]$ (x = 3 or 4) by a spray CVD process.[9] High quality epitaxial layers of $CuGaS_2$ films on GaAs (100) and GaP (100) have been deposited by LP-MOVPE using cyclopentadienylcopper triethylphosphine, tripropylgallium and di-*tert*-butyl sulfide as organometallic precursors.[10]

Over the years, a range of dithio- and diseleno-carbamato complexes of various metals have been synthesised and used to deposit a wide range of semiconductor materials.[11–13] One particularly successful modification to the sulfur/selenium containing ligands has been to develop compounds in which the parent amine is asymmetrically substituted and involves a bulky or extended alkyl substituent.[14,15] Compounds with these ligands are air stable and sufficiently volatile for the deposition of thin films of materials such as Cu_2E, In_2E_3, Ga_2E_3, ZnE and CdE (E = S or Se).[16,17] Success with the binary parents has led to deposition of ternary phases of $CuInE_2$ (E = S or Se). In this paper, we report the deposition of $CuInS_2$, $CuInSe_2$ and $CuGaS_2$ films by LP-MOCVD and AACVD processes using dual-source metal-organic precursors; preliminary results have been reported elsewhere.[18,19]

Experimental

Precursor synthesis

Preparation of bis(*N*-methyl-*N*-(*n*-hexyl)dithiocarbamato)-copper, $Cu(S_2CNMe^nHex)_2$ (1). Carbon disulfide (3.96 ml, 66 mmol) was slowly added to sodium hydroxide (2.64 g, 66 mmol) and *N*-methylhexylamine (10 ml, 66 mmol) in methanol (80 ml) at 0 °C. The yellow solution obtained was immediately added to copper(II) sulfate (5.26 g, 33 mmol) dissolved in water to give an intense dark brown precipitate which was filtered and dried. Further purification was carried out from toluene to give a black solid. Yield 64%, m.p. 48 °C, elemental analysis: $C_{16}H_{32}S_4N_2Cu$. Calculated: C: 43.29, H: 7.2, N: 6.05%. Found: C: 42.76, H: 6.97, N: 6.05%. Mass spectrum: *m/z* significant peaks $[M^+]$ 444, $[CuS_2CNCH_3C_6H_{13}]$ 253, $[S_2CNCH_2CH]$ 117, $[S_2CNCH_2C]$ 116.

Preparation of tris(*N*-methyl-*N*-(*n*-hexyl)dithiocarbamato)-indium, $In(S_2CNMe^nHex)_3$ (2). Carbon disulfide (3.96 ml, 66 mmol) was added dropwise to sodium hydroxide (2.64 g, 66 mmol) and *N*-methylhexylamine (10 ml, 66 mmol) while stirring vigorously in methanol (80 ml) at 0 °C. $InCl_3$ (4.8 g, 21 mmol) was added to the yellow solution giving a white precipitate which was filtered and dried. Further purification was carried out from toluene to give a colourless solid. Yield 67%, m.p. 100 °C, elemental analysis: $C_{24}H_{48}N_3S_6In$. Calculated: C: 42.02, H: 6.91, N: 5.88%. Found: C: 42.27, H: 6.73, N: 6.01%. ^{1}H NMR (δ, C_6D_6, 300 MHz): 0.86 (t, 9H, $-NCH_2CH_2CH_2CH_2CH_2CH_3$), 1.18 (m, 18H, $-CH_2CH_2CH_2CH_2CH_2CH_3$), 1.38 (m, 6H, $-NCH_2CH_2CH_2CH_2CH_2CH_3$), 2.8 (s, 9H, $-NCH_3$), 3.3 (t, 6H, $-NCH_2CH_2CH_2CH_2CH_2CH_3$).

 DOI: 10.1039/b302896h

Table 1 Selected bond lengths (Å) and angles (°) for $In(S_2CNMe''Hex)_3$

In(1)–S(12)	2.562(2)	S(21)–In(1)–S(22)	70.03(6)
In(1)–S(21)	2.566 (2)	S(31)–In(1)–S(22)	102.34(7)
In(1)–S(31)	2.575(2)	S(12)–In(1)–S(32)	158.44(7)
In(1)–S(22)	2.585(2)	S(21)–In(1)–S(32)	92.34(7)
In(1)–S(32)	2.587(2)	S(31)–In(1)–S(32)	69.63(6)
In(1)–S(11)	2.615(2)	S(22)–In(1)–S(32)	97.33(7)
		S(12)–In(1)—S(11)	69.66(6)
S(12)–In(1)–S(21)	99.63(7)	S(21)–In(1)–S(11)	89.55(6)
S(12)–In(1)–S(31)	100.37(6)	S(31)–In(1)–S(11)	100.02(6)
S(21)–In(1)–S(31)	159.80(7)	S(22)–In(1)–S(11)	157.49(6)
S(12)–In(1)–S(22)	103.57(7)	S(32)–In(1)–S(11)	92.74(7)

Preparation of bis(*N*-methyl-*N*-(*n*-hexyl)diselenocarbamato)-copper, $Cu(Se_2CNMe''Hex)_2$ (3). Carbon diselenide (2.4 g, 7.06 mmol) in 1,4-dioxane (100 ml) was added dropwise to sodium hydroxide (0.56 g, 7 mmol) and *N*-methylhexylamine (2 ml, 7.06 mmol) while stirring vigorously at −10 °C. The orange solution was filtered and $CuCl_2$ (0.94 g, 3.53 mmol) dissolved in water was immediately added to give a green precipitate, which was filtered and dried. Further purification was carried out from toluene to give a black solid. Yield 70%, elemental analysis: $C_{16}H_{32}Se_4N_2Cu$ Calculated: C: 30.45, H: 5.07, N: 4.44% Found: C: 30.84, H: 5.65, N: 4.45%. Mass spectrum: *m/z* significant peaks, $[CuSe_2CNCH_3CH_2C]$ 288, $[CuSe_2CNCCH_2CH_2CH]$ 300, $[CuSe_2CNCHCH_2CH_2CH_2C]$ 314.

Preparation of tris(*N*-methyl-*N*-(*n*-hexyl)diselenocarbamato)-indium, $In(Se_2CNMe''Hex)_3$ (4). Carbon diselenide (1.85 g, 1.08 mmol) in 1,4-dioxane (75 ml) was added dropwise to sodium hydroxide (0.217 g, 1 mmol) and *N*-methylhexylamine (0.8 ml, 1 mmol) while stirring vigorously in water (100 ml) at −20 °C. The orange solution was filtered and $InCl_3$ (0.4 g, 0.36 mmol) dissolved in water was immediately added to give a light yellow precipitate, which was further stirred for 4–5 hours followed by filtration and then dried. Further purification was carried out from toluene to give a yellow powder. Yield 57%, ^1H NMR (δ, C_6D_6, 300 MHz): 0.55 (t, 9H, $-NCH_2CH_2CH_2CH_2CH_2CH_2CH_3$), 0.77 (m, 18H, $-CH_2CH_2CH_2CH_2CH_2CH_3$), 1.00 (m, 6H, $-NCH_2CH_2CH_2CH_2CH_2CH_3$), 2.4 (s, 9H, $-NCH_3$), 2.9 (t, 6H, $-NCH_2CH_2CH_2CH_2CH_2CH_3$).

Preparation of tris(*N*-methyl-*N*-(*n*-hexyl)dithiocarbamato)-gallium, $Ga(S_2CNMe''Hex)_3$ (5). Sodium methyl(*n*-hexyl)dithiocarbamato (8.21 g, 46.90 mmol) was dissolved in dry benzene (~40 ml). Gallium(III) chloride (14.66 ml) in hexane solution (1.5 M) was slowly added to the solution *via* an equilibrating funnel and the mixture was stirred for an hour at room temperature. A white solid was observed in a light yellow solution. The solvent was removed *in vacuo*, yielding an oily solid, which after washing with pentane was found to be a white microcrystalline powder. Yield 68%, m.p. 85 °C, elemental analysis: $C_{24}H_{48}N_3S_6Ga$ Calculated: C: 44.99, H: 7.55, N: 6.56%. Found: C: 44.78, H: 8.14, N: 6.58%, ^1H NMR (δ, C_6D_6, 300 MHz): 0.92 (t, 9H, $-NCH_2CH_2CH_2CH_2CH_2CH_3$), 1.18 (m, 18H, $-CH_2CH_2CH_2CH_2CH_2CH_3$), 1.40 (m, 6H, $-NCH_2CH_2CH_2CH_2CH_2CH_3$), 2.8 (s, 9H, $-NCH_3$), 3.4 (t, 6H, $-NCH_2CH_2CH_2CH_2CH_2CH_3$). Mass spectrum: *m/z* significant peaks $[Ga(S_2CNCH_3C_6H_{13})_2]$ 449, $[GaS_2CNCCH_2CH_2CH_2CH_2C]$ 239, $[S_2CNCH_2CH_2CH_2CH_2C]$ 158.

Single-crystal X-ray diffraction study

Crystal data for $In(S_2CNMe''Hex)_3$: $C_{24}H_{47}InN_3S_6$, M = 684.83, monoclinic, space group $P2(1)/n$, a = 19.660(5), b = 16.984(5), c = 10.086(3) Å, α = 90, β = 104.492(9), γ = 90°, V = 3260.6(15) Å^3, Z = 4, D_c = 1.395 mg m^{-3}, μ(Mo-Kα) = 1.127 mm^{-1}, $F(000)$ = 1428, T = 100(2) K, monochromated Mo-Kα radiation, λ = 0.71073 Å. Total numbers of measured and observed independent reflections are 14238 and 6558 (R_{int} = 0.0560). R_1 = 0.0679; wR_2 = 0.1623. The structures were solved by direct methods and refined by full-matrix least squares on F^2.[20] All calculations were carried out using the SHELXTL package.[21] All non-hydrogen atoms were refined with anisotropic atomic displacement parameters. Hydrogen atoms were placed in calculated positions, assigned isotropic thermal parameters and allowed to ride on their parent carbon atoms. Selected interatomic distances and angles are summarised in Table 1.

CCDC reference number 205970. See http://www.rsc.org/suppdata/jm/b3/b302896h/ for crystallographic data in CIF or other electronic format.

Low-pressure metal-organic chemical vapour deposition (LP-MOCVD)

The growth of the thin films was carried out in a low-pressure ($\approx 10^{-2}$ Torr) MOCVD reactor tube which has been described elsewhere.[22] A graphite susceptor held the substrate (dimensions 10 mm × 15 mm) which was heated by a tungsten halogen lamp. A typical growth run (in temperature range 450–500 °C) involved the use of approximately 100 mg of stoichiometrically mixed sample, and lasted for 1–2 hours.

Films were deposited on glass microscope slides and single crystalline substrates. The precursors used were bis- and tris-complexes of methyl-*n*-hexyl-diseleno- or -dithio-carbamate with copper(II) and indium respectively, prepared as described in earlier papers. In initial experiments, these were simply mixed in a 1 : 1 ratio in the evaporator. In subsequent experiments the effect of varying the ratio of Cu : In has been investigated for the growth of $CuInS_2$ by LP-MOCVD and AACVD. In Table 2 some of the important growth experiments and the nature of the resulting films are summarised.

Table 2 Overview over some important growth experiments in the deposition of $CuInS_2$ using compounds **1** and **2** by LP-MOCVD

Ratio of **1** : **2**	Substrate	T_{pre}/°C	T_{sub}/°C	Growth time/h	Phase grown
1 : 1	glass	250	430	1.5	chalcopyrite $CuInS_2$
1 : 1	glass	250	450	1.5	chalcopyrite $CuInS_2$
1 : 1	glass	250	460	1.5	chalcopyrite $CuInS_2$
1 : 1	glass	250	480	2.5	chalcopyrite $CuInS_2$
1 : 1	glass	250	500	2.5	chalcopyrite $CuInS_2$
1 : 1	ITO coated glass	250	460	1.5	chalcopyrite $CuInS_2$
1 : 1	(100)GaAs	250	460	1	chalcopyrite $CuInS_2$
1 : 1	(100)InP	250	460	1	chalcopyrite $CuInS_2$
1 : 1	(111)Si	250	460	1	chalcopyrite $CuInS_2$
1 : 1	(111)Si	250	480	2	chalcopyrite $CuInS_2$
1 : 1.5	glass	250	480	2.5	mainly β-In_2S_3
1 : 2	glass	250	480	2.5	β-In_2S_3 and chalcopyrite $CuInS_2$
1.5 : 1	glass	250	480	2.5	chalcopyrite $CuInS_2$ and Cu_xS with $1.75 < x < 2$
2 : 1	glass	250	480	2.5	chalcopyrite $CuInS_2$ and Cu_xS with $1.75 < x < 2$

Aerosol assisted chemical vapour deposition (AACVD)

Approximately 0.25 g of precursor was dissolved in 30 ml toluene (or THF) in the round-bottomed flask. Six pieces of glass substrates (1 × 2 cm) were placed inside the reactor tube. The carrier gas flow rate was controlled by Platon flow gauges. The solution in the flask was placed in a water bath above the piezoelectric modulator of a humidifier, where aerosol droplets were generated and transferred by the carrier gas into a hot-wall zone. Then both the solvent and the precursor evaporated and the precursor vapour reached the heated substrate surface where thermally induced reactions and film deposition took place. This homemade aerosol-assisted chemical vapour deposition kit consisted of a two-necked flask, a PIFCO ultrasonic humidifier (Model No. 1077) and a CARBOLITE furnace.

Film characterization

X-ray diffraction studies were performed using secondary graphite monochromated CuK_α radiation on either a Philips PW1700 series automated diffractometer or a Bruker D8 AXS X-ray diffractometer. The sample was mounted flat and scanned from 10–90° in steps of 0.04° with a count time of 2 s. Samples were carbon coated before electron microscopic analysis. All EDAX and electron microscopy was then carried out in either a JEOL Superprobe 733 microscope or a Philips XL30 FEG. The XPS measurements were performed in the ultra-high vacuum chamber (base pressure of 10^{-8} Pa) of an ESCA 300 spectrometer using Mg-Kα excitation. The energy scale was calibrated using Au and argon was used for etching.

Results and discussion

X-Ray single crystal structure of $In(S_2CNMe''Hex)_3$

Crystals of $In(S_2CNMe''Hex)_3$ were obtained from a toluene solution at low temperature. The crystal structure of the compound is shown in Fig. 1 and selected bond angles and bond distances are given in Table 1. The crystalline phase of the compound belongs to the monoclinic space group $P2_1/n$ with $Z = 4$ units of the monomer in the unit cell. In the structure, the indium atom is coordinated to six sulfur atoms in a distorted octahedral geometry. One of the two sulfurs attached to the indium has a longer In–S separation than the other (In–S(11) = 2.615(2) Å, In–S(12) = 2.566(2) Å). Similar average In–S bond lengths are also observed in other compounds, *e.g.* $In(S_2CNEt)_3$,[23] $In[S_2P(OEt)_2]_3$,[24] In(dithiolene)$_3$[25] and $[Me_2InS_2CNEt_2]$.[26] A decrease of the ligand bite angle (S–C–S) with increasing size of metal, in this case indium compared to gallium, was observed. The average bite angles of S–C–S in the indium compound are found to be 118.1° compared to those found in gallium analogues, *e.g.* 115.9°.[27]

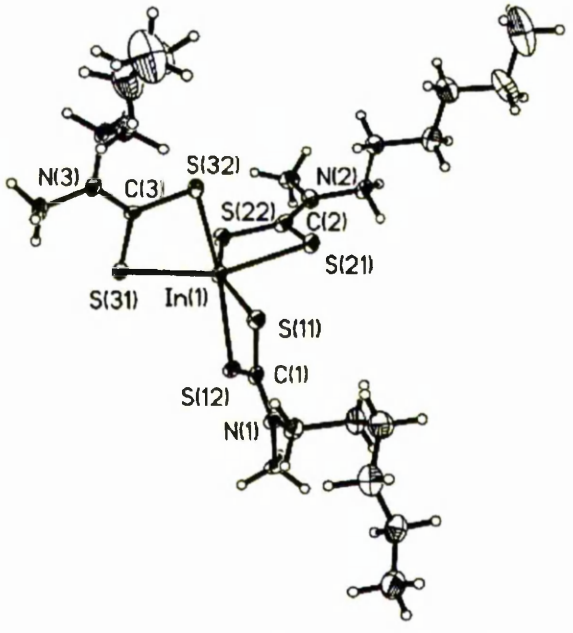

Fig. 1 X-Ray single crystal structure of $In(S_2CNMe''Hex)_3$.

Copper indium sulfide films by LP-MOCVD

Initially, stoichiometric amounts of a mixture of compounds **1** and **2** were used to deposit copper indium sulfide films. The mixture leads solely to the deposition of stoichiometric chalcopyrite $CuInS_2$ at growth temperatures above 450 °C. The 1 : 1 precursor mixture was initially utilised for growth of $CuInS_2$ on glass at different deposition temperatures and $CuInS_2$ was also deposited on various substrates such as ITO coated glass, InP(100), InP(111), GaAs(100), Si(111) and Si(100). The precursor mixture of compounds **1** and **2** in this study needs the evaporator temperature to be higher than 220 °C, and 250 °C was found to be an optimum precursor temperature in this work. If the precursor temperature is lower than 220 °C, only compound **1** is volatile enough and copper sulfide films result. Deposition of $CuInS_2$ onto the substrate was observed at substrate temperatures above 430 °C.

The shape and morphology of the particles grown on glass were not dependent on the growth temperature but the films grown at lower T_{sub} appeared to be more adherent. Films grown for less than 1 h, especially grown at low T_{sub} (450–470 °C), were dark yellow in colour and adherent with up to 5 μm thickness. Films grown for more than 2 h, with higher T_{sub} (480–500 °C), were black and tended to be less adherent probably as a result of their thickness, which was up to 8 μm. The band gap of the films was found to be 1.41 eV by UV/Vis which is close to the accepted value for the direct transition in chalcopyrite $CuInS_2$ of 1.5 eV.[28]

EDAX results indicate that the ratio of Cu : In : S is close to 1 : 1 : 2. XPS was also performed to identify elements present in the film grown at a precursor temperature of 275 °C and a growth temperature of 450 °C. The Cu $2p_{3/2}$ peak has a binding energy of 933.2 eV after etching. The In $3d_{3/2}$ and $3d_{5/2}$ features have binding energies of 452.9 eV and 445.3 eV (Fig. 2). The binding energy of the S 2p peak was found to be 162.9 eV. These values are similar to those reported elsewhere.[29]

The XRD patterns of these films on glass show very distinct peaks at all major *d*-values expected for chalcopyrite $CuInS_2$. As can be seen from the XRD patterns (Fig. 3) and SEM images (Fig. 4), $CuInS_2$ tends to grow as a flake form with a strongly favoured (112) orientation, which is typical for the chalcopyrite compounds. These flakes orientated themselves randomly on the amorphous glass substrate surface. Further attempts were made to alter the orientated growth by the use of a suitable single crystalline substrate with a lattice spacing closely matching the lattice constant of $CuInS_2$. Hence Si, InP and GaAs single crystalline substrates were used to investigate the heteroepitaxial growth of $CuInS_2$ on single crystalline substrates. Although no macromolecular orientation was observed on Si and GaAs by SEM studies, when InP(100) was used as a substrate, highly orientated growth could be observed. Thus, a very strong effect of the substrate was indicated. This is surprising for the lattice mismatch (*ca.* 6%) between $CuInS_2$ and InP(100) in this case. A comparison of the SEM images of $CuInS_2$ films on different substrates is shown in Fig. 4. The SEM and the XRD pattern of $CuInS_2$ on InP(100), where the originally dominant (112) peak is missing and the presence of (200) and (400) can be seen instead, strongly suggest heteroepitaxial growth of the $CuInS_2$ onto the InP(100) substrate with an epitaxial relationship of $CuInS_2(100)\|InP(100)$.

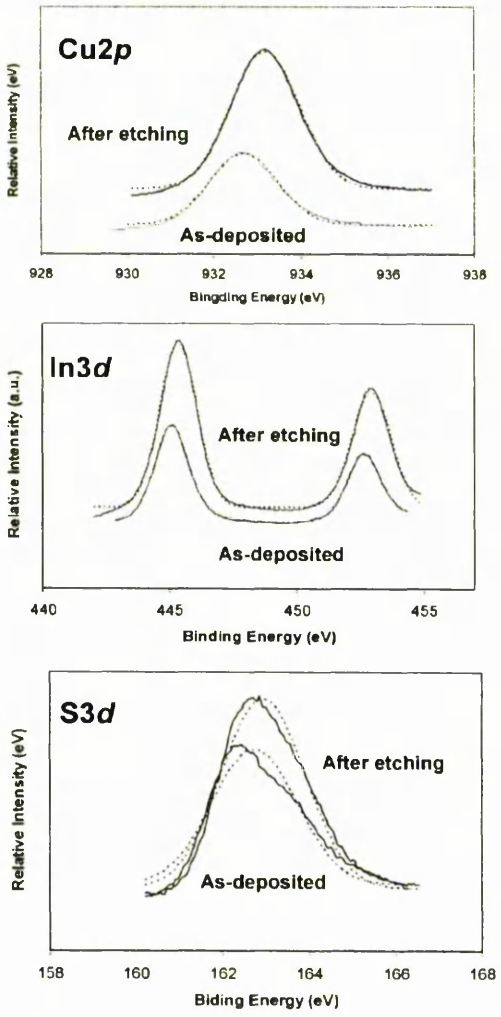

Fig. 2 XPS spectra of $CuInS_2$ grown on glass using compounds **1** and **2** by LP-MOCVD.

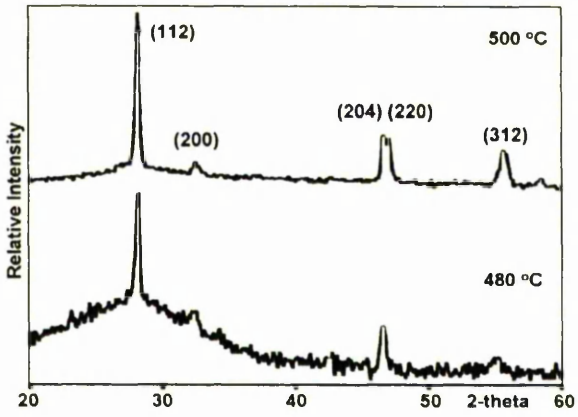

Fig. 3 XRD patterns of $CuInS_2$ grown on glass using compounds **1** and **2** by LP-MOCVD.

The growth was carried out at a T_{pre} of 250 °C and T_{sub} of 460 °C for 1 h.

Copper indium sulfide films by AACVD

$CuInS_2$ films were also successfully grown on glass at 350–450 °C by AACVD. It is interesting to note that employing

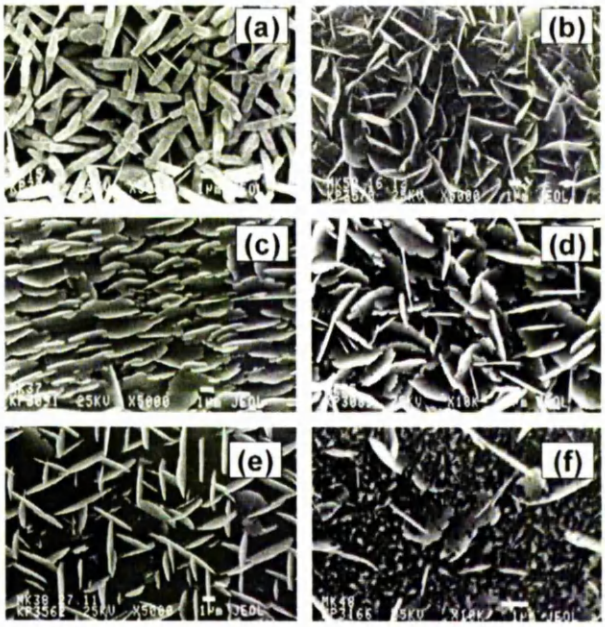

Fig. 4 SEM images of $CuInS_2$ on various substrates using compounds **1** and **2** by LP-MOCVD [a, on glass; b, ITO glass; c, InP(100); d, GaAs(100); e, InP(111) and f, Si(111)].

AACVD can reduce the deposition temperature for the growth of $CuInS_2$ to 350 °C compared to those grown by LP-MOCVD. All films grown using compounds **1** and **2** (1 : 1 ratio) gave narrow and strong peaks in the X-ray diffraction patterns and show characteristics of the tetragonal phase of $CuInS_2$ (Fig. 5). The XRD patterns of the films grown at various growth temperatures show a preferred orientation along the (112) plane regardless of the growth temperature. EDAX analysis of films grown at 450 °C showed peaks corresponding to Cu, In and S and the ratio was found to be close to 1 : 1 : 2.

SEM analysis for the as-deposited $CuInS_2$ films on glass indicates slightly different features in terms of their morphology compared to those grown by LP-MOCVD. Films grown at 450 °C show that particles are formed as flakes *ca.* 0.2 μm thick as compared to the relatively thick (*ca.* 1 μm) crystallites grown by LP-MOCVD, and the particles grown by AACVD are laid down horizontally on the glass substrate (Fig. 6). Also the shapes of the particles are very similar to those prepared on fused silica using $(Ph_3P)_2CuIn(SEt)_4$ by spray CVD.[5] In 2 hours of growth, films were found to be *ca.* 1 μm thick

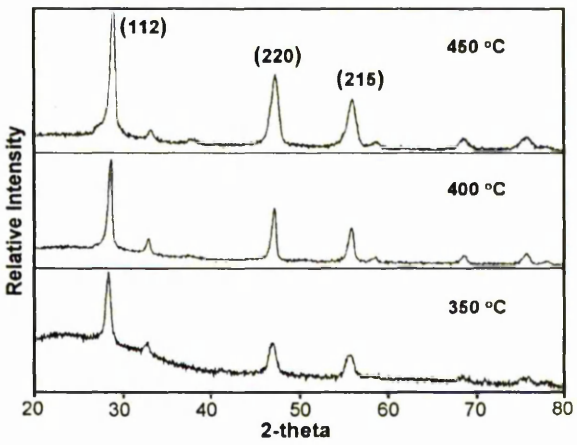

Fig. 5 XRD patterns of $CuInS_2$ on glass using compounds **1** and **2** by AACVD (temperatures indicate growth temperatures).

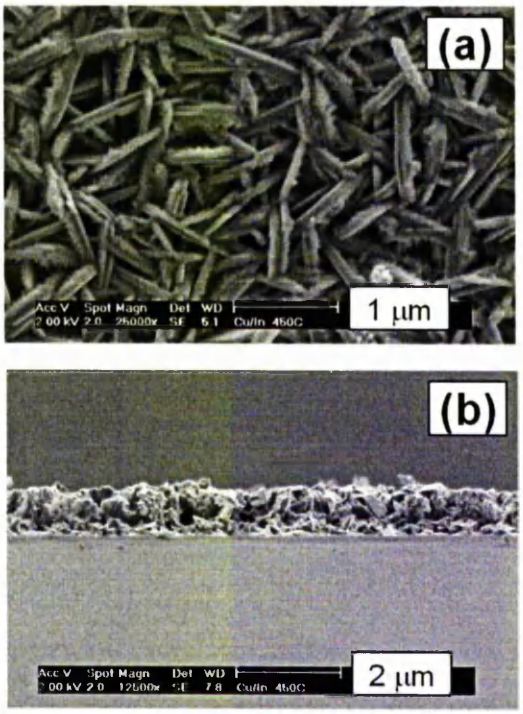

Fig. 6 SEM images of $CuInS_2$ on glass grown at 450 °C using compounds **1** and **2** by AACVD.

with a 0.5 μm h^{-1} growth rate. At lower growth temperature (350 °C), a mixture of morphologies can be seen. The particle size is found to be between 0.5–1.6 μm.

Various ratios of compounds **1** and **2** were also utilized in order to investigate stoichiometric change of $CuInS_2$ films. XRD patterns of as-deposited films grown with different ratios show that there is no evidence to trace any by-products such as either indium sulfide or copper sulfide and indicate no effect on stoichiometry of $CuInS_2$, in contrast to the LP-MOCVD work.

Copper indium selenide films by LP-MOCVD

Films were deposited on glass substrates using compounds **3** and **4**. In initial experiments, these were simply mixed in a 1 : 1 ratio in the evaporator. In subsequent experiments the effect of varying the ratio of Cu : In was also investigated. Using a 1 : 1 ratio *ca.* 2 μm thick films were deposited on glass in 2 hours of growth (source temperature T_{sub} = 180 to 250 °C, growth temperature T_{pre} = 400 to 450 °C). The films deposited using the precursors in a 1 : 1 ratio in the evaporator were specular, black and reasonably adherent and the growth rate was 1 μm h^{-1}. Typical SEM images on various substrates are shown in Fig. 7. The film on glass is composed of a mixture of acicular and hexagonal platelets of $CuInSe_2$ (Fig. 7a). The platelets in particular appear orientated orthogonal or at an acute angle to the substrate surface. Although the strongly orientated growth of $CuInS_2$ on InP(100) has been observed previously, no similar feature was found in the case of $CuInSe_2$ growth on InP(100) or other single crystalline substrates. Films grown on ITO coated glass and Si(100) show a quite different morphology compared to those prepared on glass (Fig. 7c and d). The particles are more homogenous and the average particle size is show to be 100 nm.

The XRD patterns of as-deposited films on glass with varying ratios of compounds **3** and **4** are shown in Fig. 8. The indices are assigned according to those in JCPDS 40-1487; the (112) orientation is dominant but also the other main peaks indicate that the as-grown materials are $CuInSe_2$ with the

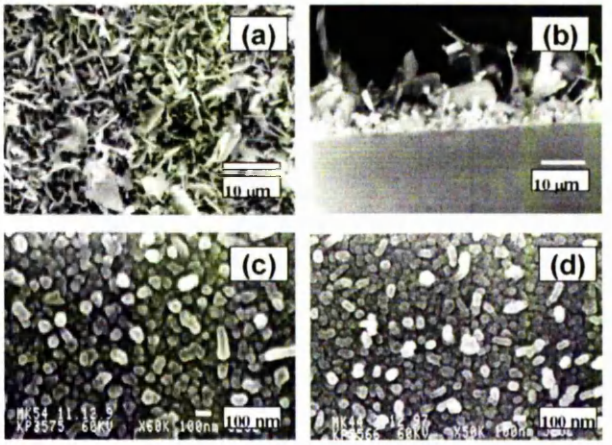

Fig. 7 SEM images of $CuInSe_2$ grown on various substrates using compounds **3** and **4** by LP-MOCVD [a and b, glass; c, ITO glass; d, Si(100)].

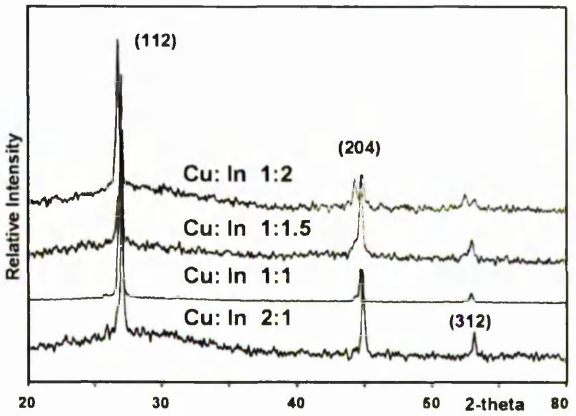

Fig. 8 XRD patterns of $CuInSe_2$ films on glass by LP-MOCVD with different ratios of compounds **3** and **4** (T_{sub}: 450 °C, T_{pre}: 250 °C, growth time: 1 h).

chalcopyrite structure. Also, varying the ratio of the compounds did not affect the deposition of $CuInSe_2$.

Qualitative EDAX results confirm that the Cu : In : Se stoichiometry is close to 1 : 1 : 2 in most cases. The optical bandgap was estimated by using the direct bandgap method as 1.08 eV. The value is in good agreement with the accepted value for $CuInSe_2$ (1.0–1.1 eV). Survey scans for the film, grown at a growth temperature of 450 °C and a precursor temperature of 275 °C, before and after the ion etching process showed that the spectrum of the sample before etching is found to be a typical oxidized surface as indicated by the O 1s core-level signal, which vanished after the etching process. The carbon peak was also minimized after etching. Details of individual elemental peaks are shown in Fig. 9. The Cu $2p_{3/2}$ peak has a binding energy of 933.1 eV after etching. The In $3d_{3/2}$ and $3d_{5/2}$ features have binding energies of 452.8 eV and 445.25 eV. The binding energy of the Se 3d peak is 55.2 eV. These values are similar to those reported elsewhere.[30]

Copper indium selenide films by AACVD

$CuInSe_2$ films were also deposited on glass using compounds **3** and **4** by AACVD. In this case, only a 1 : 1 ratio of compounds **3** and **4** was used. Films were grown at 425–475 °C with a constant argon flow rate of 180 sccm. XRD analyses (Fig. 10) suggest that as-deposited films crystallize in a tetragonal phase with a preferred orientation along the (112) direction in all

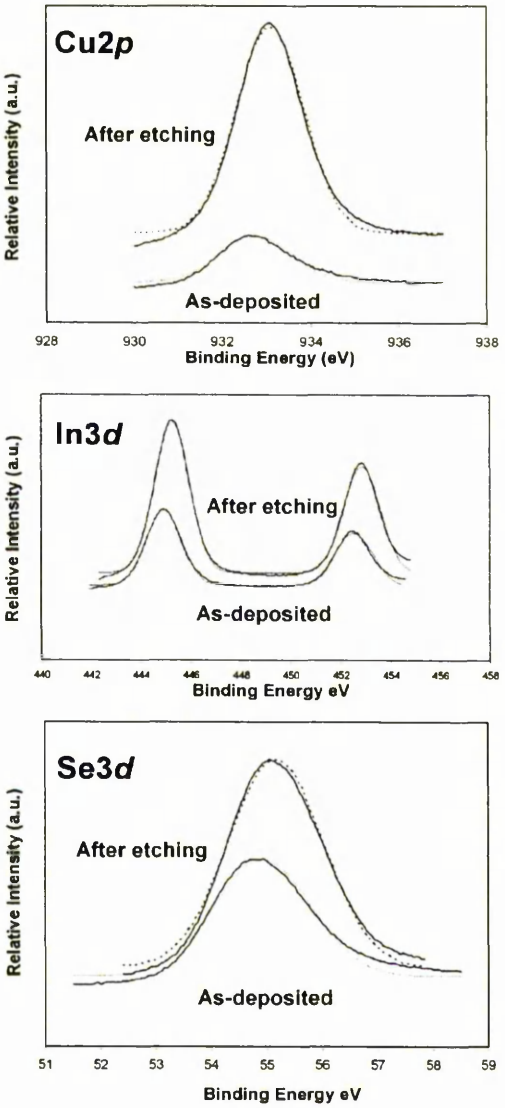

Fig. 9 XPS spectra of $CuInSe_2$ films on glass by LP-MOCVD.

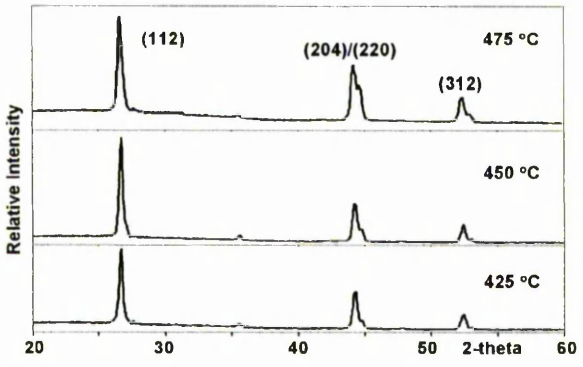

Fig. 10 XRD patterns of $CuInSe_2$ films on glass by AACVD.

cases. SEM images of the films show (Fig. 11) that the deposited materials are not homogenous and mainly consist of several different shapes of particles with poor coverage at lower growth temperature (425 °C). These findings are consistent with the LP-MOCVD study.

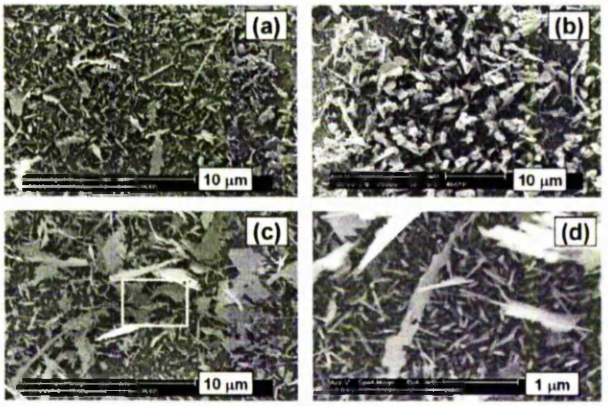

Fig. 11 SEM images of $CuInSe_2$ on glass using compounds **3** and **4** by AACVD. [(a) 425 °C, (b) 450 °C, (c) and (d) 475 °C].

Copper gallium sulfide by LP-MOCVD

In order to grow copper gallium sulfide compounds **1** and **5** were employed as precursors. 61 mg (0.138 mmol) of **1** and 90 mg (0.140 mmol) of **5** were used, representing a *ca.* 1 : 1 molar ratio. The film was grown on glass for 1.5 h at T_{pre} = 250 °C and T_{sub} = 500 °C. The XRD pattern with very low intensity is shown in Fig. 12 and the peaks could be assigned to $CuGaS_2$ from JCPDS 25-379 with some copper sulfide by-products (JCPDS 23-959 and 30-505). The morphology of the film is found to be quite random.

Copper gallium sulfide by AACVD

In the AACVD study, stoichiometric amounts of compounds **1** and **5** were employed and dissolved in THF (30 ml). In initial experiments, the Cu : In ratio was maintained at 1 : 1 and the growth time was kept constant at 2 hours (180 sccm flow rate). Glass was used as a substrate.

XRD patterns (Fig. 13) show that films deposited by AACVD have the chalcopyrite structure with a preferred orientation along the (112) direction (JCPDS 27-0279). It is also conclusive that at high temperatures the crystallinity of the deposited film is improved, as indicated by the sharpness of the peaks, whilst at low temperature (350 °C) the XRD pattern exhibits weak reflections indicating poorly crystalline films. Similar results are obtained for films grown at a lower argon flow rate (120 sccm).

SEM analysis (Fig. 14) shows that the material consists of clusters of randomly orientated platelets perpendicular to the surface for films grown at 400 and 450 °C (180 sccm flow rate).

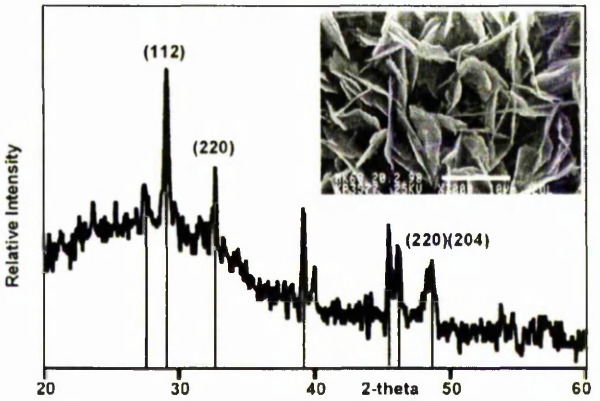

Fig. 12 XRD pattern and SEM image of $CuGaS_2$ on glass using compounds **1** and **5** by LP-MOCVD.

Table 3 Comparison of *hkl* values of films prepared in this work[a]

	$CuInS_2$			$CuInSe_2$			$CuGaS_2$		
hkl	JCPDS 27-0159	LPCVD	AACVD	JCPDS 40-1487	LPCVD	AACVD	JCPDS 25-0279	LPCVD	AACVD
112	3.19	3.19	3.12	3.35	3.30	3.34	3.06	3.07	3.07
200	2.76	2.77	2.77	2.89	N/A	N/A	2.67		2.68
211	2.41	N/A	2.47	2.53	N/A	2.52	N/A	N/A	N/A
204	1.96	1.97	1.96	2.05	N/A	2.05	1.87	1.87	1.88
220	1.95	1.95	N/A	2.04	2.02	2.02	1.89	N/A	1.89
116	1.67	1.67	1.67	1.75	1.73	1.75	1.59	N/A	1.61

[a]$CuInS_2$ and $CuGaS_2$ films were grown at T_{pre} = 250 °C and T_{sub} = 500 °C while $CuInSe_2$ films were deposited at T_{pre} = 250 °C and T_{sub} = 450 °C using LP-MOCVD. Films deposited by AACVD were grown at 450 °C.

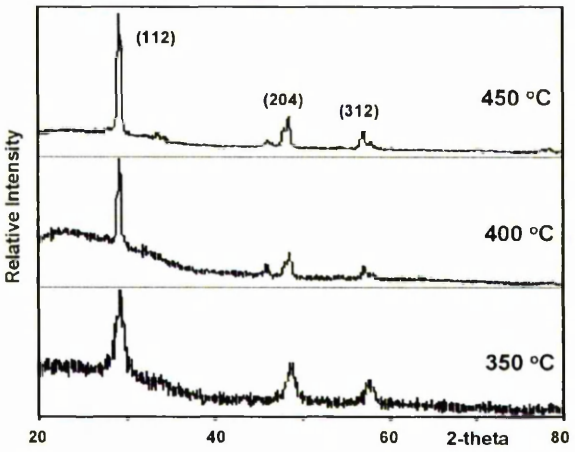

Fig. 13 XRD patterns of $CuGaS_2$ on glass using compounds **1** and **5** by AACVD (temperatures indicate growth temperatures).

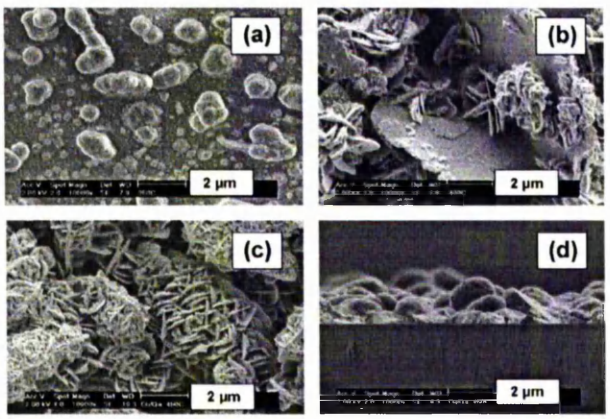

Fig. 14 SEM images of $CuGaS_2$ films grown on glass using compounds **1** and **5** by AACVD with a flow rate of 180 sccm [a, 350 °C; b, 400 °C; c and d, 450 °C].

The films deposited are dense but uneven. Growth rates are approximately 500 nm h^{-1} for films grown at 350 °C and 1 μm h^{-1} at 450 °C. As the growth temperature is decreased, the growth of $CuGaS_2$ is significantly reduced. EDAX analysis of the film shows Cu 30%, Ga 24% and S 46%. However, when the flow rate of Ar is reduced to 120 sccm, the clusters formed tended to be denser but some individual platelets were also evident. In 2 hours of growth at 450 °C, films with *ca.* 1.5 μm thickness were deposited on the glass substrate (growth rate *ca.* 0.75 μm h^{-1}). EDAX elemental atomic percentages for $CuGaS_2$ films were found to be 29%, 23% and 48% respectively.

Conclusions

The results described herein demonstrate that AACVD and LP-MOCVD using organometallic precursors, result in stoichiometric $CuME_2$ (M = In or Ga, E = S or Se) films, and the quality (*e.g.* morphology or orientations) of films are dependent on experimental parameters. Furthermore, films grown on glass by AACVD show similar XRD patterns regardless of the deposited materials. Table 3 shows some unique *hkl* values, which can be seen in the $CuME_2$ films prepared by AACVD in this study. It is evident that the CVD process and film uniformity were somewhat improved by the selection of growth techniques, deposition temperatures and substrates. As a result, it is shown that a series of asymmetrical alkyldithiocarbamate metal complexes can be used as precursors for the deposition of I–III–VI_2 films by CVD techniques.

Acknowledgements

POB thanks the EPSRC and the Leverhulme Foundation for the grants that have made this research possible. The authors wish to thank Mr. K. Pell and Dr. J. McAleese for SEM and Mr R. Sweeny for XRD measurements.

References

1 C. C. Landry, J. Lockwood and A. R. Barron, *Chem. Mater.*, 1995, **7**, 699.
2 R. Nomura, K. Kanaya and H. Matsuda, *Chem. Lett.*, 1988, **11**, 1849.
3 R. Nomura, Y. Seki and H. Matsuda, *J. Mater. Chem.*, 1992, **2**, 765.
4 W. Hirpo, S. Dhingra, A. C. Sutorik and M. G. Kanatzidis, *J. Am. Chem. Soc.*, 1993, **115**, 1597.
5 J. A. Hollingworh, A. F. Hepp and W. E. Buhro, *Adv. Mater. Chem. Vap. Deposit.*, 1999, **5**, 105.
6 K. K. Banger, J. Cowen and A. F. Hepp, *Chem. Mater.*, 2001, **13**, 382.
7 K. K. Banger, J. D. Harris, J. Cowen and A. F. Hepp, *Thin Solid Films*, 2002, **403–404**, 390.
8 M. Lin, K. P. Loh, T. C. Deivaraj and J. J. Vittal, *Chem. Commun.*, 2002, 1400.
9 K. K. Banger, J. A. Hollingworth, J. D. Harris, J. Cowen, W. E. Buhro and A. F. Hepp, *Appl. Organomet. Chem.*, 2002, **16**, 617.
10 S. Chichibu and S. Shirakata, *J. Appl. Phys.*, 2000, **87**, 3793.
11 M. Kemmler, M. R. Lazell, P. O'Brien, D. J. Otway, J.-H. Park and J. R. Walsh, *J. Mater. Sci. Mater. Electron.*, 2002, **10**, 531.
12 M. B. Hursthouse, M. A. Malik, M. Motevalli and P. O'Brien, *J. Mater. Chem.*, 1992, **2**, 949.
13 P. O'Brien, D. J. Otway and J. R. Walsh, *Thin Solid Films*, 1998, **315**, 57.
14 M. Motevalli, P. O'Brien, J. R. Walsh and I. M. Watson, *Polyhedron*, 1996, **15**, 2801.
15 P. O'Brien, J. R. Walsh, I. M. Waston, L. Hart and S. R. P. Silva, *J. Cryst. Growth*, 1996, **167**, 133.
16 S. W. Haggata, M. A. Malik, M. Motevalli, P. O'Brien and J. C. Knowles, *Chem. Mater.*, 1995, **7**, 716.

17 M. R. Lazell, P. O'Brien, D. J. Otway and J.-H. Park, *Chem. Mater.*, 1999, **11**, 3430.
18 J. McAleese, P. O'Brien and D. J. Otway, *Adv. Mater. Chem. Vap. Deposit.*, 1998, **4**, 94.
19 M. Afzaal, D. Crouch, P. O'Brien and J.-H. Park, *Mater. Res. Soc. Symp. Proc.*, 2002, **692**, 215.
20 G. M. Sheldrick, SHELXL97 and SHELXS 97, University of Göttingen, Germany, 1997.
21 SHELXTL, Version 6.10, Bruker AXS Inc., Madison, Wisconsin, USA, 2000.
22 M. A. Malik and P. O'Brien, *Adv. Mater. Opt. Electron.*, 1994, **3**, 71.
23 K. Dymock, G. J. Palenik, J. Slezak, C. L. Raston and A. H. White, *J. Chem. Soc., Dalton Trans.*, 1976, 28.
24 P. Coggan, J. D. Lebbeda, A. T. McPhail and R. A. Palmer, *J. Chem. Soc., Chem. Commun.*, 1970, 78.
25 F. W. B. Einstein and R. D. G. Jones, *J. Chem. Soc. A*, 1971, 2762.
26 S. W. Haggata, J. C. Knowles, M. A. Malik, M. Motevalli and P. O'Brien, *Chem. Mater.*, 1995, **7**, 716.
27 D. P. Dutta, V. K. Jain, A. Knoedler and W. Kaim, *Polyhedron*, 2001, **21**, 239.
28 T. Fujiwara, M. Okuya and S. Kaneko, *J. Ceram. Soc. Jpn.*, 2002, **110**, 81.
29 A. B. Mandale, S. D. Sathaye and K. R. Patil, *Mater. Lett.*, 2002, **55**, 30.
30 K. Otte, G. Lippold, D. Hirsch, A. Schindler and A. F. Bigl, *Thin Solid Films*, 2001, **361**, 498.

Deposition of II-VI Thin Films by LP-MOCVD Using Novel Single-Source Precursors

Mohammad Afzaal,[a] David Crouch,[a] Mohmmad A. Malik,[a] Majid Motevalli,[b] Paul O'Brien,*[a] Jin-Ho Park,[a] and J. Derek Woollins[c]

Keywords: Chemical vapour deposition / Chalcogens / Zinc / Cadmium

Thin films of several zinc or cadmium chalcogenides have been deposited on glass substrates by low pressure metal-organic chemical vapour deposition (LP-MOCVD) using single-source precursors, $[M\{(EP\textit{i}Pr_2)_2N\}_2]$ (M = Cd^{II}, Zn^{II} and E = S, Se). X-ray single crystal structures show that $[Zn\{(EP\textit{i}Pr_2)_2N\}_2]$ (E = S or Se) and $[Zn\{(SePPh_2)_2N\}_2]$ are tetrahedrally distorted. TGA analyses showed that the precursors are volatile, making them suitable for MOCVD studies. As-deposited films were polycrystalline as confirmed by X-ray powder diffraction (XRPD) and their morphologies were studied by scanning electron microscope (SEM).

Introduction

The direct nature of band gaps in II-VI materials makes them suitable for use in devices, such as blue/blue-green laser diodes,[1-3] which could lead to high-density optical storage systems.[4-6] Cadmium chalcogenides are also useful materials in solid-state solar cells, photoconductors, field effect transistors, sensors and tranducers.[7,8]

Single-source precursors have several potential advantages over conventional MOCVD which uses dual-sources. These include limited premature reactions and good quality homogeneous films.[1] The solid-state chemistry of cadmium and zinc with the chalcogens is typified by the formation of polymeric structures with tetrahedral metal ions,[1] the admantyl structures of many thiolates with zinc and cadmium provide well-characterised examples of such behaviour,[2-4] as do the polymeric chain complexes formed by pyridinethione and 2,3-mercaptobenzothiazole with cadmium and zinc.[5,6] Bochmann et al. have extended such chemistry by producing a range of precursors based on 2,4,6-tri-*tert*-butylphenylchalcogenolate, which have been used to deposit thin films of the metal sulfides and selenides in low-pressure growth experiments.[7-9] In related work, Arnold and co-workers have also deposited a range of chalcogenides using silicon-based ligands, i.e. $[\{MESi(SiCH_3)_3\}_2]$ (M = Zn^{II}, Cd^{II}, Hg^{II} and E = S, Se or Te).[10,11]

Other classes of molecules, which have proved useful for the deposition of thin films include coordination complexes such as dialkyl dichalcogenocarbamates or dithiophosphinates.[12-16] Various groups have studied simple $[M(S_2CNEt_2)_2]$ (M = Cd^{II}, Zn^{II}) complexes and deposited CdS or ZnS films by different deposition techniques.[13-15] However, the use of metal diethyldiselenocarbamates to deposit ZnSe and CdSe on glass substrates resulted in the deposition of elemental selenium.[16] Asymmetrical alkyl substituents as in $[M(E_2CNMeHex)_2]$ (M = Cd^{II}, Zn^{II} and E = S, Se) which were originally introduced in order to increase volatility and have been successfully used to deposit II-VI films (including ZnSe and CdSe) by low pressure metal-organic chemical vapour deposition (LP-MOCVD). An investigation into decomposition mechanisms by gas chromatography mass spectroscopy (GC-MS) and electron impact mass spectroscopy (EI-MS) showed that the deposition of selenium during growth is inhibited in such compounds.[16]

We have recently identified a new class of metal-organic single-source precursors based on bis(diphenylphosphanyl-amine) e.g., $[NH(SePPh_2)_2]$ ligands (an analogue of the β-diketonates) a system pioneered by Woollins, $[M\{(SePPh_2)_2N\}_2]$ (M = Cd^{II}, Zn^{II}) complexes which have been used as precursors for zinc/cadmium selenide films by LP-MOCVD.[17] In this paper, we report crystal structures of $[Zn\{(EP\textit{i}Pr_2)_2N\}_2]$ (E = S or Se) and $[Zn\{(SePPh_2)_2N\}_2]$. We also report the deposition and characterisation of metal chalcogenide films on glass substrates from

[a] The Manchester Materials Science Centre and Department of Chemistry, The University of Manchester,
Oxford Road, Manchester, M13 9PL, UK
Fax: (internat.) +44-(0)161-2754616
E-mail: paul.obrien@man.ac.uk
[b] Department of Chemistry, Queen Mary and Westfield College, Mile End Road, London, E1 4NS, UK
[c] School of Chemistry, University of St. Andrews, Purdie Building,
St. Andrews, Fife, KY16 9ST, UK

 DOI: 10.1002/ejic.200300101

$[M\{(EPiPr_2)_2N\}_2]$ (M = Cd^{II}, Zn^{II} and E = S, Se) complexes **1**–**4**) by low-pressure MOCVD.

Results and Discussion

The syntheses of ligands $[NH(EPiPr_2)_2]$ (E = S or Se) were carried out according to previously reported methods.[18,19] The synthesis of the precursor involves deprotonation of the N–H moiety, using sodium methoxide, to form anionic chelate complexes which is subsequently reacted with the metal chloride (Scheme 1). These reactions have some advantages over the routes via metal carbonates and higher yields are obtained particularly for the selenium complexes. The reactions occur efficiently and cleanly at room temperature in anhydrous methanol. All the compounds are soluble in organic solvents and are air-stable.

$$NH(SiMe_3)_2 + 2\ {}^iPr_2PCl \xrightarrow[\text{stirring (3 hours)}]{50\text{–}70\ ^\circ C} NH(P^iPr_2)_2 + 2\ ClSiMe_3 \quad \text{(Eq. 1)}$$

$$NH(SiMe_3)_2 \xrightarrow[\text{reflux}]{E = S,\ Se} NH(EP^iPr_2)_2 \quad \text{(Eq. 2)}$$

$$2\ NH(EP^iPr_2)_2 + MCl_2 \xrightarrow[MeOH]{NaOMe} M[(EP^iPr_2)_2N]_2 + 2\ NaCl \quad \text{(Eq. 3)}$$

Scheme 1

X-ray Structures

Crystals of $[Zn\{(SePPh_2)_2N\}_2]$ suitable for X-ray diffraction studies were obtained by slow diffusion of hexane into a chloroform solution of the complex. During attempts to synthesise the mixed-alkylzinc complexes by comproportionation reactions between dimetylzinc and $[Zn\{(EPiPr_2)_2N\}_2]$ (E = S or Se), the serendipitous formation of $[Zn\{(EPiPr_2)_2N\}_2]$ (E = S or Se) crystals from toluene solutions occurred. The molecular structures of the compounds are shown in Figures 1–3.

X-ray single crystallographic studies carried out on $[Zn\{(EPiPr_2)_2N\}_2]$ (E = S or Se) and $[Zn\{(SePPh_2)_2N\}_2]$ reveal that the complexes are tetrahedrally coordinated by two ligands. The structure of $[Zn\{(SePiPr_2)_2N\}_2]$ illustrated in Figure 1 is isostructural with its sulfur analogue (Figure 2). The Zn–Se bond lengths are in the range of 2.458(9) to 2.467(9) Å which are slightly larger than Zn–S bond lengths [2.350(11) to 2.359(11) Å]. Similarly, the Se–Zn–Se bite angles are also increased from the bite angles of S–Zn–S [111.84(4)–112.81(4)°] (Tables 2 and 3). Shortening of the P–N bonds to 1.583(3)–1.592(4) Å and

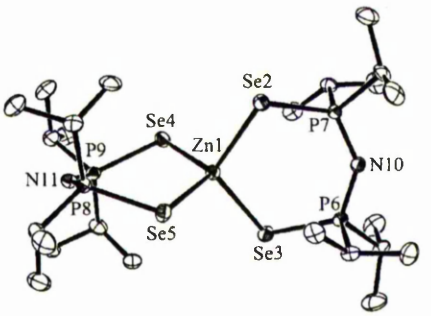

Figure 1. X-ray single crystal structure of $[Zn\{(SePiPr_2)_2N\}_2]$

Table 1. Crystallographic data collection and refinement parameters

Compound	$C_{24}H_{56}N_2P_4Se_4Zn$	$C_{24}H_{56}N_2P_4S_4Zn$	$C_{48}H_{40}N_2P_4Se_4Zn$
Formula mass	877.70	690.20	1149.91
Temperature (K)	160(2)	160(2)	433(2)
Crystal size (mm)	0.45 × 0.13 × 0.10	0.4 × 0.3 × 0.2	0.57 × 0.45 × 0.35
Crystal system	triclinic	triclinic	triclinic
Space group	$P\bar{1}$	$P\bar{1}$	$P\bar{1}$
a (Å)	9.348(2)	9.232(3)	13.727(7)
b (Å)	12.880(3)	12.678(4)	13.809(5)
c (Å)	16.389(4)	16.401(5)	14.3120(16)
α (°)	100.95(2)	92.24(2)	82.74(9)
β (°)	102.02(2)	101.77(2)	66.36(6)
γ (°)	69.64(2)	110.77(2)	70.13(4)
V (Å^3)	1794.5(7)	1744.1(10)	2337.2(15)
Z	2	2	2
$d_{calcd.}$ (mg/m^3)	1.625	1.314	1.634
Abs. coeff. (mm^{-1})	4.936	1.144	3.813
F(000)	880	736	1136
Index ranges	$0 \le h \le 11$	$-1 \le h \le 5$	$-14 \le h \le 16$
	$-14 \le k \le 15$	$-15 \le k \le 14$	$-16 \le k \le 16$
	$-19 \le l \le 19$	$-19 \le l \le 19$	$-16 \le l \le 16$
Collected/unique	6877/6313	4697/4101	8661/8661
Data/restraints/pars.	6313/0/332	4191/0/332	8661/0/4392
Goodness-of-fit on F^2	0.873	0.895	0.982
$R1$, $wR2$ [$I > 2\sigma(I)$]	0.0297, 0.0745	0.0270, 0.0662	0.0596, 0.1763
$R1$, $wR2$ (all data)	0.0592, 0.0866	0.0365, 0.0706	0.0787, 0.1963
Diff. peak, hole (e·Å^{-3})	0.545, −0.482	0.340, −0.503	1.939, −3.706

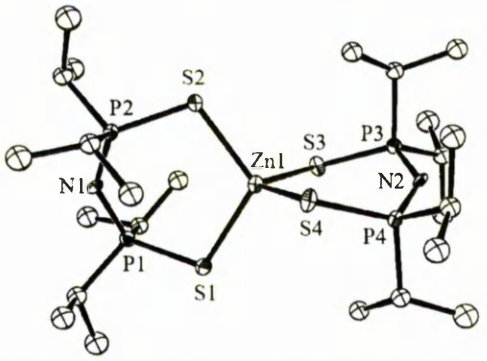

Figure 2. X-ray single crystal structure of $[Zn\{(SPiPr_2)_2N\}_2]$

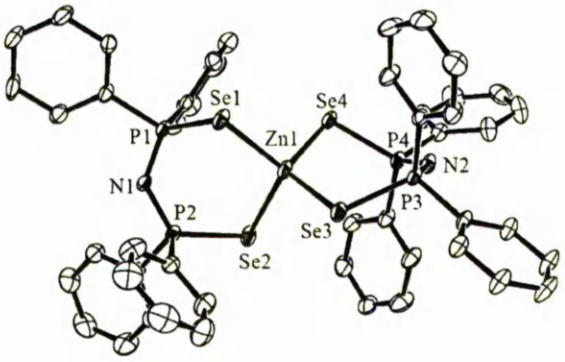

Figure 3. X-ray single crystal structure of $[Zn\{(SePPh_2)_2N\}_2]$

Table 2. Selected interatomic distances (Å) and angles (°) for $[Zn\{(SePiPr_2)_2N\}_2]$

Zn(1)−Se(2)	2.458(9)	Se(2)−Zn(1)−Se(5)	107.31(3)
Zn(1)−Se(5)	2.458(9)	Se(2)−Zn(1)−Se(4)	106.55(3)
Zn(1)−Se(4)	2.459(8)	Se(5)−Zn(1)−Se(4)	114.07(3)
Zn(1)−Se(3)	2.467(9)	Se(2)−Zn(1)−Se(3)	114.07(3)
Se(2)−P(7)	2.177(13)	Se(5)−Zn(1)−Se(3)	106.36(3)
Se(3)−P(6)	2.179(13)	Se(4)−Zn(1)−Se(3)	109.29(3)
Se(4)−P(9)	2.183(13)	P(7)−Se(2)−Zn(1)	103.30(4)
Se(5)−P(8)	2.183(13)	P(6)−Se(3)−Zn(1)	103.01(4)
P(6)−N(10)	1.592(4)	P(9)−Se(4)−Zn(1)	102.83(4)
P(8)−N(11)	1.583(3)	P(8)−Se(5)−Zn(1)	103.67(4)

Table 3. Selected interatomic distances (Å) and angles (°) for $[Zn\{(SPiPr_2)_2N\}_2]$

Zn(1)−S(4)	2.350(11)	S(4)−Zn(1)−S(2)	108.78(4)
Zn(1)−S(2)	2.347(11)	S(4)−Zn(1)−S(1)	106.98(4)
Zn(1)−S(1)	2.351(10)	S(2)−Zn(1)−S(1)	112.81(4)
Zn(1)−S(3)	2.359(11)	S(4)−Zn(1)−S(3)	111.84 (4)
S(1)−P(1)	2.027(13)	S(2)−Zn(1)−S(3)	106.59(4)
S(2)−P(2)	2.032(11)	S(1)−Zn(1)−S(3)	109.92(4)
S(3)−P(3)	2.025(11)	P(1)−S(1)−Zn(1)	105.35(5)
S(4)−P(4)	2.027(12)	P(2)−S(2)−Zn(1)	105.90 (5)
		P(3)−S(3)−Zn(1)	105.81(4)
		P(4)−S(4)−Zn(1)	105.87(4)

the subsequent extension of the P−Se bonds 2.177(13)−2.183(13) Å relative to the free ligand, indicates an increase in delocalization within the architecture due to deprotonation.[19] Crystalline $[Zn\{(SPiPr_2)_2N\}_2]$ as reported by Woollins et al. exhibits completely different unit cell parameters.[18] The unit cell described here contains two independent monomeric molecules versus four reported in the earlier paper.[18]

The zinc atom in $[Zn\{(SePPh_2)_2N\}_2]$ is also coordinated to the selenium atoms through two bidentate ligands forming six-membered chelate rings. The tetrahedral geometry around the zinc atom is distorted which is reflected in the Se−Zn−Se angles which range from 103.85(9) to 115.93(6)° (Table 4). There is no significant difference in the Zn−Se bond lengths of $[Zn\{(SePR_2)_2N\}_2]$ (R = Ph or *i*Pr). The ZnE_2P_2N (E = S or Se) rings have puckered geometries with a distorted boat conformation. This conformation appears to be the most commonly adopted for complexes containing $[R_2P(E)NP(E)R_2]^-$ (E = S or Se) ligands, although other conformations also have been reported with selenium or sulfur and phosphorous atoms at the apices.[29,30]

Table 4. Selected interatomic distances (Å) and angles (°) for $[Zn\{(SePPh_2)_2N\}_2]$

Zn(1)−Se(3)	2.459(3)	Se(3)−Zn(1)−Se(4)	115.93(6)
Zn(1)−Se(4)	2.475(15)	Se(3)−Zn(1)−Se(1)	103.85(9)
Zn(1)−Se(1)	2.482(14)	Se(4)−Zn(1)−Se(1)	111.35(8)
Zn(1)−Se(2)	2.484(19)	Se(3)−Zn(1)−Se(2)	115.03(9)
Se(1)−P(1)	2.171(3)	Se(4)−Zn(1)−Se(2)	106.10(9)
Se(2)−P(2)	2.179(2)	Se(1)−Zn(1)−Se(2)	114.71(5)
Se(3)−P(3)	2.186 (2)	P(1)−Se(1)−Zn(1)	94.11(7)
Se(4)−P(4)	2.187(2)	P(2)−Se(2)−Zn(1)	97.46(7)
		P(3)−Se(3)−Zn(1)	102.22(7)
		P(4)−Se(4)−Zn(1)	94.80(8)

Deposition Studies: In this study, metal chalcogenide thin films have been deposited using air-stable single-source precursors, $[M[(EPiPr_2)_2N\}_2]$ (M = Cd^{II}, Zn^{II} and E = S, Se). The suitability of the precursors were determined by thermogravimetric analysis (TGA) at atmospheric pressure, and all show clean sublimation without any residues, as desirable in precursors for MOCVD studies (Table 5). Deposition of thin films was attempted over a range of substrate temperatures (400 to 500 °C) on glass substrates for one hour with ca. 200 mg of precursor used for each growth experiment.

Table 5. TGA data for compounds **1**−**4**

Compound	T_s (°C)[a]	T_f (°C)[b]
$[Cd\{(SPiPr_2)_2N\}_2]$	237	355
$[Cd\{(SePiPr_2)_2N\}_2]$	310	419
$[Zn\{(SPiPr_2)_2N\}_2]$	222	366
$[Zn\{(SePiPr_2)_2N\}_2]$	240	366

[a] T_s = sublimation temp. [b] T_f = decomposition temp.

Cadmium Sulfide: CdS films were grown from $[Cd\{(SPiPr_2)_2N\}_2]$ at growth temperatures of 425 and 450 °C with a precursor temperature of 250 °C. Deposited films were yellow, transparent and well-adherent to the glass sur-

face. At higher growth temperature (475 °C), slightly dark yellow-brown film was observed after one hour of growth. As-deposited cadmium sulfide films were analysed by XRPD, which indicated that the hexagonal CdS films (Table 6) have been deposited with a preferred orientation along the (002) plane (Figure 4). SEM studies indicate that the morphology of film deposited at 450 °C consists of randomly oriented domains of compacted thin acicular crystallites with ca. 1.75 μm in thickness (Figure 5). Similar morphology was also observed for the film deposited at 425 °C. On the basis of EDAX analyses, the films were found to be slightly cadmium rich with 52%, sulfur (46%) and phosphorous (2%).

Table 6. XRPD data for CdS grown at 425 and 450 °C from $[Cd\{(SP\textit{i}Pr_2)_2N\}_2]$

hkl	JCPDS (06-0314) *d* [Å] (rel. int.)	CdS (425 °C) *d* [Å] (rel. int.)	CdS (450 °C) *d* [Å] (rel. int.)
100	3.58 (75)	3.57 (2)	3.57 (2)
002	3.36 (60)	3.35 (100)	3.36 (100)
101	3.16 (100)	3.14 (5)	3.16 (14)
102	2.45 (25)	2.43 (3)	2.45 (6)
110	2.07 (55)	2.05 (3)	2.06 (2)
103	1.90 (40)	1.89 (17)	1.90 (2)
200	1.79 (18)	N/A	N/A
112	1.76 (45)	1.76 (3)	1.77 (6)

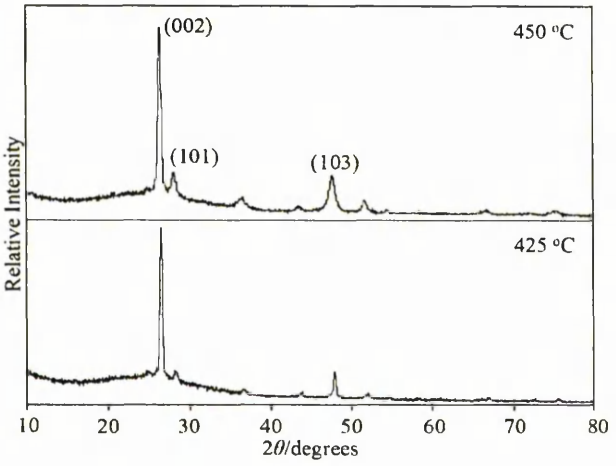

Figure 4. XRPD patterns of CdS films deposited on glass from $[Cd\{(SP\textit{i}Pr_2)_2N\}_2]$ by LP-MOCVD

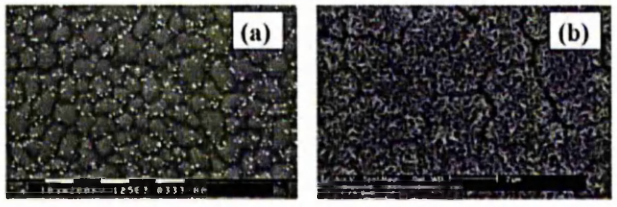

Figure 5. SEM images of CdS films from $[Cd\{(SP\textit{i}Pr_2)_2N\}_2]$ deposited at (a) 425 °C and 450 °C

Cadmium Selenide: Deposition of CdSe films was attempted at substrate temperatures of 425−500 °C, with the precursor temperature set at 325 °C using $[Cd\{(SeP\textit{i}Pr_2)_2N\}_2]$. Little or no deposition was observed below 450 °C. At higher growth temperatures, 475 and 500 °C, deposited films were black and adherent to the surface. XRPD studies of the deposited films indicate that polycrystalline hexagonal CdSe films (Table 7) have been deposited with a preferred orientation along the (100) plane (Figure 6). Film deposited at 500 °C was slightly more ordered than the film grown at 475 °C indicated by the absence of (002) plane at 25.5Θ 2θ. Films grown from $[Cd\{(SePPh_2)_2N\}_2]$ also resulted in hexagonal CdSe at 500 and 525 °C but show different preferred orientations (002) and (101) respectively.[17]

Table 7. XRPD data for CdSe grown at 475 and 500 °C from $[Cd\{(SeP\textit{i}Pr_2)_2N\}_2]$

hkl	JCPDS (08-0459) *d* [Å] (rel. int.)	CdSe (475 °C) *d* [Å] (rel. int.)	CdSe (500 °C) *d* [Å] (rel. int.)
100	3.72 (100)	3.73 (100)	3.75 (100)
002	3.51 (70)	3.51 (9)	N/A
101	3.29 (75)	3.29 (13)	3.27 (21)
102	2.55 (35)	2.55 (2)	2.54 (1)
110	2.15 (85)	2.15 (36)	2.15 (78)
103	1.98 (70)	1.98 (5)	1.97 (1)
200	1.86 (12)	1.86 (3)	1.86 (8)
112	1.83 (50)	1.83 (7)	1.83 (20)
201	1.80 (12)	1.80 (5)	1.80 (6)
202	1.65 (8)	1.64 (3)	1.64 (3)
203	1.46 (20)	1.45 (6)	1.46 (7)

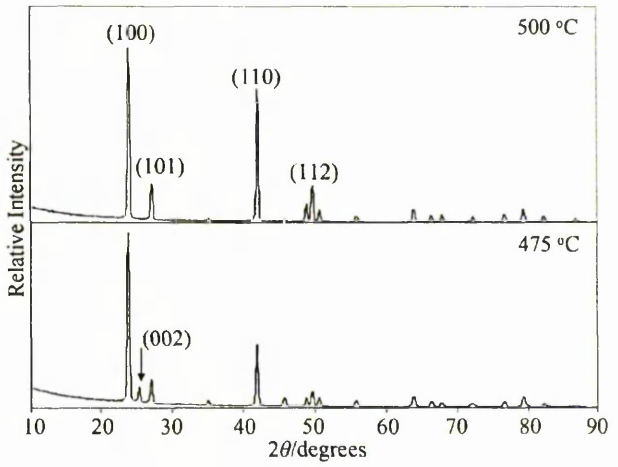

Figure 6. XRPD patterns of CdSe films deposited from $[Cd\{(SeP\textit{i}Pr_2)_2N\}_2]$ by LP-MOCVD

SEM studies indicate that the morphology of the film grown at 500 °C consists of randomly orientated platelets (ca. 1 μm in size) (Figure 7b) with a growth rate of ca. 3 μm h^{-1}. At lower growth temperature (475 °C), film morphology consists of clusters of thin particles (Figure 7a). The surface morphology can also be compared with pre-

vious attempts to deposit CdSe films from $[Cd\{(SePPh_2)_2N\}_2]$, which exhibited low degree of crystallinity and growth rate was also significantly lower (1 μm h^{-1}).[17] The EDAX spectrum of the film deposited at 500 °C from $[Cd\{(SeP\textit{i}Pr_2)_2N\}_2]$ shows the presence of cadmium (54%) and selenium (46%). No phosphorous contamination was detected in the films.

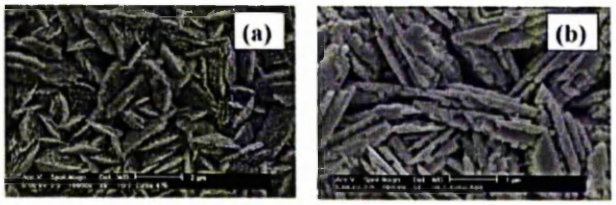

Figure 7. SEM images of CdSe films from $[Cd\{(SeP\textit{i}Pr_2)_2N\}_2]$ deposited at (a) 475 °C and 500 °C

Zinc Sulfide: Non-adherent, brown films were deposited at 450 and 475 °C maintaining precursor temperature at 250 °C using $[Zn\{(SP\textit{i}Pr_2)_2N\}_2]$. Zinc sulfide is known to exist in two phases, at low-temperature cubic polymorph (zinc blende) and at high temperature hexagonal phase (wurtzite).[31] XRPD pattern for the film deposited at 475 °C is shown in (Figure 8) and is consistent with the formation of hexagonal ZnS (JCPDS 36−1450) with a preferred orientation along the (100) plane. At higher growth temperatures (500 °C), deposited film was found to be amorphous indicated by XRPD.

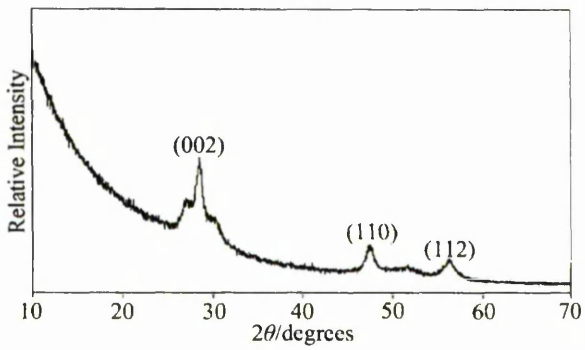

Figure 8. XRPD pattern of ZnS film deposited on glass from $[Zn\{(SP\textit{i}Pr_2)_2N\}_2]$ by LP-MOCVD

SEM micrographs for the film deposited at 475 °C shows that the film surface consists of globules ranging in size 0.25−1.25 μm. Cross-sectional SEM image of the film indicates columnar growth for ZnS and the growth rate is found to be ca. 1 μm h^{-1} (Figure 9). Similar surface morphology also has been observed for the growth of ZnS from previously studied single-source precursors by MOCVD e.g. zinc bis(diisobutyldithiophosphinate)[32] and zinc diethyldithiocarbamate.[33] EDAX indicates the presence of zinc and sulfur, however, 3% of phosphorous was also detected which is incorporated during the decomposition of precursor.

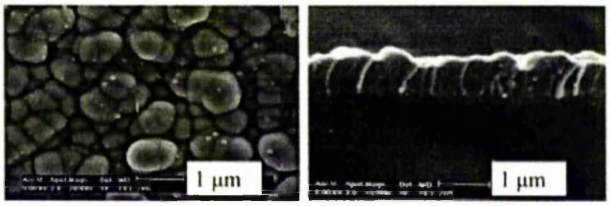

Figure 9. SEM images of ZnS films deposited at 475 °C from $[Zn\{[SP\textit{i}Pr_2)_2N\}_2]$ by LP-MOCVD

Zinc Selenide: ZnSe films were grown over a range of substrate temperatures (400−500 °C) using $[Zn\{(SeP\textit{i}Pr_2)_2N\}_2]$ but the optimum growth temperature appears to be between 425−450 °C with the precursor temperature at 275 °C. As-deposited films were orange-yellow, adherent and specular on the glass substrates. XRPD patterns indicate that the films grown at 425 and 450 °C on glass substrates showed only single-phase hexagonal ZnSe (Table 8, Figure 10). $[Zn\{(SePPh_2)_2N\}_2]$ also deposited hexagonal films at comparatively higher deposition temperatures (500 and 525 °C).[17] At higher growth temperatures

Table 8. XRPD data for ZnSe grown at 425 and 450 °C from $[Zn\{(SeP\textit{i}Pr_2)_2N\}_2]$

hkl	JCPDS (15-0105) *d* [Å] (rel. int.)	ZnSe (450 °C) *d* [Å] (rel. int.)	ZnSe (425 °C) *d* [Å] (rel. int.)
100	3.43 (100)	3.45 (95)	3.45 (100)
002	3.25 (90)	3.28 (69)	3.28 (56)
101	3.05 (70)	3.07 (28)	N/A
102	2.37 (60)	2.38 (5)	N/A
110	2.00 (100)	2.00 (100)	2.00 (70)
103	1.84 (80)	1.85 (7)	N/A
112	1.70 (70)	1.71 (41)	1.71 (25)
202	1.53 (10)	N/A	N/A
203	1.35 (60)	1.36 (2)	N/A

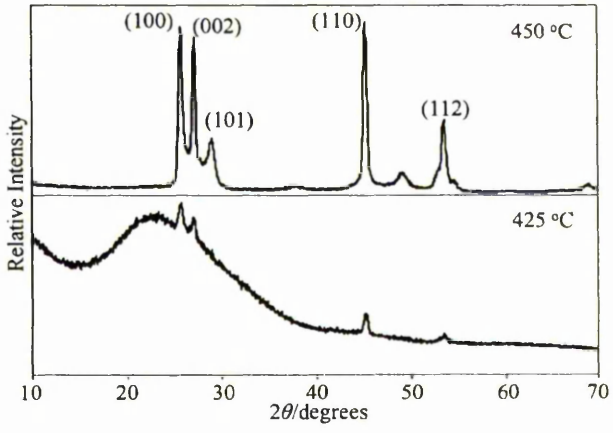

Figure 10. XRPD patterns of ZnSe films deposited from $[Zn\{(SeP\textit{i}Pr_2)_2N\}_2]$ by LP-MOCVD

(450 °C), the crystallinity of deposited film is significantly improved. However, at lower growth temperatures (425 °C), the XRPD pattern was weak indicating a less crystalline film.

SEM micrographs for the film deposited at 450 °C on glass consists of well-defined, randomly orientated particles, with an average size of ca. 0.5 μm (Figure 11). In 1 hour growth, film with ca. 2 μm thickness has been deposited. In contrast, films deposited at 425 °C had platelike morphologies with the plates laid down horizontally with respect to the glass surface. EDAX confirms that the film is close to stoichiometric ZnSe with a small amount of phosphorous (ca. 2%).

The optical properties of the films were measured by UV/Vis spectroscopy. The bandgap values extrapolated for CdS, CdSe, ZnS and ZnSe thin films are 2.30, 1.71, 3.64 and 2.63 eV, respectively. The bandgap values are all close to the literature values of 2.53 (CdS), 1.74 (CdSe), 3.8 (ZnS) and 2.58 eV (ZnSe).[34]

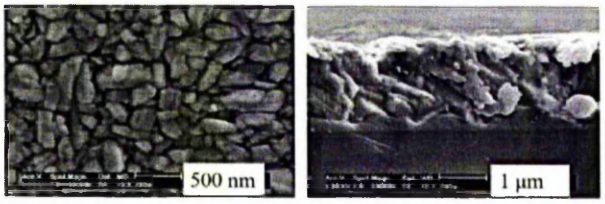

Figure 11. SEM images of ZnSe films deposited at 450 °C from $[Zn\{(SeP\textit{i}Pr_2)_2N\}_2]$ by LP-MOCVD

Conclusion

The air-stable single-source precursors $[M\{(EP\textit{i}Pr_2)_2N\}_2]$ (M = Cd^{II}, Zn^{II} and E = S, Se) have been prepared and characterised by various analytical techniques and utilised as single-source precursors for the deposition of metal chalcogenide thin films by LP-MOCVD. X-ray single crystal structures of zinc compounds indicate distorted tetrahedral geometry at the metal centres. Clean volatilisation of precursors studied by TGA makes them useful for MOCVD studies. XRPD patterns of as-deposited films show that only hexagonal phase of metal sulfide/selenide have been prepared at different growth temperatures.

Experimental Section

Precursor Synthesis: All compounds were prepared by a modified method to that reported in the literature.[18,19] The ligands $[NH(EP\textit{i}Pr_2)_2N]$ (E = S, Se) were sythesised by the reported method.[18,19]

$[Cd\{(SP\textit{i}Pr_2)_2N\}_2]$ (1):[18] In a typical preparation sodium methoxide (1.09 g, 19.7 mmol) was added to a stirred solution of $[NH(SP\textit{i}Pr_2)_2N]$ (6.00 g, 19.2 mmol) in anhydrous methanol (100 cm^3) and stirred for 10 minutes at room temperature. On addition of cadmium chloride (1.76 g, 9.5 mmol) to the resulting solution a white precipitate was formed which was furthur stirred for 2–3 hours, filtered and dried under vacuum. Recrystallisation from dichloromethane/petroleum ether (40–65 °C) yielded 6.2 g (89%) product as white solid. FT-IR: $\tilde{\nu}$ = 1224, 767 (ν P-*N*-P) cm^{-1}. ^1H NMR ($CDCl_3$): δ = 1.3 (m, 48 H, 16 CH_3-R), 2.1 (m, 8 H, 8 R-CH) ppm. ^{31}P NMR ($CDCl_3$): δ = 62.59 ppm. MS (FAB): *m/z* = 737 $[M + H^+]$. $C_{24}H_{56}CdN_2P_4S_4$: calcd. C 39.12, H 7.60, N 3.80, P, 16.81; found C 39.30, H 7.80, N 3.74, P 17.11.

$[Cd\{(SeP\textit{i}Pr_2)_2N\}_2]$ (2):[19] Recrystallisation of the white solid product from chloroform/methanol gave white crystals, yield 4.51 g (99%). FT-IR: $\tilde{\nu}$ = 1226, 763 (ν P-*N*-P), 425 (ν P-Se) cm^{-1}. ^1H NMR ($CDCl_3$): δ = 1.15 (m, 48 H, 16 CH_3-R), 2.1 (m, 8 H, 8 R-CH) ppm. ^{31}P NMR ($CDCl_3$): δ = 57.101 ppm. MS (FAB): *m/z* = 926 $[M + H^+]$. $C_{24}H_{56}CdN_2P_4Se_4$: calcd. C 31.16, H 6.10, N 3.03, P 13.39; found C 31.33, H 6.15, N 2.98, P 13.53.

$[Zn\{(SP\textit{i}Pr_2)_2N\}_2]$ (3):[18] Recrystallisation from dichloromethane/petroleum ether (40–65 °C) gave a white powder, yield 69%. FT-IR: $\tilde{\nu}$ = 1226, 773 (ν P-*N*-P) cm^{-1}. ^1H NMR ($CDCl_3$): δ = 1.3 (m, 48 H, 16 CH_3-R), 2.1 (m, 8 H, 8 R-CH) ppm. ^{31}P NMR ($CDCl_3$): δ = 63.99 ppm. MS (FAB): *m/z* = 689 $[M + H^+]$. $C_{24}H_{56}N_2P_4S_4Zn$: calcd. C 41.79, H 8.55, N 4.06, P 17.96; found C 41.83, H 8.56, N 4.03, P 18.64.

$[Zn\{(SeP\textit{i}Pr_2)_2N\}_2]$ (4):[19] Recrystallisation from chloroform/methanol gave white crystals, yield 4.21 g (98%) white crystals. FT-IR: $\tilde{\nu}$ = 1228, 762 (ν P-*N*-P), 427 (ν P-Se) cm^{-1}. ^1H NMR ($CDCl_3$): δ = 1.2 (m, 48 H, 16 CH_3-R), 2.0 (m, 8 H, 8 R-CH) ppm. ^{31}P NMR ($CDCl_3$): δ = 57.101 ppm. MS (FAB): *m/z* = 878 $[M + H^+]$. $C_{24}H_{56}N_2P_4Se_4Zn$: calcd. C 32.83, H 6.43, N 3.19, P 14.11; found C 33.02, H 6.61, N 3.12, P 14.18.

Characterisation Techniques: Unless otherwise stated, all reactions were performed under dry nitrogen using standard Schlenk techniques. All solvents and reagents were purchased from Sigma–Aldrich chemical company and used as received. In addition, toluene was distilled from over sodium under nitrogen. ^1H and ^{31}P NMR studies were carried out with a Bruker AC300 FT NMR Spectrometer. Mass spectra were recorded with a Kratos concept 1S instrument. Infrared spectra were recorded with a Specac single reflectance ATR instrument.

Growth Experiments: Low Pressure Metal-Organic Chemical Vapour Deposition (LP-MOCVD): Thin films of metal chalcogenides were grown on borosilicate glass in a low pressure (≈ 10^{-2} Torr) MOCVD reactor tube which has been described elsewhere.[21] A graphite susceptor holds the substrate dimensions (10 mm × 15 mm) which was heated by a tungsten halogen lamp.

Film Characterisations: X-ray powder diffraction studies were carried out using Philips X'Pert MPD diffractometer by using monochromated Cu-K_α radiation. The samples were mounted flat and scanned from 10° to 90° in a step size of 0.04° with a count rate of 2.5 s. Samples were carbon-coated using Edward's coating system E306A before SEM and EDAX analyses. SEM was carried out by using Philip XL30 FEG and EDAX was preformed with DX4. TGA measurements were carried out by a Seiko SSC/S200 model with a heating rate of 10 °C min^{-1} under nitrogen. Electronic absorption spectra were recorded with Helios-Beta Thermospectronic spectrophotometer.

X-ray Crystallographic Study: Single-crystal X-ray diffraction data for the compounds were collected with a CAD-4 diffractometer and Mo-K_α radiation (λ = 0.71069 Å) using ω-2θ scan. The unit cell parameters were determined by least-squares refinement on diffractometer angles (9.99° ≤ θ ≤ 12.51°) for 25 automatically centred reflections.[22] All data were corrected for absorption by empirical methods (ψ scan)[23] and for Lorentz-polarization effects

by XCAD4.[24] The structures were solved by heavy-atom method using DIRDIF-99[25] programs, refined anisotropically(non-hydrogen atoms) by full-matrix least-squares on F^2 using SHELXL-97[26] program. The H atoms were calculated geometrically and refined with a riding model. In the final stage of refinement data were correct for absorption by DIFABS.[27] The program ORTEP-3[28] was used for drawing the molecules. Crystallographic details and selected interatomic distances and angles are given in Tables 1–4.

CCDC-204283–204285 contain the supplementary crystallographic data for this paper. These data can be obtained free of charge at www.ccdc.cam.ac.uk/conts/retrieving.html [or from the Cambridge Crystallographic Data Centre, 12, Union Road, Cambridge CB2 1EZ, UK; Fax: (internat.) +44-1223/336-033; E-mail: deposit@ccdc.cam.ac.uk].

Acknowledgments

The authors thank the EPSRC, UK for the grants to POB that have made this research possible.

[1] P. O'Brien, in *Inorganic Materials* (Eds.: D. Bruce, D. O'Hare), Wiley, Chichester, **1997**, p. 523.
[2] I. G. Dance, R. G. Garbutt, D. C. Craig, M. L. Scudder, *Inorg. Chem.* **1987**, *26*, 3732–3740.
[3] I. G. Dance, R. G. Garbutt, D. C. Craig, M. L. Scudder, *Inorg. Chem.* **1987**, *26*, 4057–4064.
[4] I. G. Dance, R. G. Garbutt, M. L. Scudder, *Inorg. Chem.* **1990**, *29*, 1571–1577.
[5] M. B. Hursthouse, O. F. Z. Khan, M. Mazid, M. Motevalli, P. O'Brien, *Polyhedron* **1990**, *9*, 541–544.
[6] O. F. Z. Khan, P. O'Brien, *Polyhedron* **1991**, *10*, 325–332.
[7] M. Bochmann, K. J. Webb, M. Harman, M. B. Hursthouse, *Angew. Chem. Int. Ed. Engl.* **1990**, *29*, 638–639.
[8] M. Bochmann, K. J. Webb, M. B. Hursthouse, M. Mazid, *J. Chem. Soc., Dalton Trans.* **1991**, 2317–2323.
[9] M. Bochmann, K. J. Webb, *J. Chem. Soc., Dalton Trans.* **1991**, 2325–2329.
[10] B. O. Dabbousi, P. J. Bonasia, J. Arnold, *J. Am. Chem. Soc.* **1991**, *113*, 3186–3188.
[11] P. J. Bonasia, J. Arnold, *Inorg. Chem.* **1992**, *31*, 2508–2514.
[12] C. Byrom, M. A. Malik, P. O'Brien, A. J. P. White, D. J. Williams, *Polyhedron* **2000**, *19*, 211–215.
[13] R. Nomura, T. Murai, T. Toyosaki, H. Matsuda, *Thin Solid Films* **1995**, *271*, 4–7.
[14] M. B. Hurthouse, M. A. Malik, M. Motevalli, P. O'Brien, *Polyhedron* **1992**, *11*, 45–48.
[15] M. Motevalli, P. O'Brien, J. R. Walsh, I. M. Watson, *Polyhedron* **1996**, *15*, 2801–2808.
[16] M. Chunggaze, M. A. Malik, P. O'Brien, *J. Mater. Chem.* **1999**, *10*, 2433–2437.
[17] M. Afzaal, S. M. Aucott, D. Crouch, P. O'Brien, J.-H. Park, J. D. Woollins, *Adv. Mater. Chem. Vap. Dep.* **2002**, *5*, 187–189.
[18] D. Cupertino, R. Keyte, A. M. Z. Slawin, D. J. Williams, J. D. Woollins, *Inorg. Chem.* **1996**, *35*, 2695–2697.
[19] D. Cupertino, D. J. Birdsall, A. M. Z. Slawin, J. D. Woollins, *Inorg. Chim. Acta* **1999**, *290*, 1–7.
[20] V. Garcia-Montalvo, J. Novosad, P. Kilian, J. D. Woollins, A. M. Z. Slawin, P. G. Y. Garcia, M. Lopez-Cardoso, G. Espinosa-Perez, R. Cea-Olivares, *J. Chem. Soc., Dalton Trans.* **1997**, 1025–1029.
[21] M. A. Malik, P. O'Brien, *Adv. Mater. Opt. Electron* **1994**, *7*, 117–121.
[22] Enraf–Nonius CAD-4/PC Software. Version 1.5c, Enraf–Nonius, Delft, The Netherlands, **1994**.
[23] A. C. T. North, D. C. Phillips, F. S. Mathews, *Acta Crystallogr., Sect. A* **1968**, A24, 351–359.
[24] Harms, S. Wocadlo, *XCAD4 – CAD4 Data Reduction*, University of Marburg, Marburg, Germany, **1995**.
[25] P. T. Beurskens, G. Beursken, W. Bosman, R. De Gelder, S. Garci-Granda, R. O. Gould, R. Israel, J. M. M. Smiths, *The DIRDIF-96 Programme system*, Crystallography Laboratory, University of Nijmegen, The Netherlands, **1996**.
[26] G. Sheldrick, M. SHELXL-97, University of Göttingen, **1997**.
[27] L. J. Farrugia, ORTEP-3 for Windows, *J. Appl. Crystallogr.* **1997**, *30*, 565.
[28] L. J. Farrugia, *WinGX – A Windows Program for Crystal Structure Analysis*, University of Glasgow, Glasgow, **1998**.
[29] J. R. Philips, A. M. Z. Slawin, A. J. P. White, D. J. Williams, J. D. Woollins, *J. Chem. Soc., Dalton Trans.* **1995**, 2467–2468.
[30] N. Zuniga-Villarreal, C. Silvestru, R. R. Lezama, S. H. Ortega, C. A. Toledano, *J. Organomet. Chem.* **1995**, *496*, 169–174.
[31] P. O'Brien, R. Nomura, *J. Mater. Chem.* **1995**, *5*, 1761–1773.
[32] Y. Takahashi, R. Yuki, M. Sugiura, S. Motijima, K. Sugiiyama, *J. Cryst. Growth* **1980**, *50*, 491–497.
[33] N. H. Tran, R. N. Lamb, G. L. Mar, *Colloids Surfaces A., Physicochem. Eng. Aspects* **1999**, *155*, 93–100.
[34] J. I. Pankove, *Optical processes in semiconductors*, Dover Publications Inc., New York, **1970**, 1327.

Received February 19, 2003
Early View Article
Published Online October 23, 2003

JOURNAL OF Materials Communication CHEMISTRY

Deposition of CdSe thin films using a novel single-source precursor; $[MeCd\{(SeP^iPr_2)_2N\}]_2$

Mohammmad Afzaal,[a] David Crouch,[a] Mohammad A. Malik,[a] Majid Motevalli,[b] Paul O'Brien*[a] and Jin-Ho Park[a]

[a]*The Manchester Materials Science Centre and Department of Chemistry, The University of Manchester, Oxford Road, Manchester, UK M13 9PL. E-mail: paul.obrien@man.ac.uk*
[b]*Department of Chemistry, Queen Mary and Westfield, Mile End Road, London, UK E1 4NS*

Received 15th January 2003, Accepted 22nd January 2003
First published as an Advance Article on the web 6th February 2003

The novel complex $[MeCd\{(SeP^iPr_2)_2N\}]_2$ has been synthesised and its structure determined by X-ray single crystal methods. The compound is suitable for the deposition of cadmium selenide films by low pressure chemical vapour deposition.

In recent years, there has been rapid development in the field of II–VI semiconductors because their intermediate energy band gaps have led to their use in a variety of devices.[1] Cadmium chalcogenides have applications in solid-state solar cells and photoconductors, in field-effect transistors, sensors and transducers.[2–4] A number of reports have appeared concerning single-source precursors for the deposition of II–VI materials,[5] such as thiocarbamates,[6] selenocarbamates,[7] thiophosphinates,[8] 2,4,6-tri-*tert*-butylphenyl chalcogenides,[9] silicon-based systems (*e.g.* $M[ESi(SiCH_3)_3]_2$: M = Zn, Cd, Hg; E = Se, Te)[10] and alkylmetal thio- and selenocarbamates.[11] In this paper, we report the synthesis and characterisation† of $[MeCd\{(SeP^iPr_2)_2N\}]_2$, which is the first example of a cadmium mixed-alkyl diselenoimidodiphosphinate complex, and its use as a single-source precursor to deposit CdSe films by low pressure metal–organic chemical vapour deposition (LP-MOCVD).

The complex $[MeCd\{(SeP^iPr_2)_2N\}]_2$ was prepared by the comproportionation of Me_2Cd and $Cd[(SeP^iPr_2)_2N]_2$‡ in anhydrous toluene.§

The structure of the compound (Fig. 1) was determined by X-ray crystallography¶ and consists of dimeric molecular units; each diselenoimidodiphosphinate chelates to one cadmium atom and bridges to the next. Each cadmium is four-coordinate and bound to three selenium atoms and one carbon. The structure resembles the dimeric structure of bis(diethyldiselenocarbamato)cadmium(II), but with the alkyl group replacing the chelating-only carbamato group, as in $NpCd(Se_2CNEt_2)$ and in $MeCd(S_2CNEt_2)$.[12,13] The Cd–Se bond lengths are in the range Cd(1)–Se(1) 2.672(3) to Cd(1)–Se(2a) 2.934(2) Å, which are slightly longer than the parent cadmium compound 2.622(2)–2.636(2) Å. The bite angle Se(1)–Cd(1)–Se(2) 109.61(10)° is less acute than the Se–Cd–Se angle in $Cd[(SeP^iPr_2)_2N]_2$ [111.32(6)°].[14] The Cd–C bond length (2.156 Å) is similar to those observed in other cadmium alkyls.[12,13,15]

Thermogravimetric analysis (TGA) showed the complex to sublime between 275 and 410 °C, but with a 14.2 wt% final residue. X-Ray powder diffraction (XRPD) of the final residue obtained from pyrolysis‖ of the compound indicated predominantly bulk hexagonal CdSe.

Deposition of films was attempted over a range of substrate temperatures (425–475 °C) for 1 h, using *ca.* 200 mg of the precursor for each experiment, whilst the volatisation temperature for the precursor was kept constant at 285 °C. The films deposited at 425 and 450 °C were black and adhered well to glass substrates (Scotch tape test) but could be removed by scratching the surface with a scalpel. However, at a higher deposition temperature (475 °C), a powdery film was deposited and was found to be amorphous.

XRPD of the deposited films confirmed the formation of hexagonal CdSe (JCPDS file 08-0459) with a preferred orientation along the (002) plane (Fig. 2). In contrast, films deposited from the parent complex $[Cd\{(SeP^iPr_2)_2N\}]_2$ on glass substrates by LP-MOCVD also resulted in hexagonal CdSe at 475 and 500 °C, but showed a different preferred orientation—along the (100) plane.[16]

Scanning electron microscopy (SEM) studies indicated that there is a dramatic change in the morphologies of the deposited films with the growth temperature. The morphology of the films grown at 450 °C consists of randomly orientated flakes

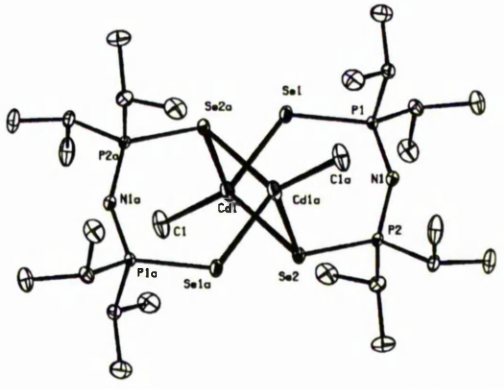

Fig. 1 Molecular structure of $[MeCd\{(SeP^iPr_2)_2N\}]_2$. Selected bond distances (Å) and angles (°): Cd(1)–C(1) 2.156(5), Cd(1)–Se(1) 2.672(3), Cd(1)–Se(2) 2.703(3), Cd(1)–Se(2a) 2.934(2), Se(1)–P(1) 2.171(3), Se(2)–P(2) 2.210(3); C(1)–Cd(1)–Se(1) 112.48(15), C(1)–Cd(1)–Se(2) 122.56(15), Se(1)–Cd(1)–Se(2) 109.61(10), C(1)–Cd(1)–Se(2a) 121.19(14), Se(1)–Cd(1)–Se(2a) 96.86(8), Se(2)–Cd(1)–Se(2a) 89.68(8), P(1)–Se(1)–Cd(1) 106.62(10), P(2)–Se(2)–Cd(1) 100.01(9).

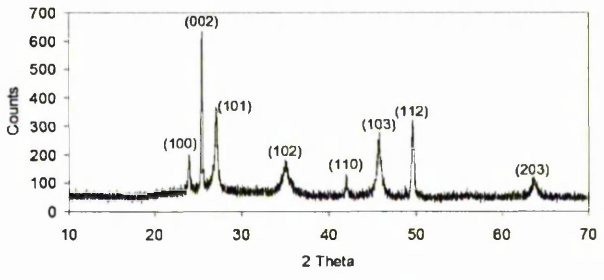

Fig. 2 XRPD pattern of CdSe film deposited on glass at 450 °C.

DOI: 10.1039/b300608p

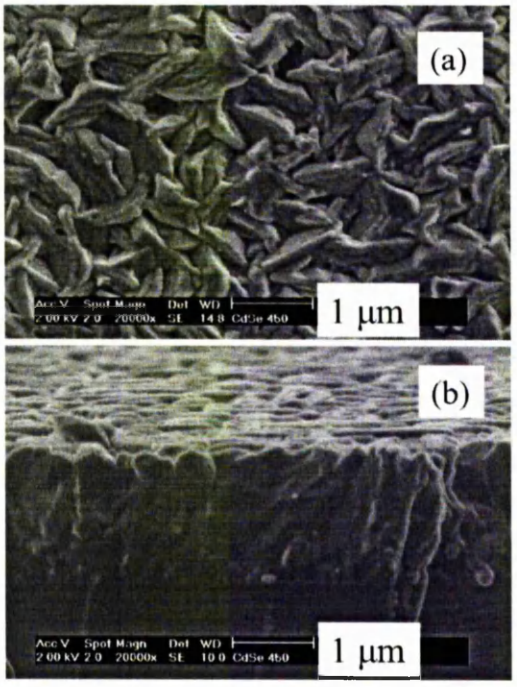

Fig. 3 SEM images of CdSe film deposited on glass at 450 °C: (a) top view, (b): cross-sectional view.

and the growth rate was found to be *ca.* 1.2 μm h^{-1} (Fig. 3). At 425 °C, the film consists of randomly orientated platelets. Energy-dispersive X-ray (EDAX) analyses of the films show that the films are slightly selenium-rich, consisting of 52% Se and 48% Cd. No phosphorous was detected in the films.

The optical band gap of the film was estimated by using the direct band gap method (α^2 *vs.* $h\nu$), which provided a value of 1.73 eV for the CdSe films, the reported value for hexagonal CdSe is 1.7 eV.[17]

The significance of the current study is two-fold. First of all, we have synthesised and characterised a new dimeric cadmium compound containing the imidodiphosphinate moiety. Secondly, its use as a single-source precursor for the deposition of hexagonal CdSe films on glass substrates by LP-MOCVD has been clearly demonstrated. Further studies will focus on the effect of modifying alkyl groups on the volatility of the precursors.

J. H. P. and M. A. are supported by EPSRC grants to P. O. B. Dimethylcadmium was a gift from Epichem Ltd.

Notes and references

†Characterisation: XRPD studies were carried out with a Bruker D8 AXS diffractometer using monochromated Cu-K_α radiation. The samples were mounted flat and scanned from 10 to 70° in a steps of 0.04° with a count rate of 2.5 s. Films were carbon coated using an Edwards E306A coating system before SEM and EDAX analyses. SEM was carried out using a Philips XL30 FEG instrument and EDAX was performed with a Philips DX4. TGA measurements were carried out under nitrogen using a Seiko SSC/S200 instrument. Electronic absorption spectra were recorded on a Helios-Beta thermospectronic spectrophotometer.

‡$Cd[(SeP^iPr_2)_2N]_2$ was prepared according to the reported method.[14] Toluene (BDH) was distilled over Na–benzophenone and degassed prior to use. All manipulations and reactions were carried out in an inert atmosphere using Schlenk techniques and a vacuum line. Thin films were deposited on borosilicate glass in a low pressure ($\sim 10^{-2}$ Torr) MOCVD reactor tube, which has been described elsewhere.[18] A graphite susceptor held the substrate (dimensions: 10 mm × 15 mm), which was heated by a tungsten halogen lamp.

§A solution of cadmium iminobis(diisopropylphosphine selenide) (2.4 g, 2.59 mmol) in dry toluene (~50 ml) was stirred with dimethylcadmium (0.38 g, 2.59 mmol) at room temperature for 1 h. After removal of solvent under vacuum, a yellow solid was obtained. Some of this product was recrystallised in toluene to give transparent crystals. Yield: 2.4 g (87%). M.p. 191 °C. ^{1}H NMR (C_6D_6, 300 MHz): δ 0.10 (6H, s, $CdCH_3$); 0.8 [48H, m, $CH(CH_3)_2$]; 1.5 [8H, m, $CH(CH_3)_2$]. ^{31}P NMR (C_6D_6, 400 MHz): δ 54.76 (m). Microanalysis calculated for $C_{26}H_{62}Cd_2N_2P_4Se_4$: C, 29.28; H, 5.81; N, 2.63; found: C, 30.40; H, 6.12; N, 2.84%. FT-IR [major bands and tentative assignments (cm^{-1})]: 671 [δ(Cd–C)], 1227, 754 [δ(P–N–P)].

¶*Crystal data*: $C_{26}H_{62}Cd_2N_2P_4Se_4$; M = 1067.3; triclinic; space group $P\bar{1}$; a = 9.625(8), b = 10.143(9), c = 11.180(9) Å; α = 103.44(8), β = 80.97(9), γ = 111.88(9)°; V = 982.1(14) $Å^3$; Z = 1; D = 1.805 g cm^{-1}. Total number of measured and observed independent reflections: 3715 and 3449 (R_{int} = 0.01490), respectively. R_1 = 0.0283; wR_2 = 0.0705. CCDC reference number 193982. See http://www.rsc.org/suppdata/jm/b3/b300608p/ for crystallographic data in CIF or other electronic format.

‖The pyrolysis experiment was performed in a quartz glass reactor using a heating furnace. The sample was heated to 475 °C under a constant flow of argon.

1 P. O'Brien and R. Nomura, *J. Mater. Chem.*, 1995, **5**, 1761.
2 G. Y. Chung, H.-D. Kim, B.-T. Ahn and H.-B. Im, *Thin Solid Films*, 1993, **232**, 28.
3 S. C. Sahn and S. N. Sahn, *Thin Solid Films*, 1993, **225**, 17.
4 A. Yoshikawa, S. Yamaga, K. Tanaka and H. Kasai, *J. Cryst. Growth*, 1985, **72**, 13.
5 A. N. Gleizes, *Chem. Vap. Deposition*, 2000, **6**, 155.
6 D. M. Frigo, O. F. Z. Khan and P. O'Brien, *J. Cryst. Growth*, 1989, **96**, 989.
7 M. B. Hursthouse, M. A. Malik, M. Motevalli and P. O'Brien, *Polyhedron*, 1992, **11**, 45.
8 Y. Takahashi, R. Yuki, M. Motojima and K. Sugiyama, *J. Cryst. Growth*, 1980, **50**, 491; M. A. H. Evans and J. O. Williams, *Thin Solid Films*, 1982, **87**, L1.
9 M. Bochmann, K. J. Webb, M. Harman and M. B. Hursthouse, *Angew. Chem., Int. Ed. Engl.*, 1990, **29**, 638.
10 B. O. Dabbousi, P. J. Bonasia and J. Arnold, *J. Am. Chem. Soc.*, 1991, **113**, 3186.
11 M. B. Hursthouse, M. A. Malik, M. Motevalli and P. O'Brien, *Organometallics*, 1991, **10**, 730; M. A. Malik and P. O'Brien, *Chem. Mater.*, 1991, **3**, 999.
12 I. Abrahams, M. A. Malik, M. Motevalli and P. O'Brien, *J. Organomet. Chem.*, 1994, **465**, 73.
13 M. B. Hursthouse, M. A. Malik, M. Motevalli and P. O'Brien, *Organometallics*, 1991, **10**, 730.
14 D. Cupertino, D. J. Birdsall, A. M. Z. Slwain and J. D. Woollins, *Inorg. Chim. Acta*, 1999, **290**, 1.
15 M. J. Henderson, R. Papasergio, C. L. Raston, A. H. White and M. F. Lappert, *Chem. Commun.*, 1986, 672; G. W. Bushnell and S. R. Stobart, *Can. J. Chem.*, 1980, **58**, 672.
16 M. Afzaal, P. O'Brien and J. H. Park, unpublished results.
17 R. G. Weller and J. O. Dimmock, *Phys. Rev.*, 1962, **125**, 1805.
18 M. A. Malik and P. O'Brien, *Adv. Mater. Opt. Electron.*, 1994, **3**, 71.

ARTICLE

Journal of Materials Chemistry
www.rsc.org/materials

The synthesis, X-ray structures and CVD studies of some group 11 complexes of iminobis(diisopropylphosphine selenides) and their use in the deposition of I/III/VI photovoltaic materials

Mohammad Afzaal,[a] David J. Crouch,[a] Paul O'Brien,*[a] James Raftery,[a] Peter J. Skabara,[a] Andrew J. P. White[b] and David J. Williams[b]

[a]*Department of Chemistry, University of Manchester, Oxford Road, Manchester, UK M13 9PL. E-mail: Paul.O'Brien@man.ac.uk*
[b]*Department of Chemistry, Imperial College London, South Kensington, London, UK SW7 2AZ*

Received 23rd September 2003, Accepted 5th November 2003
First published as an Advance Article on the web 27th November 2003

Reaction of $NH(P^iPr_2)_2$ with elemental selenium in concentrated solvent conditions enables large scale preparation and improved yields of $NH(PSe^iPr_2)_2$ that may be deprotonated with sodium methoxide to give $NaN(PSe^iPr_2)_2$. Treatment of the sodium salt with appropriate Group 11 metal salts in methanol yields a range of trinuclear complexes. The protic solvent conditions utilized facilitate the reduction of copper(II) salts resulting in the isolation of copper(I) complexes. These new Group 11 complexes have been characterised by ^1H and ^{31}P NMR and IR spectroscopy, APCI mass spectrometry, microanalysis and X-ray crystallography. Thermolytic decomposition of the copper(I) precursors in the presence of the indium precursor, $In[(SeP^iPr_2)_2N]_2Cl$, has been carried in the solid state using AA-MOCVD to give copper indium diselenide solid state materials $CuInSe_2$.

Introduction

Dichalcogenoimidodiphosphinato anions $[R_2P(E)–N–P(E)R_2]$ [where E = O (**1**), S (**2**), and Se (**3**)] are versatile ligands, with a strong tendency to form inorganic (carbon free) chelate rings.[1–4] Transition metal complexes incorporating such ligands have demonstrated improved thermal and chemical stability over organic based ligands such as β-diketone complexes, which are susceptible to oxidation, polymerisation and hydration.[5] Metal complexes incorporating **2** and **3** are excellent as single source precursors for CVD[6] and quantum dot applications.[7]

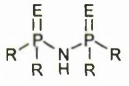

1 E = O
2 E = S
3 E = Se

a R = phenyl
b R = methyl
c R = butyl
d R = *iso*-propyl

Although the chemistry of **1** and **2** is relatively well developed, with numerous chalcogenide/phosphinate combinations having been reported, the majority of studies have described the coordination chemistry of phenyl substituted systems[4,8] (R = C_6H_5–, **a**). However, other alkyl functionalities have been described for dithioimidodiphosphinates **2**, such as methyl[9] [R = CH_3–, **b**], butyl[10] [R = $CH_3(CH_2)_3$–, **c**] and isopropyl[11] [R = $(CH_3)_2CH$–, **d**] analogues. The vast majority of examples describing the chemistry of **3** have again incorporated phenyl architecture.[4,8] There have been few reports on the diisopropyl analogue, $NH(PSe^iPr_2)_2$ **3d**,[4] and transition metal complexes subsequently prepared from it.[12] The major advantages of the EPNPE system are its flexibility and the large X···X "bite" (*ca.* 4 Å), allowing the formation of chelate rings and resulting in a symmetrical coordination pattern through the donor atoms.

In this paper we report on the synthesis and structural characterisation of group 11 diselenoimidodiphosphinato complexes. Compared to previous methods,[3,4] a more efficient synthesis of **3d** is reported, enabling conveniently large quantities (~70 g per batch) to be prepared. Formed by the reaction of **3d** under basic conditions with the appropriate metal centre examples of copper(I) **4**, silver(I) **5** and gold(I) **6** coordination complexes (see Scheme 1) are described along with their structural characterisation.

Such single source precursors are of particular interest as the generation of group 11 chalcogenide solid state materials has demonstrated a multitude of potential uses. For example, silver and gold chalcogenide nanoparticles have been used in the preparation of super-lattices[13] and electro-active materials.[14] Other applications of group 11 nanoparticles include their use as biomarkers in TEM experiments[15] and, more recently, in single-electron transistors.[16] Such applications make use of compounds **4**, **5**, and **6**, a potentially interesting area of endeavour as to our knowledge group 11 selenides have received scant attention. The ease and efficiency of their preparation also makes them commercially attractive.

Analogue **4** has been studied under aerosol-assisted chemical

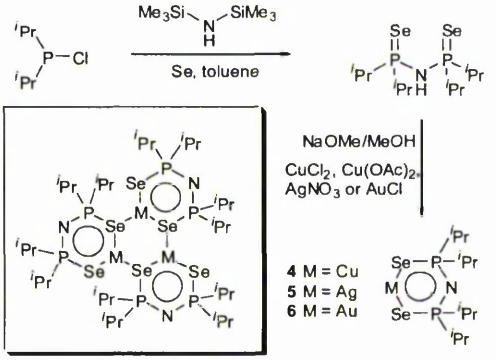

Scheme 1 Synthetic route to $M''[N(SeP^iPr_2)_2]_n$ chelate complexes.

DOI: 10.1039/b311743j

vapour deposition (AACVD) conditions and when used in conjunction with the indium precursor $In[(SeP^iPr_2)_2N]_2Cl$, **7**[17] affords copper indium diselenide solid state materials. Ternary metal chalcogenide $CuInSe_2$ has been the focus of much recent research for use in high efficiency, radiation-hard solar cells.[18] There have only been a few reports on the deposition of $CuInSe_2$ by CVD methods. Bougnot *et al.*[19] have deposited $CuInSe_2$ films contaminated with In_2Se_3 by MOCVD using copper(II) hexafluoroacetylacetonate mixed with trimethylamine, triethylindium and hydrogen selenide. Successful growth of $CuInSe_2$ films by metal–organic vapour phase expitaxy (MOVPE) has also been reported using cyclopentadienylcopper-triethylphosphine, trimethylindium and diethyl selenide as the precursors.[20]

Examples of complexes comprising of copper, indium and selenium atoms in a molecule as single-source precursors for $CuInSe_2$ are very few. Only Kanatzidis and co-workers have reported the preparation of hetero-binuclear complexes, $(Ph_3P)_2Cu(\mu\text{-}ER)_2In(ER)_2$ (E = S, Se; R = Et, ^{t}Bu) and pyrolysis studies have revealed that the selenium derivative could be converted into $CuInSe_2$ at 400–450 °C, yet none of the precursors had been evaluated in thin film deposition studies.[21]

Previously, we have grown $CuInSe_2$ films at 425–450 °C by AACVD using stoichiometric amounts of asymmetrically substituted diselenocarbamates, $Cu(Se_2CNMe^nHex)_2$ and $In(Se_2CNMe^nHex)_3$, as dual-source metal–organic precursors.[22] The goal of the current research is to deposit metal chalcogenide thin films based on diselenoimidodiphosphinato complexes. Complexes of these ligands are air-stable and sufficiently volatile for the deposition of thin films of materials such as ZnSe, CdSe, In_2Se_3 and Bi_2Se_3.[6c,23,24] Successful growth of In_2Se_3 from $In[(SeP^iPr_2)_2N]_2Cl$ has encouraged us to attempt the deposition of a ternary phase. Here, we report on a simple thermal AACVD preparation of copper indium diselenide films from metal–organic precursors.

Results and discussion

The generation of $NH(SeP^iPr_2)_2$ **3d**, in a one-pot synthesis from chlorodiisopropylphosphine, is relatively straightforward and has been documented elsewhere.[3,4] However we have established[25] that under reduced solvent conditions (*i.e.* when solvent : reagent mole ratio is $\leqslant 14:1$) the reaction yield can be improved upon,[3,4] enabling the procedure to be conveniently scaled up and permitting larger quantities (~ 70 g) of **3d** to be prepared with relative ease. We have also studied the reactions of **3d** and their salts with group 11 metal salts.[25] Improved complex formation was observed in the reaction of **3d** with sodium methoxide in anhydrous methanol yielding the sodium salt $NaN(PSe^iPr_2)_2$: *in situ* treatment of the salt, $NaN(PSe^iPr_2)_2$, with the appropriate group 11 metal salt yields compounds **4**–**6** in good-to-excellent yields. For example, the reaction of silver(I) nitrate with $NaN(PSe^iPr_2)_2$ directly produces $Ag[(^iPr_2PSe)_2N]$ **5** as an *off-white* powder in 82% yield (Scheme 1). The analogous reaction of **3d** with gold(I) chloride gave **6** as a *khaki green* powder in 73% yield.

Reaction of $CuCl_2$ or $Cu(OAc)_2$ with $NH(SeP^iPr_2)_2$–NaOMe in anhydrous methanol did not give the expected $Cu[(^iPr_2PSe)_2N]_2$ precursor. Instead a trinuclear copper(I) complex $\{Cu^I[(^iPr_2PSe)_2N]\}_3$ is isolated in good yield (72% for $CuCl_2$). The reaction is carried out using an excess of **3d**. We found that the overall yield is reduced if the ratio of reactants is changed. In this reaction we assume that the reducing agent is the protic solvent itself. Similar behaviour has been demonstrated in related sulfur containing systems.[26] For example the role of the solvent as the reducing agent was first postulated by Herrmann *et al.*,[26a] who obtained $\{Cu^I[(C_6H_5O)_2\text{–}P(S)NC(S)N(C_2H_5)_2]\}_3$ with a Cu_3S_3 core from the reaction in ethanol using a Cu(II) nitrate salt. Woollins and co-workers[26b] have demonstrated similar behaviour in the related copper dithioimidodiphosphinates, in which a Cu_3S_3 core is obtained from the reaction of $CuCl_2$ and **2d** under similar conditions.

CVD studies

Deposition of $CuInSe_2$ films has been carried out by AACVD using 1 : 1 molar ratios of $In[(SeP^iPr_2)_2N]_2Cl$ and $\{Cu[(SeP^iPr_2)_2N]\}_3$ in 30 cm^3 THF . Both copper and indium precursors were analysed by TGA which indicated decomposition temperatures of 287.5–343 °C for copper and 225–380 °C for indium precursors leading to the formation of metal selenides, as indicated by XRPD. These results encouraged us to perform the stoichiometric reactions of copper and indium precursors leading to growth of $CuInSe_2$ films. The deposition of films was observed at growth temperatures of 375 to 450 °C on glass substrates over 2 hours. The deposited films were black and fairly adherent to the substrates. All the as-deposited films gave narrow and strong peaks in the X-ray powder diffraction spectra (XRPD) and show the characteristic tetragonal phase of $CuInSe_2$ (Fig. 1). XRPD patterns of the films grown at various growth temperatures show a preferred orientation along the (112) plane regardless of growth temperature. Similarly, $CuInSe_2$ films with a preferred orientation along the (112) plane have also been grown from methyl-^{n}hexyl diselenocarbamato complexes of copper and indium by AACVD.[22]

Scanning electron microscopy (SEM) was used to analyse the morphology of the deposited films. It can be seen that the deposited layers are not homogeneous and mainly consist of thin plate-like particles, laid down perpendicularly on the substrate with random orientation (Fig. 2). The heterogeneous morphology of the thin film layer can be altered by using single crystalline substrates such as InP(111) and Si(111) which may lead to homogeneous growth. Such growth was observed in the LP-MOCVD of $CuInSe_2$ from $Cu(Se_2CNMe^nHex)_2$ and $In(Se_2CNMe^nHex)_3$.[27] Energy dispersive X-ray analysis (EDAX) confirms the presence of Cu (23%), In (27%) and Se (50%).

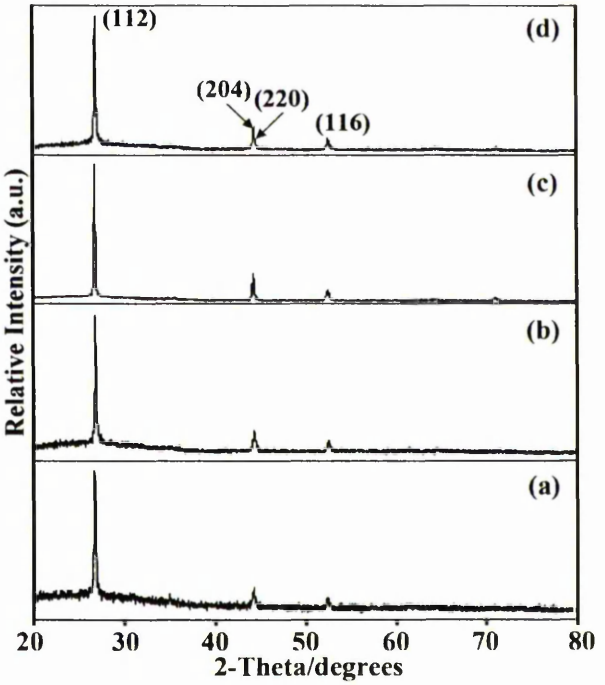

Fig. 1 XRPD patterns of $CuInSe_2$ on glass at (a) 375 °C, (b) 400 °C, (c) 425 °C and (d) 450 °C.

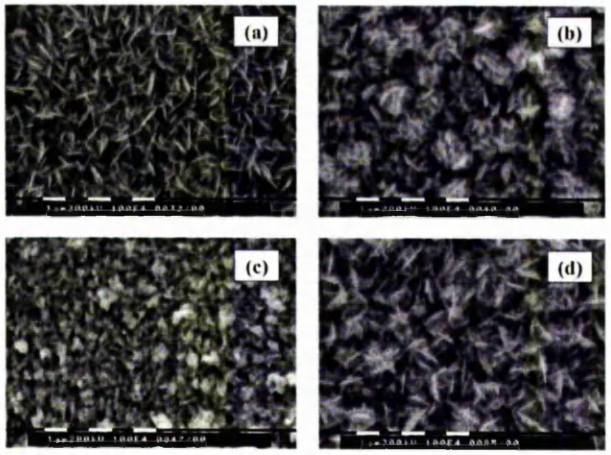

Fig. 2 SEM images of $CuInSe_2$ films deposited on glass at (a) 375 °C, (b) 400 °C, (c) 425 °C and (d) 450 °C.

Solid state structure

The structures of two members of this series, $\{Cu[(^tPr_2PSe)_2N]\}_3$ **4**† and $\{Ag[(^tPr_2PSe)_2N]\}_3$ **5**‡, were determined by X-ray crystallography. Both were shown to have trimeric structures (Figs. 3 and 4) very similar to that of the copper–sulfur analogue $\{Cu[(^tPr_2PS)_2N]\}_3$ published by Woollins *et al.*[26b] Each metal centre has a distorted trigonal planar geometry (Tables 1 and 2) but with the Se–M–Se angles within the central six-membered M_3Se_3 ring approaching tetrahedral [105.91(6)–111.44(6)° for **4** and 106.47(3)–112.53(3)° for **5**]; the largest deviation from planarity occurs at Cu(2) in **4** where the metal lies *ca.* 0.13 Å out of the plane of its substituents. As was seen for the Cu–S bonds in the literature analogue,[26b] in both **4** and **5** the M–Se bonds within the central M_3Se_3 ring [Cu–Se 2.3408(16)–2.3756(16) Å; Ag–Se 2.5798(9)–2.6137(10) Å] are noticeably longer than those within the MSe_2P_2N rings [Cu–Se 2.3146(19)–2.3400(16) Å; Ag–Se 2.5527(10)–2.5590(10) Å]. The geometry of the M_3S_3 ring in the two complexes is very different, there being a pronounced boat conformation in **4** [{Cu(2),Cu(3),Se(1),Se(3)} coplanar to within 0.01 Å, Cu(1) and Se(5) lying 1.29 and 0.44 Å out of this plane respectively] whilst in **5** a chair arrangement is observed [{Ag(1),Ag(2),-Se(4),Se(6)} coplanar to within 0.02 Å, Ag(3) and Se(2) lying 1.11 and −1.72 Å out of this plane respectively]. In both complexes, each of the three peripheral six-membered MSe_2P_2N rings adopts a very similar folded conformation with the metal,

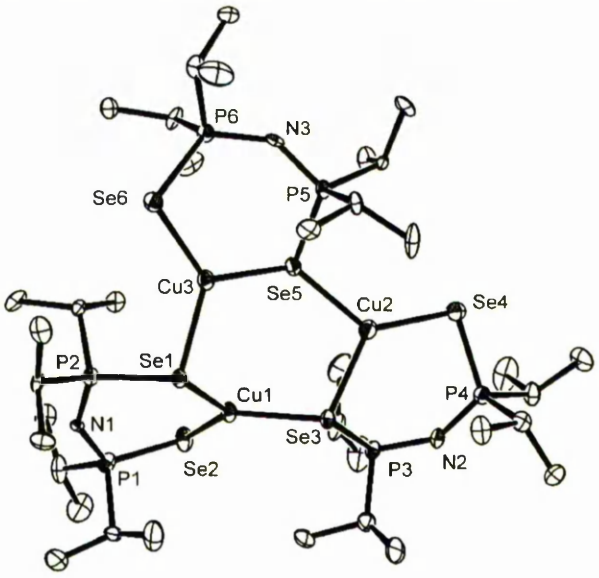

Fig. 3 The molecular structure of $\{Cu[N(SeP^iPr_2)_2]\}_3$ (**4**) showing 50% thermal ellipsoids.

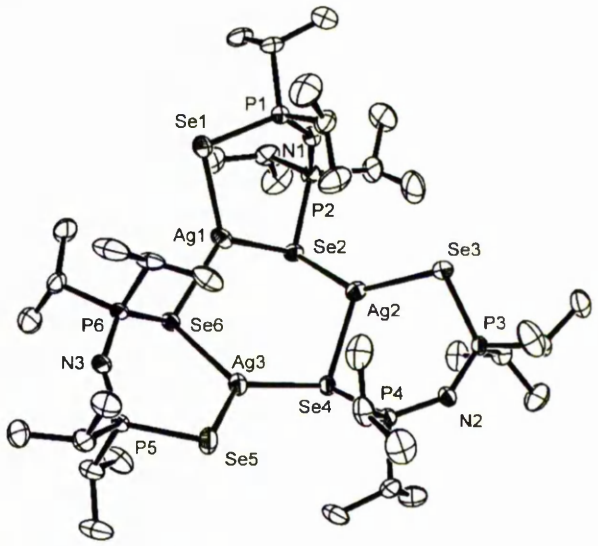

Fig. 4 The molecular structure of $\{Ag[N(SeP^iPr_2)_2]\}_3$ (**5**) showing 50% thermal ellipsoids.

Table 1 Selected bond lengths (Å) and angles (°) for **4**

Cu(1)–Se(1)	2.3712(15)	Cu(1)–Se(2)	2.3400(16)
Cu(1)–Se(3)	2.3756(16)	Cu(2)–Se(3)	2.3635(16)
Cu(2)–Se(4)	2.3146(19)	Cu(2)–Se(5)	2.3408(16)
Cu(3)–Se(1)	2.3755(16)	Cu(3)–Se(5)	2.3692(19)
Cu(3)–Se(6)	2.3318(18)	N(1)–P(1)	1.575(6)
N(1)–P(2)	1.602(6)	N(2)–P(3)	1.601(6)
N(2)–P(4)	1.599(6)	N(3)–P(5)	1.585(6)
N(3)–P(6)	1.598(6)	Se(1)–P(2)	2.226(2)
Se(2)–P(1)	2.163(3)	Se(3)–P(3)	2.202(2)
Se(4)–P(4)	2.172(3)	Se(5)–P(5)	2.191(2)
Se(6)–P(6)	2.182(2)		
P(2)–Se(1)–Cu(1)	99.71(7)	P(2)–Se(1)–Cu(3)	103.84(7)
Cu(1)–Se(1)–Cu(3)	103.63(6)	P(1)–Se(2)–Cu(1)	96.68(7)
P(3)–Se(3)–Cu(2)	95.68(8)	P(3)–Se(3)–Cu(1)	112.12(7)
Cu(2)–Se(3)–Cu(1)	109.38(5)	P(4)–Se(4)–Cu(2)	97.86(7)
P(5)–Se(5)–Cu(2)	111.69(8)	P(5)–Se(5)–Cu(3)	98.38(7)
Cu(2)–Se(5)–Cu(3)	128.20(5)	P(6)–Se(6)–Cu(3)	99.42(7)
Se(2)–Cu(1)–Se(1)	122.98(5)	Se(2)–Cu(1)–Se(3)	128.34(6)
Se(1)–Cu(1)–Se(3)	108.39(5)	Se(4)–Cu(2)–Se(5)	128.39(5)
Se(4)–Cu(2)–Se(3)	124.68(6)	Se(5)–Cu(2)–Se(3)	105.91(6)
Se(6)–Cu(3)–Se(5)	120.86(5)	Se(6)–Cu(3)–Se(1)	127.68(6)
Se(5)–Cu(3)–Se(1)	111.44(6)		

† *Crystal data for* **4**: $C_{36}H_{84}Cu_3N_3P_6Se_6$, M = 1409.26, monoclinic, $P2_1/c$ (no. 14), a = 13.178(8), b = 30.108(17), c = 14.691(9) Å, β = 109.423(12)°, V = 5497(6) Å^3, Z = 4, D_c = 1.703 g cm^{-3}, μ(Mo-Kα) = 5.325 mm^{-1}, T = 100 K, colourless plates; 11700 independent measured reflections, F^2 refinement, R_1 = 0.053, wR_2 = 0.102, 5898 independent observed absorption corrected reflections [$|F_o| > 4\sigma(|F_o|)$, $2\theta_{max}$ = 54°], 511 parameters. CCDC 215924. See http://www.rsc.org/suppdata/jm/b3/b311743j/ for crystallographic files in .cif or other electronic format.

‡ *Crystal data for* **5**: $C_{36}H_{84}Ag_3N_3P_6Se_6$, M = 1542.25, triclinic, $P\bar{1}$ (no. 2), a = 14.0717(11), b = 14.7803(8), c = 17.3186(12) Å, α = 114.918(4), β = 92.242(6), γ = 115.042(5)°, V = 2854.1(3) Å^3, Z = 2, D_c = 1.795 g cm^{-3}, μ(Mo-Kα) = 5.040 mm^{-1}, T = 183 K, colourless platy prisms; 7910 independent measured reflections, F^2 refinement, R_1 = 0.038, wR_2 = 0.076, 6030 independent observed absorption corrected reflections [$|F_o| > 4\sigma(|F_o|)$, $2\theta_{max}$ = 47°], 488 parameters. CCDC 215924. See http://www.rsc.org/suppdata/jm/b3/b311743j/ for crystallographic files in .cif or other electronic format.

Table 2 Selected bond lengths (Å) and angles (°) for **5**

Ag(1)–Se(1)	2.5590(10)	Ag(1)–Se(2)	2.6085(9)
Ag(1)–Se(6)	2.5863(9)	Ag(2)–Se(2)	2.5798(9)
Ag(2)–Se(3)	2.5527(10)	Ag(2)–Se(4)	2.6137(10)
Ag(3)–Se(4)	2.5923(8)	Ag(3)–Se(5)	2.5580(9)
Ag(3)–Se(6)	2.6134(9)	Se(1)–P(1)	2.181(2)
Se(2)–P(2)	2.206(2)	Se(3)–P(3)	2.169(2)
Se(4)–P(4)	2.206(2)	Se(5)–P(5)	2.167(2)
Se(6)–P(6)	2.212(2)	P(1)–N(1)	1.598(6)
P(2)–N(1)	1.577(6)	P(3)–N(2)	1.600(6)
P(4)–N(2)	1.583(6)	P(5)–N(3)	1.580(6)
P(6)–N(3)	1.591(6)		
Se(1)–Ag(1)–Se(2)	120.26(3)	Se(1)–Ag(1)–Se(6)	129.63(3)
Se(2)–Ag(1)–Se(6)	109.74(3)	Se(2)–Ag(2)–Se(3)	139.92(3)
Se(2)–Ag(2)–Se(4)	106.47(3)	Se(3)–Ag(2)–Se(4)	113.17(3)
Se(4)–Ag(3)–Se(5)	128.27(3)	Se(4)–Ag(3)–Se(6)	112.53(3)
Se(5)–Ag(3)–Se(6)	119.18(3)	Ag(1)–Se(1)–P(1)	97.27(6)
Ag(1)–Se(2)–Ag(2)	91.07(3)	Ag(1)–Se(2)–P(2)	95.36(5)
Ag(2)–Se(2)–P(2)	110.11(6)	Ag(2)–Se(3)–P(3)	98.11(6)
Ag(2)–Se(4)–Ag(3)	105.25(3)	Ag(2)–Se(4)–P(4)	101.27(6)
Ag(3)–Se(4)–P(4)	104.87(5)	Ag(3)–Se(5)–P(5)	96.64(5)
Ag(1)–Se(6)–Ag(3)	104.12(3)	Ag(1)–Se(6)–P(6)	105.55(6)
Ag(3)–Se(6)–P(6)	94.08(5)		

the two seleniums and one of the phosphorus atoms being essentially planar with the other phosphorus centre and the nitrogen being *ca.* 1.2 and 0.7 Å out of this plane (on the same side) respectively. There is in both complexes an asymmetry between the P–Se bond lengths within the $N(SeP^iPr_2)_2$ ligands, with those to the three-coordinate selenium centres being slightly longer [2.191(2)–2.226(2) Å] than those to the two-coordinate atoms [2.163(3)–2.182(2) Å]; the corresponding bond lengths in the protonated free ligand **3d** are 2.0961(8) and 2.1027(9) Å.[3b] The P–N bond lengths range between 1.575(6) and 1.602(6) across the two complexes, *cf.* 1.686(3) and 1.693(3) Å in **3d**.

Experimental

Unless otherwise stated, all reactions were performed under an inert atmosphere of dry nitrogen using standard Schlenk techniques. All glassware was flame dried under vacuum prior to use. All solvents and reagents were purchased from Sigma-Aldrich and used as received. ^{1}H and ^{31}P NMR studies were carried out using a Bruker AC300 FTNMR instrument. Mass spectra were recorded on a Kratos concept 1S instrument. Infrared spectra were recorded on a Specac single reflectance ATR instrument (4000–400 cm^{-1}, resolution 4 cm^{-1}). Elemental analyses were performed by the University of Manchester micro-analytical laboratory. Melting points were recorded on a Gallenkamp melting point apparatus and are uncorrected.

1. $^iPr_2P(Se)NHP(Se)^iPr_2$ (3d)

A solution of chlorodiisopropylphosphine (72 g, 0.472 mol) in anhydrous toluene (100 cm^3) was added dropwise over 45 minutes to a stirred solution of 1,1,1,3,3,3-hexamethyldisilazane (38.07 g, 0.236 mol) in anhydrous toluene (150 cm^3) at 60 °C. The reaction was stirred at 60–70 °C for 4 hours and cooled to room temperature. Selenium powder (37.27 g, 0.472 mol) was added and the suspension heated at reflux for 12 hours. The resulting orange homogeneous solution was concentrated to *ca* 100 cm^3 and cooled at 0 °C for 12 hours. The resulting white precipitate was recovered and washed with diethyl ether (100 cm^3) and cold toluene (100 cm^3). Recrystallisation from chloroform–hexane yielded 68.21 g (71%) as an off white powder. Mp 171–173 °C; FT-IR (KBr): 3209 (ν N–H), 1385 (δ N–H), 907, 879 (ν P–N–P), 489 (ν P–Se) cm^{-1}; ^{1}H NMR ($CDCl_3$): δ = 1.3 (m, 24 H, 12CH_3–R), 2.75 (m, 4 H, 4C*H*–R), 3.1 ppm (s, 1 H, N–*H*); ^{31}P–{^{1}H} NMR ($CDCl_3$): δ = 90.829 ppm [s, ^1Jpar;^{31}P–^{77}Se) 757 Hz]; MS (FAB): *m/z* = 408 (100%, M + H) (Found: C 35.31, H 7.26, N 3.49, P 15.28%. $C_{12}H_{29}NP_2Se_2$ requires C 35.39, H 7.18, N 3.44, P 15.10%.)

2. $Cu[(^iPr_2PSe)_2N]$ (4)

Sodium methoxide (0.28 g, 4.91 mmol) was added to a stirred solution of **3d** (2.00 g, 4.91 mmol) in anhydrous methanol (100 cm^3). The resulting pink solution was stirred at room temperature for 10 minutes. Copper(II) acetate (0.50 g, 2.46 mmol) was added and the reaction stirred at room temperature for 2 hours. The resulting suspension was filtered and the recovered solid washed with methanol (100 cm^3) before drying under vacuum. Recrystallisation from chloroform–methanol yielded 0.84 g (72%) of a brick red powder. Mp 118–121 °C; FT-IR (KBr): 1257, 1217, 755(ν P–N–P), 422 (ν P–Se) cm^{-1}; ^{1}H NMR ($CDCl_3$): δ = 1.28 (m, 24 H, 12CH_3–R), 2.17 ppm (m, 4 H, 4C*H*–R); ^{31}P–{^{1}H} NMR ($CDCl_3$): δ = 54.34 ppm [m, CuSeP, ^1Jpar;^{31}P–^{77}Se) 534 Hz]; MS (APCI): *m/z* = 470 (100%, M + H) (Found: C 31.27, H 5.95, N 2.80, P 12.80, Cu 12.98%. $C_{12}H_{28}NP_2Se_2Cu$ requires C 30.68, H 6.01, N 2.98, P 13.19, Cu 13.53.)

3. $Ag[(^iPr_2PSe)_2N]$ (5)

Sodium methoxide (0.56 g, 9.82 mmol) was added to a stirred solution of **3d** (4.00 g, 9.82 mmol) in anhydrous methanol (100 cm^3). The resulting pink solution was stirred at room temperature for 10 minutes. Silver(I) nitrate (1.67 g, 9.82 mmol) was added yielding an immediate gelatinous white precipitate. The suspension was stirred at room temperature for 2 hours. The recovered solid was washed with methanol (100 cm^3) and dried under vacuum. Recrystallisation from chloroform–methanol yielded 4.15 g (82%) of a white powder. Mp 108–111 °C; FT-IR (KBr): 1223, 750(ν P–N–P), 429 (ν P–Se) cm^{-1}; ^{1}H NMR ($CDCl_3$): δ = 1.25 (m, 24 H, 12CH_3–R), 2.2 ppm (m, 4 H, 4C*H*–R); ^{31}P–{^{1}H} NMR ($CDCl_3$): δ = 54.06 ppm [m, AgSeP, ^1Jpar;^{31}P–^{77}Se) 499 Hz]; MS (APCI): *m/z* = 515 (100%, M + H) (Found: C 28.23, H 5.64, N 2.73, P 12.46%. $C_{12}H_{28}NP_2Se_2Ag$ requires C 28.03, H 5.49, N 2.72, P 12.05%.)

4. $Au[(^iPr_2PSe)_2N]$ (6)

Sodium methoxide (0.12 g, 2.15 mmol) was added to a stirred solution of **3d** (0.87 g, 2.15 mmol) in anhydrous methanol (50 cm^3). The resulting pink solution was stirred at room temperature for 10 minutes. Gold(I) chloride (0.50 g, 2.15 mmol) was added and the reaction stirred at room temperature for 16 hours. The resulting khaki green suspension was filtered and the recovered solid washed with methanol (100 cm^3) before drying under vacuum. Recrystallisation from chloroform–methanol yielded 0.95 g (73%) of a khaki green powder. Mp 224–227 °C; FT-IR (KBr): 1226, 756 (ν P–N–P), 431 (ν P–Se) cm^{-1}; ^{1}H NMR ($CDCl_3$): δ = 1.35 (m, 24 H, 12CH_3–R), 2.45 ppm (m, 4 H, 4C*H*–R); ^{31}P–{^{1}H} NMR ($CDCl_3$): δ = 54.85 ppm [m, AuSeP, ^1Jpar;^{31}P–^{77}Se) 358 Hz]; MS (APCI): *m/z* = 604 (98%, M + H); (Found: C 23.82, H 4.90, N 2.27, P 10.31%. $C_{12}H_{28}NP_2Se_2Au$ requires C 23.89, H 4.68, N 2.32, P 10.27%.)

X-Ray crystallography

Crystals suitable for X-ray diffraction studies were obtained by slow diffusion of hexane into dichloromethane or carbon disulfide solutions of the appropriate compound. Data for **4** and **5** were collected on Bruker SMART and Bruker P4 diffractometers at the University of Manchester and Imperial College London respectively. The structures were solved and

refined (based on F^2) using the SHELX-97 and SHELXTL program systems.[28,29]

CVD experimental

Aerosol-assisted chemical vapour deposition (AACVD). Approximately 0.25 g of precursor was dissolved in 30 cm^3 THF in a round-bottomed flask. Six glass substrates (1 × 2 cm) were placed inside the reactor tube. The carrier gas flow rate was controlled by Platon flow gauges. The solution in the flask was placed in a water bath above the piezoelectric modulator of a humidifier, where aerosol droplets were generated and transferred by the carrier gas into a hot-wall zone. Both the solvent and the precursor were evaporated and the precursor vapour reached the heated substrate surface where thermally induced reactions and film deposition took place. This home-made aerosol-assisted chemical vapor deposition kit consists of a two-neck flask, a PIFCO ultrasonic humidifier (Model No. 1077) and a CARBOLITE furnace.

Film characterizations. X-Ray powder diffraction studies were done on a Bruker AXS D8 diffractometer using monochromated Cu-Kα radiation. The samples were mounted flat and scanned from 5° to 80° in a step size of 0.01 or 0.02° with a count rate of 2 or 5 s. Films were carbon coated using an Edward's E306A coating system before SEM and EDAX analyses. SEM was carried out on a Philips XL30 FEG and EDAX was preformed using a DX4.

Conclusion

This paper describes the synthesis and characterisation of iminobis(diisopropylphosphine chalcogenide) complexes of copper, silver and gold. These air stable complexes have been shown to be trimeric in the solid state by X-ray single crystal diffraction, possessing M_3Se_3 configurations with extended P–Se bonds. The protic solvent conditions utilized facilitate the reduction of copper(II) salts resulting in copper(I) complexes being isolated. Thermolytic decomposition of the copper(I) precursors in the presence of the indium precursor, $In[(SeP^iPr_2)_2N]_2Cl$, was carried out in the solid state using AA-MOCVD to give copper indium diselenide solid state materials $CuInSe_2$. Our results illustrate that such dichalcogenoimidodiphosphinato compounds are excellent as molecular single source precursors for the preparation of group 11 chalcogenide and other ternary metal chalcogenide solid-state materials.

Acknowledgements

M. A. and D. J. C are supported by EPSRC grants to P. O. B. This work is part of the program studying new precursors for chalcogenides funded by the EPSRC.

References

1 F. T. Wang, J. Najdzionek, K. L. Leneker, H. Wasserman and D. M. Braitsch, *Synth. React. Inorg. Met.-Org. Chem.*, 1978, **8**(2), 119.
2 R. O. Day, R. R. Holmes, A. Schmidpeter, K. Stoll and L. Howe, *Chem. Ber.*, 1991, **124**, 2443.
3 (*a*) P. Bhattacharyya, A. M. Z. Slawin and M. B. Smith, *J. Chem. Soc., Dalton Trans.*, 1998, 2467; (*b*) D. Cupertino, D. J. Birdsall, A. M. Z. Slawin and J. D. Woollins, *Inorg. Chim. Acta*, 1999, **290**, 1
4 (*a*) J. D. Woollins, *J. Chem. Soc., Dalton Trans.*, 1996, 2893 and references within; (*b*) P. Bhattacharyya and J. D. Woollins, *Polyhedron*, 1995, **14**(23), 3367.
5 R. C. Mehrotra, R. Bohra and D. P. Gaur, *Metal β-Diketonates and Allied Derivatives*, Academic Press, London, 1978.
6 (*a*) N. Revaprasadu, M. A. Malik, P. O'Brien, M. M. Zulu and M. Wakefield, *J. Mater. Chem.*, 1998, **8**, 1885; (*b*) B. Ludolph, M. A. Malik, P. O'Brien and N. Revaprasadu, *Chem. Commun.*, 1998, 1849; (*c*) M. Green and P. O'Brien, *Chem. Commun.*, 1999, 2235; (*d*) N. L. Pickett and P. O'Brien, *Chem. Rec.*, 2001, **1**, 467; (*e*) M. Afzaal, S. M. Ascott, D. Crouch, P. O'Brien, J. D. Woollins and J.-H. Park, *Chem. Vap. Deposition*, 2002, **8**(5), 187; (*f*) M. Afzaal, D. Crouch, M. A. Malik, M. Motevalli, P. O'Brien and J.-H. Park, *J. Mater. Chem.*, 2003, **13**(1–3), 1; (*g*) A. N. Gleizes, *Chem. Vap. Deposition*, 2000, **6**(4), 155.
7 D. J. Crouch, P. O'Brien, M. A. Malik, P. J. Skabara and S. P. Wright, *Chem. Commun.*, 2003, 1454.
8 (*a*) P. Bhattacharyya, J. Novosad, J. Phillips, A. M. Z. Slawin, D. J. Williams and J. D. Woollins, *J. Chem. Soc., Dalton Trans.*, 1995, 1607; (*b*) R. Cea-Olivares, V. García-Montalvo, J. Novosad, J. D. Woollins, R. A. Toscano and G. Espinosa-Pérez, *Chem. Ber.*, 1996, **129**, 919; (*c*) Q.-F. Zhang, H. Zheng, W.-Y. Wong, W.-T. Wong and W.-H. Leung, *Inorg. Chem.*, 2000, **39**, 5255.
9 C. Silvestru, R. Rosler, I. Haiduc, R. Cea-Olivares and G. Espinosa-Perez, *Inorg. Chem.*, 1995, **34**, 3352.
10 D. C. Cupertino, R. W. Keyte, A. M. Z. Slawin and J. D. Woollins, *Polyhedron*, 1999, **18**, 707.
11 (*a*) D. C. Cupertino, R. W. Keyte, A. M. Z. Slawin, D. J. Williams and J. D. Woollins, *Inorg. Chem.*, 1996, **35**, 2695; (*b*) Q.-F. Zhang, K.-K. Lau, J. L.C. Chim, T. K. T. Wong, W.-T. Wong, I. D. Williams and W.-H. Leung, *J. Chem., Soc., Dalton Trans.*, 2000, 3027.
12 (*a*) L. M. Gilby and B. Piggott, *Polyhedron*, 1999, **18**, 1077; (*b*) M.-A. Muñoz-Hernández, A. Singer, D. A. Atwood and R. Cea-Olivaries, *J. Organomet. Chem.*, 1998, **571**, 15.
13 J. Fink, C. J. Kiely, D. Bethell and D. J. Schiffrin, *Chem. Mater.*, 1998, **10**, 922.
14 D. Gittens, D. J. Schiffrin, R. Nichols and D. Bethell, *Adv. Mater.*, 1999, **11**, 737.
15 J. W. Slot and H. J. Geuze, *J. Cell Biol.*, 1981, **90**, 533.
16 T. Sato, H. Ahmed, D. Brown and B. F. G. Johnson, *J. Appl. Phys.*, 1997, **82**, 696.
17 K. Darwin, L. M. Gilby, P. R. Hodge and B. Piggott, *Polyhedron*, 1999, **18**, 3729.
18 M. Contreras, B. Egass, K. Ramanathan, J. Hiltner, A. Swartlander, F. Hasson and R. Noufi, *Prog. Photovoltaics*, 1999, **7**, 311.
19 (*a*) V. Sagnes, A. Salesse, M. C. Artaud, S. Duchemin, J. Bougnot and G. Bougnot, *J. Cryst. Growth*, 1992, **124**, 620; (*b*) F. Ouchin, P. Gallon, M. C. Artaud, J. Bougnot and S. Duchemin, *Cryst. Res. Technol.*, 1996, **31**, S513.
20 S. Chichibu, *Appl. Phys. Lett.*, 1997, **70**, 1840.
21 W. Hirpo, S. Dhingra, A. C. Sutorik and M. G. Kanatzidis, *J. Am. Chem. Soc.*, 1993, **115**, 597.
22 M. Afzaal, D. Crouch, P. O'Brien and J.-H. Park, *Mater. Res. Soc. Symp. Proc.*, 2002, **692**, 61.
23 M. Afzaal, D. Crouch, P. O'Brien and J.-H. Park, *Thin Solid Films*, in press.
24 D. J. Crouch, M. Helliwell, P. O'Brien, J.-H. Park, J. Waters and D. J. Williams, *J. Chem Soc., Dalton. Trans.*, 2003, 1500.
25 D. J. Crouch and P. O'Brien, unpublished data.
26 (*a*) E. Herrmann, R. Richter and N. T.T. Chau, *Z. Anorg. Allg. Chem.*, 1997, **623**, 403; (*b*) D. J. Birdsall, A. M. Z. Slawin and J. D. Woollins, *Inorg. Chem.*, 1999, **38**, 4152.
27 J. McAleese, P. O'Brien and D. J. Otway, *Chem. Vap. Deposition*, 1998, **4**, 94.
28 G. M. Sheldrick, SHELX-97, University of Göttingen, Germany, 1997.
29 (*a*) SHELXTL PC version 5.03, Siemens Analytical X-Ray Instruments, Inc., Madison, WI, 1994; (*b*) SHELXTL PC version 5.1, Bruker AXS, Madison, WI, 1997.

Chemical Vapor Deposition of Indium Selenide and Gallium Selenide Thin Films from Mixed Alkyl/Dialkylselenophosphorylamides

Jin-Ho Park, Mohammad Afzaal, Madeleine Helliwell, Mohmmad A. Malik, Paul O'Brien,* and Jim Raftery

The Manchester Materials Science Centre and Department of Chemistry, The University of Manchester, Oxford Road, Manchester, M13 9PL, United Kingdom

Received February 24, 2003. Revised Manuscript Received May 15, 2003

The syntheses and characterizations of the mixed alkyl/dialkylselenophosphorylamides, $[Me_2Ga(SeP^iPr_2)_2N]$ (**1**) and $[R_2In(SeP^iPr_2)_2N]$ (R = Me (**2**), Et (**3**)) are reported together with the X-ray single-crystal structures of $[Me_2M(SeP^iPr_2)_2N]$ (M = Ga(III) or In(III)), which have Se_2C_2 coordination at the metal centers. These compounds have been used as single-source precursors for the deposition of metal (Ga or In) selenides films on glass substrates by MOCVD. Ga_2Se_3 thin films have been deposited from compound **1** by aerosol-assisted chemical vapor deposition (AACVD) and low-pressure metal-organic chemical vapor deposition (LP-MOCVD). X-ray powder diffraction (XRPD) studies show that the films are composed of cubic Ga_2Se_3. Indium selenide (In_2Se_3) thin films have been grown from compound **2** by AACVD and all the as-deposited indium selenide films are found to be hexagonal γ-In_2Se_3.

Introduction

Thin films of III−VI materials are potential alternatives to II−VI materials in optoelectronic and photovoltaic devices[1,2] and also have a potential application as passivating layers for III−V devices.[3] In addition, there are related ternary and quaternary phases such as $CuInE_2$ and $CuIn_{1-x}Ga_xE_2$ (E = S or Se) with uses in solar cells.[1]

Compounds containing a chalcogen and a group 13 metal (Al, Ga or In) have often been used as single molecular precursors for the deposition of III−VI materials.[4] A variety of single-source precursors have been reported for the deposition of III−VI thin films by various deposition processes.[1,5−15] Barron and co-workers have reported a number of complexes with cubane structures, for example, $[^tBuGaS]_4$, and deposited cubic GaS using atmospheric pressure CVD. They suggested that the formation of cubic GaS is influenced by the cubic nature of the core of $[^tBuGaS]_4$ precursor, which is maintained throughout deposition.[4,8,9] The same group has also reported the growth of GaS films using mixed-alkyl gallium dithiocarbamate precursors, $(^tBu)Ga(S_2CNR_2)_2$ (R = Me, Et), by atmospheric pressure (AP-MOCVD),[10] while films prepared by our group from an air-stable precursor, $Ga(S_2CNMeHex)_3$, by LP-MOCVD on GaAs(111) substrates resulted in the deposition of α-Ga_2S_3 films.[11] Our efforts also include the synthesis of precursors based on monothiocarbamate ligands, such as $[In(SOCNEt_2)_3]$ and $[Et_2In(SOCNEt_2)]_n$, and utilization of one of these compounds to deposit β-In_2S_3 thin films on glass by LP-MOCVD.[12] In addition, several mixed alkyl group 13 dithiocarbamate precursors were utilized to deposit III−VI materials, e.g., $[R_2M(S_2CNEt_2)]$ (M = In, Ga and R = Me, Et, Np).[14]

Recently, we have identified a new class of metal-organic single-source precursors based on bidentate bis(diphenylselenophosphoryl)amide ligand, $[NH(SePPh_2)_2]$, and deposited II−VI thin films by low-pressure MOCVD using $M[(SePPh_2)_2N]_2$ [M = Cd(II) or Zn(II)].[16] These selenium-containing ligands are relatively easy to prepare from elemental selenium and obviate the need for the use of noxious CSe_2 as used in preparing diselenocarbamates. The aim of the present study is to extend the chemistry to group 13 and synthesize novel gallium

* To whom correspondence should be addressed: Professor Paul O'Brien, Department of Chemistry, The University of Manchester, Oxford Road, Manchester, M13 9PL, UK. E-mail: paul.obrien@man.ac.uk. Tel: +44-161-275-4652. Fax: +44-161-275-4616.

(1) Lazell, M. R.; O'Brien, P.; Otway, D. J.; Park, J.-H. *J. Chem. Soc., Dalton Trans.* **2000**, 4479.
(2) *Semiconductor: other than Group IV Elements and III−V Compounds*; Madelung, O., Poerschke, R., Eds.; Springer-Verlag: Berlin, 1992.
(3) *CVD of Nonmetals*; Rees, W. E., Jr., Ed.; VCH: New York, 1996.
(4) Barron, A. R. *Adv. Mater. Opt. Electron.* **1995**, *5*, 245.
(5) Gysling, H. J.; Wernberg, A. A.; Blanton, T. N. *Chem. Mater.* **1992**, *4*, 900.
(6) Kanatzidis, M. G.; Dihingra, S. *Inorg. Chem.* **1989**, *28*, 2024.
(7) Nomura, R.; Konishi, K.; Matsuda, H. *Thin Solid Films* **1991**, *198*, 339.
(8) MacInnes, A. N.; Power, M. B.; Barron, A. R. *Chem. Mater.* **1992**, *4*, 11.
(9) MacInnes, A. N.; Power, M. B.; Barron, A. R. *Chem. Mater.* **1993**, *5*, 1344.
(10) Keys, A.; Bott, S. G.; Barron, A. R. *Chem. Mater.* **1999**, *11*, 3578.
(11) Lazell, M. R.; O'Brien, P.; Otway, D. J.; Park, J.-H. *Chem. Mater.* **1999**, *11*, 3430.
(12) Horley, G. A.; Chunggaze, M.; O'Brien, P.; White, A. J. P.; Williams, D. J. *J. Chem. Soc., Dalton Trans.* **1998**, 4205.
(13) Bessergenev, V. G.; Ivanova, E. V.; Kovalevskaya, Y. A.; Gromilov, S. A.; Kirichenko, V. N.; Larionov, S. V. *Inorg. Mater.* **1996**, *6*, 1639.
(14) Haggata, S. W.; Knowles, J. C.; Malik, M. A.; Motevalli, M.; O'Brien., P. *Chem. Mater.* **1995**, *7*, 716.
(15) Suh, S.; Hoffman, D. M. *Chem. Mater.* **2000**, *12*, 2794.
(16) Afzaal, M.; Aucott, S. M.; Crouch, D.; O'Brien, P.; Park, J.-H.; Woollins, J. D. *Adv. Mater. Chem. Vap. Depostion* **2002**, *5*, 187.

10.1021/cm0310420 CCC: $25.00
Published on Web 10/14/2003

and indium complexes by reacting group 13 metal alkyls with [NH(SeP^{i}Pr$_2$)$_2$] moiety and utilize these compounds for the deposition of III–VI thin films by MOCVD.

Experimental Section

Trimethylgallium, trimethylindium, and triethylindium were kindly donated by Epichem Ltd. Solvents were obtained from BDH and were dried and degassed before use. The ligand [NH(SeP^{i}Pr$_2$)$_2$] was prepared by the literature method.[17] All reactions were performed in an inert atmosphere using Schlenk techniques and a vacuum line.

Preparation of [Me$_2$Ga(SeP^{i}Pr$_2$)$_2$N] (1). The compound was prepared by the addition of Me_3Ga (0.75 g, 6.54 mmol) in toluene (25 mL) to a stirred solution of NH(SeP^{i}Pr$_2$)$_2$ (2.7 g, 6.55 mmol) in toluene. Removal of solvent and volatiles in vacuo led to a viscous liquid, which was crystallized by adding hexane. Yield: 2.9 g, 84%. mp 61 °C. ^{1}H NMR (δ, C_6D_6, 300 MHz): 0.60 [6H, s, Ga–CH_3], 1.1 [24H, m, C–CH_3], 1.95 [4H, m, C–H]. ^{31}P NMR (δ, C_6D_6, 400 MHz): 57.43 [m]. Microanalysis. Calculated for [$C_{14}H_{34}N_1P_2Se_2Ga$]: C, 33.23; H, 6.77; N, 2.77; P, 12.24%. Found: C, 32.75; H, 6.85; N, 2.77; P, 11.86%. FT-IR (major bands and tentative assignments cm^{-1}): 515, 569 (δ (Ga–C)), 1223 (δ (P–N–P)). Mass spectrum: *m/z* 507 [M + H$^+$], 491 [MeGa(SeP^{i}Pr$_2$)$_2$N]$^+$.

Preparation of [Me$_2$In(SeP^{i}Pr$_2$)$_2$N] (2). Compound **2** was synthesized in a manner similar to **(1)**; the reaction of NH(SeP^{i}Pr$_2$)$_2$ (1.1 g, 2.69 mmol) in toluene (40 mL) and trimethylindium (0.43 g, 2.69 mmol) resulted in a yellow solid. Product was re-crystallized from toluene. Yield: 0.93 g, 75%. mp 57 °C. ^{1}H NMR (δ, C_6D_6, 300 MHz): 0.47 [6H, s, In–CH_3], 1.1 [24H, m, C–CH_3], 1.90 [4H, m, C–H]. ^{31}P NMR (δ, C_6D_6, 400 MHz): 58.22 [m]. Microanalysis. Calculated for [$C_{14}H_{34}N_1P_2Se_2In$]: C, 30.53; H, 6.17; N, 2.54%. Found: C, 29.07; H, 5.98; N, 2.24%. FT-IR (major bands and tentative assignments cm^{-1}): 512 (δ (Ga–C)), 1229 (δ (P–N–P)). Mass spectrum: *m/z* 551 [M + H$^+$], 535 [MeIn(SeP^{i}Pr$_2$)$_2$N]$^+$.

Preparation of [Et$_2$In(SeP^{i}Pr$_2$)$_2$N] (3). Similarly, compound **3** was synthesized from NH(SeP^{i}Pr$_2$)$_2$ (1.5 g, 3.68 mmol) in toluene (40 mL) and triethylindium (0.75 g, 3.67 mmol), which resulted in a white solid. Recrystallization was carried out from toluene. Yield: 1.64 g, 76%. mp 62–64 °C. ^{1}H NMR (δ, C_6D_6, 300 MHz): 1.1 [24H, m, C–CH_3], 1.2 [4H, q, In–CH_2], 1.5 [6H, t, C–CH_3], 1.9 [4H, m, C–H]. ^{31}P NMR (δ, C_6D_6, 400 MHz): 58.45 [m]. Microanalysis. Calculated for [$C_{16}H_{38}N_1P_2Se_2In$]: C, 33.18; H, 6.61; N, 2.42; P, 10.70%. Found: C, 33.54; H, 6.81; N, 2.41; P, 10.71%. FT-IR (major bands and tentative assignments cm^{-1}): 513 (δ (Ga–C)), 1231 (δ (P–N–P)). Mass spectrum: *m/z* 579 [M + H$^+$], 549 [EtIn(SeP^{i}Pr$_2$)$_2$N]$^+$.

Physical Measurements. NMR spectra were carried out using a Bruker AC300 FT-NMR spectrometer. Mass spectra were recorded on a Kratos concept 1S instrument. Infrared spectra were recorded on a Specac single reflectance ATR instrument. Melting points were measured in sealed tubes with an electrothermal melting point apparatus. X-ray powder diffraction studies were carried out by a Bruker AXS D8 diffractometer using monochromated Cu Kα radiation. The samples were mounted flat and scanned from 10° to 60° in a step size of 0.04° with a count rate of 2.5 s. Samples were carbon-coated using Edward's coating system E306A before SEM and EDAX analyses. SEM was carried out using Philip XL30 FEG and EDAX was performed using DX4. TGA measurements were carried out by a Seiko SSC/S200 model with a heating rate of 10 °C min^{-1} under nitrogen. Electronic absorption spectra were recorded on Helios-Beta thermospectronic spectrophotometer. Pyrolysis experiments were performed in a quartz glass reactor using a heating furnace at atmospheric pressure. The samples were heated to 475 °C under a constant flow of argon (120 sccm) for 1 h.

Single-Crystal X-ray Diffraction Study. Measurements were made using graphite monochromated Mo Kα radiation (λ = 0.71073Å) on a Bruker APEX diffractometer. The structures were solved by direct methods and refined by full-matrix least-squares on F^2.[18] All calculations were carried out using the SHELXTL package.[19] All non-hydrogen atoms were refined with anisotropic atomic displacement parameters. Hydrogen atoms were placed in calculated positions, assigned isotropic thermal parameters, and allowed to ride on their parent carbon atoms. Crystallographic details and selected interatomic distances and angles are summarized in Tables 1, 2, and 3.

CCDC reference numbers for the compounds are 203742 and 203743.

Deposition of Thin Films. In_2Se_3 and Ga_2Se_3 thin films were grown on glass substrates by AACVD for 2 h, with a constant argon flow rate of 120 sccm by dissolving ca. 150 mg of precursor in 20 mL of toluene.[20] Deposition of gallium selenide thin films was also carried out in a cold wall low-pressure (ca. 10^{-2} Torr) MOCVD reactor tube described previously.[21] A graphite susceptor holds the glass substrate dimensions (10 × 15 mm), which was heated by a tungsten halogen lamp. Growth of films was attempted over a range of

Table 1. Crystal Data and Structure Refinement Parameters

compound	$C_{14}H_{34}GaNP_2Se_2$	$C_{14}H_{34}InNP_2Se_2$
fw	506	551.10
λ (Å)	0.71073	0.71073
crystal system	monoclinic	monoclinic
a (Å)	13.989(2)	14.6027(14)
b (Å)	10.4987(18)	17.9871(18)
c (Å)	14.254(2)	16.5824(16)
α (deg)	90	90
β (deg)	94.094	99.774(2)
γ (deg)	90	90
V (Å^3)	2088.1(6)	4292.3(7)
Z	4	8
space group	$P2_1/n$	$P2_1/n$
d_{calcd} (mg/m^3)	1.610	1.706
μ (mm^{-1})	4.950	4.636
no. of reflcns collcd	17046	33762
no. of unique collcd	4931	8734
R indices [$I > 2\sigma(I)$]	R1 = 0.0267 wR2 = 0.0690	R1 = 0.0387 wR2 = 0.0957
R indices (all data)	R1 = 0.0306 wR2 = 0.0710	R1 = 0.0498 wR2 = 0.1025
max peak and hole	1.205, −0.557	1.351, −2.070

Table 2. Selected Interatomic Distances (Å) and Angles (deg) for [Me$_2$Ga(SeP^{i}Pr$_2$)$_2$N]

Ga(1)–C(1)	1.979(2)	C(2)–Ga(1)–C(1)	120.14(10)
Ga(1)–C(2)	1.970(2)	C(2)–Ga(1)–Se(2)	110.39(7)
Ga(1)–Se(1)	2.5038(5)	C(1)–Ga(1)–Se(2)	104.58(7)
Ga(1)–Se(2)	2.4901(5)	C(2)–Ga(1)–Se(1)	100.21(7)
Se(1)–P(1)	2.1925(6)	C(1)–Ga(1)–Se(1)	112.36(6)
Se(2)–P(2)	2.1919(6)	Se(2)–Ga(1)–Se(1)	108.947(11)
N(1)–P(1)	1.5934(17)	P(1)–Se(1)–Ga(1)	106.054(17)
N(1)–P(2)	1.5877(18)	P(2)–Se(2)–Ga(1)	105.831(19)

Table 3. Selected Interatomic Distances (Å) and Angles (deg) for [Me$_2$In(SeP^{i}Pr$_2$)$_2$N]

In(1)–C(13)	2.154(4)	C(13)–In(1)–C(14)	125.00(17)
In(1)–C(14)	2.153(4)	C(13)–In(1)–Se(2)	101.67(13)
In(1)–Se(1)	2.6835(5)	C(14)–In(1)–Se(2)	112.22(12)
In(1)–Se(2)	2.6746(5)	C(13)–In(1)–Se(1)	109.41(12)
Se(1)–P(1)	2.1827(11)	C(14)–In(1)–Se(1)	100.32(12)
Se(2)–P(2)	2.1886(10)	Se(2)–In(1)–Se(1)	107.417(16)
N(1)–P(1)	1.584(17)	P(1)–Se(1)–In(1)	104.77(3)
N(1)–P(2)	1.579(3)	P(2)–Se(2)–In(1)	104.28(3)

(17) Cupertino, D.; Birdsall, D. J.; Slawin, A. M. Z.; Woollins, J. D. *Inorg. Chim. Acta* **1999**, *290*, 1.

(18) Sheldrick, G. M. *SHELXL97 and SHELXS 97*; University of Göttingen: Göttingen, Germany, 1997.

(19) Bruker. *SHELXTL*, Version 6.10; Bruker AXS Inc.: Madison, WI, 2000.

(20) Horley, G. A.; Lazell, M. R.; O'Brien, P. *Adv. Mater. Chem. Vap. Deposition* **1996**, *2*, 242.

(21) Malik, M. A.; O'Brien, P. *Adv. Mater. Opt. Electron.* **1994**, *3*, 171.

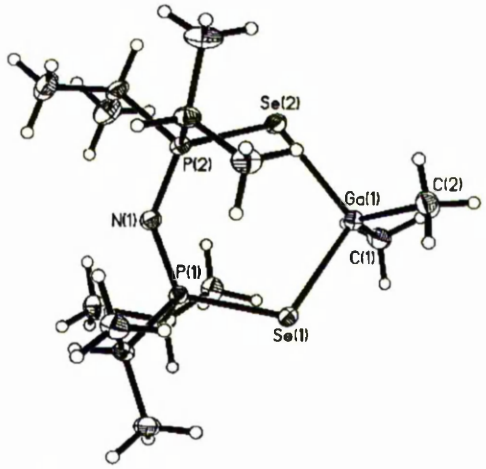

Figure 1. X-ray single-crystal structure of $[Me_2Ga(SeP^iPr_2)_2N]$.

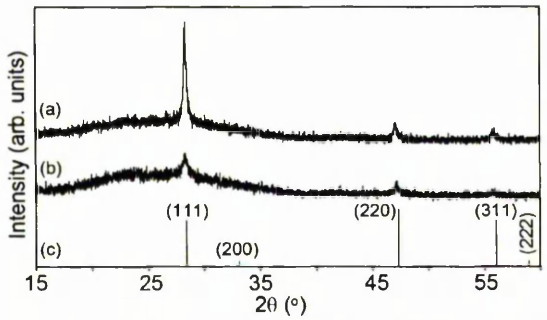

Figure 2. XRPD patterns of Ga_2Se_3 films deposited by AACVD at (a) 475 °C and (b) 450 °C. The standard pattern for cubic Ga_2Se_3 (JCPDS 5-724) is shown for comparison (c).

deposition temperatures, maintaining a precursor temperature of 185 °C for 1 h with ca. 200 mg of precursor used for each experiment.

Results and Discussion

The synthesis of $[NH(SeP^iPr_2)_2]$ was carried out according to the previously reported method.[17] The acidic nature of the imino proton in the ligand makes it a good candidate for the alkane elimination reactions with group 13 metal alkyls.[22]

The reactions were carried out in 1:1 stoichiometric amounts of the ligand and metal alkyl in anhydrous toluene and good yields were obtained. All the compounds are soluble in common organic solvents and are generally air-stable. ^1H NMR spectra of compounds **1** and **2** show a singlet for methyl protons and a triplet and a quartet for *N*-ethyl groups in compound **3**.

X-ray Single-Crystal Structures of $[Me_2Ga(SeP^iPr_2)_2N]$ (1) and $[Me_2In(SeP^iPr_2)_2N]$ (2). Crystals of compound **1** were obtained from hexane at low temperature (−25 °C). The crystal structure of the compound is shown in Figure 1 and selected bond lengths and angles are summarized in Table 2. The structure of compound **1** shows a dimethylgallium moiety coordinated to the imidophosphineselenate ligand in a distorted tetrahedral geometry. The Ga−Se bond lengths are 2.4901(5) and 2.5038(5) Å, which are comparable to those reported for $[Et_2Ga(SePPh_2)_2N]$ (2.5139(10) and 2.5347(10) Å)[22] and $[Cp^*Ga(\mu_3-Se)]_4$ (ranging between 2.445 and 2.499 Å).[23] The complex $[Tp(Bu^t)_2]GaSe$ synthesized by Parkin and Kuchta has the shortest known Ga−Se bond lengths, which are consistent with multiple bond character (2.214(1) Å).[24] The bite angle of Se(2)−Ga(1)−Se(1) is 108.95(1)°, which is similar to the reported value.[22] The structure of compound **1** has a smaller C−Ga−C angle (120.14(10)°) in comparison to the angle observed for $[Et_2Ga(SePPh_2)_2N]$ (125.5(4)°).[22] Shortening of the P−N bonds to 1.5877(18) and 1.594(2) Å and the subsequently extended P−Se bonds 2.1919(6) and 2.1925(6) Å relative to free ligand indicate an increase in delocalization within the structure due to deprotonation.[17]

Crystals of compound **2** were obtained from toluene undisturbed for a period of time at low temperature. The asymmetric unit of the crystal structure contains two similar molecules and is isostructural with the gallium analogue (Figure 1). Similarly, the indium atom is in a distorted tetrahedral coordination environment, with the Se(2)−In(1)−Se(1) angle being smaller than the C(13)−In(1)−C(14) angle as a consequence of the imidophosphineselenate chelate ring (Table 3). The bite angle of Se−In−Se (107.42(2)°) is considerably greater than the bite observed in a tris-chelate compound, $In[(SePPh_2)_2N]_3$ (95.55°), due to the greater steric requirements of three ligands around a six-coordinate metal center in comparison to compound **2**, which is four-coordinate.[25] The C(13)−In(1)−C(14) angle is 125.0(2)°, which is similar to the value (123(1)°) reported for $[Bu_2^tIn(\mu\text{-}SeBu^t)]_2$.[26] The In−Se bond lengths (2.6746(5) and 2.6835(5) Å) are shorter than $[In(SePPh_2)_2N]_3$ (average 2.75 Å),[25] $[(2,4,6\text{-trimethylphenyl})_2In(\mu\text{-}SePh)]_2$ (average 2.732 Å),[27] and $[(Me_3CCH_2)_2In(\mu\text{-}SePh)]_2$ (average 2.743 Å).[28] In comparison with compound **1**, compound **2**

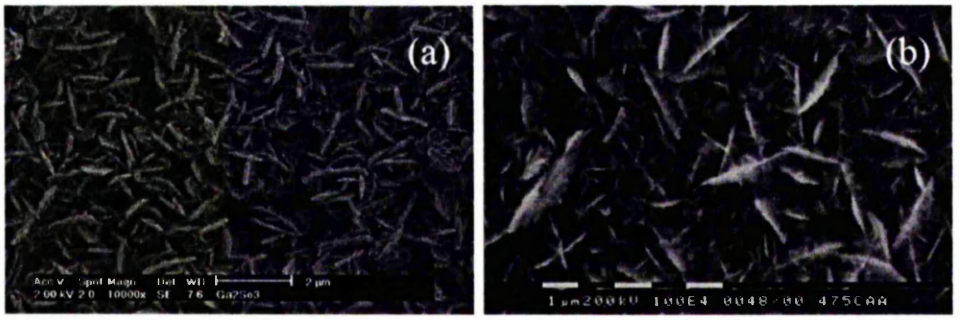

Figure 3. SEM images of Ga_2Se_3 films deposited by AACVD at (a) 450 °C and (b) 475 °C.

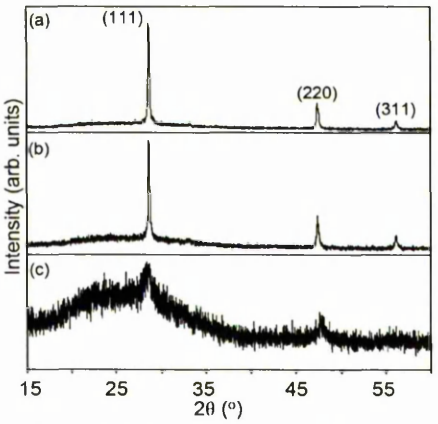

Figure 4. XRPD patterns of Ga_2Se_3 films deposited by LP-MOCVD at (a) 500 °C, (b) 475 °C, and (c) 450 °C.

shows a longer metal−selenium bond, as expected due to the larger size of indium.

Gallium Selenide Thin Films. Gallium selenide films have been grown from $[Me_2Ga(SeP^iPr_2)_2N]$ by AACVD and LP-MOCVD. Thermogravimetric analysis (TGA) shows that the precursor sublimes in one step between 175 and 400 °C but with a 35 wt % final residue at atmospheric pressure. The brown-colored residue obtained from the pyrolysis of the compound was analyzed by XRPD; however, the pattern was not definitive. The broad peaks in the pattern could be tentatively cubic Ga_2Se_3. EDAX analysis was also consistent with the comparative Ga_2Se_3.

Deposition of films by AACVD was attempted over a range of deposition temperatures (400−475 °C) with ca. 150 mg of the precursor used for each experiment. However, growth of films was only observed at higher growth temperatures (450 and 475 °C). As-deposited films were dark brown, nonuniform, and nonadherent to the glass substrates.

XRPD patterns of the films grown by AACVD are shown in Figure 2. The patterns are consistent with the formation of cubic Ga_2Se_3 (JCPDS 5-724) with a preferred orientation along the (111) direction. The film deposited at 450 °C produced broad peaks, indicating small particle sizes, but at higher deposition temperature the peaks sharpened. In contrast, Ga_2Se_3 film deposited from a cubane complex, $[Cp^*Ga(\mu_3\text{-}Se)]_4$, showed a relatively broad XRPD pattern even after annealing the film at 500 °C.[23] However, when similar cubane complexes, $[(R)Ga(\mu_3\text{-}Se)]_4$ (R = CMe_3, $CEtMe_2$, and CEt_2Me) where cyclopentadienyl derivative is replaced by alkyl groups, were used, they resulted in deposition of GaSe films between 325 and 370 °C.[29]

A SEM image of the film deposited at 450 °C shows that the film surface consists of randomly oriented and poorly defined particles with ca. 0.75 μm in thickness (Figure 3a). In contrast, the film grown at 475 °C consists of thin platelike particles, laid down perpendicularly onto the substrate with random orientation (Figure 3b). The growth rate at 475 °C is ca. 0.75 μm h^{-1}. EDAX analyses of the grown films at random sites showed that a gallium-to-selenium ratio is close to 2:3.

As an alternative, deposition was also attempted by LP-MOCVD on glass substrates for 1 h. Deposition was attempted over a range of substrate temperatures (400−500 °C), while the precursor temperature was maintained at 185 °C. Little or no deposition was observed below 450 °C. The films obtained were yellow and transparent at 450 °C, light-red at higher temperatures, and adherent to the glass substrate surface (Scotch tape test).

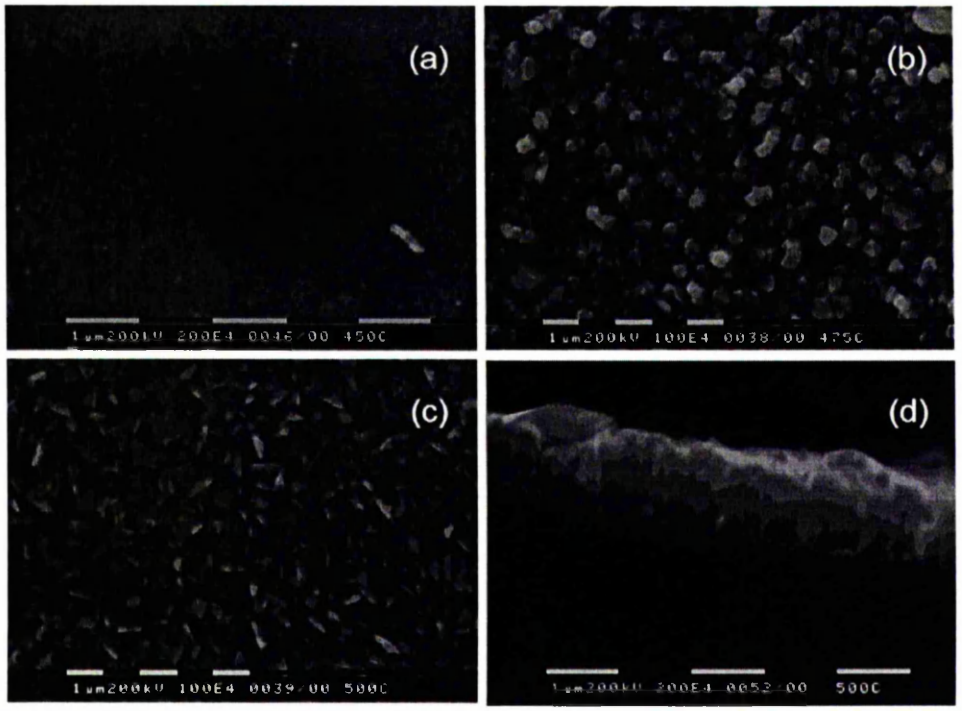

Figure 5. SEM images of Ga_2Se_3 films deposited by LP-MOCVD at (a) 450 °C, (b) 475 °C, and (c) and (d) 500 °C.

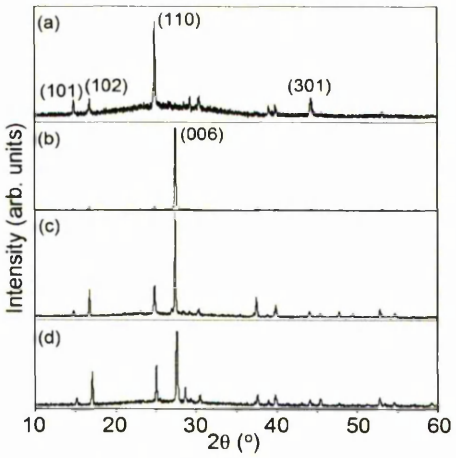

Figure 6. XRPD patterns of In_2Se_3 films deposited by AACVD at (a) 475 °C, (b) 450 °C, (c) 425 °C, and (d) 400 °C.

XRPD analysis show that the films are cubic Ga_2Se_3 at all growth temperatures with a preferred orientation along the (111) plane (Figure 4). The XRPD patterns indicate that the crystallinity of deposited films is dependent on the growth temperatures. Deposition carried out at 450 °C yielded relatively poor crystalline Ga_2Se_3 film, while higher deposition temperature results in improved crystallinity.

Figure 5 shows SEM micrographs of the deposited films at different growth temperatures. The film deposited at 450 °C has featureless microcrystalline morphology and poor coverage is also observed. At higher growth temperatures (475 and 500 °C), dense morphology is evident and particles have irregular shapes. The growth rate at 500 °C is ca. 1.25 μm h^{-1}. EDAX analyses of the films show that the films are slightly selenium-rich, 64%, and gallium is 36%.

Indium Selenide Thin Films. Deposition of indium selenide films from $[Et_2In(SeP^iPr_2)_2N]$ was achieved by AACVD. TGA of the compound suggests that it decomposes in a two-step mechanism in which $(P^iPr_2)_2N$ moiety dissociates between ca. 137 and 307 °C at atmospheric pressure. The XRPD pattern of the final residue (18 wt %) obtained from pyrolysis of the compound indicated the formation of γ-In_2Se_3. Films grown on glass between 400 and 475 °C were found to be purple, uniform, and fairly adherent.

Indium selenide films analyzed by XRPD indicated that the hexagonal γ-In_2Se_3 phase (JCPDS 40-1407) has been grown with a preferred orientation along the (006) plane except for the film deposited at 475 °C. which showed a preferred orientation along the (110) plane (Figure 6). In contrast, γ-In_2Se_3 films grown from $In[(SeP^iPr_2)_2N]_2Cl$ at 475 and 525 °C by LP-MOCVD also showed a preferred orientation along the (006) plane.[30] On the other hand, the use of $(Me_2InSePh)_2$ in spray MOCVD experiments (In/Se ratio), using argon as a carrier gas, has led to the growth of nonstoichiometric cubic InSe at 365 °C.[5]

Figure 7 shows the SEM micrographs of the various changes observed at different growth temperatures. The films deposited at 425 and 450 °C have similar morphologies with columnar aggregates (Figure 7b,c). As the deposition temperature decreases to 400 °C, the morphology consists of anhedral grains (Figure 7a). At 475 °C, the surface consists of randomly oriented platelets. The thickness of the films as obtained from the cross-sectional views was found to be ca. 0.5 μm at 400 °C, 1.5 μm at 425 °C, and 1 μm at 450 °C on glass substrates after 2 h of growth. EDAX analysis shows that the indium-to-selenium ratio is close to 2:3 for the film grown at 450 °C but a small trace of phosphorus (<1%) was also found, which was incorporated during the decomposition of the precursor.

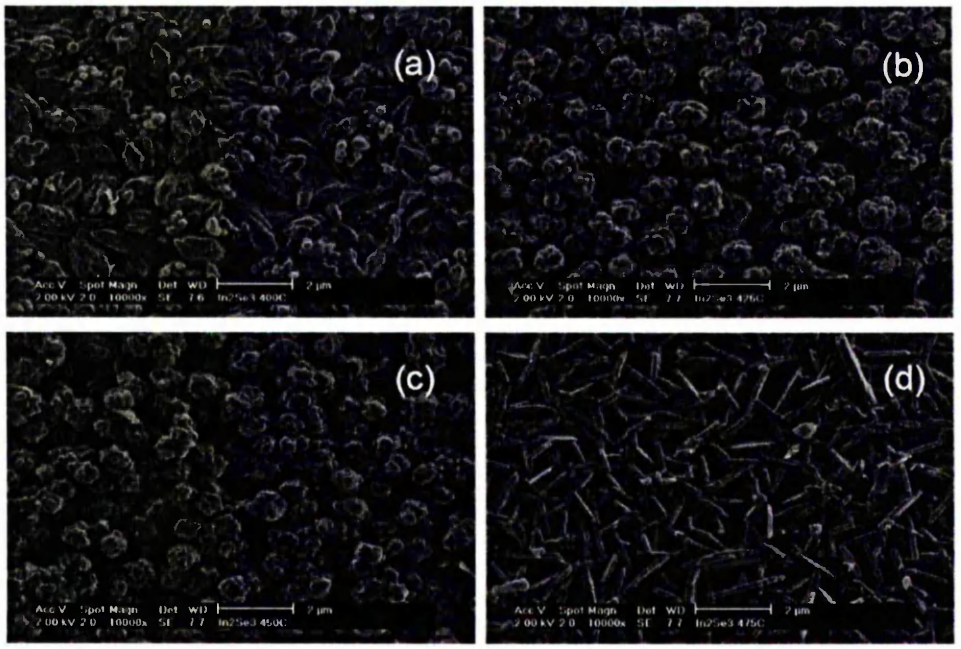

Figure 7. SEM images of In_2Se_3 films deposited by AACVD at (a) 400 °C, (b) 425 °C, (c) 450 °C, and (d) 475 °C.

Band gaps of the films were determined using UV/vis spectroscopy, which provided values of 2.74 eV for Ga_2Se_3 and 1.78 eV for In_2Se_3. The results are consistent with the literature values.[31,32]

Conclusions

$[Me_2Ga(SeP^iPr_2)_2N]$ and $[Et_2In(SeP^iPr_2)_2N]$ have been synthesized and used as single-source precursors for the growth of gallium selenide and indium selenide films. X-ray single-crystal structures of $[Me_2M(SeP^iPr_2)_2N]$ (M = Ga or In) show distorted tetrahedral geometry at the metal centers. XRPD studies show that cubic Ga_2Se_3 and hexagonal γ-In_2Se_3 films have been deposited on glass substrates. These compounds form a useful addition to the family of single-molecule precursors for selenides. The ligand itself is quite straightforward to prepare. Further studies will focus on the properties of films and the effect of modifying alkyl groups on the volatility of the precursors.

Acknowledgment. Authors thank the EPSRC for the grants to P.O.B. that have made this research possible. The authors would also like to thank Mr. Ian Borough (MMSC) for SEM analysis.

Supporting Information Available: Crystallographic data for the gallium and indium selenide compounds (CIF). This material is available free of charge via the Internet at http://pubs.acs.org.

CM0310420

(22) Munoz-Hernández, M. Á.; Singer, A.; Atwood, D. A.; Cea-Olivares, R. *J. Organomet. Chem.* **1998**, *571*, 15.
(23) Schultz, S.; Gillan, E. G.; Ross, J. L.; Rogers, L. M.; Rogers, R. D.; Barron, A. R. *Organometallics* **1996**, *15*, 4880.
(24) Kuchta, M. C.; Parkin, G. *Inorg. Chem.* **1997**, *36*, 2492.
(25) Cea-Olivares, R.; Garcia-Montalvo, V.; Novosad, J.; Woollins, J. D.; Toscano, R. A.; Espinosa-Pérez, G. *Chem. Ber.* **1996**, *129*, 919.
(26) Stoll, S. L.; Bott, S. G.; Barron, A. R. *J. Chem. Soc., Dalton Trans.* **1997**, 1315.
(27) Rahbarnoohi, H.; Kumar, R.; Heeg, M. J.; Oliver, J. P. *Organometallics* **1995**, *14*, 3869.
(28) Beachley, O. T., Jr.; Lee, J. C., Jr.; Gysling, H. J.; Chao, S.-H. L.; Churchill, M. R.; Lake, C. H. *Organometallics* **1992**, *11*, 3144.
(29) Gillan, E. G.; Barron, A. R. *Chem. Mater.* **1997**, *9*, 3037.
(30) Afzaal, M.; Crouch, D.; O'Brien, P.; Park, J.-H. *Thin Solid Films*, in press.
(31) Wright, A.; Williams, J.; Krost, A.; Richter, W.; Zahn, D. *J. Cryst. Growth* **1992**, *121*, 111.
(32) Julien, C.; Chevy, A.; Siapkas, D. *Phys. Status Solidi A* **1990**, *118*, 553.